

AD-A102 330

CRANFIELD INST OF TECH (ENGLAND) SCHOOL OF MECHANICA--ETC F/6 13/7
UNSTEADY EFFECTS OF CIRCUMFERENTIAL PRESSURE DISTORTED INLET FL--ETC(U)
JUN 81 R E PEACOCK AFOSR-77-3305

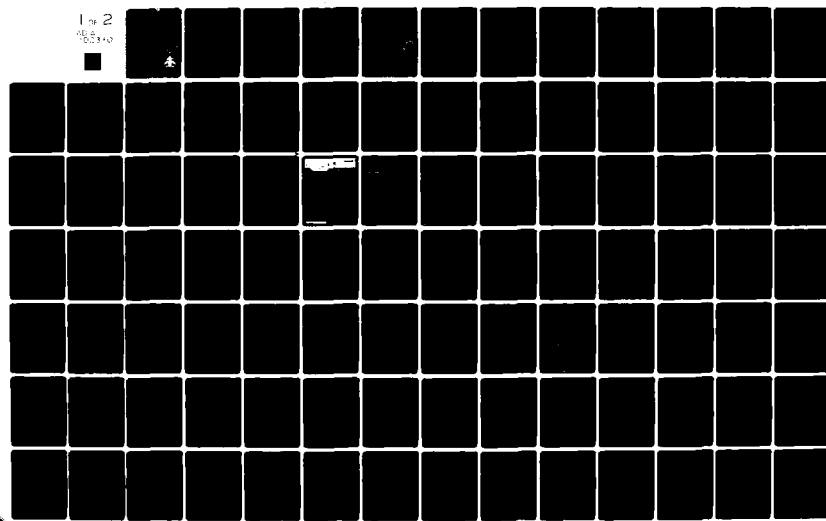
UNCLASSIFIED

AFOSR-TR-81-0604

NL

Line 2
AFOSR-77-3305

本



Cranfield

AD A102330

**School of Mechanical Engineering
Thermal Power Group**

DDIC FILE COPY

Approved for public release;
distribution unlimited.

THIS DOCUMENT IS BEST QUALITY PRACTICABLE.
THE COPY FURNISHED TO DDC CONTAINED A
SIGNIFICANT NUMBER OF PAGES WHICH DO NOT
REPRODUCE LEGIBLY.



Cranfield Bedford MK 43 0AL England
Telephone 0234 - 750111 (Bedford 750111) Telex 825072

Approved for public release
distribution unlimited.

818 03 069

UNCLASSIFIED

SECURITY CLASSIFICATION OF THIS PAGE (When Data Entered)

19 REPORT DOCUMENTATION PAGE		READ INSTRUCTIONS BEFORE COMPLETING FORM	
18. REPORT NUMBER AFOSR-TR-81-0604	12. GOVT ACCESSION NO. AD-A102330	3. RECIPIENT'S CATALOG NUMBER	
4. TITLE (and Subtitle) UNSTEADY EFFECTS OF CIRCUMFERENTIAL PRESSURE DISTORTED INLET FLOWS IN COMPRESSORS		5. TYPE OF REPORT & PERIOD COVERED FINAL	
6. AUTHOR(s) R. E. PEACOCK	7. CONTRACT OR GRANT NUMBER(s) AFOSR-77-3305		
9. PERFORMING ORGANIZATION NAME AND ADDRESS CRANFIELD INSTITUTE OF TECHNOLOGY CRANFIELD, BEDFORD, GREAT BRITAIN	10. PROGRAM ELEMENT, PROJECT, TASK AREA & WORK UNIT NUMBERS 2307/A4 61102F		
11. CONTROLLING OFFICE NAME AND ADDRESS AIR FORCE OFFICE OF SCIENTIFIC RESEARCH/NA BOLLING AFB, DC 20332	12. REPORT DATE JUN 1981		
14. MONITORING AGENCY NAME & ADDRESS (if different from Controlling Office) 12 151	13. NUMBER OF PAGES 146		
15. SECURITY CLASS. (of this report) UNCLASSIFIED			
15a. DECLASSIFICATION/DOWNGRADING SCHEDULE			
16. DISTRIBUTION STATEMENT (of this Report) Approved for public release; distribution unlimited.			
17. DISTRIBUTION STATEMENT (of the abstract entered in Block 20, if different from Report)			
18. SUPPLEMENTARY NOTES			
19. KEY WORDS (Continue on reverse side if necessary and identify by block number) AXIAL FLOW COMPRESSORS ROTATING STALL INLET DISTORTION UNSTEADY FLOW			
20. ABSTRACT (Continue on reverse side if necessary and identify by block number) <p>An investigation of the mechanics of rotor unsteady response in the presence of both upstream generated planar distortion and rotating stall is described. To this end, a system for the measurement and analysis of on-rotor pressure data was developed on a single stage, low speed rig. Two areas of investigation based on the compressor operating conditions were pursued: operation on the negative slope of the characteristic (nominally stable flow) and on the positive and zero slope (rotating stall). Compressor overall performance and detailed</p>			

UNCLASSIFIED
SECURITY CLASSIFICATION OF THIS PAGE(When Data Entered)

Response followed trends anticipated by the blockage effects of the inlet disposed screens. Two classes of rotating stall were isolated, each with different characteristics. One was present under low flow uniform inlet conditions and the other when an inlet distortion was present.

5

UNCLASSIFIED
SECURITY CLASSIFICATION OF THIS PAGE(When Data Entered)

1.

NO BETTER COPY AVAILABLE

29 APR 82

DISCLAIMER NOTICE

THIS DOCUMENT IS BEST QUALITY
PRACTICABLE. THE COPY FURNISHED
TO DTIC CONTAINED A SIGNIFICANT
NUMBER OF PAGES WHICH DO NOT
REPRODUCE LEGIBLY.

4

CRANFIELD INSTITUTE OF TECHNOLOGY

FINAL REPORT

Prepared for

UNITED STATES AIR FORCE OFFICE OF SCIENTIFIC RESEARCH (AFSC) USA
EUROPEAN OFFICE OF AEROSPACE RESEARCH AND DEVELOPMENT
LONDON, GREAT BRITAIN

UNSTEADY EFFECTS OF CIRCUMFERENTIAL PRESSURE DISTORTED INLET FLOWS IN COMPRESSORS

GRANT AFOSR 77-3305 ✓

(061392)

PRINCIPAL INVESTIGATOR: R. E. PEACOCK*



The School of Mechanical Engineering
Cranfield Institute of Technology
Cranfield, Bedford, Great Britain
Telephone (0234) 750111, Ext. 523

June, 1981

AIR FORCE OFFICE OF SCIENTIFIC RESEARCH (AFSC)
NOTICE OF TRANSMITTAL TO DDC
This technical report has been reviewed and is
approved for public release IAW AFR 190-12 (7b).
Distribution is unlimited.
A. D. BLOSE
Technical Information Officer

LIST OF CONTENTS

1.0 INTRODUCTION

2.0 OBJECTIVE

3.0 THE RESEARCH FACILITY

- 3.1 The Rig (fig.1)
- 3.2 Steady State Instrumentation
- 3.3 The Rotor-Borne Instrumentation (Table 1)
 - 3.3.1 Requirements
 - 3.3.2 The Rotor-borne Components
 - 3.3.3 Installation
 - 3.3.4 The Effect of Centrifugal Force
 - 3.3.5 Rotor-borne Signal Conditioning (fig. 2)
 - 3.3.6 The Peripheral Equipment (fig. 2)
- 3.4 Data Acquisition Systems
- 3.5 Software Development
- 3.6 Distortion Generators

4.0 DATA ACQUISITION

5.0 THE EXPERIMENTAL PROGRAMME

- 5.1 Negative Slope Operation
- 5.2 Positive Slope Operation
- 5.3 Derived Parameters

6.0 DISCUSSION OF RESULTS

6.1 Negative Slope Operation

- 6.1.1 Compressor Overall Performance
- 6.1.2 Rotor Unsteady Pressure Data

6.2 Positive Slope Operation

7.0 FURTHER RECOMMENDED WORK

8.0 CONCLUSIONS

9.0 REFERENCES

TABLES 1 & 2

Accession For	
NTIS GRA&I	<input type="checkbox"/>
DTIC TAB	<input type="checkbox"/>
Unannounced	<input type="checkbox"/>
Justification	
By	
Distribution/	
Availability Codes	
Avail and/or	
Dist Special	
23	
PAC	

LIST OF CONTENTS

APPENDIX 1	A DIGITAL TECHNIQUE FOR THE ANALYSIS OF THE RESPONSE OF COMPRESSOR/DUCT SYSTEMS IN UNSTEADY FLOW
APPENDIX 2	DISTORTION GENERATION SCREENS
APPENDIX 3	DERIVED AERODYNAMIC AND ASSOCIATED PARAMETERS
APPENDIX 4	COMPRESSOR ROTATING STALL IN UNIFORM AND NON-UNIFORM FLOW
FIGURES	1 - 30

1-
app. 1 deleted
Illegible
29 apr 82

1.0 INTRODUCTION

While it is always designed using steady state assumptions, the compressor, under all régimes of operation is essentially an unsteady flow device. The relative movement between succeeding blade rows ensures that the shed wakes impose cyclic, small scale, changes both of incidence and velocity on succeeding blade rows. More important however are the unsteady flows sensed at and beyond the stability limit line of a compressor: these are recognised either as a planar perturbation, rotating stall, or as a spatial perturbation, system surge. Because there appears to be evidence that rotating stall, the fundamental destabilising feature of a compressor pre-dates surge its mechanism is of considerable interest.

These classes of unsteady flow, which are internally generated in the machine, are all reproducible in a compressor/duct system which has initially uniform flow. Other time-dependent flows, which may be of large magnitude and make a significant contribution to the performance and may be life of a compressor may be generated externally and ingested into the compressor. These include planar distortions in the inlet flow due to partial blockage of the intake, the generation of secondary flows due to bends in the intake duct, or wake-shedding from upstream support struts. While such distortions may be steady in an absolute frame of reference, relative to the rotor they are sensed as time-wise unsteadiness. The rotor then may be expected to have a time-wise response somewhat similar to that in rotating stall since both the distortion wake and the rotating stall cell are characterised by regions of reduced absolute velocity yielding changes in rotor relative velocity and incidence.

It was to examine the mechanics of rotor unsteady response both in the presence of upstream generated planar distortion and rotating stall that the research programme (AFOSR-77-3305) was established. The programme was based upon a proposal (1) which followed a previous period of research (AFOSR-74-2708) reported in (2).

This document forms the final report on the programme (AFOSR-77-3305) and covers the whole of the research period. Progress reports have been issued during the course of the programme (3, 4, 5).

2.0 OBJECTIVE

The overall long-term aim of the Cranfield research programme is to produce:

1. an improved parameter for quantifying distortion
2. improvements in performance prediction techniques for compressors in quasi-steady distorted flows
3. a prediction technique for compressors in pulsating flows
4. a design method that will reduce compressor sensitivity to inlet flow distortions.

This involves an integrated programme of research in which five experimental rigs are being used. In parallel, mathematical models of distorted flows and compressor reactions to them are under development.

The detailed aim of that part of the programme covered by the research grant AFOSR-77-3305 may be quantified as:

1. the development of a custom-designed data acquisition and analysis system.
2. evaluation of rotating stall phenomena
3. evaluation of distortion on rotor transients and compressor behaviour.
4. the provision of a databank that may be of subsequent value in the development of analytical programmes.

3.0 THE RESEARCH FACILITY

3.1 The Rig (fig.1)

The compressor upon which the research was executed was of single-stage and lightly loaded. The annulus, which was of constant cross-section was 20.00" tip diameter and 10.00" hub diameter. Rotational speeds used in the programme reported were 1000 and 1250 rev/min. Blading, which was of C4 section was of free vortex zero α_0 design: details are listed in Table 1. Mass flow was controlled by a throttle valve sited downstream of the compressor and separated from it by a long duct.

3.2 Steady State Instrumentation

The rig was fitted with the usual instrumentation required to evaluate the overall compressor performance. Inner and outer wall static tappings were positioned ahead and behind every blade row, and the downstream stagnation pressures were measured by four rakes placed orthogonally, each having nine shrouded pitot heads. All pressure readings were taken from inclined multiple manometer banks.

The compressor pressure ratio was calculated from the stagnation pressure measured downstream of the stage by the 36 stagnation pressure probes. Using averaged value of static pressure from the inner and outer wall tappings downstream of the stage, together with the 36 total pressure readings, the velocity distribution was obtained radially. Area weighted integration provided the compressor mass flow.

3.3 The Rotor-Borne Instrumentation (Table 1)

Two rotor blades were instrumented at blade mid-height (bmh) with eight static pressure tappings; blade A on the pressure surface and the blade B on the suction surface. High-frequency response transducers (70 KH₂) were mounted at bmh at all tappings. The pressure was fed from the blade surface to the transducer volume within the blade via a 0.015" diameter transfer tube (maximum length of 0.06"). The transducers had a miniature silicon diaphragm (0.125" diameter) on which a full wheatstone bridge network was diffused. The electrical output wires were routed down

through the blade root to a remotely controlled switching circuit mounted on the rotor disc. The signal was then taken from the rotating frame via a precision slipring assembly (noise $< 5 \mu\text{V}/\text{mA}$) to an external switch control device and finally to amplification and recording equipment.

The system was designed so that any eight transducers could be recorded simultaneously.

3.3.1 Requirements

The basic requirements of the rotor-borne system were that mechanical integrity and calibrations would be maintained under high 'g' conditions and that the frequency response would be sensibly higher than the disturbance frequency in the flow: (In the application to be discussed 'g' loads of up to 800 and disturbance frequencies of 25 Hz. would be encountered.)

With an analogue output from the rotor-borne system it was also necessary to have a comprehensive peripheral data recording and analysis system. To achieve this it was necessary to be able to:

1. record many channels simultaneously
2. detect any non-synchronous data, such as rotating stall
3. detect non-periodic data
4. record in real time

3.3.2 The Rotor-Borne Components

Since the unsteady pressures around the compressor blades were a good indication of the flow field behaviour the pressure transducers were mounted on the rotor assembly. Compactness, low weight, mechanical integrity, shock resistance, good frequency response with high natural frequency, low hysteresis characteristic, high resolution, temperature and acceleration insensitivity are characteristics of a good transducer for this application. Of those examined a miniature silicon diaphragm with a fully active wheatstone bridge was selected.

3.3.3 Installation

The high natural frequency of such a transducer could only be exploited if the diaphragm was directly exposed to the unsteady pressure. For compressor blades this called for surface mounting that would destroy the blade contour, so a buried system was adopted and an accompanying reduction in natural frequency of the system accepted. The pressure amplitude ratio, that of sensed pressure (P_2) to forcing pressure (P_1) and the phase-lag has been theoretically evaluated by Bergh and Tijdeman (6) and simplified by Schweikhard (7) to yield:

$$\text{amplitude ratio } \frac{P_2}{P_1} = \frac{1}{\sqrt{1 - \left(\frac{\omega}{\omega_n}\right)^2 + \left(\frac{2\zeta\omega}{\omega_n}\right)^2}}$$

$$\text{phase angle } \phi = \tan^{-1} \frac{2\zeta}{\left(\frac{\omega}{\omega_n} - \frac{\omega_n}{\omega}\right)}$$

(ω is frequency of fluctuating pressure)

$$\text{where the damping ratio } \zeta = \frac{4V}{r^3} \cdot \sqrt{\frac{L}{\pi} \left(\frac{\rho}{\gamma P}\right) \left(V + \frac{4r^2L}{\pi}\right)}$$

$$\text{and the natural frequency: } \omega_n = \sqrt{\frac{\gamma P}{\rho} \frac{r^2}{4\pi L \left(V + \frac{4r^2L}{\pi}\right)}}$$

(γ is the ratio of specific heats, P and ρ are mean air pressure and density respectively).

During installation every effort was made to keep r as large and V as small as possible in order to minimise response problems.

For a system with the transducer mounted in the blade adjacent to the tapping, the natural frequency became very high and beyond the range of concern.

3.3.4 The Effect of Centrifugal Force

The mass of the transducer diaphragm responded, for blade-mounted transducers in the installation considered, in the following manner to centrifugal force.

<u>Rotational Speed rev/min.</u>	<u>g.</u>	<u>% error F.S.</u>
750	120	0.24
1000	213	0.43
1250	333	0.67
1500	479	0.96

For a transducer of full scale deflection pressure of 51b/in^2 the maximum error was 0.0479 lb/in^2 .

With a blade mounted transducer system the transducer was connected to the static pressure tapping by a short pneumatic tube. The effect of centrifugal force on the volume of air was very low.

3.3.5 Rotor-Borne Signal Conditioning (fig. 2)

The transducer signal passed through a 24-way slip ring, with a multiplexing system permitting up to 10 signals out of 20 to be carried simultaneously. Good signal-to-noise ratio was achieved using a high quality slip-ring assembly. Signal conditioning for thermal stability was carried out on-rotor.

3.3.6 The Peripheral Equipment (fig. 2)

Signal amplification took place in the stationary framework using specially designed amplifiers. The data (if time invariant) was recorded on an oscilloscope or digital volt-meter.

Instrumentation comprised two data reduction and storage systems which included an analogue-to-digital converter, a micro-processor, visual display unit, a digital-to-analogue converter and a cartridge record/playback unit.

3.4 Data Acquisition Systems

Two data acquisition systems were developed for this programme. Basically similar in operation they each received the set of analogue signals which were digitised via a logging control on a teletype console. The digitised data were either stored for subsequent analysis on a magnetic cartridge in conjunction with a record/playback unit or analysed using a suite of computer programmes developed for the purpose.

The main difference between the two systems in operation was that one was limited to a digitisation frequency of 4 kHz while the other was capable of a digitisation rate of 1 MHz. The low speed unit is described in greater detail in (4) and the high speed unit in (8) which is included as Appendix 1.

3.5 Software Development

The development of software for the peripheral data logging and analysis provided a major hazard in the programme. Undetected software errors led to malsynchronisation of the experimental data which, because the technique involved direct on-line digitisation resulted in substantial abortion of the programme. This was subsequently repeated satisfactorily after the necessary corrections.

3.6 Distortion Generators

The flow through the compressor was upset by implanting a series of screens in the intake region one chord upstream of the rotor leading edge in the constant annulus section of the ductwork. Every screen was of uniform blockage circumferentially and radially, promoting a nominally constant pressure drop in its wake in both radial and circumferential directions. As will be seen though, this uniformity was disturbed by a rotor blade interaction.

8.

Screens of three circumferential extents 60° , 90° and 120° were employed and screen resistance coefficients, calculated by the method employed by Bruce ((9) and Appendix 2). For the 60° and 120° screen the resistance coefficient $K = 4.37$ and for the 90° screen, in which two identical layers of gauze were used, the resistance coefficient $K = 8.74$.

4.0 DATA ACQUISITION

Steady state data which were used to establish the compressor characteristic were acquired in the traditional manner from manometer banks and appropriate steady state recorders.

The unsteady pressure data from the rotor surfaces were handled in two ways. In each case, the peripheral recording system was limited in the number of possible channels to be used and so data were taken sequentially from suction and pressure surfaces of the blades.

For measurements taken on the negative slope of the compressor characteristic, away from rotating stall effects, twenty-five sets of consecutive data were ensemble averaged, averaging taking place at a prescribed set of locations around the annulus and each average being at one location. Early tests had confirmed that twenty-five sets of data effectively smeared out the electrical and aerodynamic noise.

Within the rotating stall régime, ensemble averaging at any circumferential position was meaningless since the rotating stall cell moved within the annulus at a non-synchronous speed. Attempts to ensemble-average at points relative to the stall cell rather than the fixed annulus were not successful. There was evidence from another research programme that the rotating stall cell was itself unstable changing its magnitude and shape on successive cycles and this further deterred the attempts to average such data. The rotating stall data were then not ensemble averaged but represented that measured over one or two consecutive cycles.

5.0 THE EXPERIMENTAL PROGRAMME

Two areas of investigation comprised the experimental programme, that with the compressor operating on the negative slope of its characteristic, the nominally stable régime and that with operation in the positive and zero slope areas of the characteristic, the region of rotating stall.

5.1 Negative Slope Operation

Two rotational speeds were used in this phase of the work, 1000 rev/min. and 1250 rev/min.

Four screens of uniform blockage radially and circumferentially were also employed. Three screens, all of the same blockage were respectively of 60° , 90° and 120° circumferential extent and the use of these yielded not only the trend in overall performance change with increasing extent of blockage but also the effect of the circumferential extent of the blockage upon the rotor reaction. One further screen of 90° circumferential extent was made of a double layer of the screen mesh and the derived data, when compared with that of the 90° single mesh screen, showed the effects of blockage density.

In evaluating the compressor characteristics, four or five throttle positions were used in general. Detailed analysis was however confined to three points, all on the negative slope.

5.2 Positive Slope Operation

Rotating stall measurements were all made at the rotational speed of 1250 rev/min.

Two inlet geometries were used in the investigation, that with a clean inlet flow and that with a 90° uniform single mesh screen placed in the intake.

5.3 Derived Parameters

The parameters describing the unsteady aerodynamics and associated features are defined in Appendix 3.

6.0 DISCUSSION OF RESULTS6.1 Negative Slope Operation6.1.1 Compressor Overall Performance

The compressor characteristics both for clean flow and inlet distorted flow at the two compressor speeds are plotted in figs. 3-6. The data at the two speeds, while not identical are closely similar.

The progressive increase in screen size (figs. 3,4) yielded a reduction in pressure rise coefficient at any particular mass flow coefficient and also a reduction in the open throttle mass flow. From the derived data it is seen that the maximum mass flow at $\theta = 60^\circ$ did not quite fit this trend. It is additionally noted that with increase in screen size up to $\theta = 90^\circ$ the positive slope and hence stability limit moved to progressively higher mass flows. At $\theta = 120^\circ$ this trend was reversed.

The effect upon overall performance of the intensity of the distortion may be observed in figs. 5,6. Increased blockage led to progressively reduced pressure rise and open throttle mass flow.

6.1.2 Rotor Unsteady Pressure Data

Rotor unsteady pressure measurements are presented graphically as follows:

	Flow Rate	1000 rev/in.			1250 rev/in.		
		1	2	3	1	2	3
Figures							
60° single mesh screen		7	8	9	10	11	12
90° single mesh screen		13	14	15	16	17	18
120° single mesh screen		19	20	21	22	23	24
90° double mesh screen		25	26	27	28	29	30

The form of figs. a & b is three-dimensional, each graph indicating the pressure distribution for either the rotor suction or pressure surface with respect to axial chord and time. The matrix drawn to represent the

resulting surface was derived from computer interpolation routines and is not representative of the number of chordwise tapping positions which were always eight. In comparing the trailing edge data for both suction and pressure surface at one particular condition it is noted that Kutta condition is apparently violated. Trailing edge data are extrapolated from the rearward static pressure tappings set at 92% of the chord on both surfaces. Because there is evidence that in unsteady flow operation the Kutta condition is not maintained, no attempt was made to close the pressure loop at the trailing edge.

Figs. 7a,b indicate at 1000 rev/min the rotor reaction to the single mesh 60^0 distortion screen under open throttle conditions. In otherwise uniform behaviour the rotor reaction to the screen shadow is clearly defined in the region $25^0 < \theta < 110^0$ on the convex surface and $0 < \theta < 150^0$ on the concave surface. The pressure reduction in the screen wake yielded reduced pressure at the blade surfaces which recovered in the clean flow of the remainder of annulus. Because the screen wake spread in the axial direction (fig. 7c) and there was vorticity in the flow at the wake edges the effect upon the rotor was wider spread than the geometric extent of the screen.

As well as indicating the circumferential change in incidence and axial velocity ratio, fig. 7c shows the blade normal force coefficient and the position of the centre of pressure gained by integration of the data in figs. 7a, b. The normal force coefficient rose sharply with incidence at entry to the screen shadow and then followed a wavy pattern characteristic of dynamic stall. In the region $90^0 < \theta < 120^0$ the sharp changes in the normal force coefficient were due to activity on the blade concave surface (fig 7b).

A plot of normal force coefficient v incidence (fig. 7d) shows large scale hysteresis in the blade reaction.

A general observation may be made about the form of these plots. They comprise a series of points in one C_n v i region for operation in the clean region of the annulus and a second concentration in a second region of generally higher C_n v i , the two regions being joined by transit lines. Such data support the concept of the two compressors in parallel hypothesis and are worthy of close investigation in the light of the parallel compressor theory.

The data were not altered in character with reduction in mass flow (figs. 8, 9) or with increased rotational speed (figs. 10-12).

The use of a 90^0 single mesh screen led to a similar spreading of the unsteady flow reaction which in the region of the screen shadow contained, at 1000 rev/min. three well-defined peaks (fig. 13c) as had been observed in earlier work (fig. 10). In addition, the flow distortion left a short periodic residual wave in the data, four cycles of which can generally be seen in figs. 13a, c. In certain other tests, in which attempts were made to ensemble average rotating stall conditions the observed ripple was characteristic of rotating stall. In this case though, the effect was not that of rotating stall data being incorrectly superimposed by the averaging technique, but was a real aerodynamic effect.

At 1250 rev/min. compressor speed, the three-peak unsteady character of the normal force coefficient was not as evident (fig. 16c).

The effect of using the 120^0 single mesh screen was to spread the primary effect of its shadow on the rotor over a longer period, resulting in a multi-peak unsteadiness in the normal force coefficient and a reaction which did not become steady at any time during the blade rotation.

Comparing data from tests with the 90^0 double mesh screen (figs. 25-30) with those from the 90^0 single mesh screen it is seen that the increased blockage produced a larger change of axial velocity ratio and incidence in the shadow. This was reflected in larger perturbations of the rotor surface pressures.

A synopsis of the maximum, minimum and mean values of axial velocity, incidence and normal force coefficient for all data points is given in Table 2.

6.2 Positive Slope Operation

The different technique of data acquisition and analysis used in evaluating rotating stall has already been discussed.

The results of the investigation are presented in Appendix 4 which also contains a full discussion.

In brief, two classes of rotating stall were identified each with its own characteristic frequency and stall inception point. One class of rotating stall, which propagated across the blade from trailing to leading edge had a rotational frequency of 66% of the compressor speed and was isolated with clean inlet flow conditions. The other which was leading edge propagated was 50% of the compressor speed and was sensed with an upstream distortion of a 90° screen.

7.0 FURTHER RECOMMENDED WORK

The data gained in the programme are presented in a form that enables further analysis and digestion. Areas in which the data may be used are:

1. in giving positive support to the parallel compressor theory and offering modifications to the theory to allow both for time-lag effects in passing from one sector of the compressor to the other and for large perturbation effects such as rotor blade dynamic stall
2. in developing unsteady stage characteristics and compressor unsteady overall characteristics
3. in quantifying the unsteady and large perturbation effects which cannot currently be modelled accurately.

8.0 CONCLUSIONS

A system for the measurement and analysis of on-rotor data was developed on a single-stage low speed rig for the purpose of evaluating rotor response to circumferentially varying flows either created by inlet distortion screens or rotating stall.

The two-part programme that ensued granted an understanding and a databank of rotor reaction to a range of inlet distortions and to rotating stall.

Compressor overall performance and detailed response followed trends anticipated by the blockage effects of the inlet disposed screens. Two classes of rotating stall were isolated each with different characteristics. One was present under low flow uniform inlet conditions and the other when an inlet distortion was present.

REFERENCES

1. PEACOCK R. E. 'Unsteady Effects of Circumferential Pressure Distorted Inlet Flows in Compressors' Research Proposal 959:REP:132 Dec. 1976
2. PEACOCK R. E. 'Square-Wave Circumferential Distortion Effects in Compressors' Final Research Report (AFOSR-74-7208)(061345) March 1977
3. PEACOCK R. E. 'Unsteady Effects of Circumferential Pressure Distorted Internal Flows in Compressors' First Progress Report (USAFOSR-77-3305) November 1976
4. PEACOCK R. E. 'Unsteady Effects of Circumferential Pressure Distorted Internal Flows in Compressors' Second Progress Report (USAFOSR-77-3305) April 1977
5. PEACOCK R. E. 'Unsteady Effects of Circumferential Pressure Distorted Internal Flows in Compressors' Third Progress Report (USAFOSR-77-3305) November 1978
6. BERGH H. TIJDEMAN H 'Theoretical and Experimental Results for a Dynamic Response of Pressure Measuring Systems' REP.NLR-TR-F238 National Aero and Astronautical Research Inst., Amsterdam, 1965
7. SCHWEIKHARD W. G. 'Test Techniques, Instrumentation and Data Processing'. AGARD-LS-72 Distortion Induced Engine Instability November 1974
8. PEACOCK R. E. DAS D. K. FORD J. KELLY C. J. 'Digital Data Handling of Unsteady Aerodynamic Phenomena' Microsystems 81, 4th Annual Conference 11-13 March 1981, London, UK
9. BRUCE E.P. 'Design and Evaluation of Screens to Produce Multi-Cycle \pm 20% Amplitude Sinusoidal Velocity Profiles.' AIAA 8th Aerodynamic Testing Conference, Bethesda, Maryland, USA July 1974
10. PEACOCK R. E. OVERLI J. 'Dynamic Internal Flows in Compressors with Pressure Maldistributed Inlet Conditions' AGARD 46th PEP Conference 1975

TABLE 1

Blade Data and Tapping Locations

	Stators t/c = .10							Rotors t/c = .12							Units
	Dia.	10.2	12.5	14.6	15.0	17.0	19.4	10.2	12.5	14.6	15.0	17.0	19.4		
θ	53.2	47.6	43.0	42.4	39.4	36.0	52.4	38.6	29.6	28.6	23.3	17.0	17.0	deg.	
γ	13.6	13.0	11.9	11.7	10.5	-9.0	-9.2	21.6	30.9	31.8	38.3	45.0	45.0	deg.	
β_1	40.2	36.8	33.4	32.9	30.2	27.0	35.4	40.9	45.7	46.1	49.9	53.5	53.5	deg.	
β_2	13.0	10.8	-9.6	-9.5	-9.2	-9.0	-16.9	2.2	16.1	17.5	26.6	36.5	36.5	deg.	
s/c	.615	.750	.886	.905	1.03	1.17	.623	.761	.898	.917	1.04	1.18	-		

	C ins.	No.	R_e	AR
Stators	1.86	28	1.39	5.37
Rotors	3.02	17	2.29	3.29

Rotor Tapping Positions:

No.	Inches from LE	%C
1	0.152	5.03
2	0.393	13.01
3	0.677	22.42
4	1.076	35.63
5	1.494	49.47
6	1.831	60.63
7	2.148	71.13
8	2.413	79.90

SYNOPSIS OF MEASURED UNSTEADY FLOW DATA

TABLE 2

60° SINGLE MESH

	Vax			C _N			i deg.		
	Max	Min	Mean	Max	Min	Mean	Max	Min	Mean
1000 rpm Q1	1.095	0.348	0.833	1.462	0.348	0.826	24.6	-11.7	1.9
1000 rpm Q2	1.089	0.410	0.853	1.250	0.289	0.683	24.2	- 5.8	4.8
1000 rpm Q3	1.332	0.398	0.933	1.273	0.281	0.598	29.7	- 3.7	10.2
1250 rpm Q1	1.099	0.377	0.843	1.415	0.375	0.845	23.2	-11.0	1.8
1250 rpm Q2	1.115	0.409	0.837	1.458	0.372	0.802	23.9	- 8.6	4.9
1250 rpm Q3	1.225	0.531	0.945	1.328	0.251	0.653	24.7	- 0.6	10.1

120° SINGLE MESH

	Vax			C _N			i deg.		
	Max	Min	Mean	Max	Min	Mean	Max	Min	Mean
1000 rpm Q1	1.154	0.369	0.696	1.566	0.467	0.979	24.9	- 8.4	10.3
1000 rpm Q2	1.188	0.375	0.693	1.156	0.191	0.736	26.9	- 3.1	14.9
1000 rpm Q3	1.450	0.462	0.888	1.537	0.450	0.900	29.6	- 3.1	14.9
1250 rpm Q1	1.164	0.370	0.698	1.617	0.689	1.198	25.0	- 9.0	9.9
1250 rpm Q2	1.176	0.356	0.686	1.588	0.699	1.174	27.1	- 7.3	12.1
1250 rpm Q3	1.516	0.469	0.907	1.758	0.711	1.138	29.8	- 2.9	15.3

90° SINGLE MESH

	Vax			C _N			i deg.		
	Max	Min	Mean*	Max	Min	Mean*	Max	Min	Mean*
1000 rpm Q1	1.040	0.237	0.762	1.510	0.612	0.995	32.1	- 5.5	7.1
1000 rpm Q2	1.025	0.209	0.743	1.606	0.385	0.852	33.6	- 4.8	8.3
1000 rpm Q3	1.084	0.259	0.779	1.399	0.393	0.772	33.7	- 1.1	11.8
1250 rpm Q1	1.184	0.317	0.841	1.279	0.493	0.946	30.2	- 5.7	8.0
1250 rpm Q2	1.259	0.341	0.879	1.436	0.512	0.907	30.9	- 4.3	9.5
1250 rpm Q3	1.328	0.380	0.939	1.341	0.506	0.839	32.2	- 2.1	12.9

90° DOUBLE MESH

	Vax			C _N			i deg.		
	Max	Min	Mean*	Max	Min	Mean*	Max	Min	Mean*
1000 rpm Q1	1.261	0.240	0.749	1.918	0.248	1.100	34.8	-14.0	9.1
1000 rpm Q2	1.330	0.227	0.774	1.759	0.240	1.078	36.7	-13.3	11.3
1000 rpm Q3	1.476	0.269	0.860	1.727	0.312	1.012	36.1	- 6.8	14.6
1250 rpm Q1	1.256	0.235	0.758	1.998	0.449	1.163	35.3	-14.5	8.4
1250 rpm Q2	1.293	0.219	0.781	2.049	0.682	1.282	36.8	-13.1	10.2
1250 rpm Q3	1.470	0.298	0.886	1.869	0.681	1.173	35.6	- 6.1	13.9

* - Arithmetic mean across 360°

Q1 - open throttle

Q3 < Q2 < Q1

DISTORTION GENERATION SCREENS

Wire mesh screens were used to generate square-wave distortions.

Three different screens were used, 60° (50 mesh/inch), 90° (2 x 50 mesh/inch) and 120° (50 mesh/inch). The screens were placed 1 chord upstream of the rotor blades leading edge.

The screen resistance coefficient (K) was calculated. $K = 4.37$ for 50 mesh/inch and $K_2 = 8.74$ for 2 x 50 mesh/inch.

In the screen resistance coefficient calculation (K)
By E.P. Bruce (g) it is suggested that ;

$$K = \frac{\Delta P}{\frac{1}{2} \rho V_{REF}^2}$$

where;

K = Resistance coefficient

ρ = Fluid density

V_{REF} = Reference axial velocity,
the uniform axial velocity at
a point far upstream of the
screen.

and

$$K = \frac{CS}{(1-S)^2}$$

where;

C = Screen loss coefficient
(C = 0.8 for wire diameter based
Reynolds numbers are small, i.e.
 $R_e < 4000$)

S = Solidity, the ratio of blocked
area to total area.

$$S = 2 \left[\frac{d}{m} \right] - \left[\frac{d}{m} \right]^2$$

where;

d = wire diameter

m = spacing between centres of wires

$$d = 0.007 \text{ inch} \quad m = 0.017 \text{ inch}$$

$$S = 0.654$$

$$C = 0.8 \text{ since } R_{ed} = 300 < 4000$$

$$K = \frac{CS}{(1-S)^2} \quad K = 4.37$$

APPENDIX 3

DERIVED AERODYNAMIC & ASSOCIATED PARAMETERS

Corrected Speed

The compressor corrected speed is

$$N_{corr} = N_{act} \left(\frac{T_{ref}}{T_{act}} \right)^{\frac{1}{2}}$$

where; N_{corr} = Corrected rotor speed

N_{act} = Measured rotor speed

T_{ref} = Reference temp. in $^{\circ}$ K

T_{act} = Measured temp. in $^{\circ}$ K

Blade Static Pressure Coefficient, C_p

$$C_p = \frac{p - p_{amb}}{\frac{1}{2} \rho U^2}$$

where; p = Measured pressure

p_{amb} = Ambient pressure

ρ = Air density

U = Blade speed at b.m.h.

Blade Normal Force Coefficient, C_N

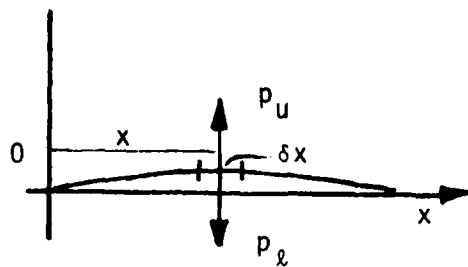
Integration of the C_p vs x/c plot for both pressure and suction surfaces is directly proportional to C_N .

The normal force per unit span is then;

$$C_N = \frac{\int p d(x/c)}{\frac{1}{2} \rho U^2} = \int C_p d(x/c)$$

Pitching Moment Coefficient, C_M

Pitching moment is taken about the leading edge.



The net force acting on an element of an aerofoil is given by:

$$\delta F = (p_u - p_x) \delta x \text{ per unit span}$$

The pitching moment due to this element of force about the L.E. 0 is given by:

$$\delta M = (p_u - p_x) x \cdot \delta x$$

The total pitching moment is:

$$M = (p_u - p_x) x \cdot dx \quad \text{A.3.1}$$

In non-dimension form

$$C_M = \frac{M}{\frac{1}{2} \rho U^2 S C} \quad \text{where,}$$

S = is the area of blade surface (Here, since we are considering unit span $S = C$, chord)

then,

$$C_M = \frac{M}{\frac{1}{2} \rho U^2 C^2}$$

Thus (A.3.1) may be defined in coefficient form as :

$$C_M = \int_0^c (C_{p_u} - C_{p_l}) x/c d(x/c) \dots \dots \dots \quad (A.3.2)$$

$$\text{i.e. } C_M = \int_0^c C_{p_u} \cdot x/c d(x/c) - \int_0^c C_{p_l} \cdot x/c d(x/c)$$

$$\text{i.e. } C_M = \sum (C_p x/c \Delta(x/c))_u - \sum (C_p x/c \Delta(x/c))_l \dots \dots \quad (A.3.3)$$

Summations on the C_p vs x/c curves may be executed using trapezoidal rule if C_p is known on both upper and lower surfaces at a known common x/c , then, e.g. (A.3.2) may be used in simplified form as :

$$C_M = \int_0^c (\Delta C_p x/c) d x/c$$

$$\text{i.e. } C_M = \sum (\Delta C_p \cdot x/c) \Delta (x/c)$$

Centre of Pressure, x

The position of the centre of pressure, x , from the L.E. is

$$x = \frac{C_M}{C_N}$$



an ASME
publication

\$3.00 PER COPY
\$1.50 TO ASME MEMBERS

The Society shall not be responsible for statements or opinions advanced in papers or in discussion at meetings of the Society or of its Divisions or Sections, or printed in its publications. Discussion is printed only if the paper is published in an ASME journal or Proceedings. Released for general publication upon presentation. Full credit should be given to ASME, the Technical Division, and the author(s).

Compressor Rotating Stall in Uniform and Non-Uniform Flow

B. F. J. COSSAR

Assistant Professor

R. E. PEACOCK

Senior Lecturer,
The School of Mechanical Engineering,
Cranfield, Bedford, U.K.

W. C. MOFFATT*

Professor

Mechanical Engineering Dept.,
Royal Military College of Canada,
Kingston, Ontario, Canada

Rotating stall in axial compressors consists of regions or cells of retarded flow moving around the annulus relative to the blades. Planar symmetry is destroyed, resulting in stalled blades in part of the annulus and unstalled blades in the remainder. The stall cell moves in the direction opposite to the rotor, relative to the blades, but since the relative speed of propagation is usually less than the rotor speed, the cell is seen to move in the same direction as the rotor from an absolute reference frame. The presence of the stall cells results in a deterioration of compressor performance since the maximum pressure ratio is not achieved in regions of retarded flow. Furthermore, since this self-induced distortion is periodic, the forced frequencies generated may coincide with the natural harmonics of the blading, tending to cause structural damage. This paper describes a series of experiments in which a single-stage, lightly loaded compressor operated under stall-free conditions and with rotating stall, both with uniform inlet flow and with distortions generated by an upstream screen of uniform porosity. Not only was the overall compressor performance determined in the traditional manner, but the distribution of static pressure over the rotor suction and pressure surfaces was measured with high response instrumentation. The rotor pressure profiles measured in both undistorted and distorted flow are presented for operation before and after the onset of rotating stall and the latter are compared with the steady flow results. It is observed that two distinctly different types of rotating stall exist depending upon whether or not an inlet flow distortion is present. These cells differ not only in macroscopic properties—rotational speed, circumferential extent, mass-averaged flow conditions etc.—but also in detailed flow characteristics as evidenced by the rotor blade static pressure distributions. It is further observed that not all inlet distortion geometries lead to the development of rotating stall.

*Presently Visiting Professor, von Karman Institute for Fluid Dynamics, Rhode-St-Geneve, Belgium.

Contributed by the Gas Turbine Division of The American Society of Mechanical Engineers for presentation at the 1979 Israel Joint Gas Turbine Congress, Haifa, Israel, July 9-11, 1979. Manuscript received at ASME Headquarters May 11, 1979.

Copies will be available until March 1, 1980.

Compressor Rotating Stall In Uniform and Non-Uniform Flow

B. F. J. COSSAR

W. C. MOFFATT

R. E. PEACOCK

NOMENCLATURE

a, b, \dots, j = compressor operating points on characteristic in undistorted flow
 q, r, \dots, v = compressor operating points on characteristic in distorted flow
 c_p = blade surface coefficient of pressure
 $= \frac{P - P_1}{\frac{1}{2} \rho_1 W_1^2}$
 c^* = dimensionless blade surface pressure change due to stall or distortion
 $= \frac{P - P_\theta}{\frac{1}{2} \rho W_1^2}$
 $c.p.r.$ = compressor stagnation pressure ratio
 $c_{\Delta T}$ = stagnation pressure coefficient
 $= \frac{P - P_1}{\frac{1}{2} \rho_0 V_0^2}$
 c_s = static pressure coefficient = $\frac{P - P_1}{\frac{1}{2} \rho V_0^2}$
 m = Mass flow rate
 N = Rotor rotational speed
 P = Stagnation pressure
 P_s = static pressure
 P_θ = blade surface static pressure in distorted flow rotating stall

Δp = blade surface static pressure relative to atmospheric pressure
 R_b = $P_\infty - P$
 T = Reynolds' Number based upon blade chord
 V = Absolute temperature
 W = gas velocity in absolute frame of reference
 x/c = gas velocity relative to the rotor
 θ = dimensionless chordal distance
 θ_D = circumferential position with respect to a fixed reference
 θ' = circumferential extent of distortion
 θ^* = circumferential position of stall cell with respect to a reference fixed to the rotor
 U = rotor blade speed
 i = flow incidence to blade
 ρ = fluid density
 τ = angular extent of rotating stall cell period, expressed in absolute degrees of rotor rotation

Subscripts

0 = upstream of distortion screen
 1 = upstream of rotor
 ∞ = ambient

Superscripts

= mass averaged quantity

INTRODUCTION

The existence of large-scale non-uniformities in the inlet flow of axial compressors has recently received widespread attention. The mathematical difficulties in handling other than linearised models of such flows have however limited theoretical developments: furthermore, the complexities of data acquisition and presentation and even the development of suitable parameters by which to describe these unsteady phenomena have severely hampered the experimentalist. Nevertheless, continued improvement to axial compressor performance, particularly in surge-margin and operating range, must include an improved understanding of unsteady effects.

For compressors operating near the surge line, the development of rotating stall cells appear to be a common or maybe universal (1, 2), precursor to complete breakdown of performance. This phenomenon consists of regions or cells of retarded flow moving around the annulus relative to the blades. Axial symmetry is destroyed, resulting in stalled blades in parts of the annulus and unstalled blades in the remainder. The stall cell moves in the direction against that of the rotor relative to the blades, but since the relative speed of propagation is usually less than the rotor speed, the cell is seen to move in the same direction as the rotor in an absolute frame of reference.

The presence of the stall cells results in a deterioration of compressor performance since the maximum pressure ratio is not achieved in regions of retarded flow. Furthermore, since this self-induced distortion is periodic, the forced frequencies generated may coincide with the natural harmonics of the blading, tending to cause structural damage.

The effects of non-uniform inlet conditions and the development of rotating stall are clearly not unrelated; one results from an external influence upstream of the stage, the other can be generated within the blade row, but both result in non-axisymmetric and therefore unsteady flow conditions within rotor rows. The distortions may be from one to many blade passages in circumferential extent and therefore have associated frequencies of the order of the rotor rotating speed. These are of course, much lower than the blade passage frequencies encountered when considering blade wake effects.

This Paper describes a series of experiments in which a fully instrumented axial compressor was tested over a wide range of operating conditions. Not only was the compressor overall performance obtained, but the distribution of static pressure along the rotor blade surfaces was measured with high response instrumentation. Data were obtained both for undistorted and distorted inlet flows, the latter being generated by uniform porosity screens of various circumferential extent mounted at the compressor inlet.

Of particular interest was the development of rotating stall cells when the compressor operated near the stability limit line. The on-rotor pressure measurements showed very clearly the formation of these cells, whose development, circumferential extent and speed of rotation were found to be significantly affected by the nature of the upstream flow.

THE EXPERIMENTAL FACILITY

The test rig (fig 1) was a lightly-loaded, single stage axial compressor, having constant annulus cross-section measuring 25.4 cm diameter at the hub and 50.8 cm. at the tip. All blades were built up from C4 sections. A variable-speed, 5hp motor drove the compressor at speeds up to a maximum of 1500 rpm. The mass flow was controlled by a throttle-valve situated at the tailpipe exit.

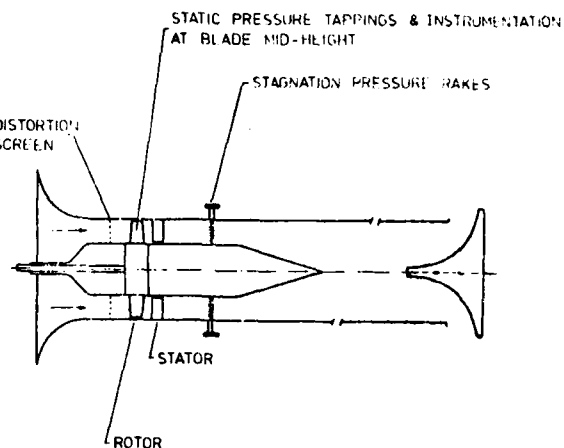


FIG 1 THE SINGLE STAGE COMPRESSOR RIG

The rig was fitted with the usual instrumentation required to evaluate overall compressor performance. Inner and outer wall static tappings were positioned ahead of and behind every blade row, and the downstream stagnation pressures were measured by four rakes disposed orthogonally, each having nine shrouded pitot heads. All pressure readings were taken from inclined multiple manometer banks. Hot wire anemometer measurements were taken with the probe situated in the compressor inlet, providing both mean and turbulence velocities for a selected number of operating conditions.

The compressor pressure ratio was calculated from the total pressure measured downstream of the stage by the 36 stagnation pressure probes. Using the averaged value of static pressure from the inner and outer wall tappings downstream of the stage, together with the 36 stagnation pressure readings, the velocity distribution was obtained radially. Area weighted integration of this distribution yielded the compressor mass flow.

The rotor speed was measured by mounting a 60 tooth gear wheel on the drive shaft. An inductive pick-up sensed the passage of each tooth and the number counted over a period of one second was displayed on a frequency meter (yielding speed in rev/min directly).

Two rotor blades were instrumented at blade mid-height (bmh), one with eight static pressure tappings on the pressure surface, and the other with eight tappings on the suction surface. A high-frequency response transducer (70 kHz) was mounted

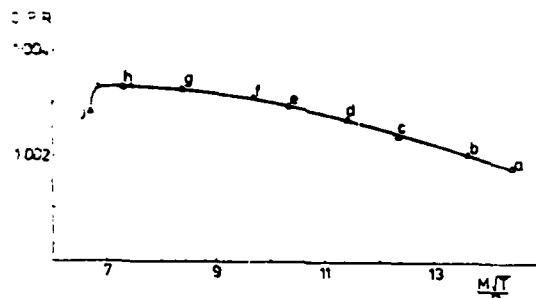


FIG. 2 UNDISTURBED COMPRESSOR CHARACTERISTIC - 1250 rev/min.

at bmh for each tapping. The pressure was fed from the blade surface to the transducer volume within the blade via a 0.038 cm diameter transfer tube (maximum length of 0.152 cm). The transducers had a miniature silicon diaphragm (0.318 cm) on which a full Wheatstone bridge network was diffused. The electrical output wires were routed down through the blade root to a remotely-controlled switching circuit mounted on the rotor disc. The signals were then taken from the rotating rig via a precision slipring assembly (noise < 5µV/mA) to an external switch control device and finally to amplification/recording equipment.

The entire pick-up and recording system had a frequency response in excess of 1000 Hz, sufficiently high to handle all frequencies encountered.

A yawmeter was located one-half chord upstream of the rotor, permitting calculation of the upstream static pressure and inlet relative velocity.

The blade surface pressure distribution data were evaluated in the usual pressure coefficient (C_p) form, where:-

$$C_p = \frac{p - p_1}{\frac{1}{2} \rho W_1^2}$$

In the case of the unsteady experiments, where only time averaged values of p_1 and V_1 were known, a new pressure coefficient C^* was utilized, where:-

$$C^* = \frac{p - p_0}{\frac{1}{2} \rho W_1^2}$$

p_0 is the static pressure measured at the same blade tapping at the same flow conditions in steady flow and the denominator represents the time-averaged dynamic pressure as seen by the rotor. Thus C^* represents the change in the blade surface static pressure distribution resulting from the presence of the rotating stall and/or inlet flow distortion.

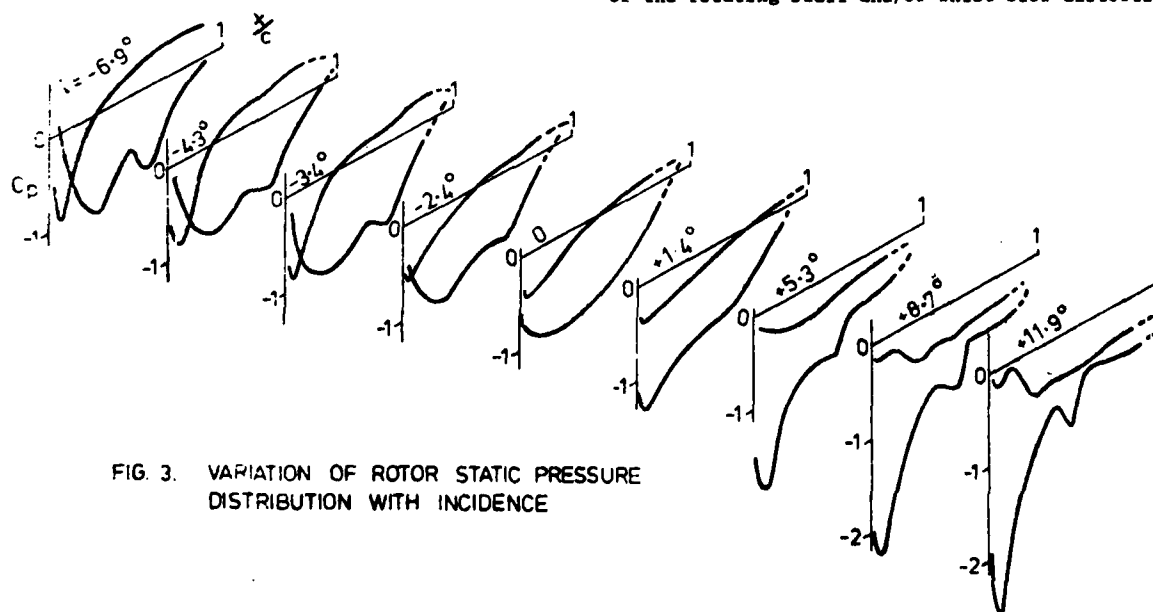


FIG. 3. VARIATION OF ROTOR STATIC PRESSURE DISTRIBUTION WITH INCIDENCE

The system was designed so that any eight transducers could be recorded simultaneously. This was wired for four channels (combinations) of eight transducers. Selection of channel A connected the eight pressure surface transducers to eight galvanometers in an ultraviolet recorder. The other three channels were: B) 8 suction; C) 4 leading edge (LE) suction and 4 LE pressure; D) 4 trailing edge (TE) suction and 4 TE pressure tappings. Channels C and D were included to permit time-matching of suction and pressure surface measurements (taken from different blades) during unsteady flow.

EXPERIMENTAL RESULTS IN UNDISTORTED INLET FLOW

Unstalled Flow

The experimental compressor performance map is shown in fig 2. Data are shown for ten operating points at a constant rotational speed of 1250 rev/min. Measured rotor blade surface pressure distributions are plotted in fig 3 for the nine stalled operating conditions (a - i) of fig 2.

While at the higher and lower incidences these data show unexpected excursions, they are in good agreement with other data near the design incidence. Fig. 4 shows a comparison between the present results and those reported in (1) and (4) for similar blades operating at similar incidences and Reynolds' numbers for rotor and cascade respectively. Fig. 5 shows a comparison between the present and experimental data and those calculated by the analytical method of Martensen (5). In all cases the agreement is good. It may be observed that the ripple in the convex surface measured by Rhoden (4) and followed by the data reported here, was ascribed to the presence of a laminar separation bubble, a phenomenon which, in any case, could not be predicted by the inviscid model of Martensen (5).

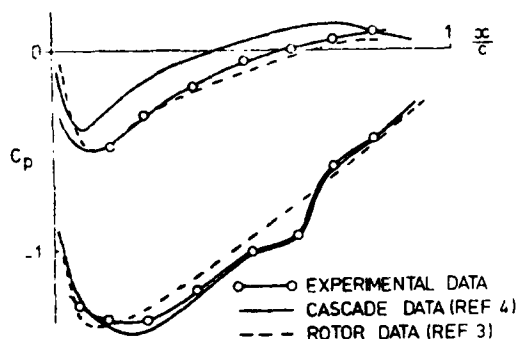


FIG 4 COMPARISON OF DATA WITH OTHER EXPERIMENTS

Rotating Stall

Further reduction of the compressor mass flow from point i of fig 2 to point j led to the inception of rotating stall in the rotor. Fig. 6 shows the variation of rotor blade pressure surface static pressure as a function of circumferential location at a constant flow condition indicated by point j (fig 2). Data are given for seven chordal locations, with tapping 1 being nearest the leading edge. Rotor movement was in the direction of increasing θ .

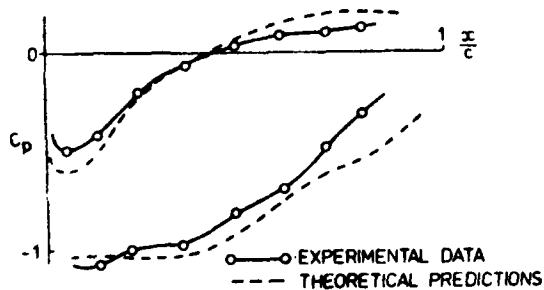


FIG 5 COMPARISON OF DATA WITH THEORY

Examination of fig 6 reveals that at a given tapping, the pressure pattern repeated itself approximately every 540° of absolute rotor rotation and thus the stall pattern moved in the same direction as the rotor at one-third its rotational

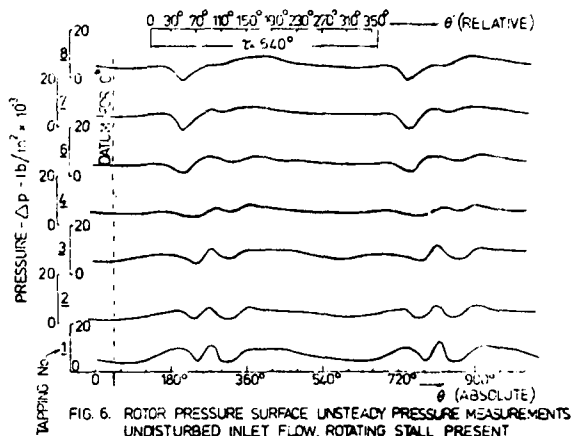


FIG. 6. ROTOR PRESSURE SURFACE UNSTEADY PRESSURE MEASUREMENTS

speed when viewed in the absolute frame of reference. Relative to the rotor however, the stall pattern moved in the opposite direction at roughly two-thirds the rotor rotational speed.

It may also be seen from fig 6 that the rotating stall cell first appeared at the rearmost portion of the rotor blade and moved upstream requiring about 20° of relative rotation (i.e. three blade passages) to reach the leading edge and become fully established. The cell occupied roughly 20 per cent of the circumferential extent to the annulus.

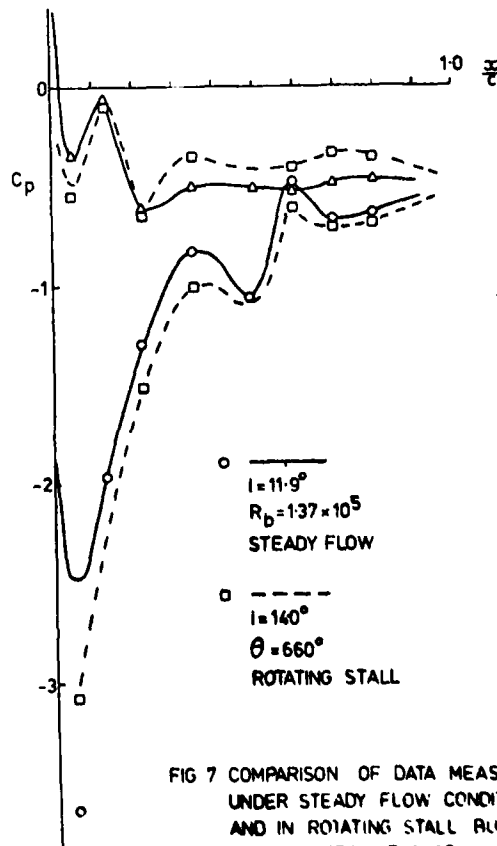


FIG 7 COMPARISON OF DATA MEASURED UNDER STEADY FLOW CONDITIONS AND IN ROTATING STALL BUT REMOTE FROM THE STALL CELL

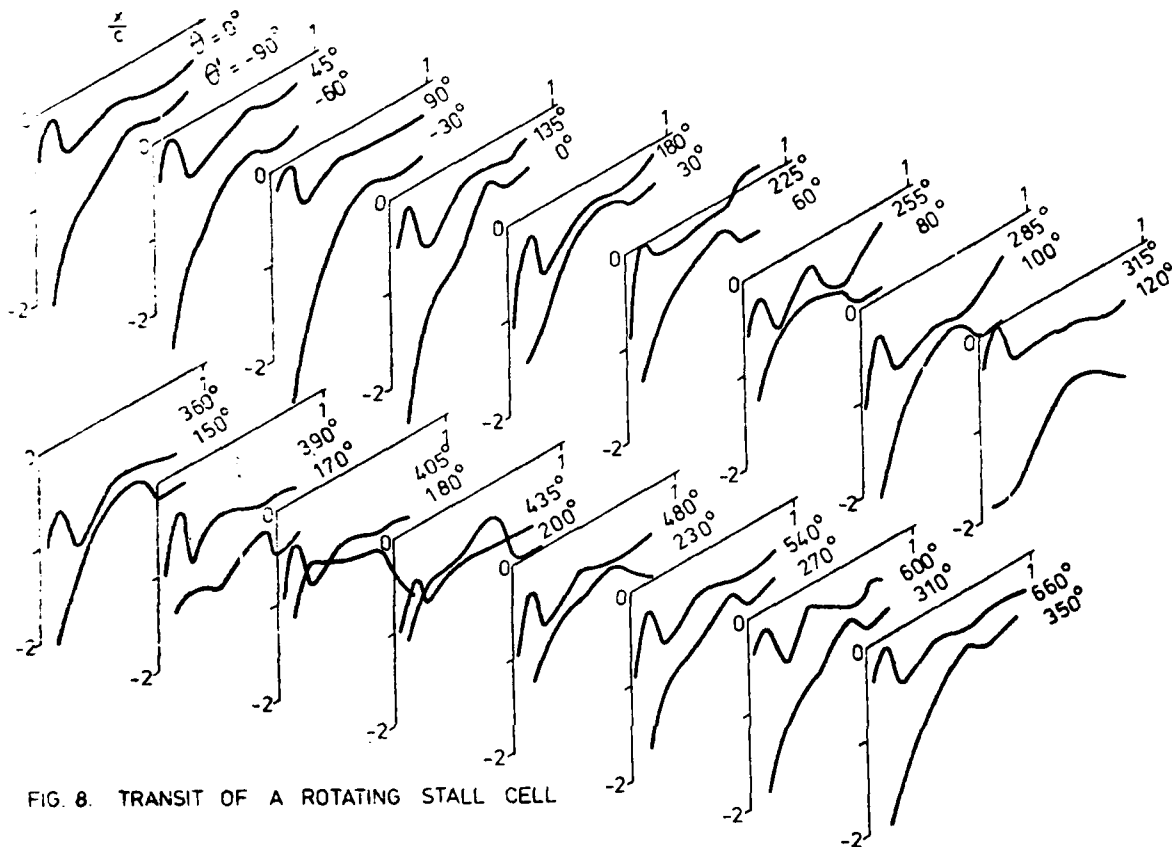


FIG. 8. TRANSIT OF A ROTATING STALL CELL

The data of fig 6 are replotted in the form of pressure coefficient and chordal dimension in fig 7 and 8. Fig 7 shows a comparison of the results obtained in the unstalled flow ($i = 11.9^\circ$) with those for flow with rotating stall at a point circumferentially remote from the stall cell ($\delta = 660^\circ$). The incidence at the latter condition was approximately 14° . Given the modest difference in incidence, the two results are in excellent agreement, showing that the flow had adequate opportunity to re-establish its steady state flow pattern between successive passages of the stall (a key assumption in the parallel compressor model of the rotating stall flow). Fig 8 shows the measured rotor pressure coefficient for a number of azimuthal positions (the reference position for θ and θ' are shown in fig 6). It is clear that at $\theta = 180^\circ$ a significant pressure distribution change had been experienced by the suction surface and the leading edge region of the pressure surface. By the time the rotor had moved to $\theta = 225^\circ$ both surfaces experienced gross changes in pressure distribution. Not until the rotor had rotated nearly a full revolution (to $\theta = 540^\circ$) was the flow fully re-established.

To illustrate more clearly the effect of the rotating stall cell on blade element performance fig 9 shows a plot of C^* v chord. The reference state

for p_0 and hence C^* was the pressure distribution obtained at $\theta = 45^\circ$, a condition sufficiently removed from the stall cell that 'clear flow' prevailed. Absolute values of C^* are not particularly meaningful in view of the averaging required in computing the denominator, but shifts from the zero reference are a qualitative measure of change in blade surface pressure distribution as a result of the pressure of rotating stall. As was observed by Day (6), the rotating stall cell is a highly active region of flow; and this is supported by these data; the rapid changes of surface pressure in the region of $\theta = 405^\circ$ are evidence that reversed flow existed in the blade passage.

EXPERIMENTAL RESULTS IN DISTORTED FLOW

Unstalled Flow

To assess the effects of inlet distortion on the blade pressure distributions a 90° squarewave distortion was generated by positioning a uniform low porosity wire-mesh screen one-half diameter upstream of the stage. The resulting overall compressor characteristic is shown in fig 10 superimposed for comparison upon the undistorted flow characteristic. The movement of the stability line, yielding a surge-margin reduction for an operational compressor, is evident.

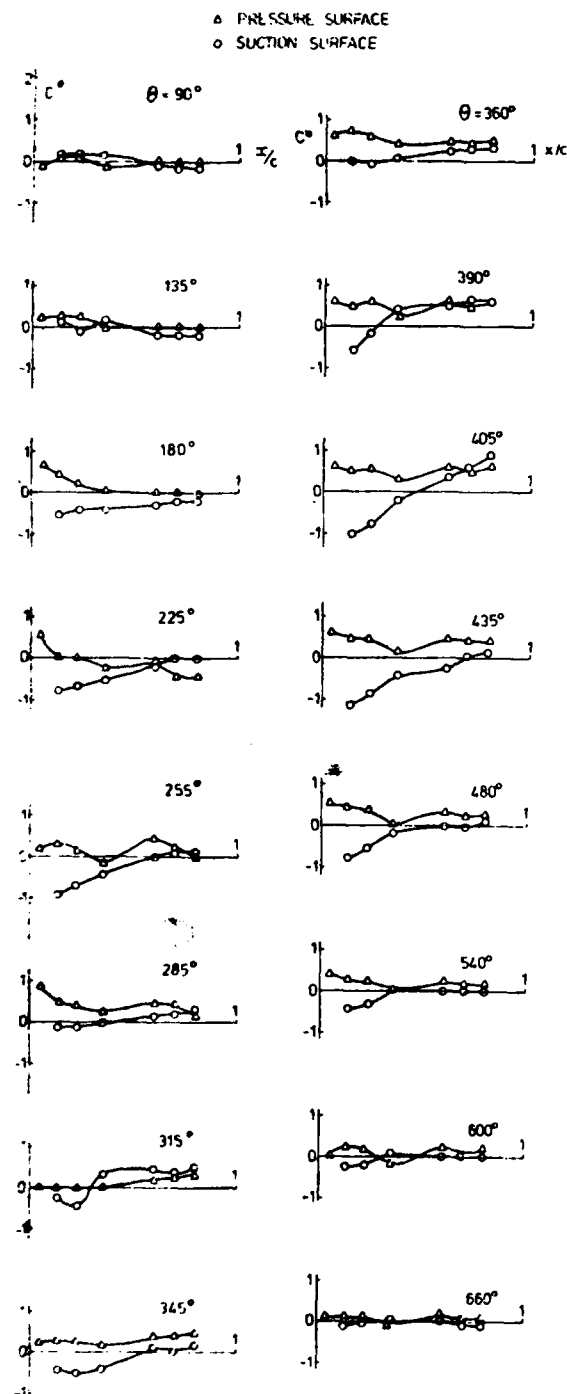


FIG 9 EFFECT OF ROTATING STALL ON THE UNSTEADY PRESSURE COEFFICIENT C^*

The associated variation of stagnation and static pressure upstream of the stage is indicated in fig 11 for the operating points $q - v$ on the characteristic (fig 10). A discussion of the seemingly anomalous rise in static pressure upstream of the rotor as it emerged from the distortion region is given in (3). The corresponding circumferentially varying stagnation and static pressures downstream of the stage are presented in fig 12 for an operating point, v , close to the stability limit.

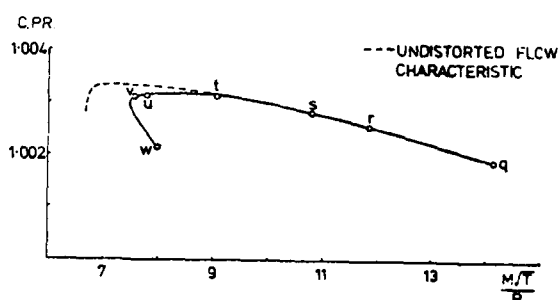


FIG. 10 DISTORTED FLOW COMPRESSOR CHARACTERISTIC
-1250 rev/min $\theta = 90^\circ$

An example of a typical rotor blade concave surface pressure distribution at the same operating condition is shown in fig 13. The blade clearly experienced a significant pressure disturbance every revolution, but the effect was generally limited to the forward portion of the passage. The effect of the distortion screen may be seen more clearly in fig 14 in which C^* is plotted as a function of blade chord for a number of tangential locations. In this instance C^* is a measure of the difference in static pressure between that at a given and that prevailing at a reference value of θ for comparatively undisturbed flow - in this case at $\theta = 150^\circ$. If the undistorted flow pressure distribution is taken to correspond roughly to that shown for $\theta = -90^\circ$, it is clear that major pressure changes began to take place some 30° before the rotor entered the shadow of the screen and persisted for at least 60° after it emerged from behind the screen. This observation is consistent with the spread in upstream static pressure (fig 11) and the corresponding downstream stagnation pressure distribution (fig 12).

Rotating Stall

Closure of the throttle to move the compressor operating point from v to w on fig 10 led into what, from instrument observation, may be described as a classic rotating stall mode. For example, fig 15 shows rotor blade concave surface pressure distributions as a function of θ . While superficially similar to those data found in the rotating stall case without inlet distortion screens (fig 6) several important differences may be observed. The period of the rotating stall cell cycle lengthened from 540° to 720° of rotor rotation, meaning that the cell was rotating at one-half the rotor speed relative to a stationary observer (c.f. one-third rotor speed in the case of undistorted inlet flow). Thus the cell was moving at $U/2$ relative to the rotor, compared with $2U/3$ for flow without a dis-

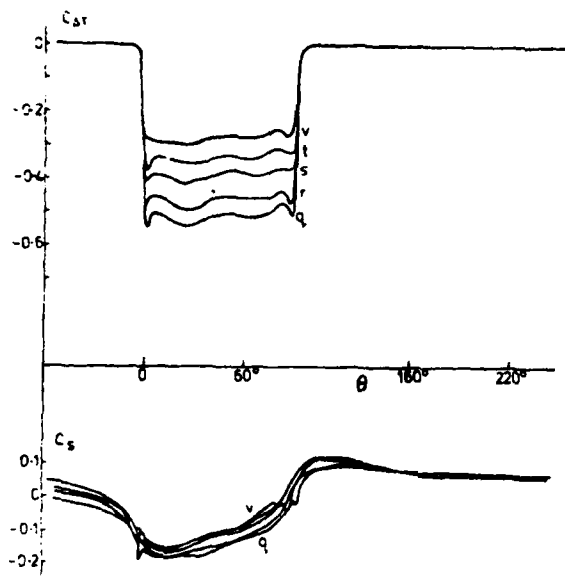


FIG 12 EFFECT OF COMPRESSOR OPERATING POINT UPON DISTORTION PROFILE - 1250 rev/min $\theta_0 = 90^\circ$

tortion screen. It is also clear that the pressure perturbation propagated from the leading to the trailing edge of the blade, unlike the distorted flow case (fig 6) in which the reverse was true. Furthermore, on alternate revolutions, when the instrumented blade passed through the screen shadow but the stall cell was diametrically opposite in the compressor annulus, only a minor perturbation

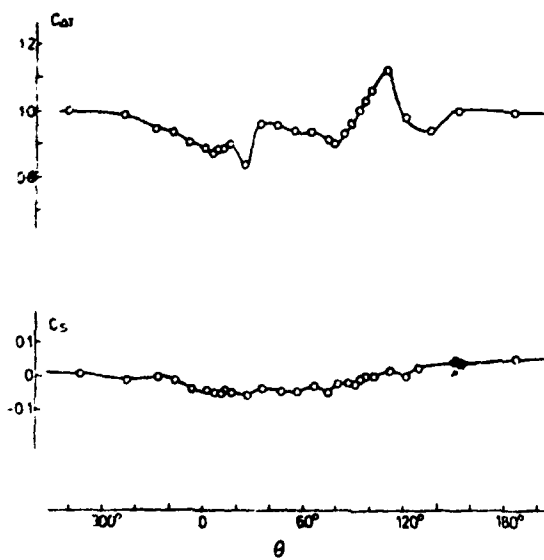


FIG 12 CIRCUMFERENTIAL PRESSURE VARIATION DOWNSTREAM OF COMPRESSOR - 1250 rev/min, POINT 'v', $\theta_0 = 90^\circ$

in static pressure was experienced at the forward three measuring stations. The remainder were unaffected.

The rotor blade surface pressure distributions were plotted in the form of $C^* v \frac{\partial}{\partial C}$ in fig 16 where the reference condition for C^* was taken at $\theta = 225^\circ$ (see fig 15). In the region $0^\circ < \theta < 75^\circ$, following the transit of the stall cell the flow was being re-established in the blade passage. For the range $75^\circ < \theta < 150^\circ$ the flow was apparently stabilized, the apparently unusual pressure distribution being a consequence of selecting $\theta = 225^\circ$ as the reference condition for C^* . For $150^\circ < \theta < 330^\circ$ the blade experienced modest pressure fluctuations as a result of passing through the distorted inlet flow, but major pressure excursions did not commence until $\theta = 630^\circ$. In the range $630^\circ < \theta < 780^\circ$ the rotor blade clearly experienced rapid changes in loading, characteristic of the transit of a rotating stall cell. Finally ($\theta > 810^\circ$) the flow was restored to the state which prevailed 720° earlier.

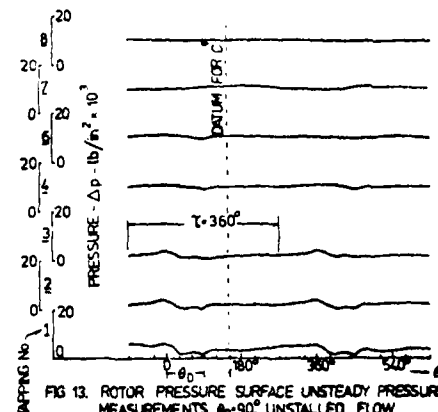


FIG 13. ROTOR PRESSURE SURFACE UNSTEADY PRESSURE MEASUREMENTS $\theta_0 = 90^\circ$ UNSTALLED FLOW

Other distortion screens of different circumferential coverage (15° to 120°) and varying porosity were investigated, but in no other instance was rotating stall observed. For example, a 15° screen of the same (low) porosity as that described above did not produce rotating stall.

DISCUSSION AND CONCLUSIONS

It would be inappropriate to draw general conclusions from the limited data presented in this paper. Our purpose, rather, is to present detailed blade element information for a lightly loaded compressor operating in two distinctly different regimes of rotating stall in the hope that current models of cell structure and behaviour may be reinforced by this addition to the body of experimental data.

The existence of two different stall regimes suggests that two different mechanisms of rotating stall initiation on the rotor are possible. In the undistorted flow case, the rotor blade surface pressure distributions indicate a disturbance moving forward in the blade row. This is not inconsistent with the observations of others (e.g. (6)

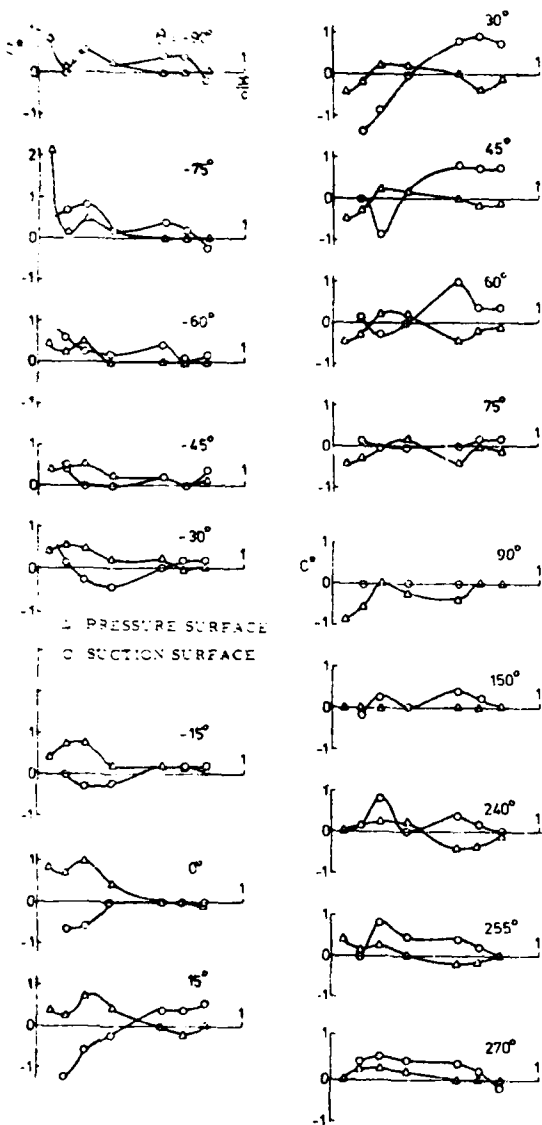


FIG 14 EFFECT OF DISTORTION ON THE UNSTEADY PRESSURE UNDISTORTED C^*

who, on the basis of observations made upstream and downstream of the blade row, concluded that reverse flow is possible. It further suggests the rotating stall cell has its origins in the stator and that the rotor is responding to a rotating downstream blockage. To check this, further experiments would be needed.

In the case of the distorted inlet flow, the stall cell is clearly rotor initiated. The perturbation resulting from passage of the stall cell is much greater than that caused solely by the distortion screen and in fact, once rotating stall is established, the unstalled portion of the annulus is virtually unaffected by the distortion. This latter observation lends support to the stall model of (1) in which it is suggested that the unstalled portion of the flow is operating well

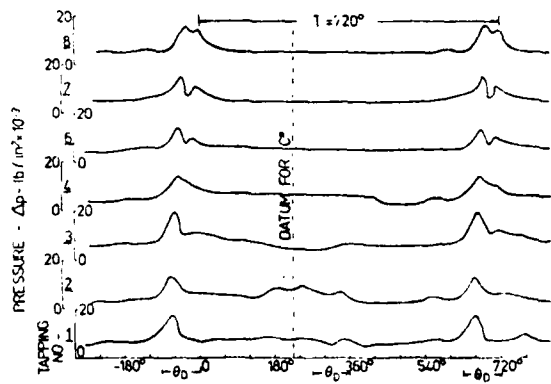


FIG 15 ROTOR PRESSURE SURFACE UNSTEADY PRESSURE MEASUREMENTS $\theta_0 = 90^\circ$ WITH ROTATING STALL

below the stall line on the operating curve; it is therefore comparatively immune to upstream perturbations. This flow, combined with the small mass flow rate passing through the stall cell, results in the mass-averaged performance given by the point w in fig 10.

The inception of rotating stall and the flow pattern within a stall cell and the mechanism controlling the flow pattern within the stall cell are not currently well understood. This presentation, with the detailed information on flow within the rotating blade row may have some value in improving knowledge in this complex flow situation, which is still a limitation in axial compressor performance.

ACKNOWLEDGEMENTS

The experimental phase of this work was carried out in the U.K. under the United States Air Force Research Grant AFOSR-77-3305. Analysis in Canada was supported by the Defence Research Board of Canada under grant number 3610-147. These sources of sponsorship are gratefully acknowledged.

REFERENCES

1. Greitzer E.M. 'Surge and rotating stall in axial flow compressors, Part I: Theoretical compression system model' Trans. ASME Journal of Engineering for Power, April 1976 Vol. 98, 190-198.
2. Greitzer E.M. 'Surge and rotating stall in axial flow compressors, Part II: Experimental results and comparison with theory' Trans. ASME Journal of Engineering for Power. April 1976 Vol 98, 199-211.
3. Peacock R.E. 'Dynamic internal flows in compressors with pressure maldistributed inlet conditions' AGARD-CP-177 46th P.E.P. Conference of AGARD Monterey, California September 1975.

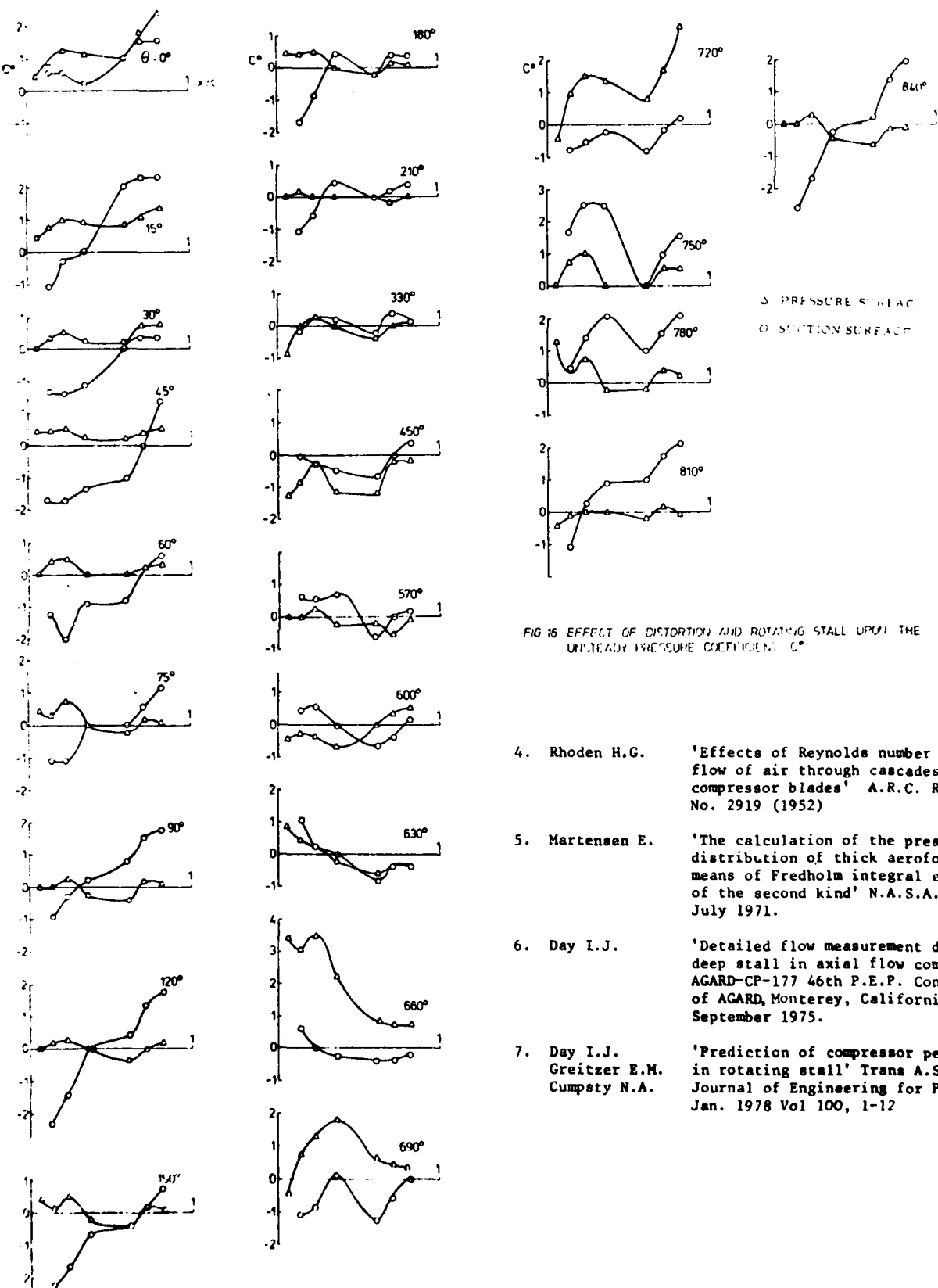


FIG 16 EFFECT OF DISTORTION AND ROTATING STALL UPON THE UNSTEADY PRESSURE COEFFICIENT C_p

4. Rhoden H.G. 'Effects of Reynolds number on the flow of air through cascades of compressor blades' A.R.C. R & M No. 2919 (1952)
5. Martensen E. 'The calculation of the pressure distribution of thick aerofoils by means of Fredholm integral equations of the second kind' N.A.S.A. TTF-70 July 1971.
6. Day I.J. 'Detailed flow measurement during deep stall in axial flow compressors' AGARD-CP-177 46th P.E.P. Conference of AGARD, Monterey, California September 1975.
7. Day I.J. Greitzer E.M. Cumpsty N.A. 'Prediction of compressor performance in rotating stall' Trans A.S.M.E. Journal of Engineering for Power. Jan. 1978 Vol 100, 1-12

SECTIONAL VIEW OF COMPRESSOR

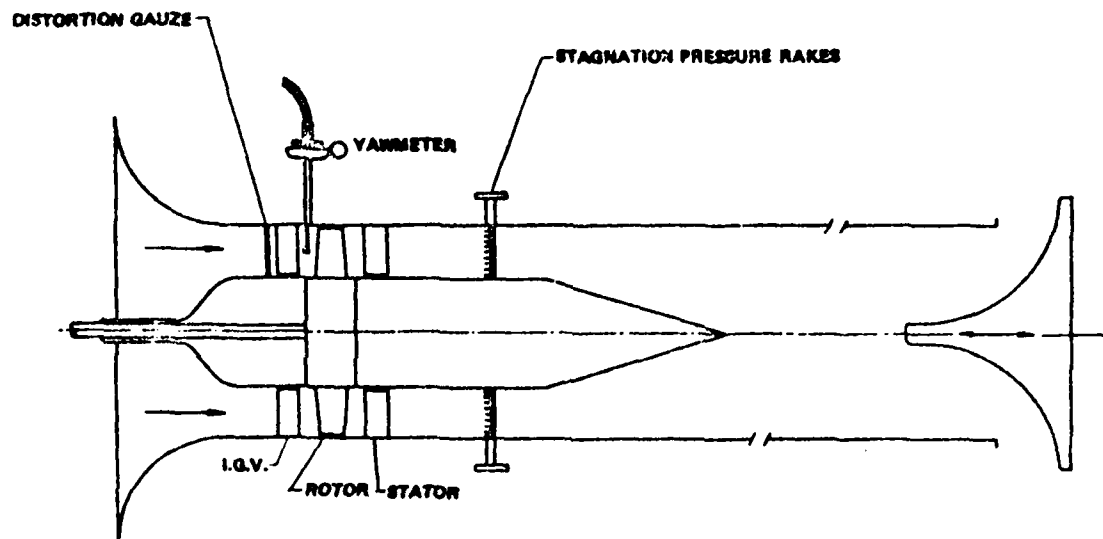


FIG. 2

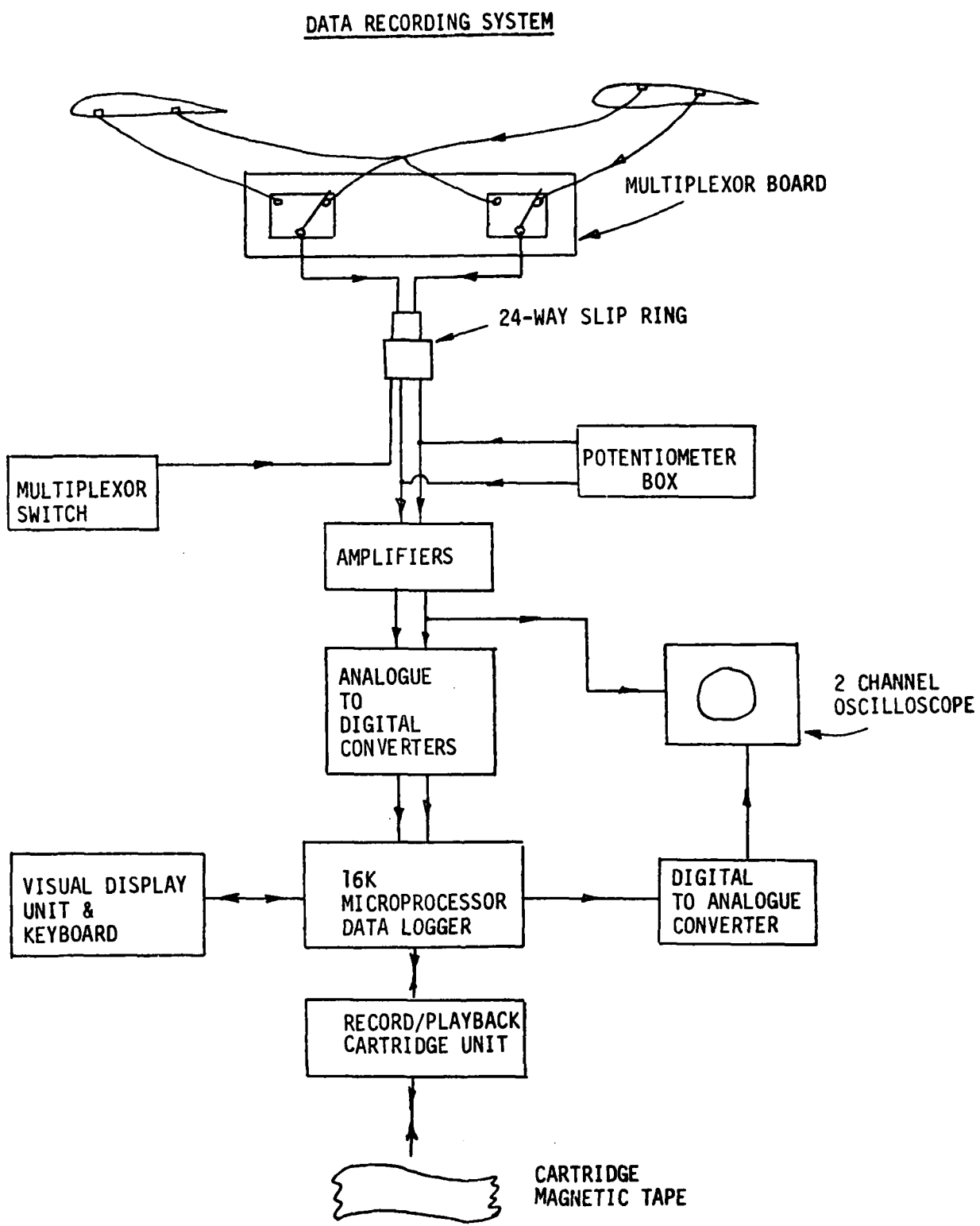


FIG. 3

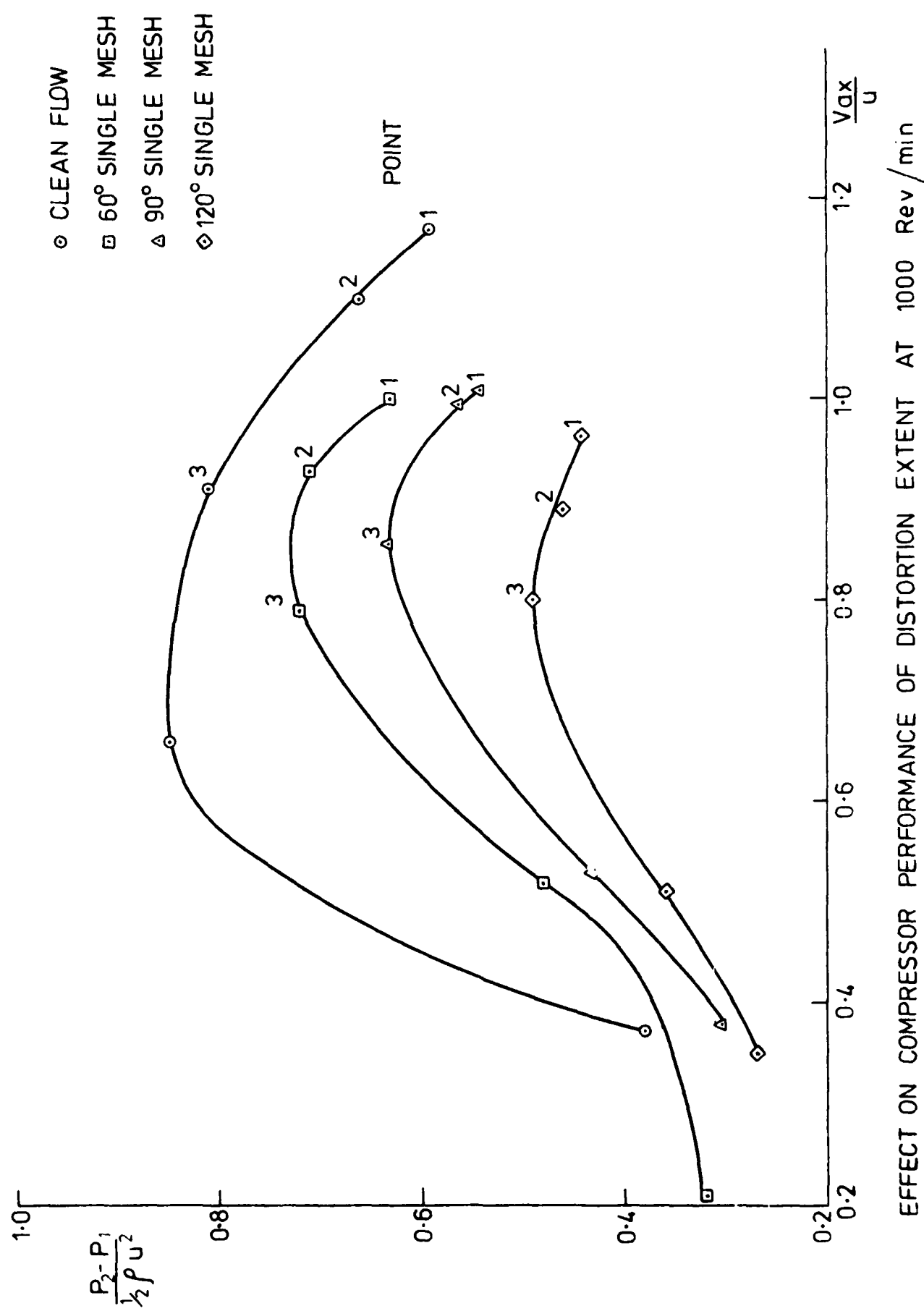


FIG. 4

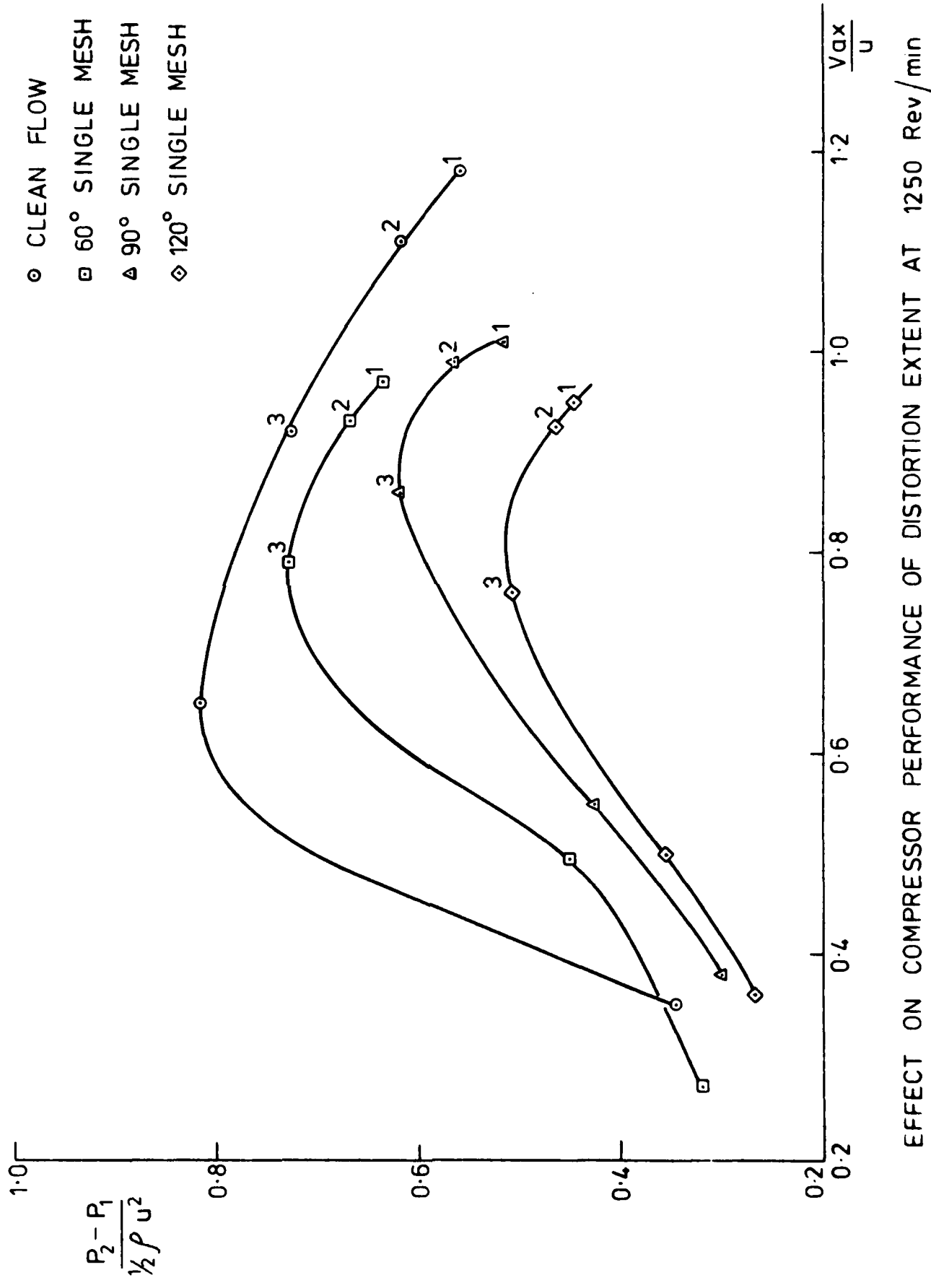


FIG. 5

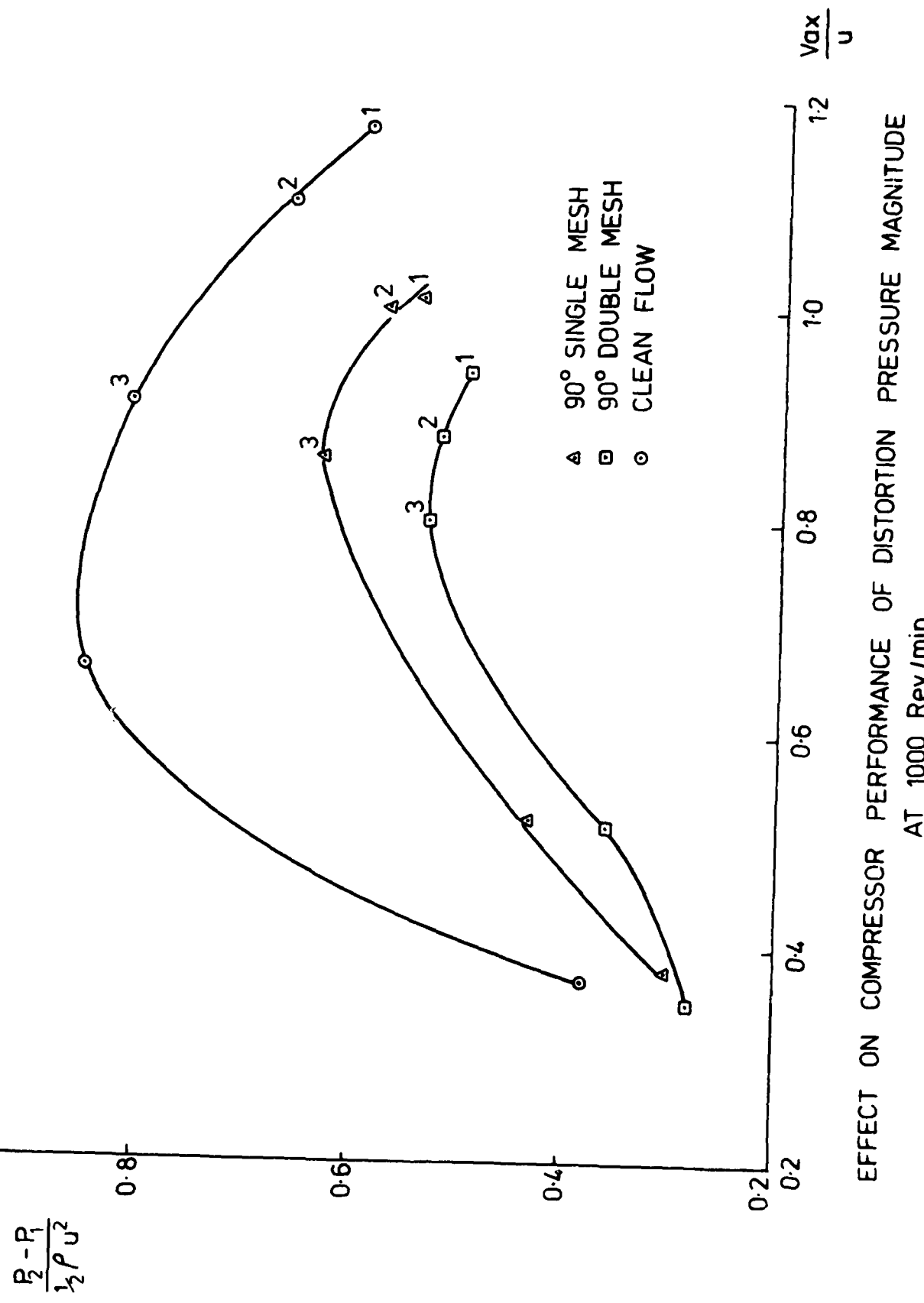
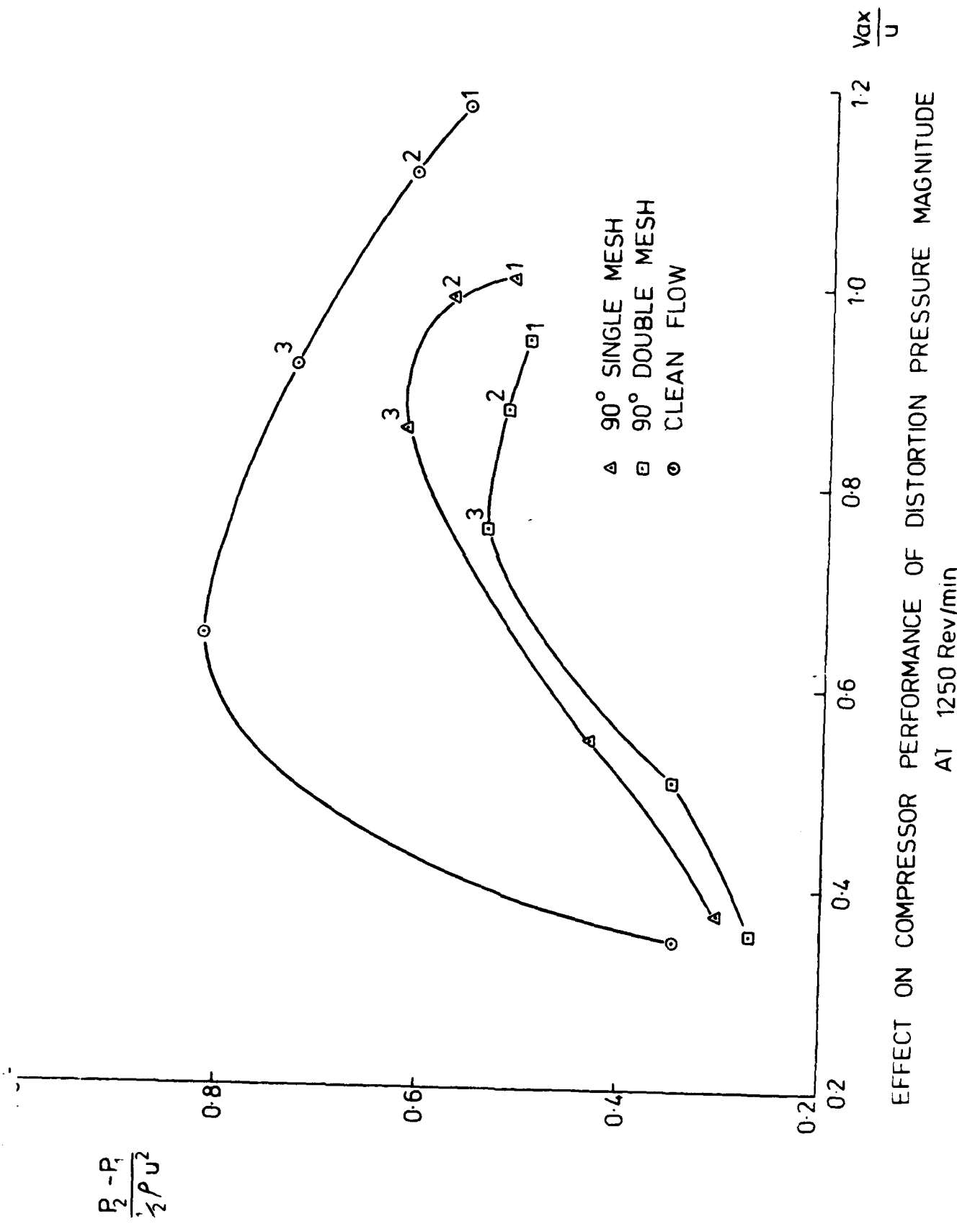


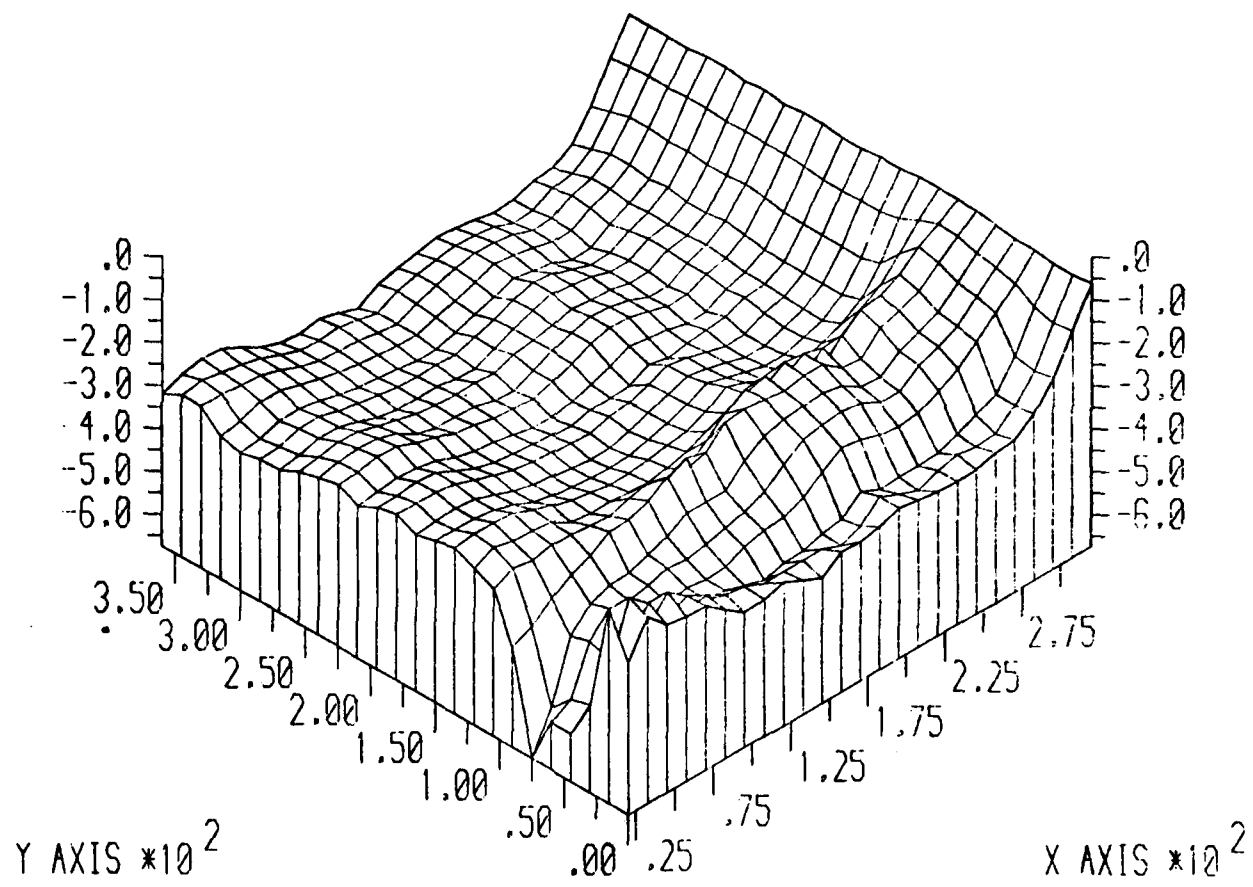
FIG. 6



2

GENERATED DISTORTION AND
ASSOCIATED RESPONSE DATA

FIG. 7a



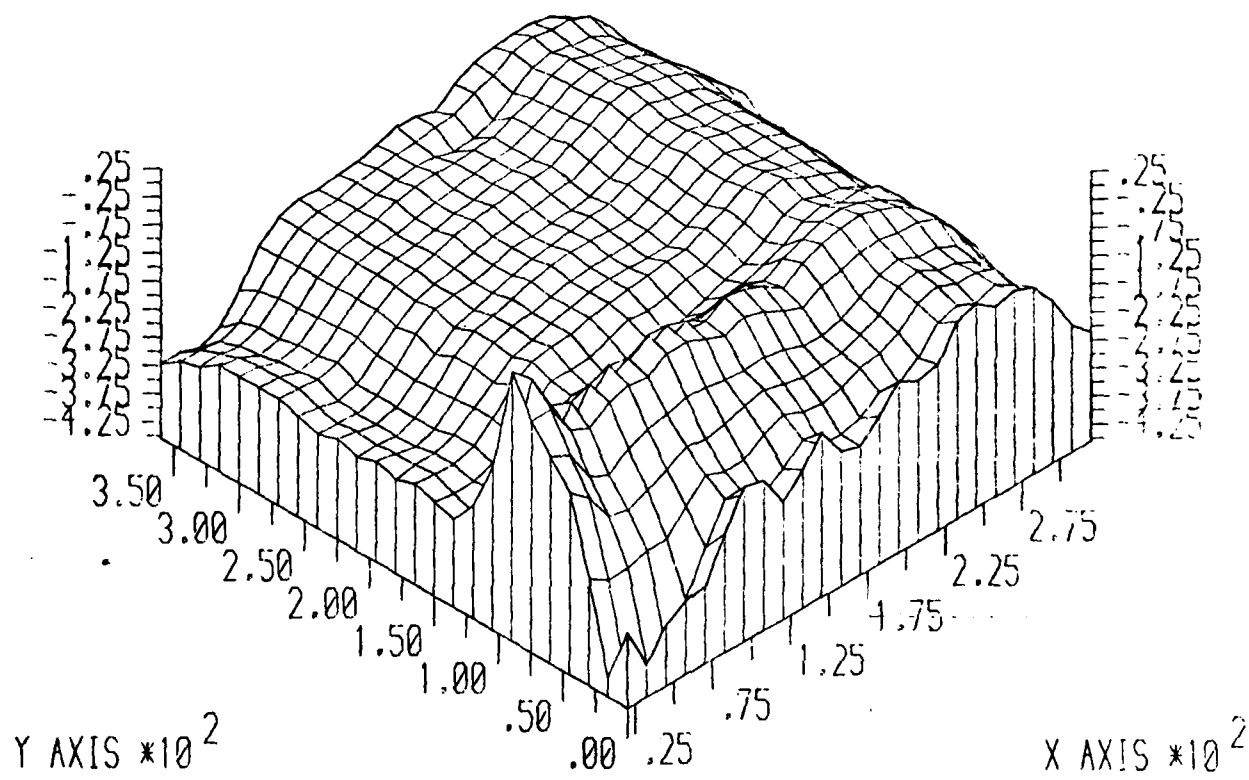
60° SQ.WAVE TEST @1000 RPM FLOW RATE NO=1

SUCTION SURFACE PRESSURE DISTRIBUTION

GDR7

02/09/90 00.15

FIG. 7b



60° SQ.WAVE TEST @1000 RPM FLOW RATE NO=1
PRESSURE SURFACE PRESSURE DISTRIBUTION

GDR7

02/09/80 00.17

FIG. 7c

ROTOR RESPONSE TO SQUARE WAVE SCREEN -- TEST 13

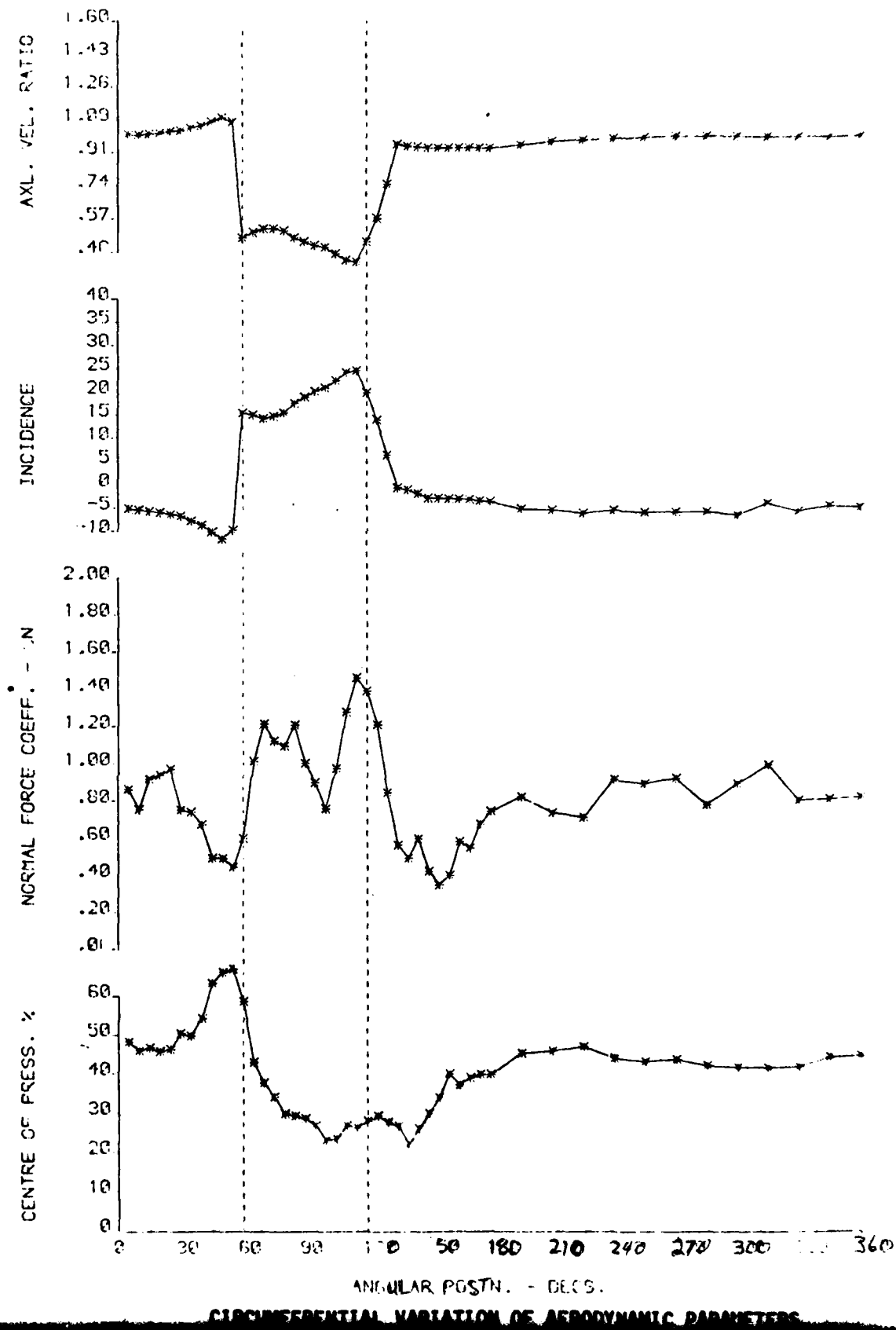


FIG. 7d

NORMAL FORCE VS. INCIDENCE --TEST 13

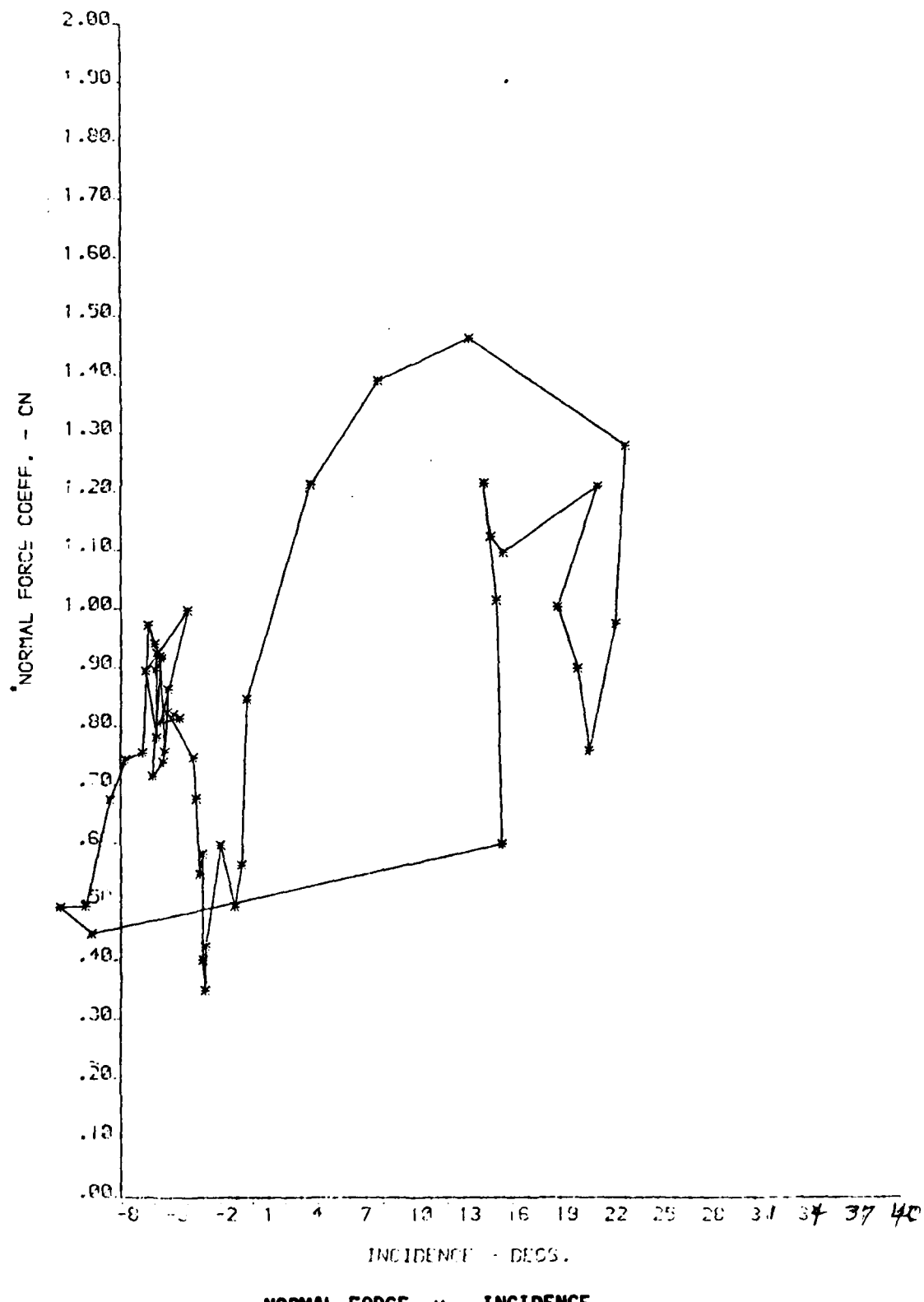
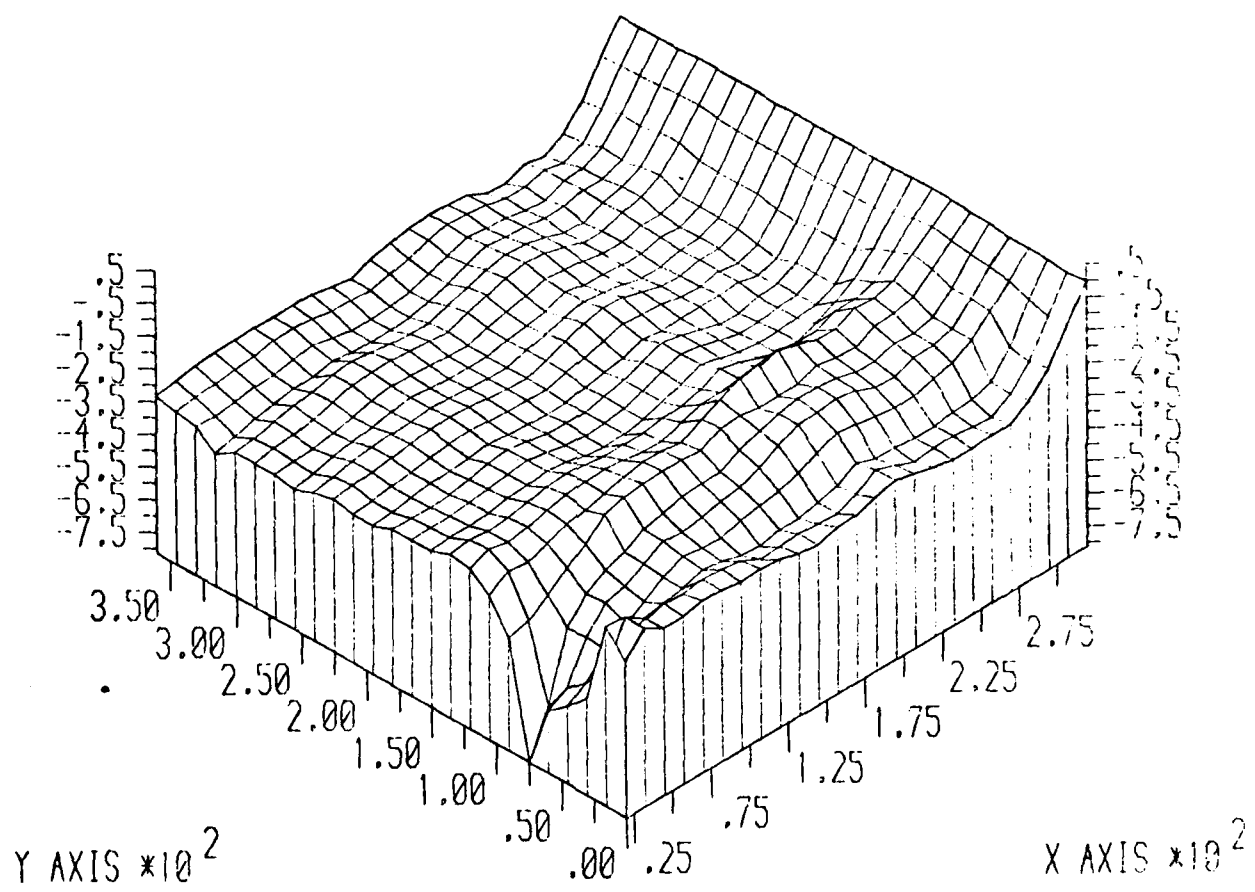


FIG. 8a



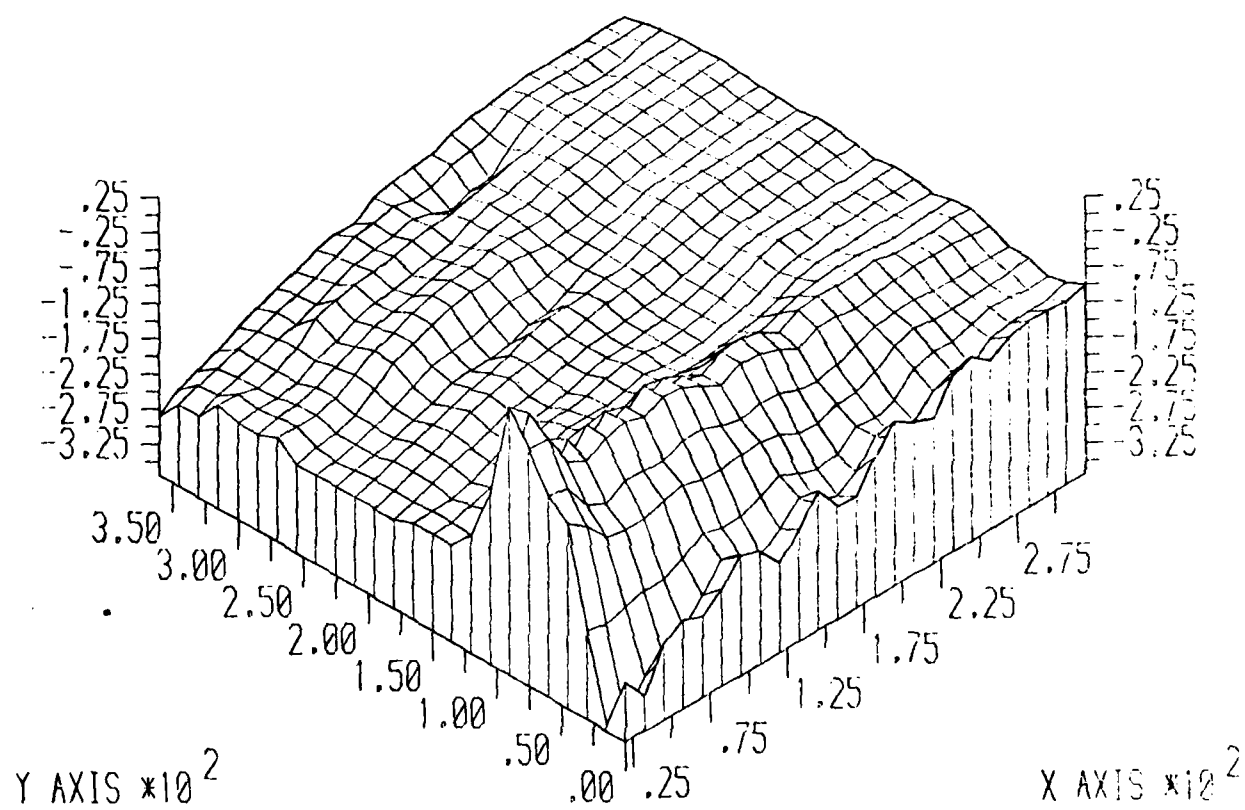
60° SQ. WAVE TEST @ 1000 RPM FLOW RATE NO-2

SUCTION SURFACE PRESSURE DISTRIBUTION

GDR7

13/08/80 18.13

FIG. 8b



60° SQ. WAVE TEST @ 1000 RPM FLOW RATE NO=2
PRESSURE SURFACE PRESSURE DISTRIBUTION

GDR7

13/08/80 18.16

FIG. 8c
ROTOR RESPONSE TO SQUARE WAVE SCREEN - TEST 14.

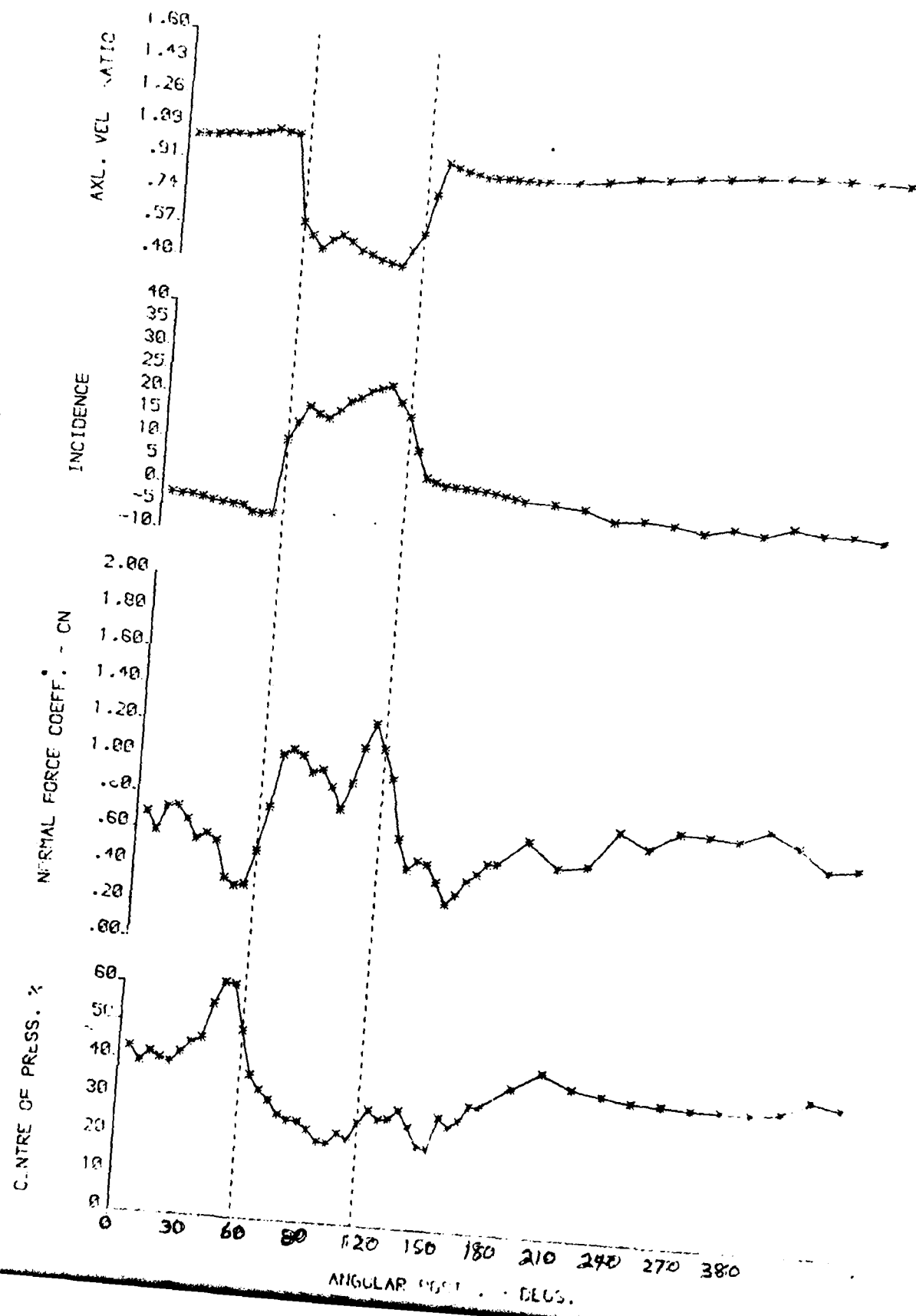


FIG. 8d

NORMAL FORCE VS. INCIDENCE --TEST 14

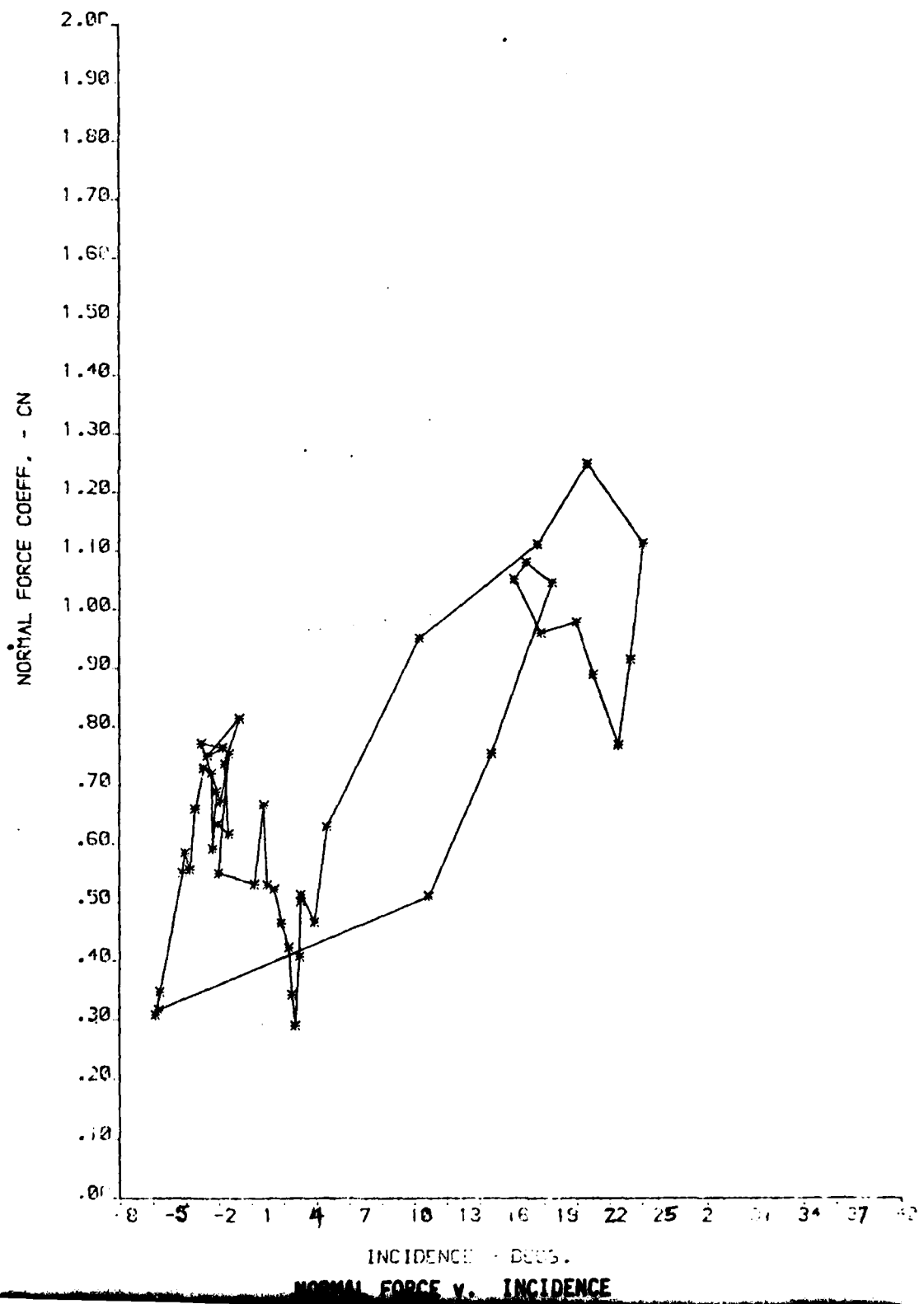
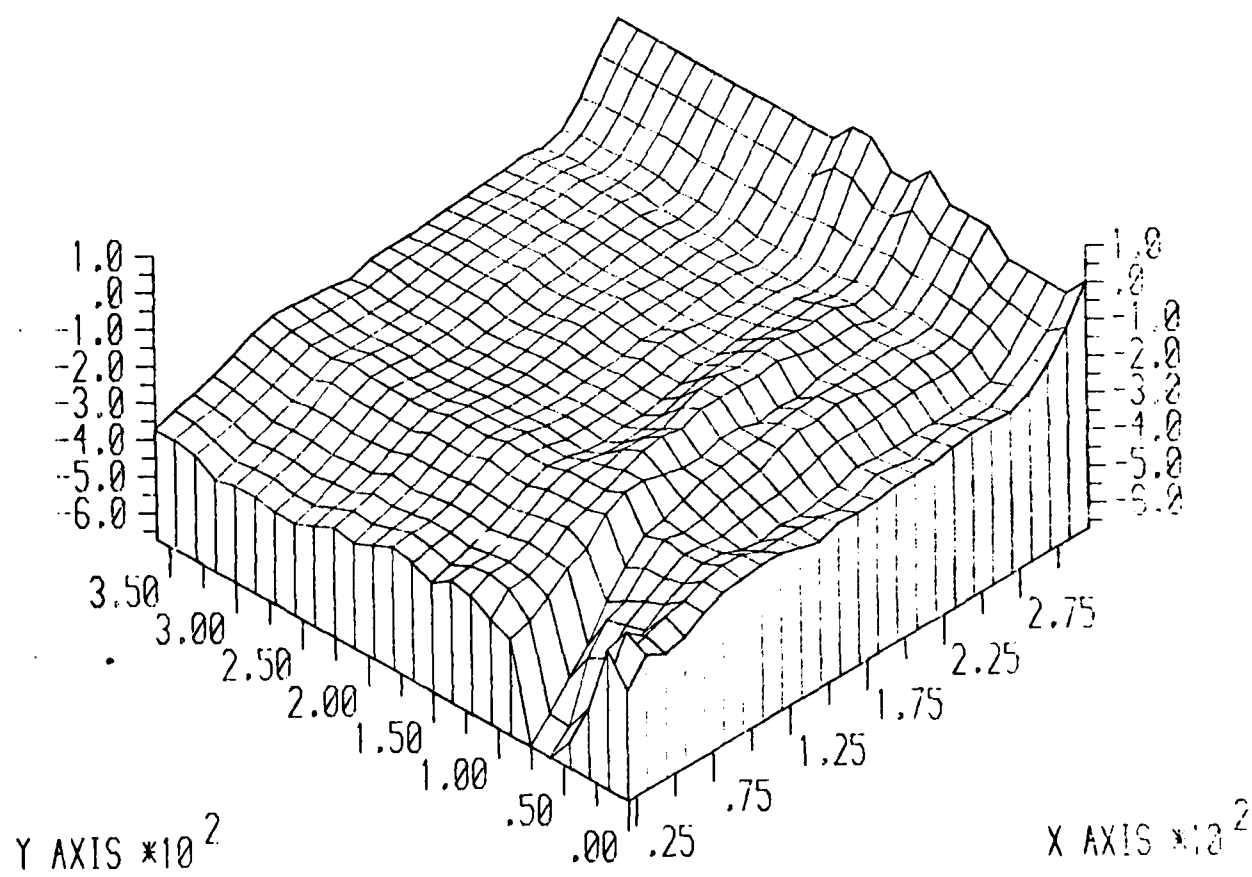


FIG. 9a



60° SQ. WAVE TEST @ 1000 RPM FLOW RATE NC=3

SUCTION SURFACE PRESSURE DISTRIBUTION

FIG. 9b

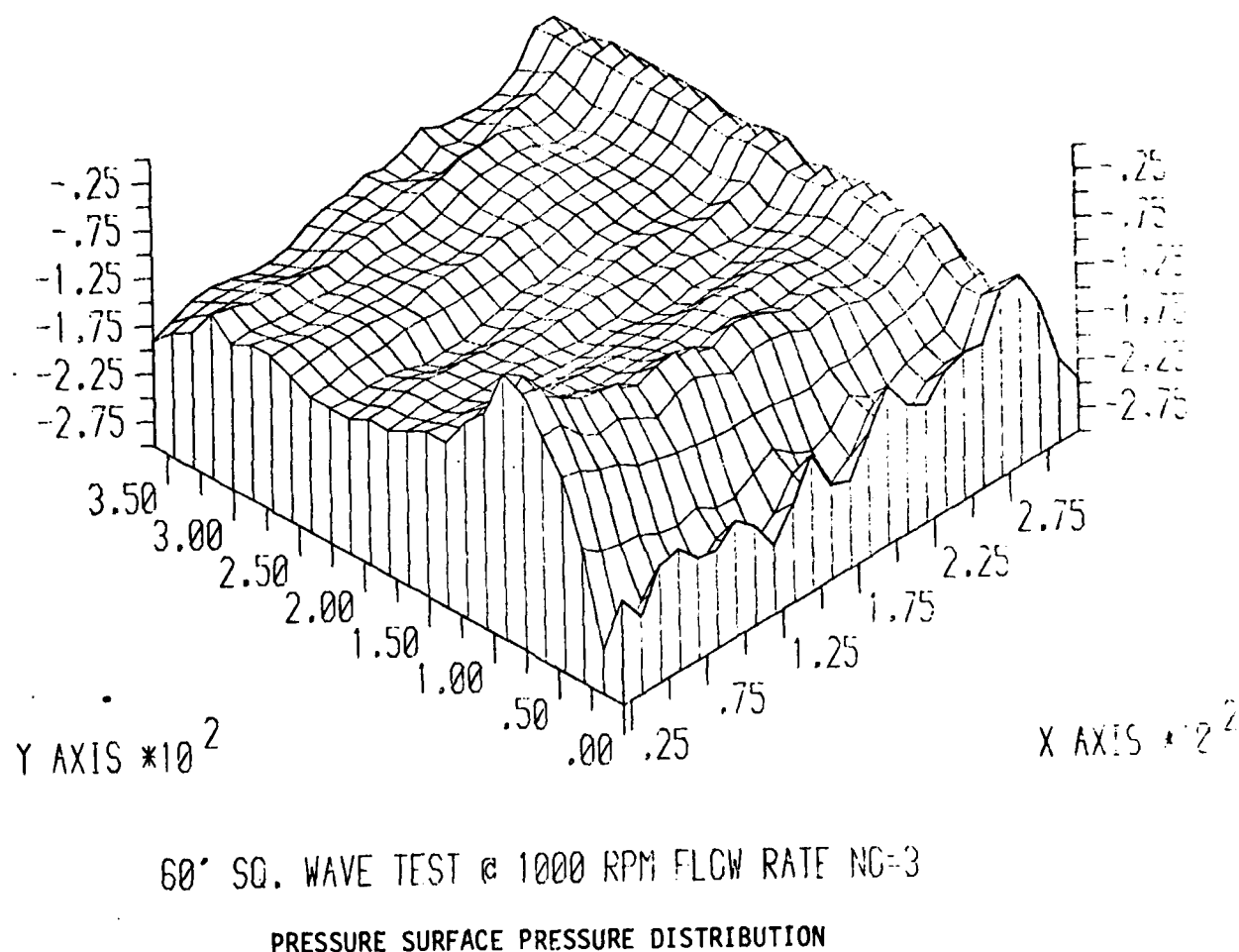


FIG. 9c

PILOT RESPONSE TO SQUARE WAVE SCREEN - TEST 15

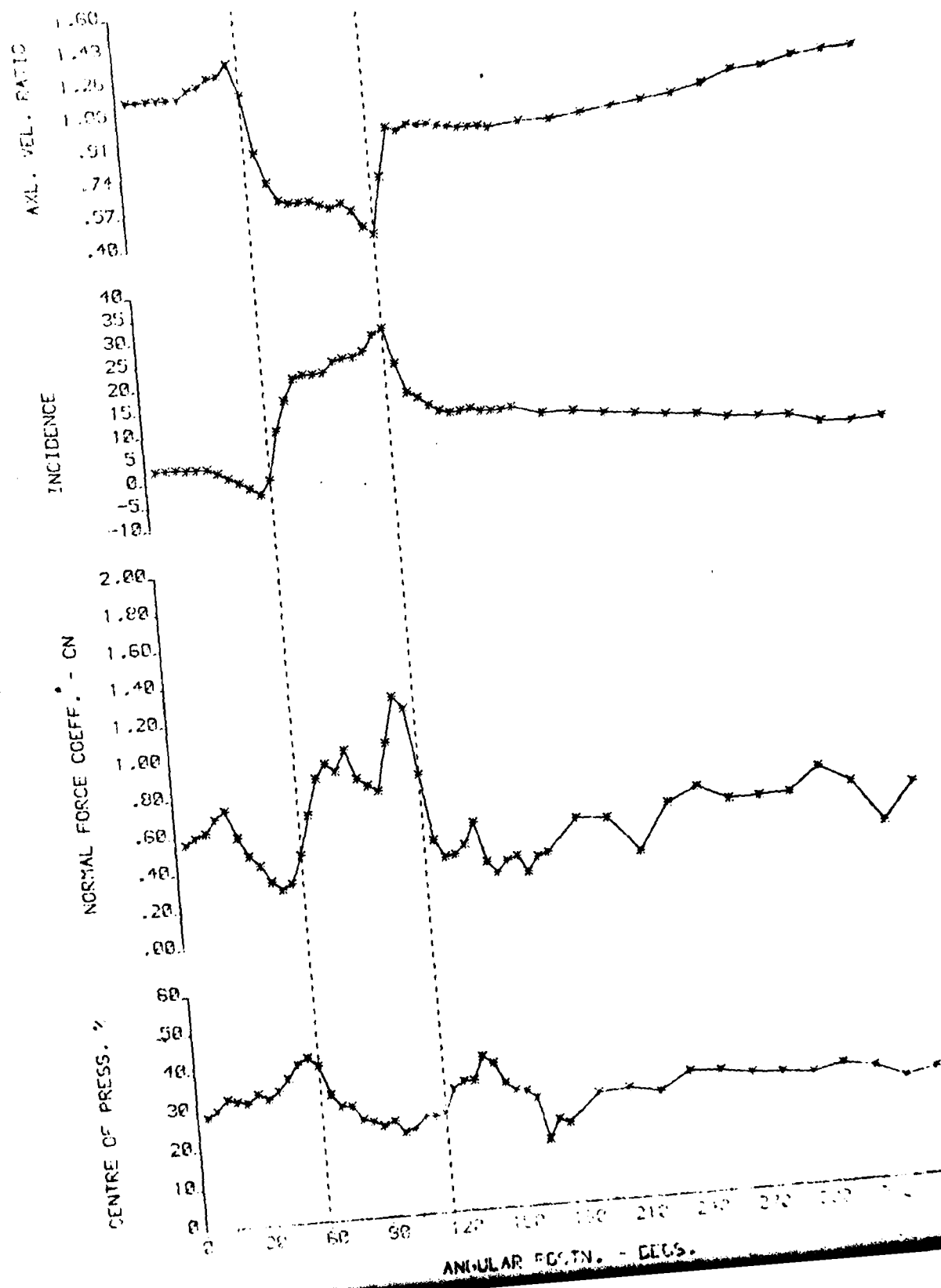


FIG. 9d

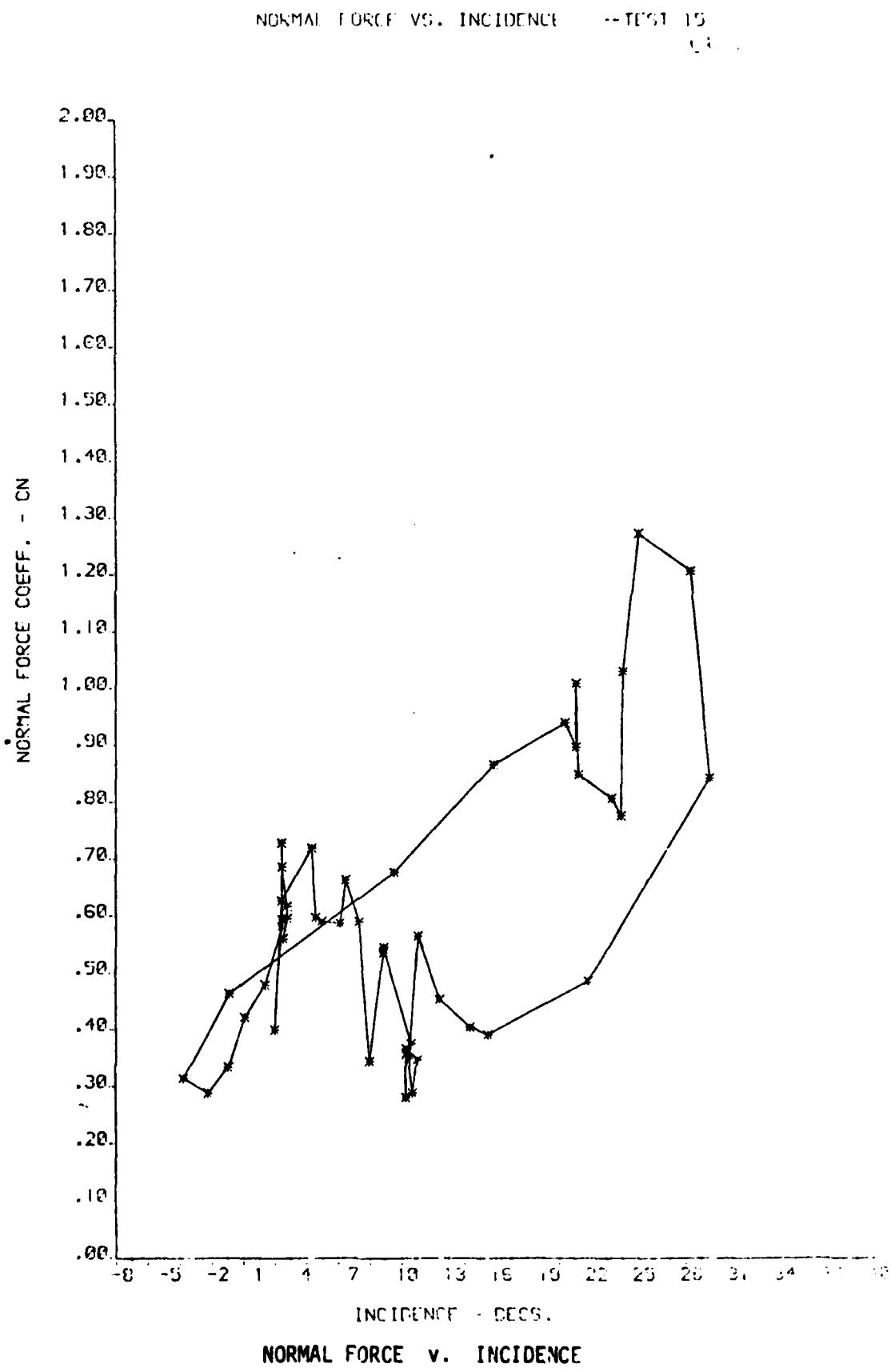
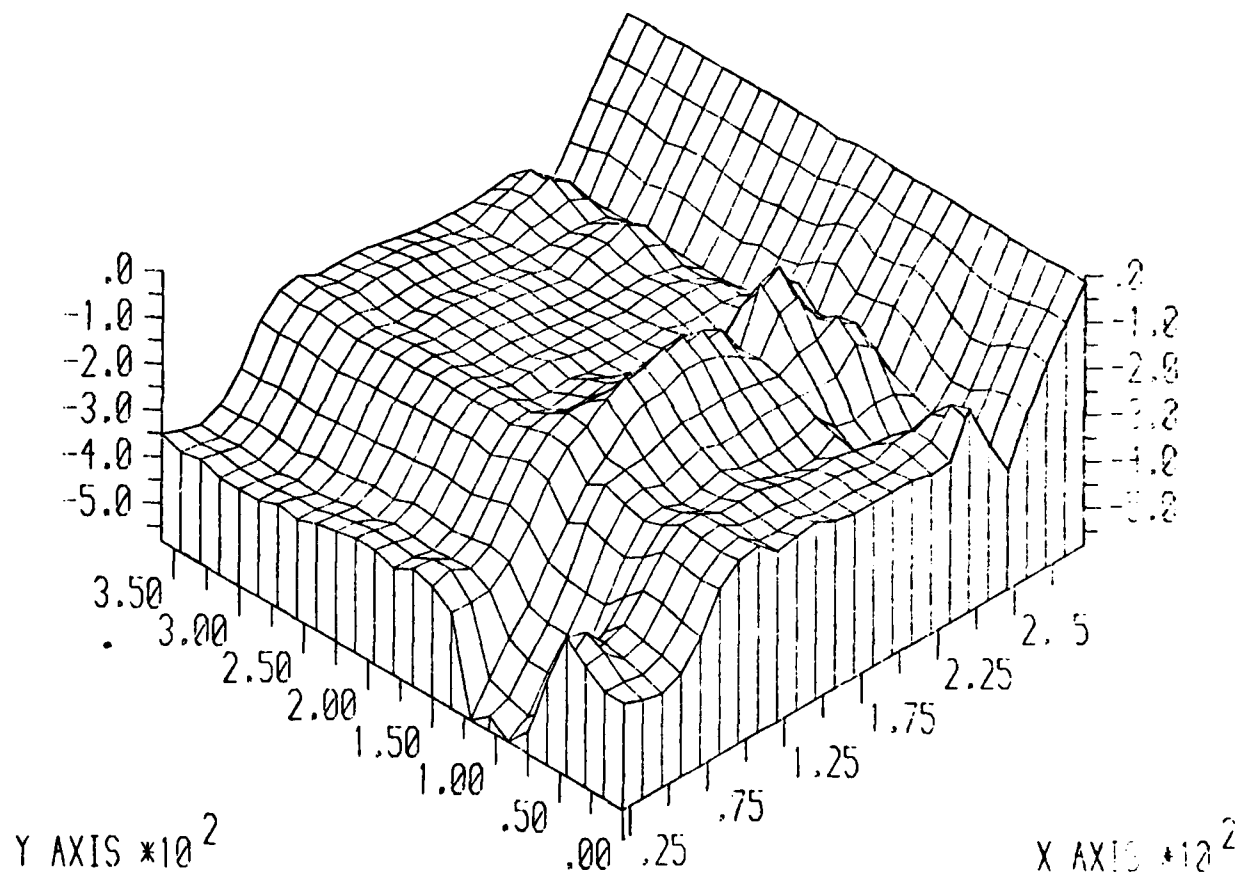


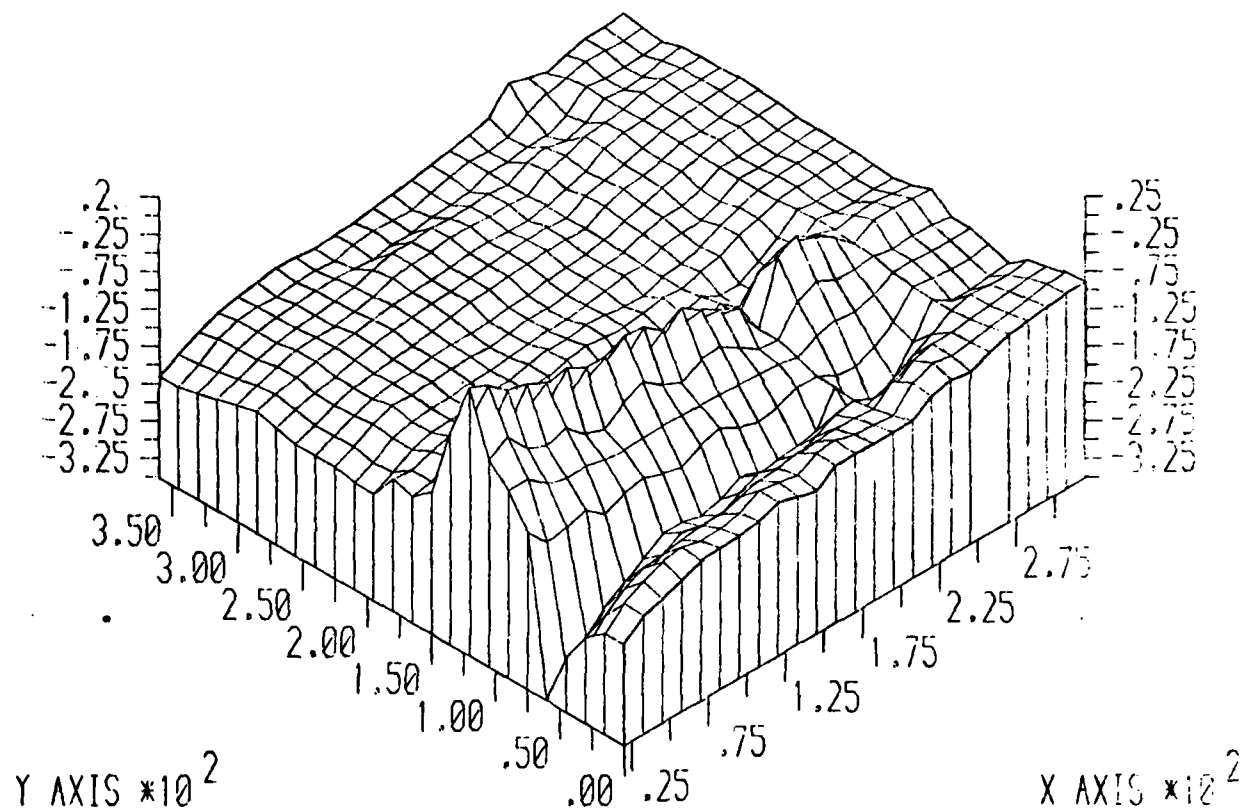
FIG. 10a



60' SQ. WAVE TEST @ 1250 RPM FLOW RATE NO. 1

SUCTION SURFACE PRESSURE DISTRIBUTION

FIG. 10b

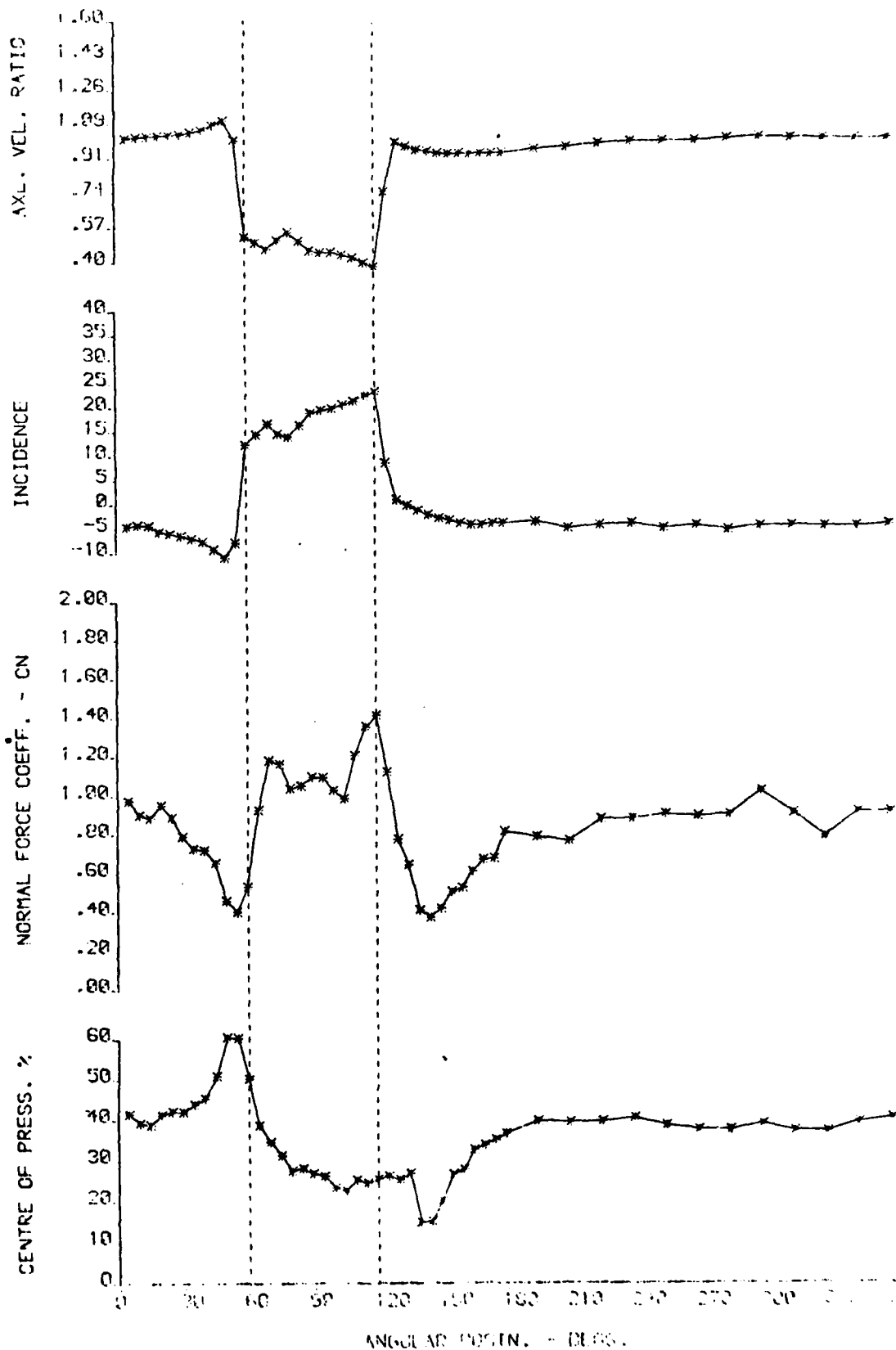


60° SQ. WAVE TEST @ 1250 RPM FLOW RATE NO-1

PRESSURE SURFACE PRESSURE DISTRIBUTION

FIG. 10c

ROTOR RESPONSE TO SQUARE WAVE SCREEN - TEST 17



CIRCUMFERENTIAL VARIATION OF AERODYNAMIC PARAMETERS

FIG. 10d

NORMAL FORCE VS. INCIDENCE --TEST 17

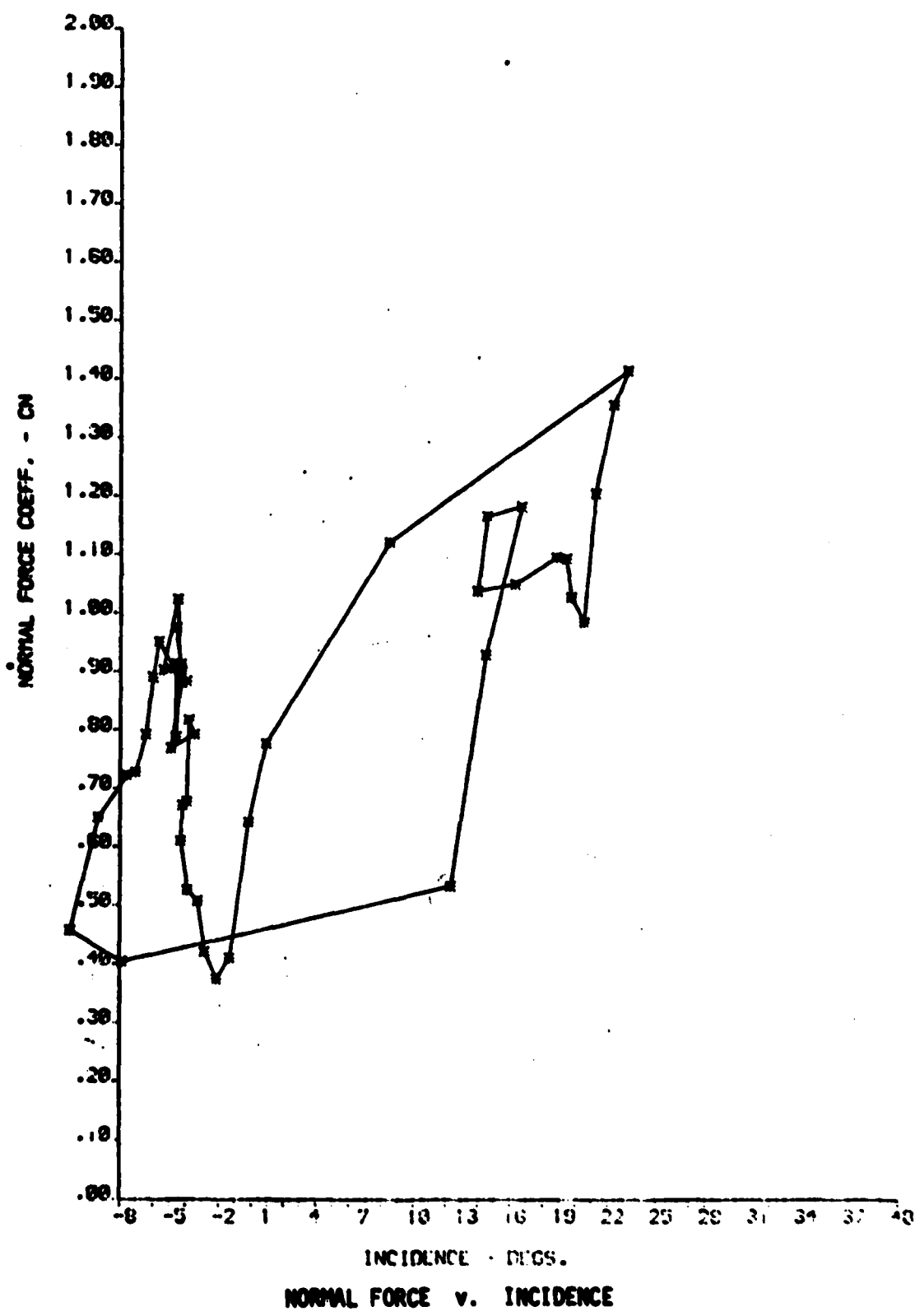
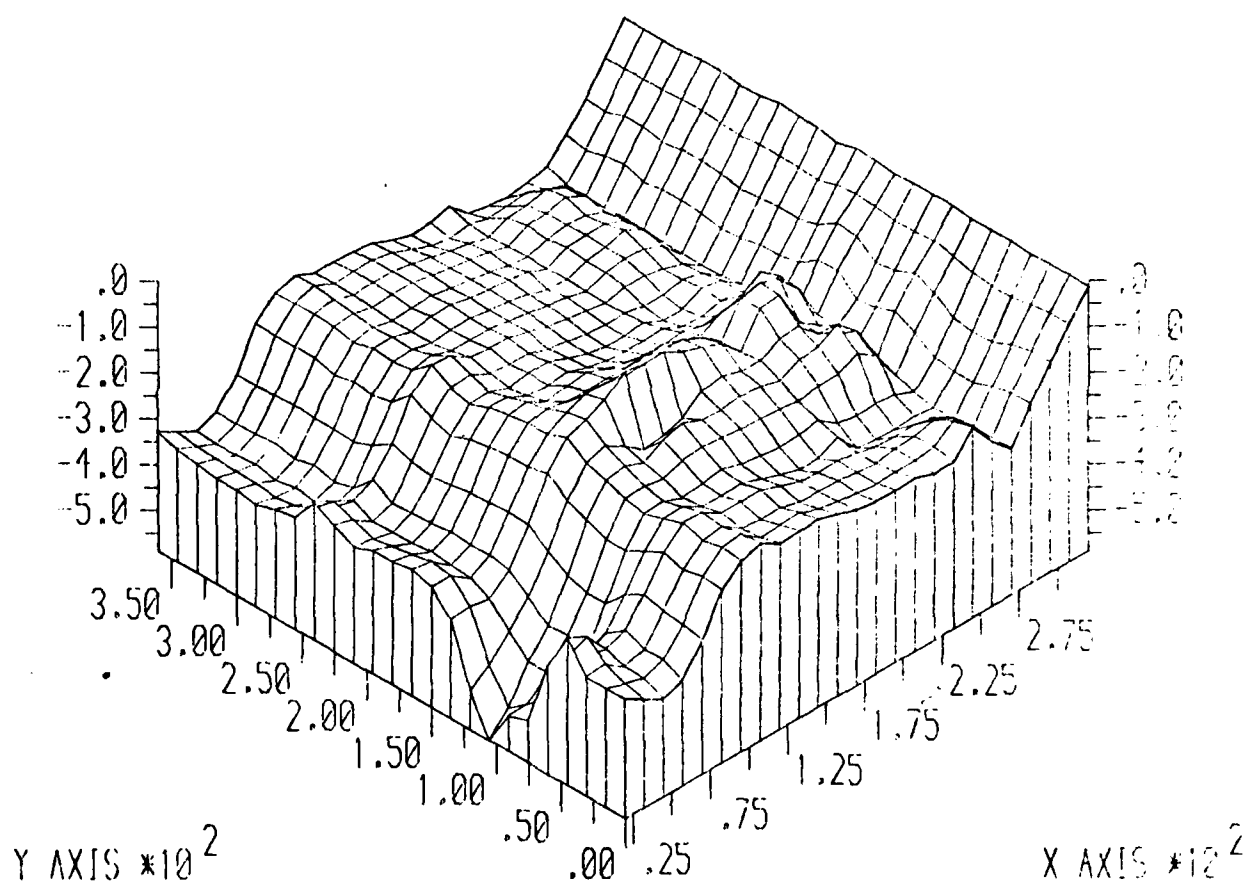
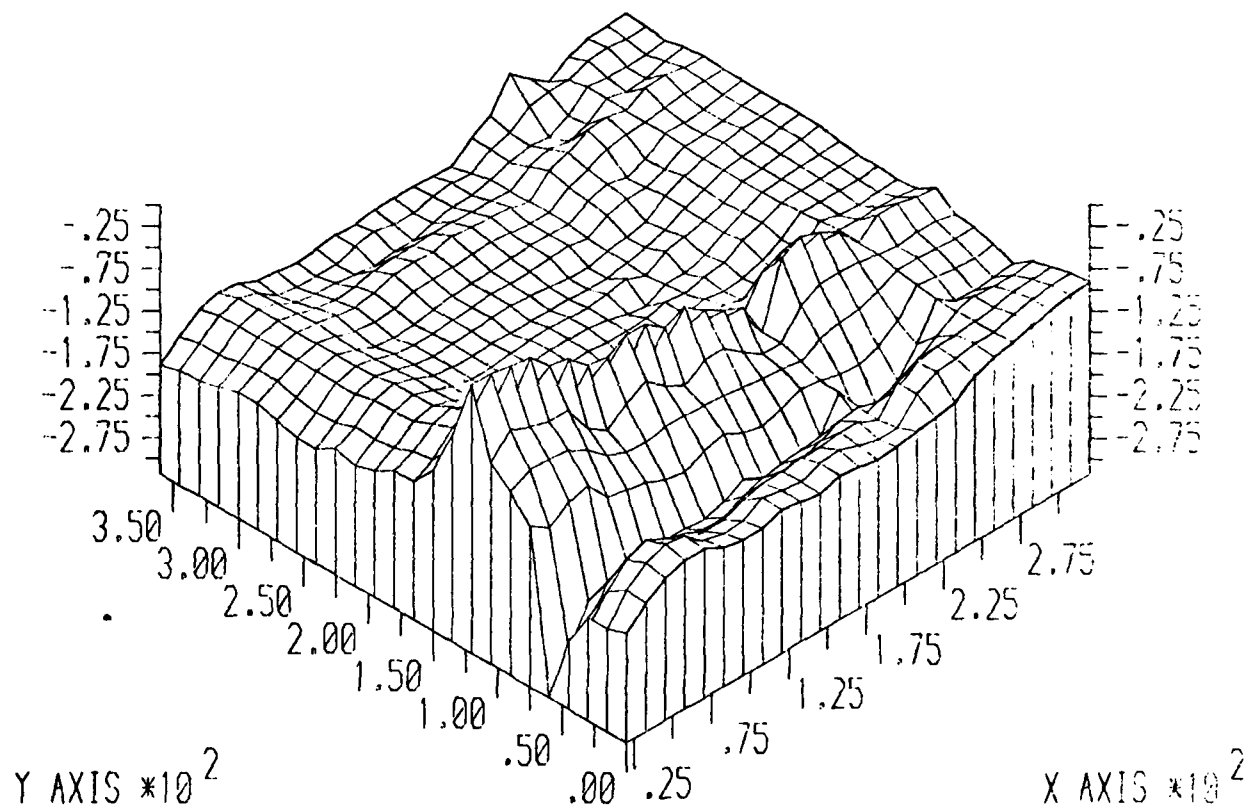


FIG. 11a



60° SQ. WAVE TEST @ 1250 RPM FLOW RATE NO-2
SUCTION SURFACE PRESSURE DISTRIBUTION

FIG. 11b



60° SQ. WAVE TEST @ 1250 RPM FLOW RATE NO-2

PRESSURE SURFACE PRESSURE DISTRIBUTION

ROTOR RESPONSE TO SQUARE WAVE SCREEN - TEST 10

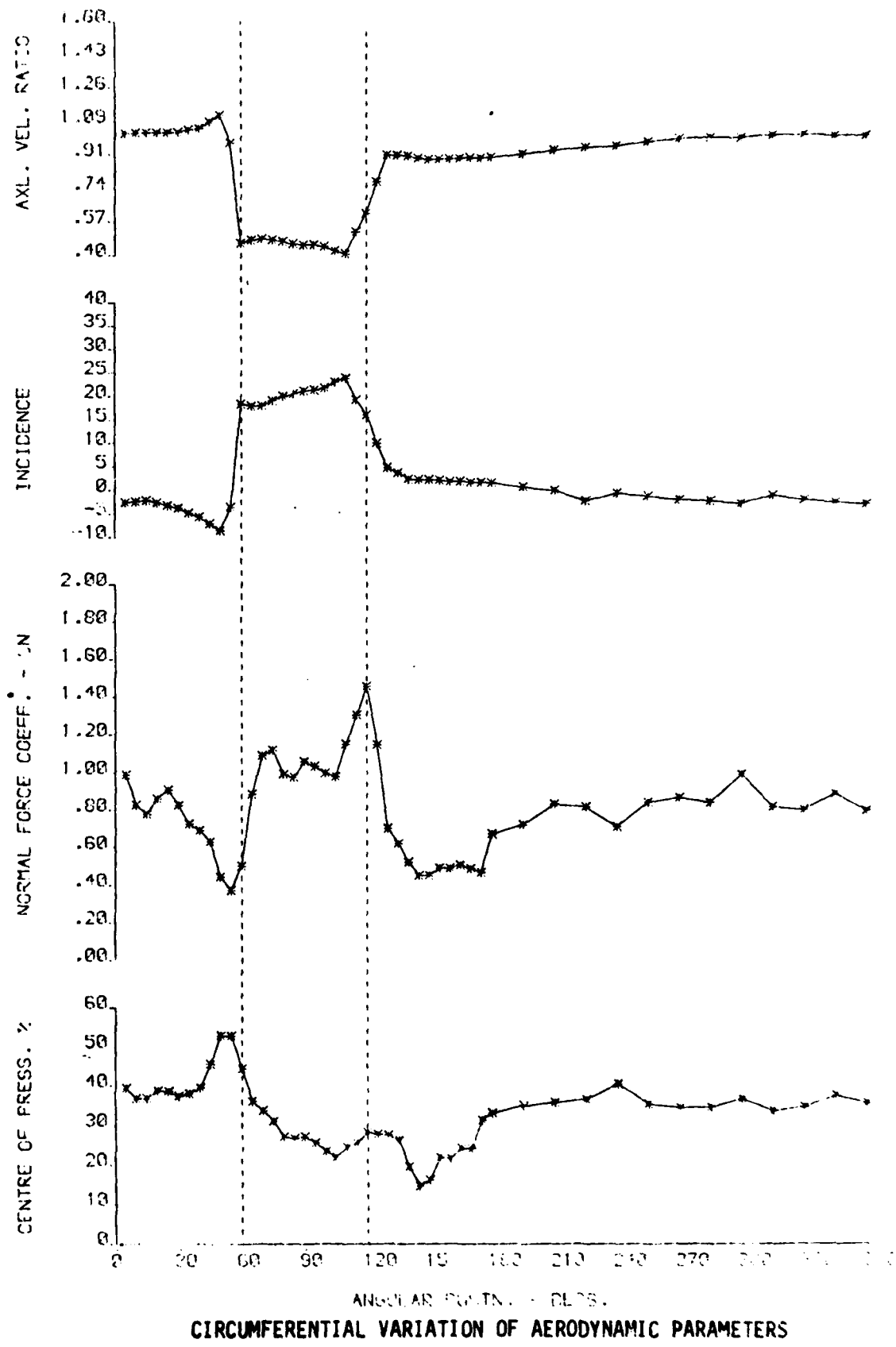


FIG. 11d

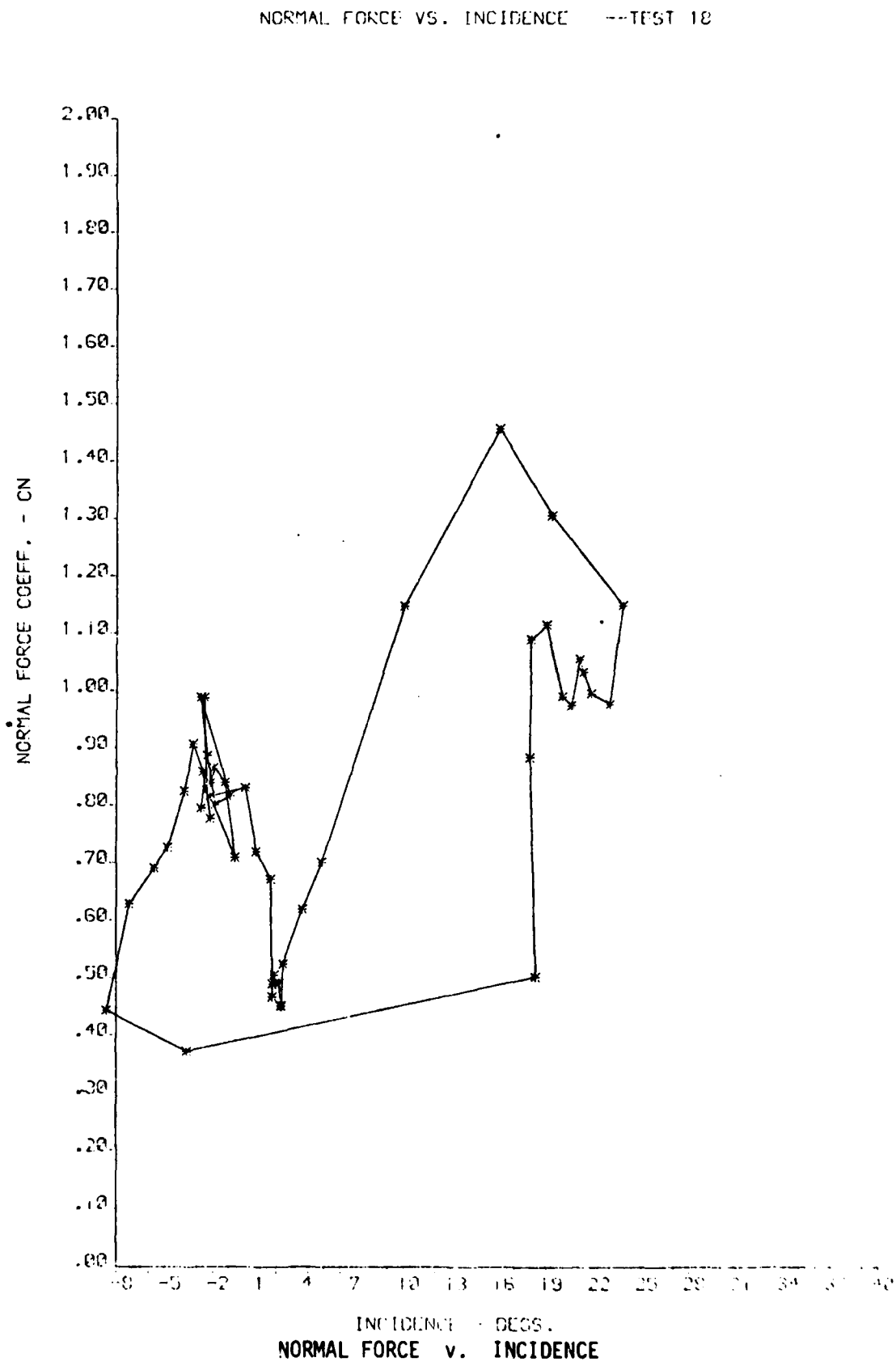
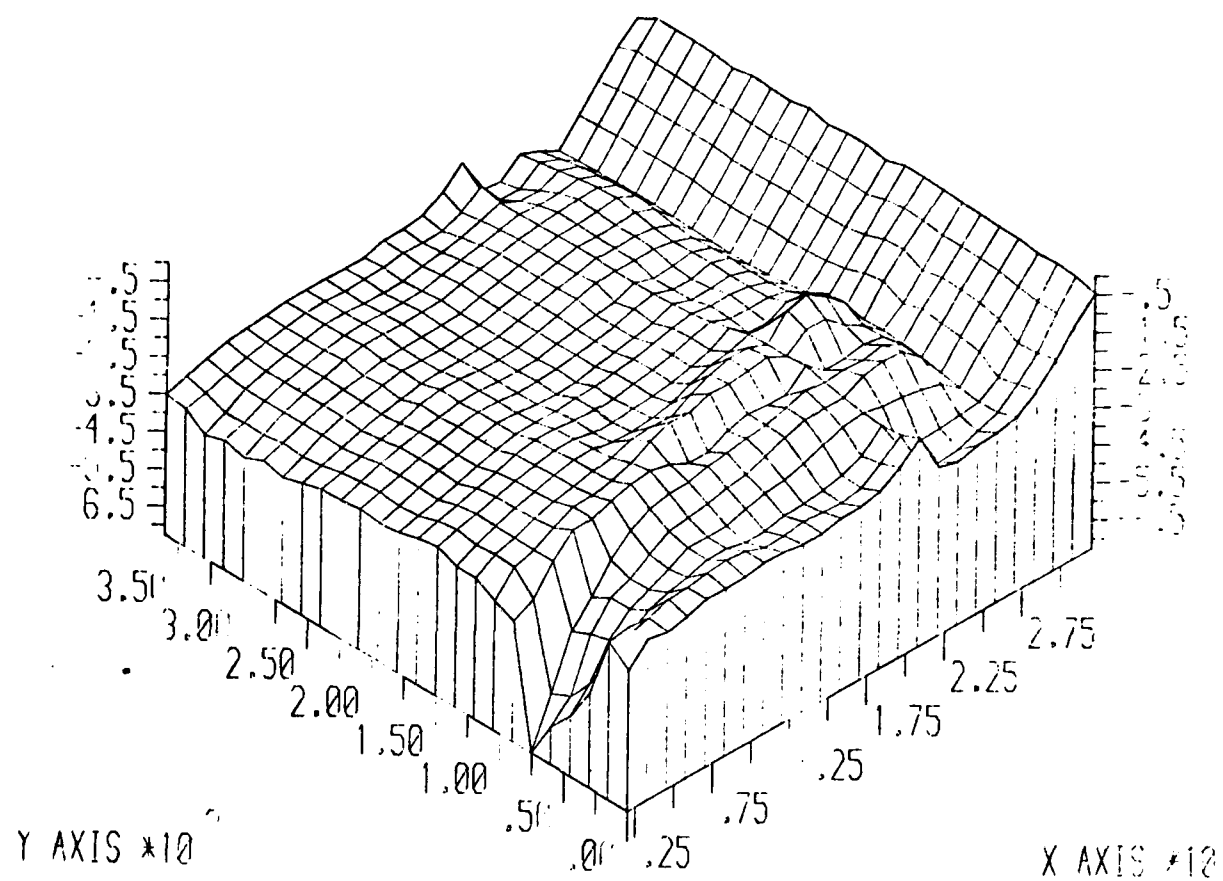


FIG. 12a



0° SQ.WAVE TEST @ 1250 RPM FLOW RATE NO. 3

SUCTION SURFACE PRESSURE DISTRIBUTION

FIG. 12b

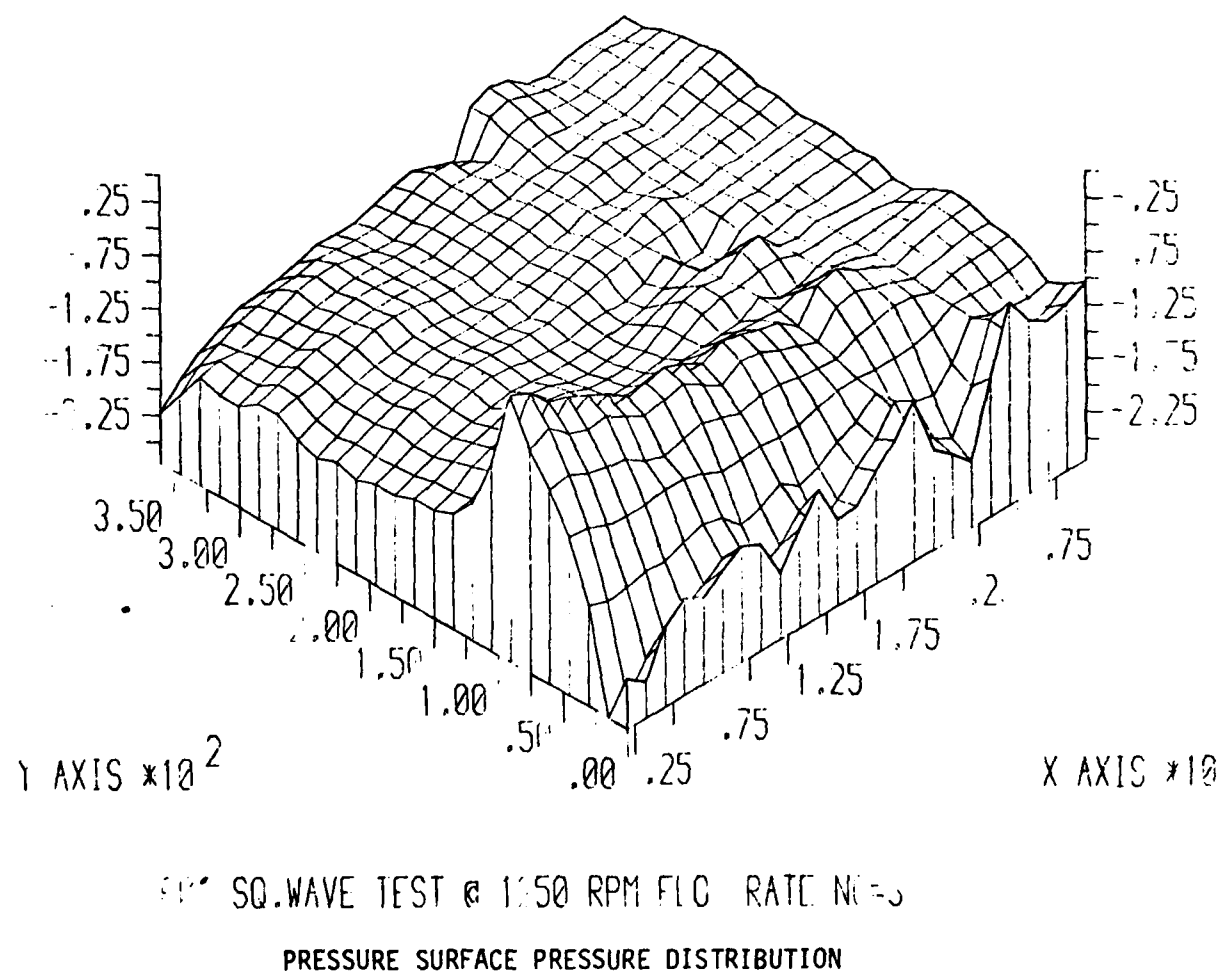


FIG. 12c

POLE RESPONSE TO SQUARE WAVE SPEED TEST 15

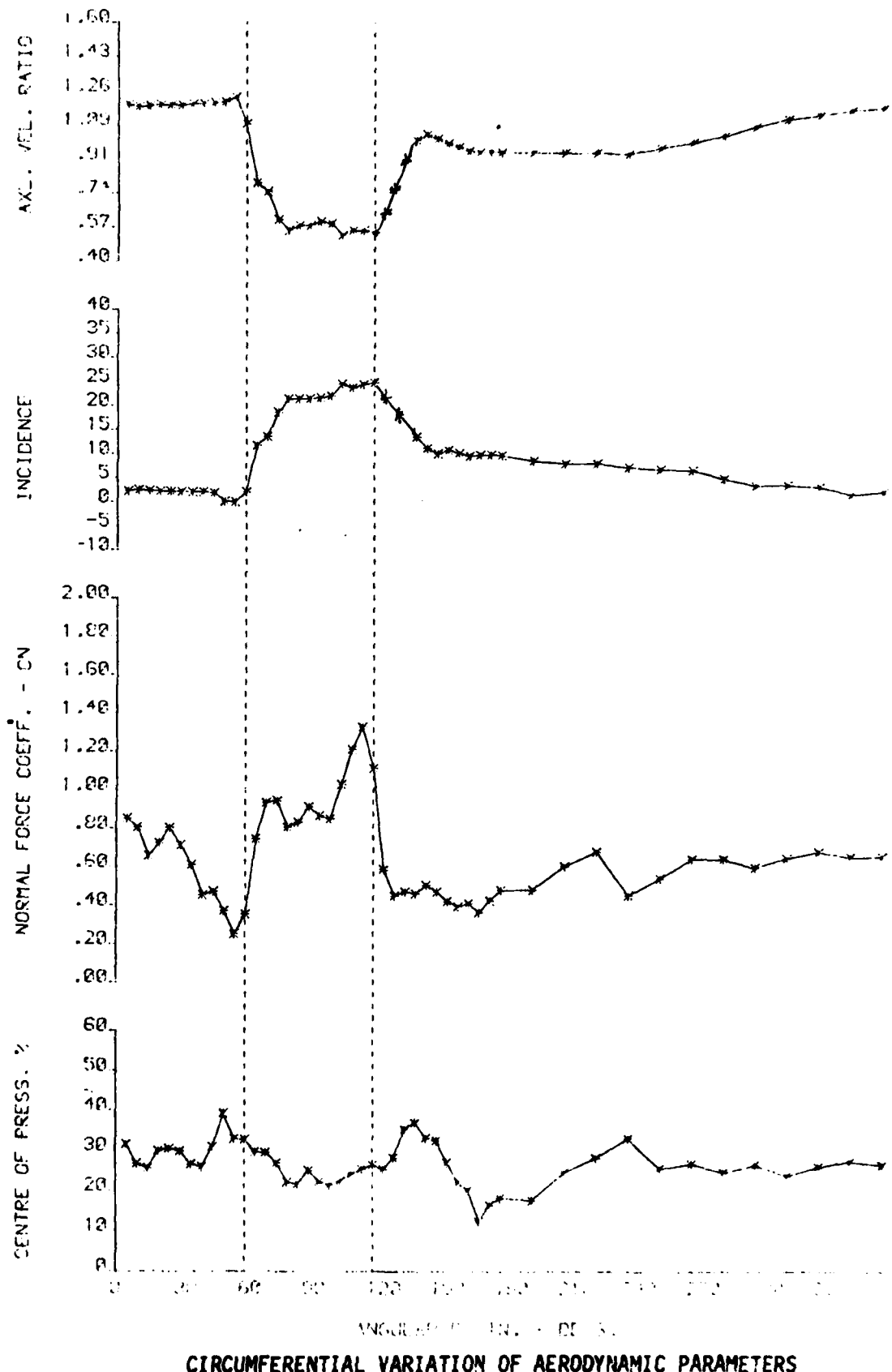


FIG. 12d

NORMAL FORCE VS. INCIDENCE -- TEST 19

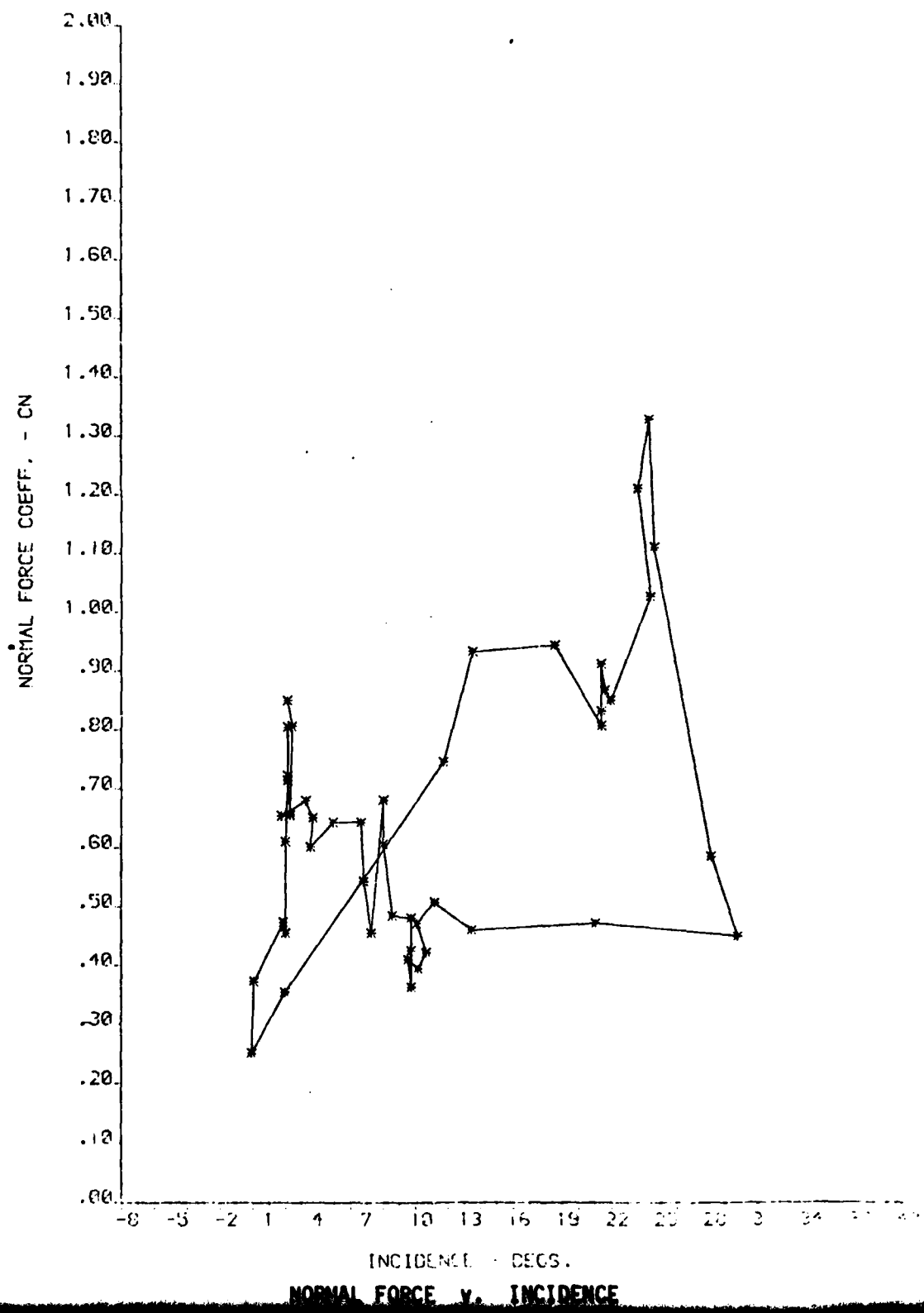
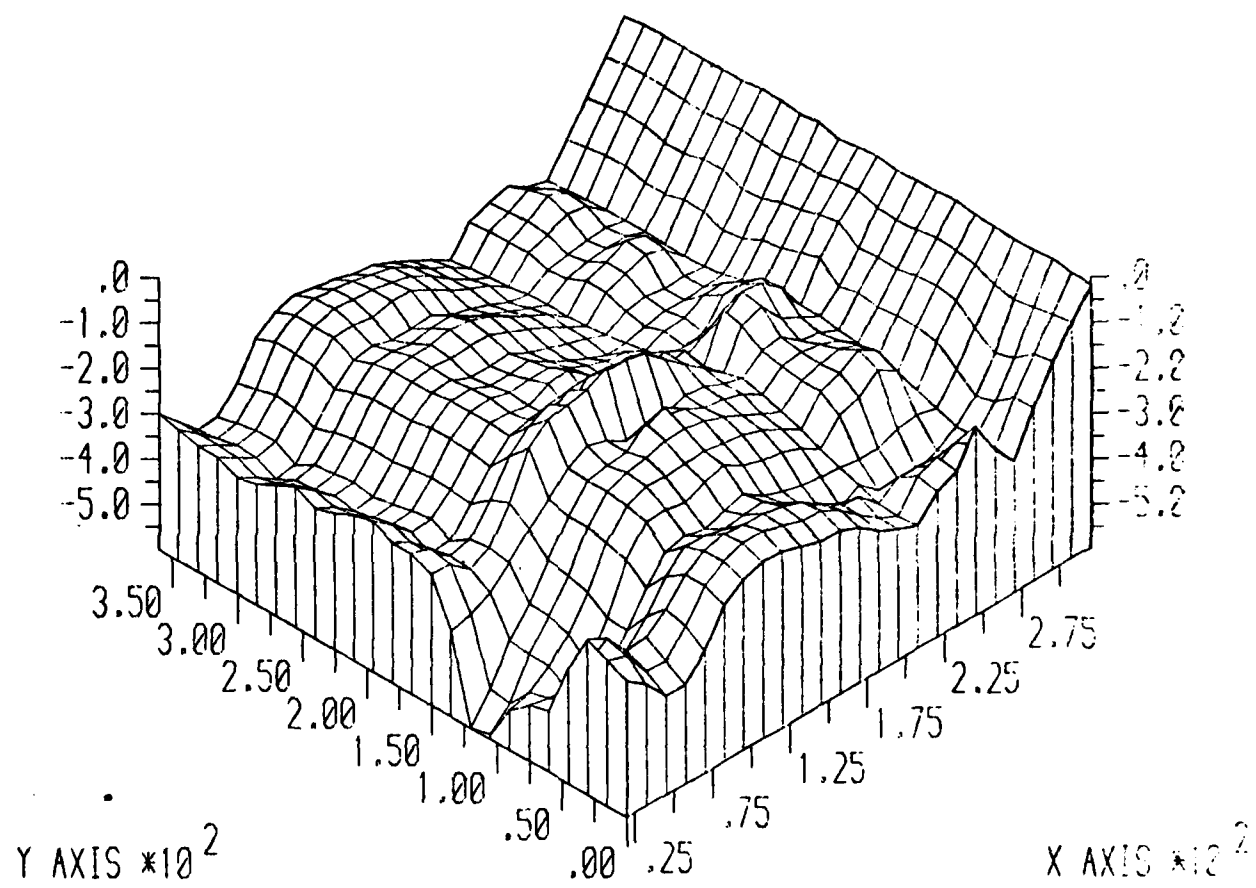


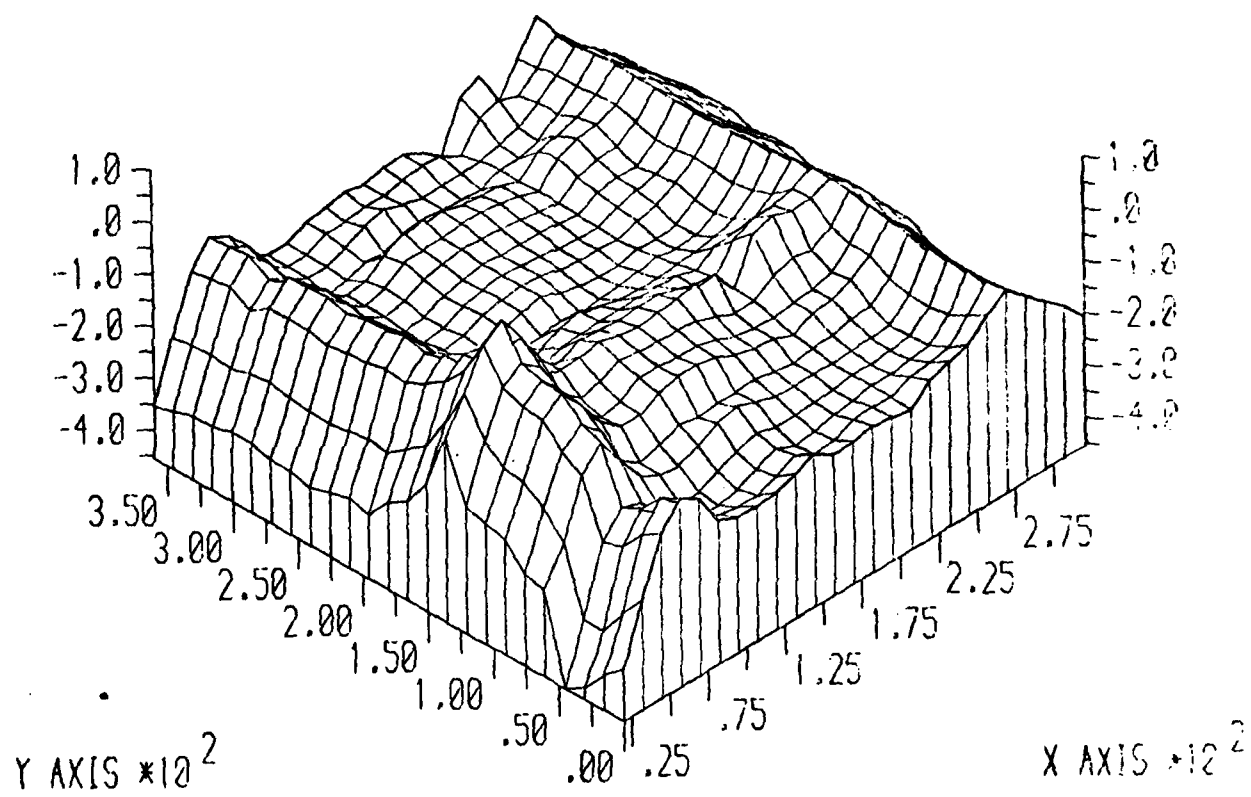
FIG. 13a



90° SQ. WAVE TEST @1200 RPM FLOW RATE NO-1

SUCTION SURFACE PRESSURE DISTRIBUTION

FIG. 13b



90° SQ. WAVE TEST @1000 RPM FLOW RATE NO:1

PRESSURE SURFACE PRESSURE DISTRIBUTION

FIG. 13c

ROTOR RESPONSE TO SQUARE WAVE SCREEN - TEST 1

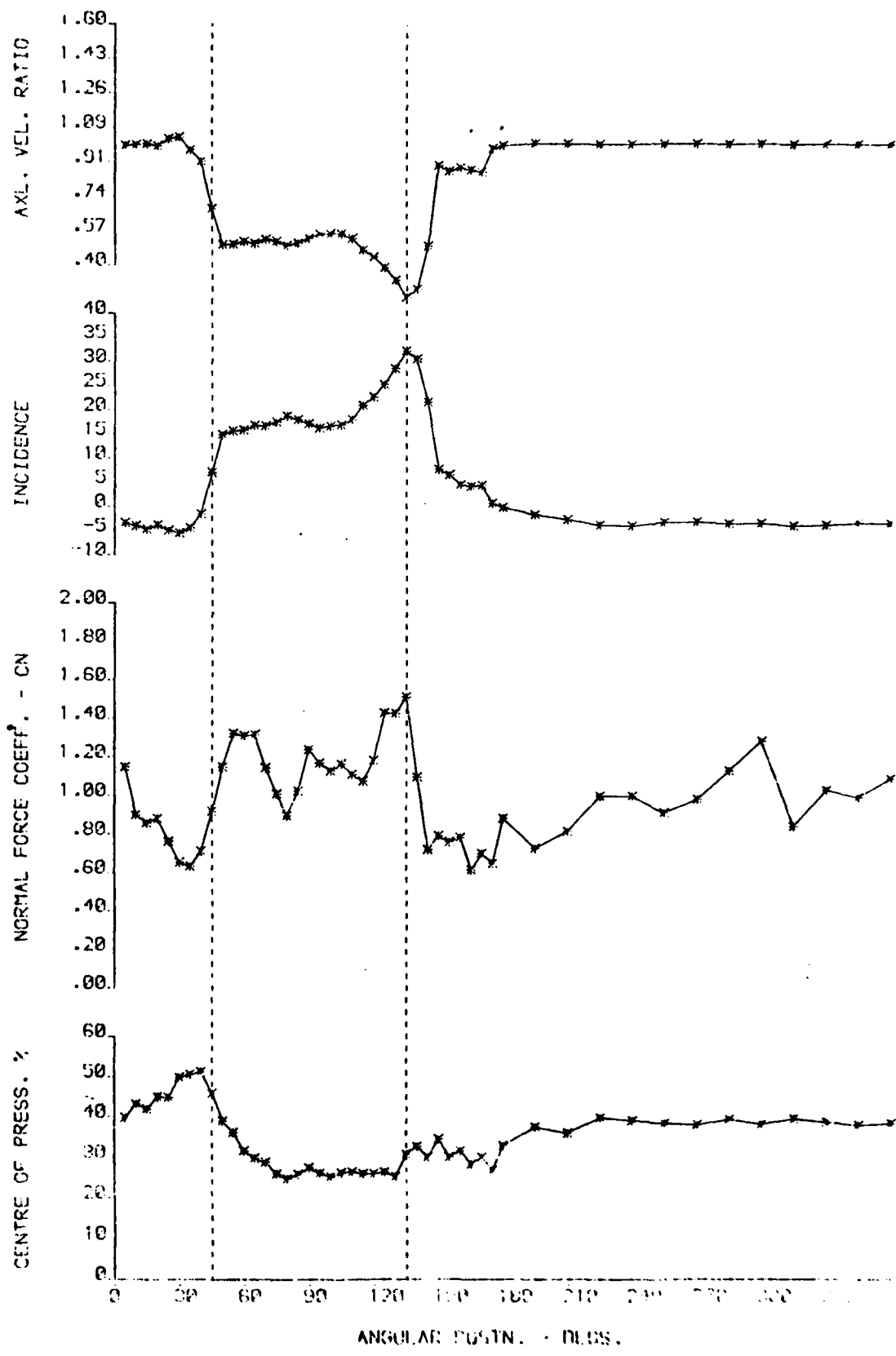


FIG. 13.d

NORMAL FORCE VS. INCIDENCE --TEST 1

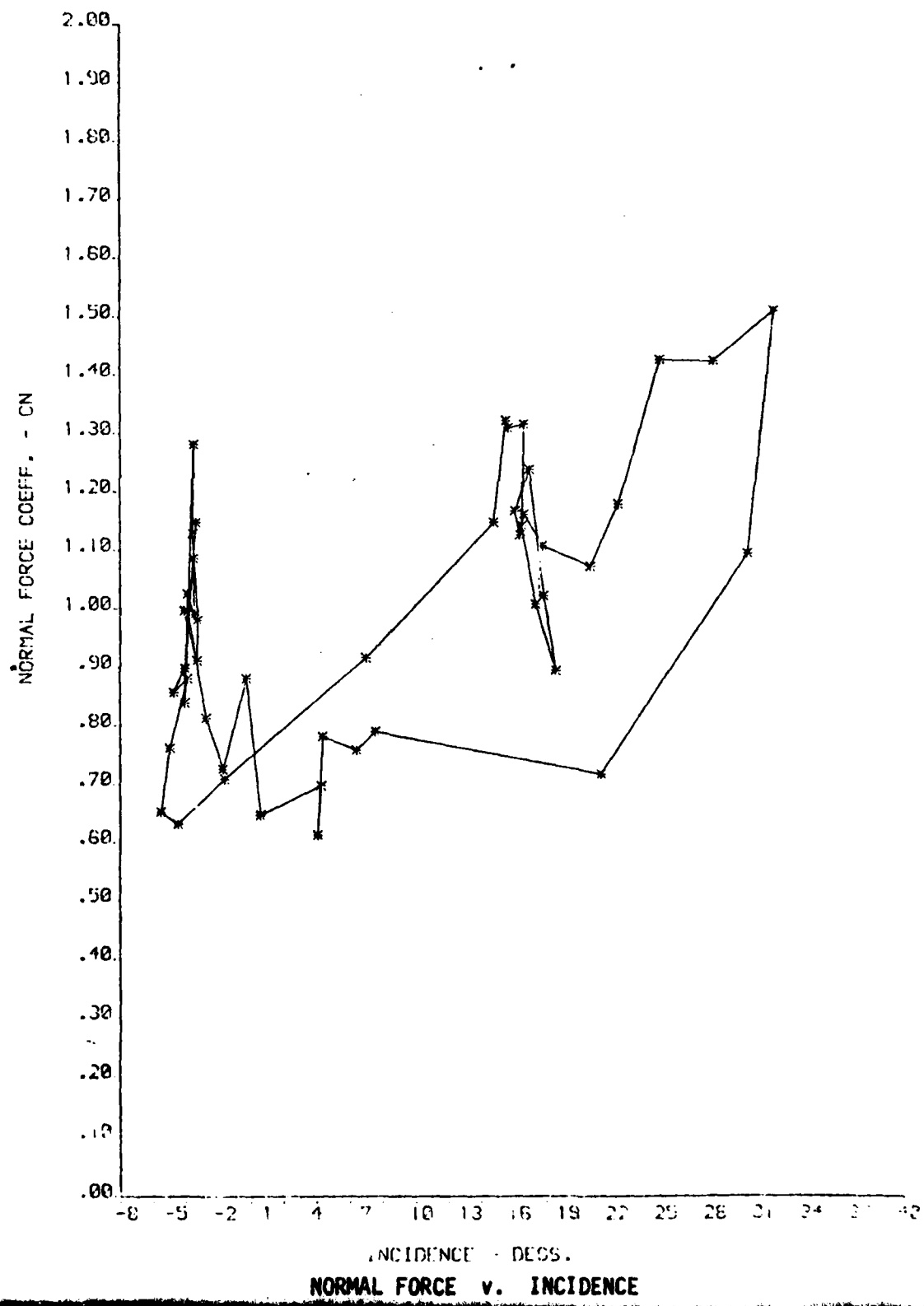


FIG. 14a

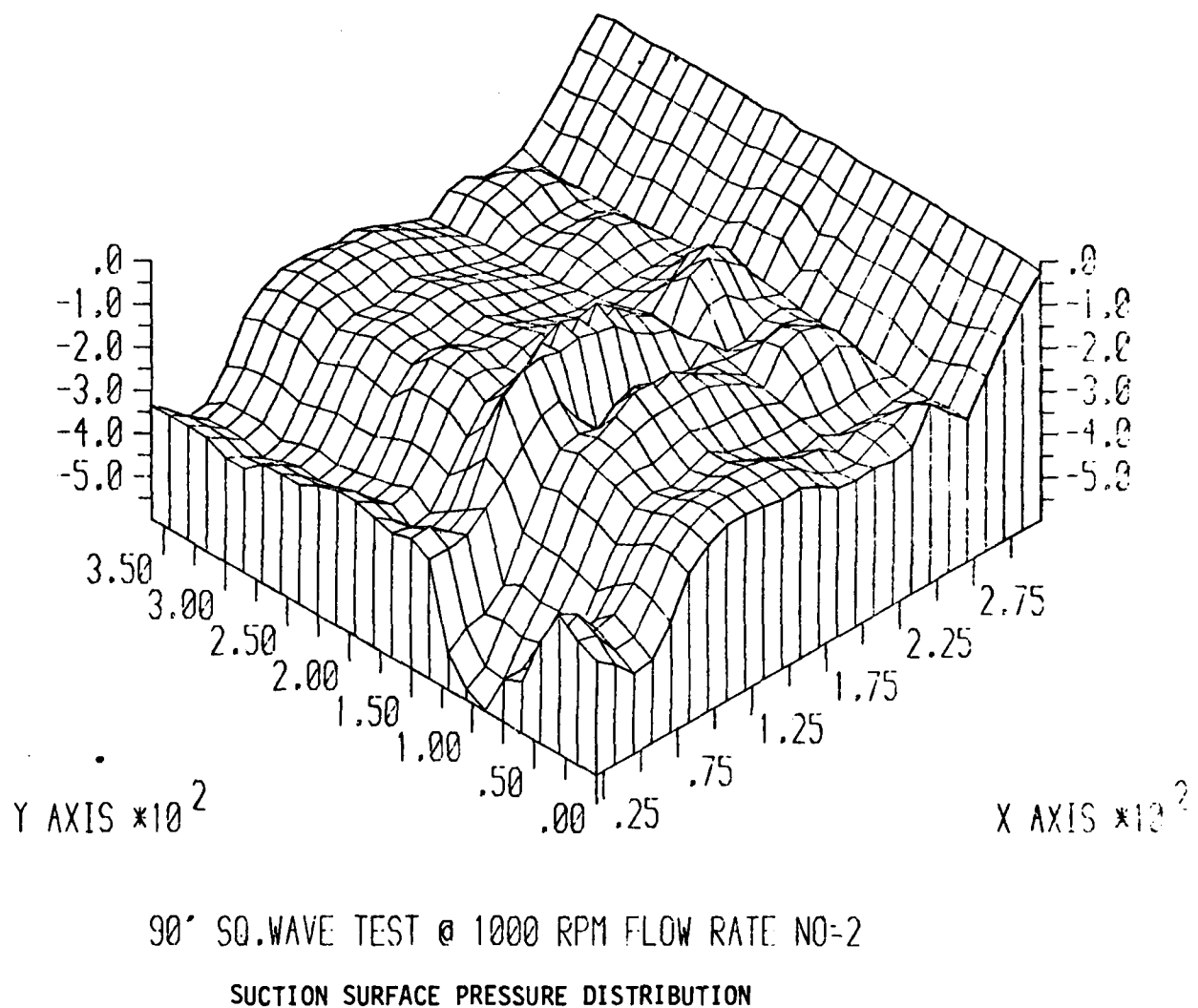
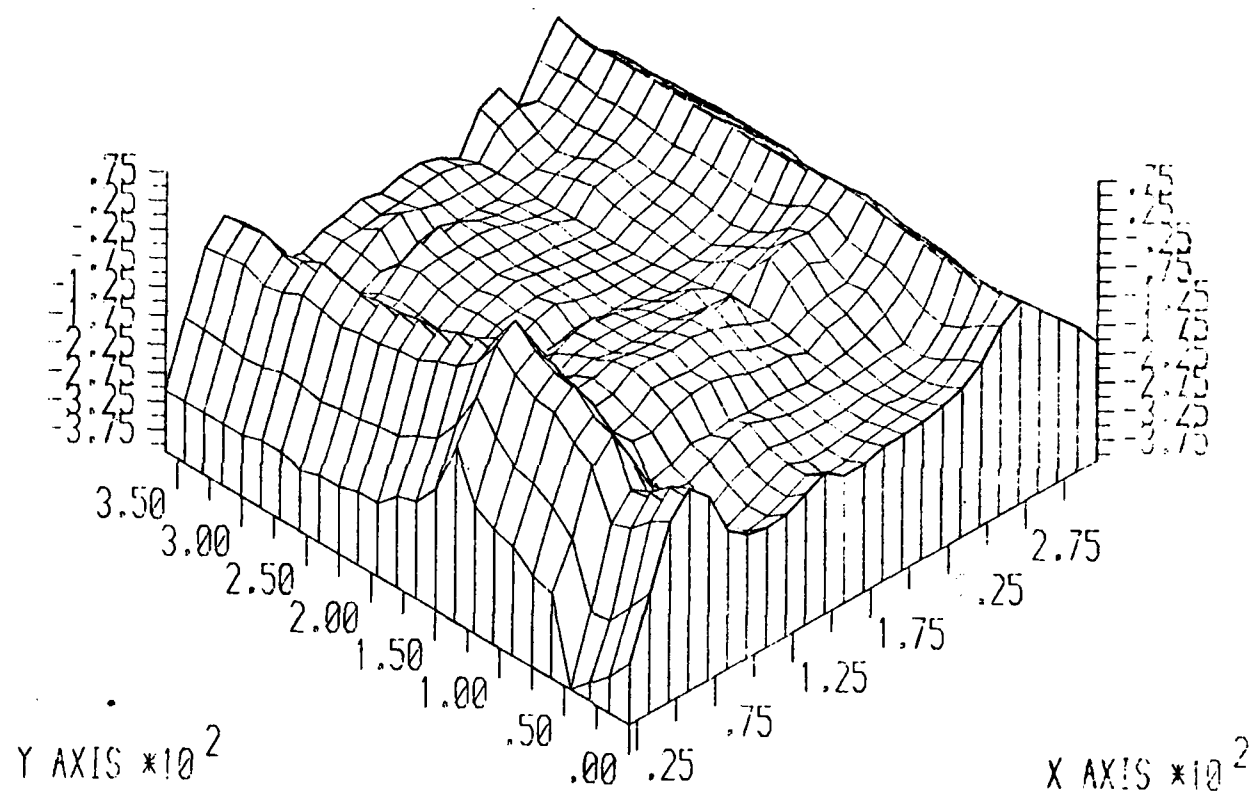


FIG. 14b



90° SQ.WAVE TEST @ 1000 RPM FLOW RATE NO-2

PRESSURE SURFACE PRESSURE DISTRIBUTION

FIG. 14c

ROTOR RESPONSE TO SQUARE WAVE SCREEN -- TEST 2

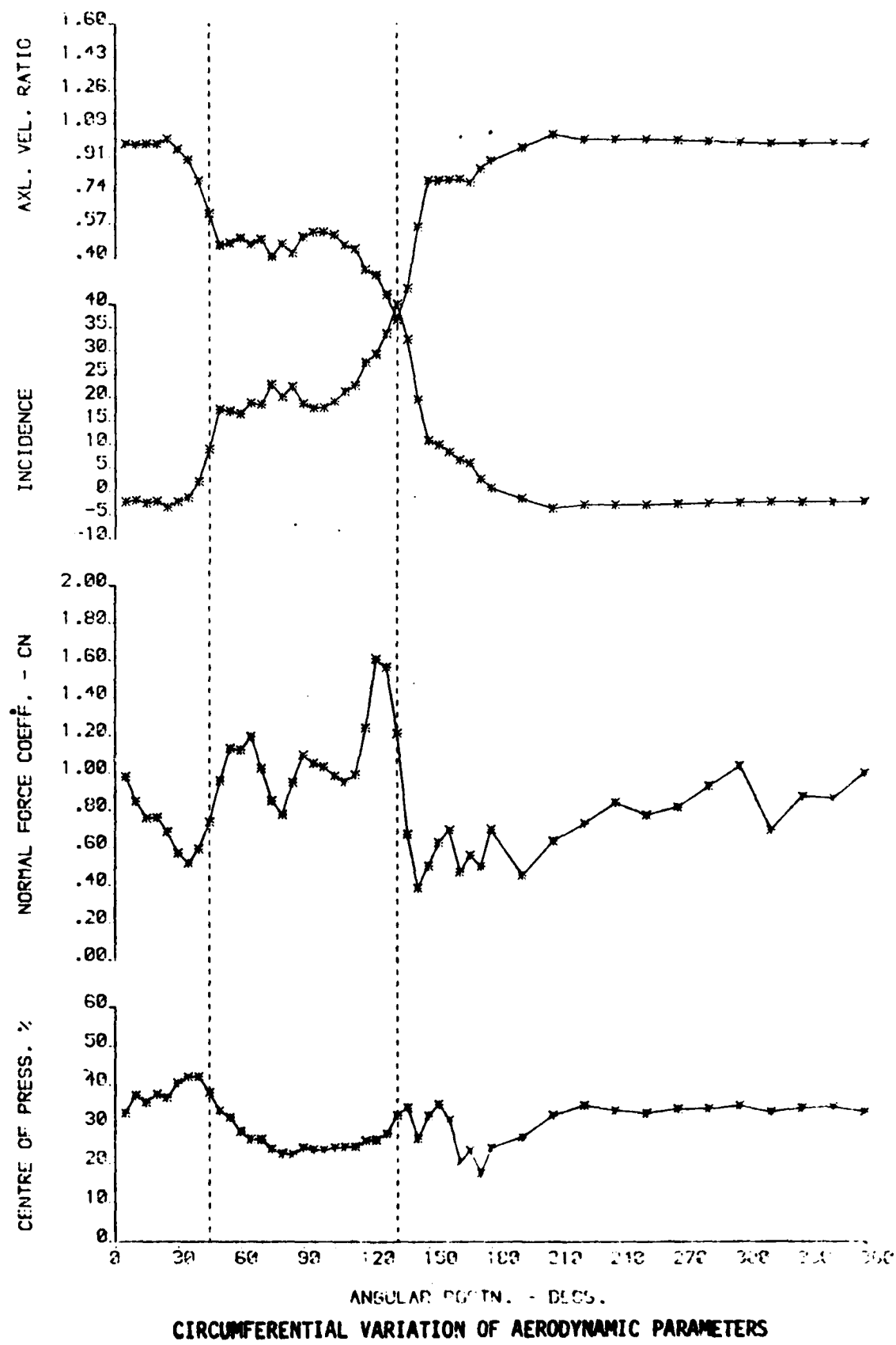


FIG. 14d

NORMAL FORCE VS. INCIDENCE -- TEST 2

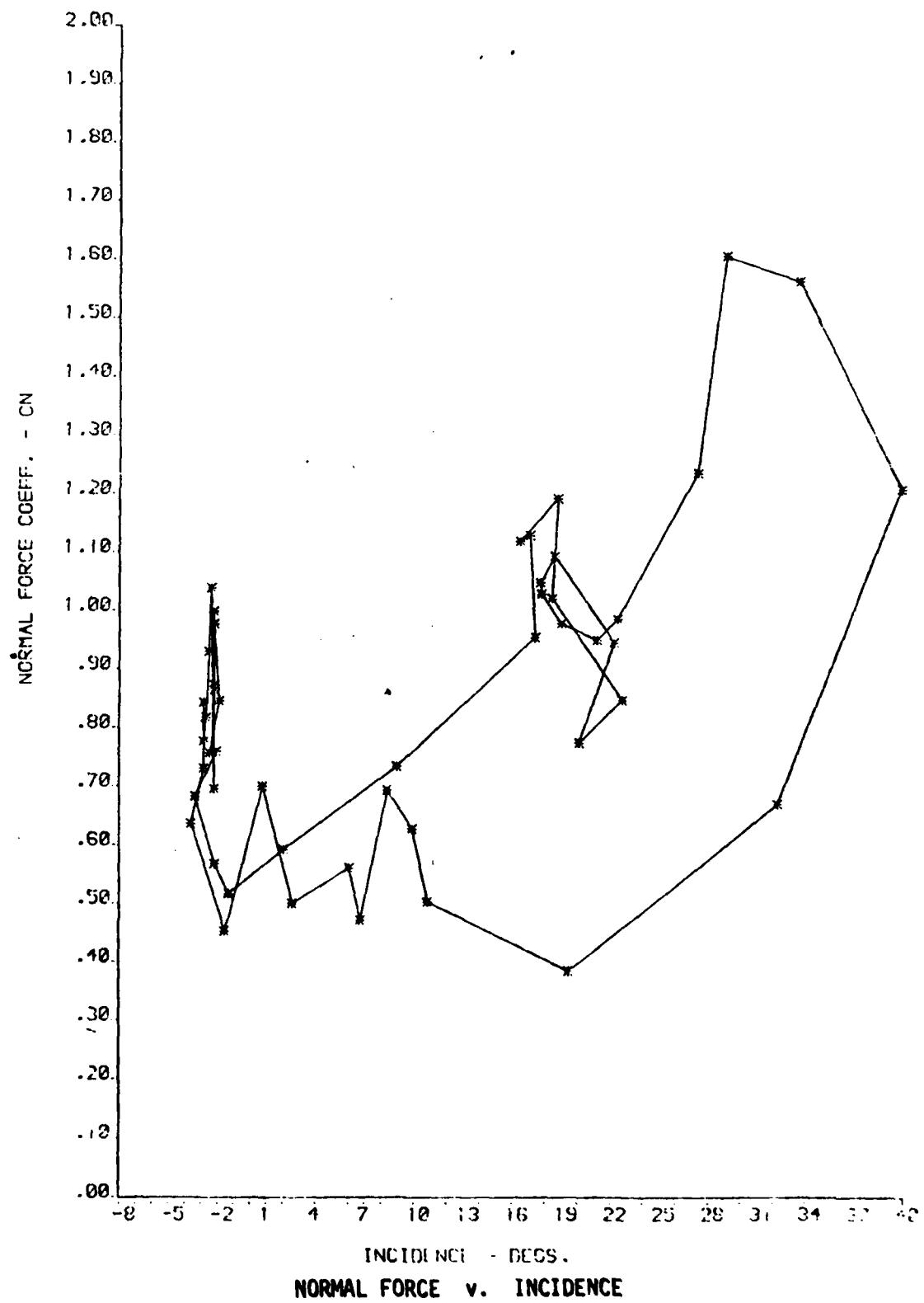
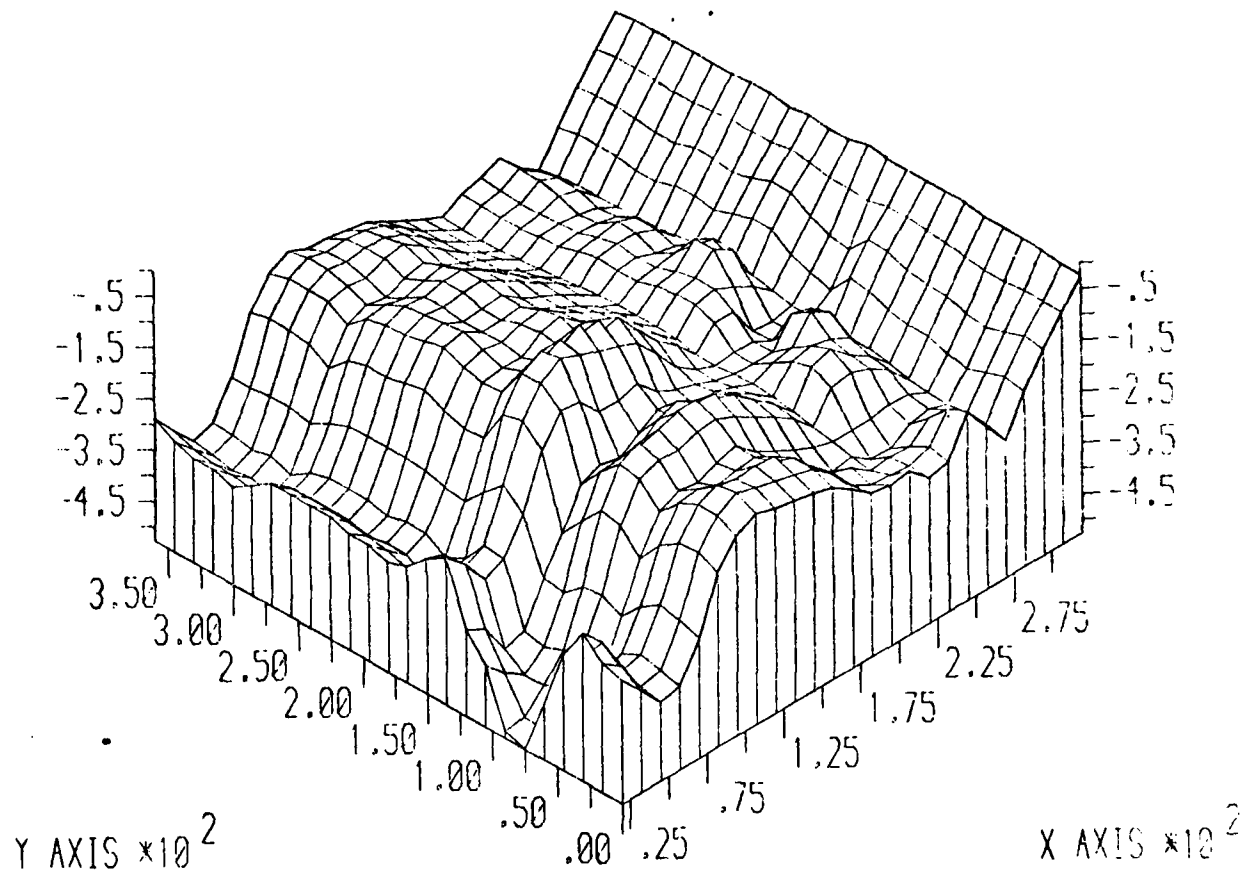


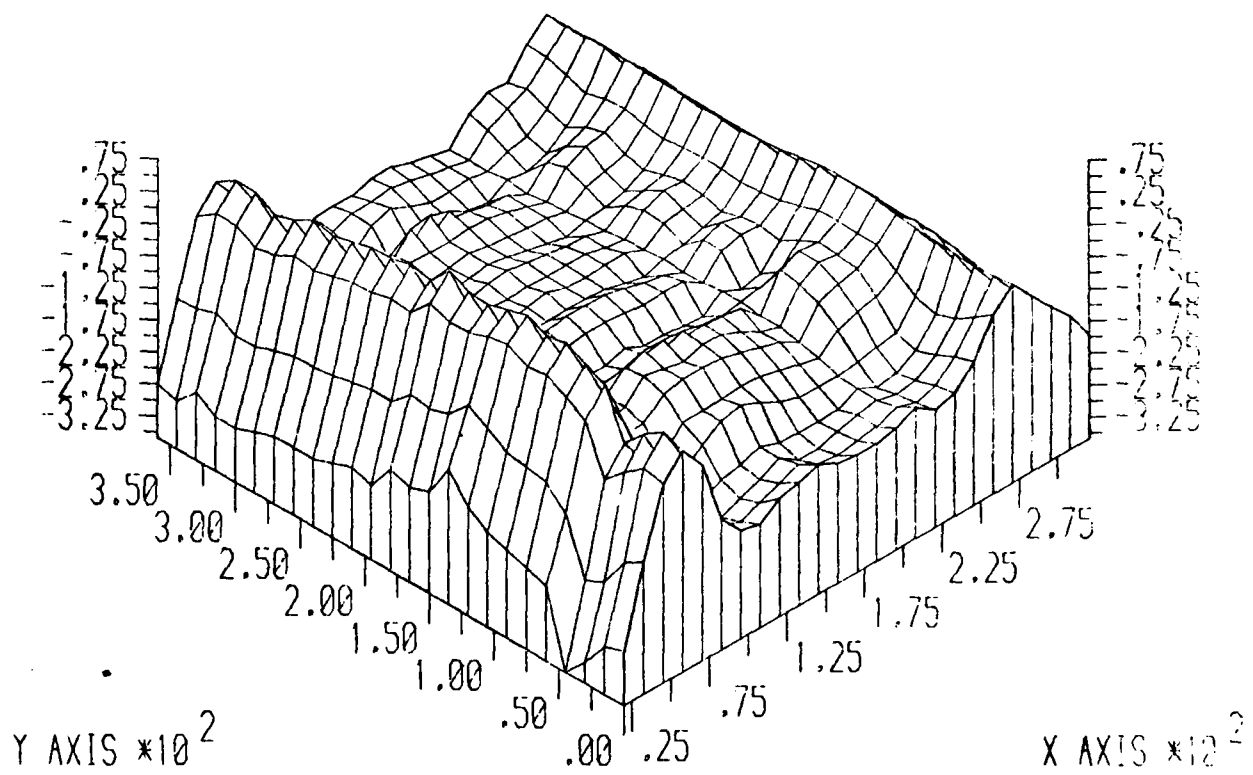
FIG. 15a



90° SQ.WAVE TEST @ 1000 RPM FLOW RATE NO-3

SUCTION SURFACE PRESSURE DISTRIBUTION

FIG. 15b

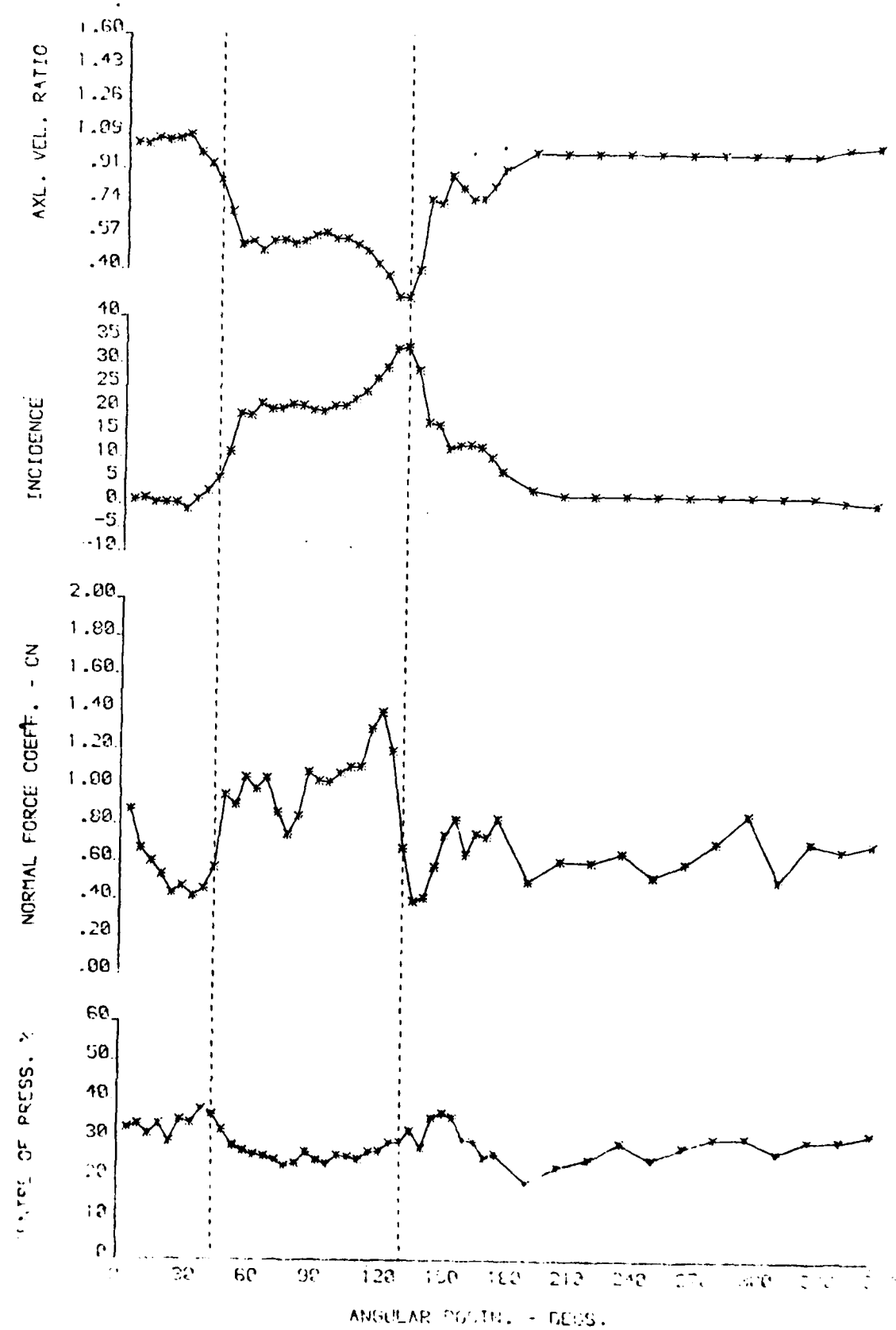


90° SQ.WAVE TEST @ 1000 RPM FLOW RATE NO-3

PRESSURE SURFACE PRESSURE DISTRIBUTION

FIG. 15c

ROTOR RESPONSE TO SQUARE WAVE GROUND -- TEST 3



CIRCUMFERENTIAL VARIATION OF AERODYNAMIC PARAMETERS

FIG. 15d

NORMAL FORCE VS. INCIDENCE --TEST 3

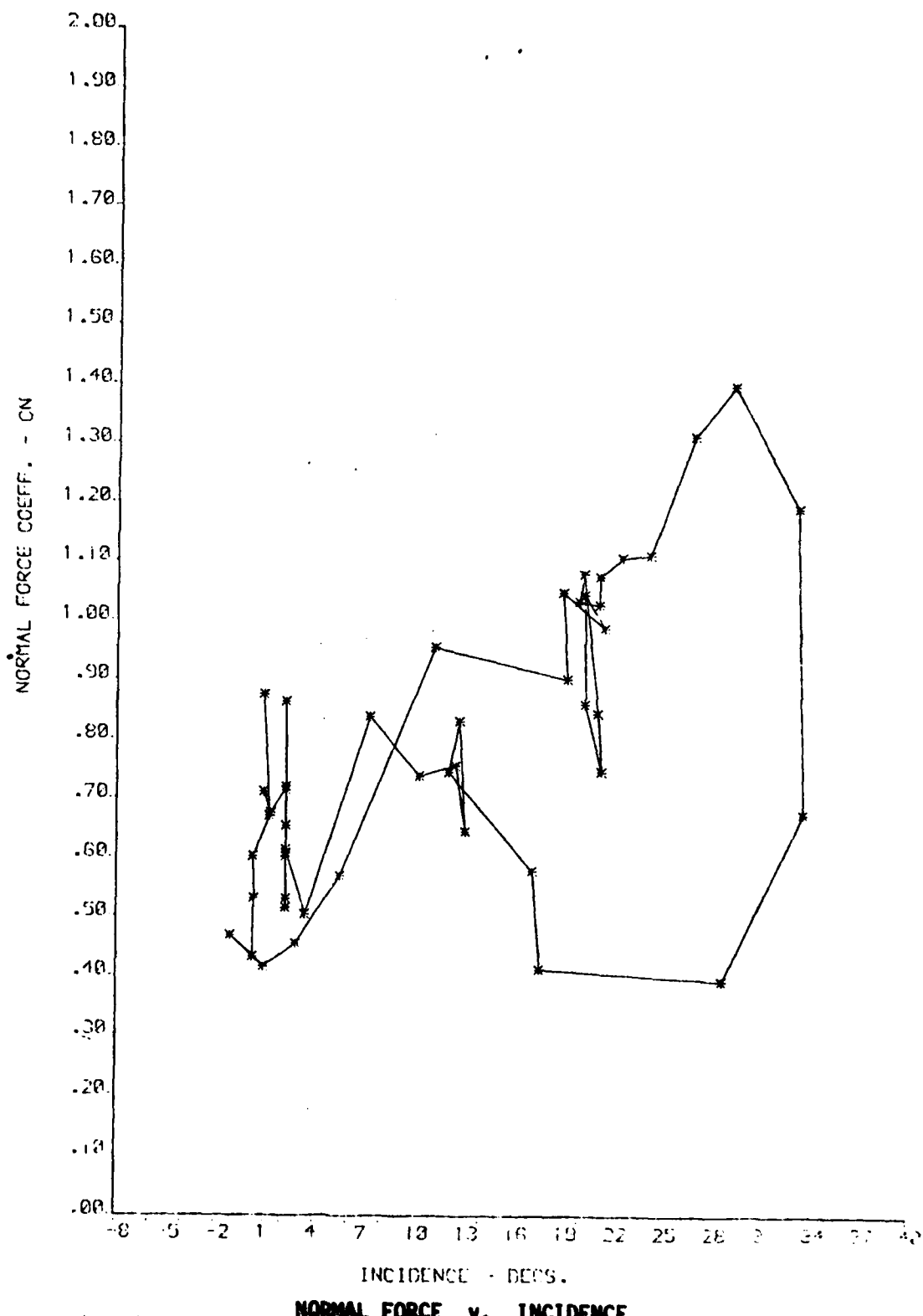


FIG. 16a

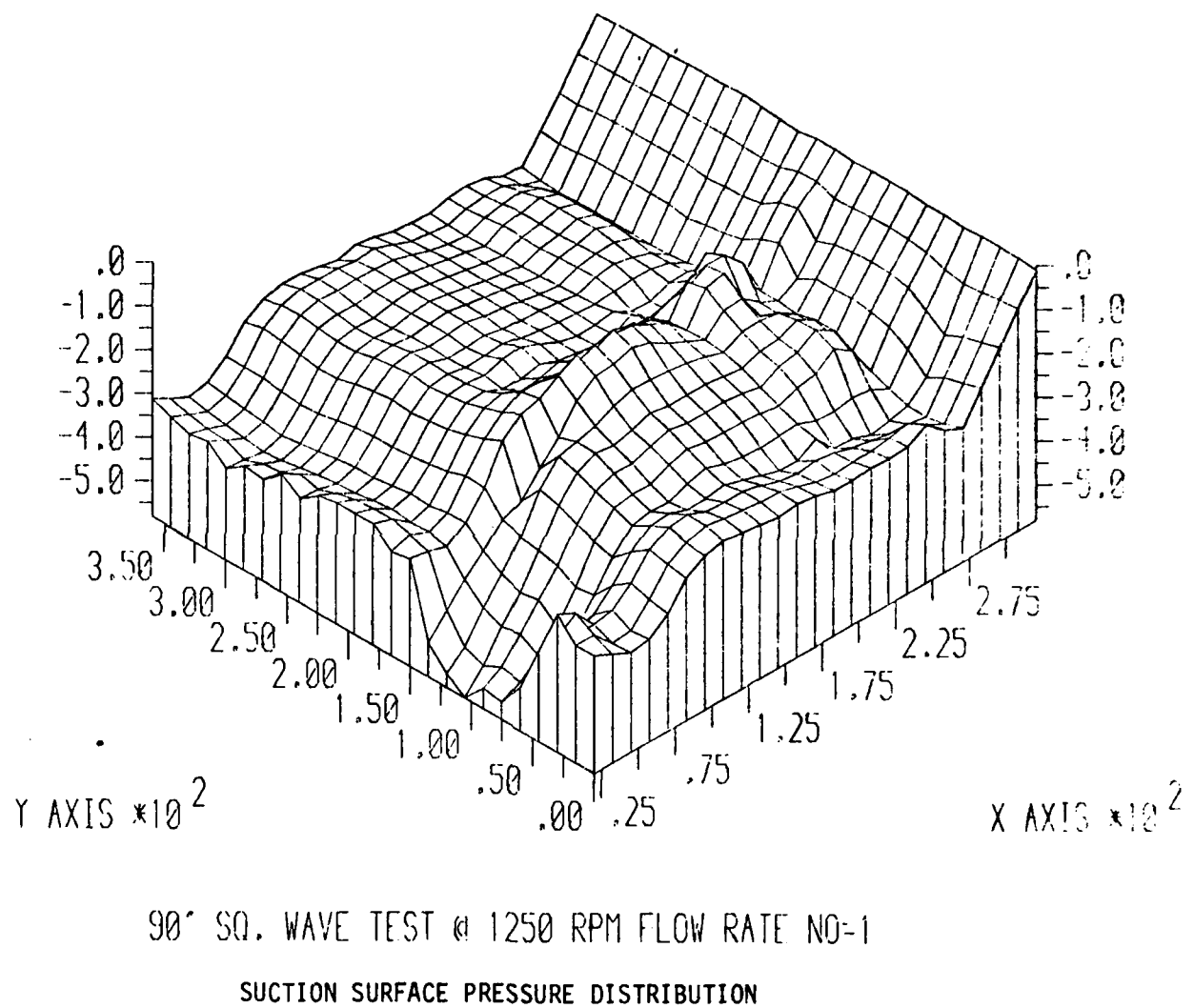
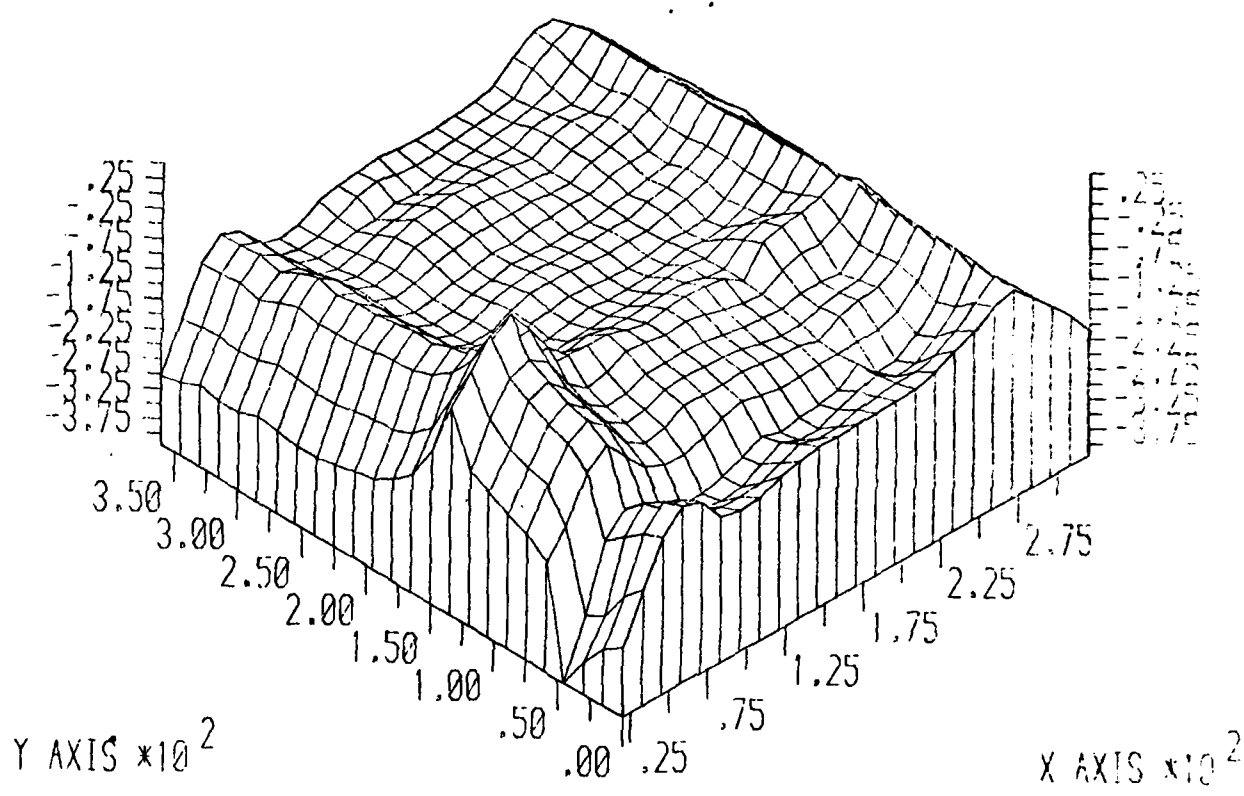


FIG. 16b



90° SQ. WAVE TEST @ 1250 RPM FLOW RATE NO=1

PRESSURE SURFACE PRESSURE DISTRIBUTION

FIG. 16c
ROTOR RESPONSE TO SQUARE WAVE SCREEN - TEST 1

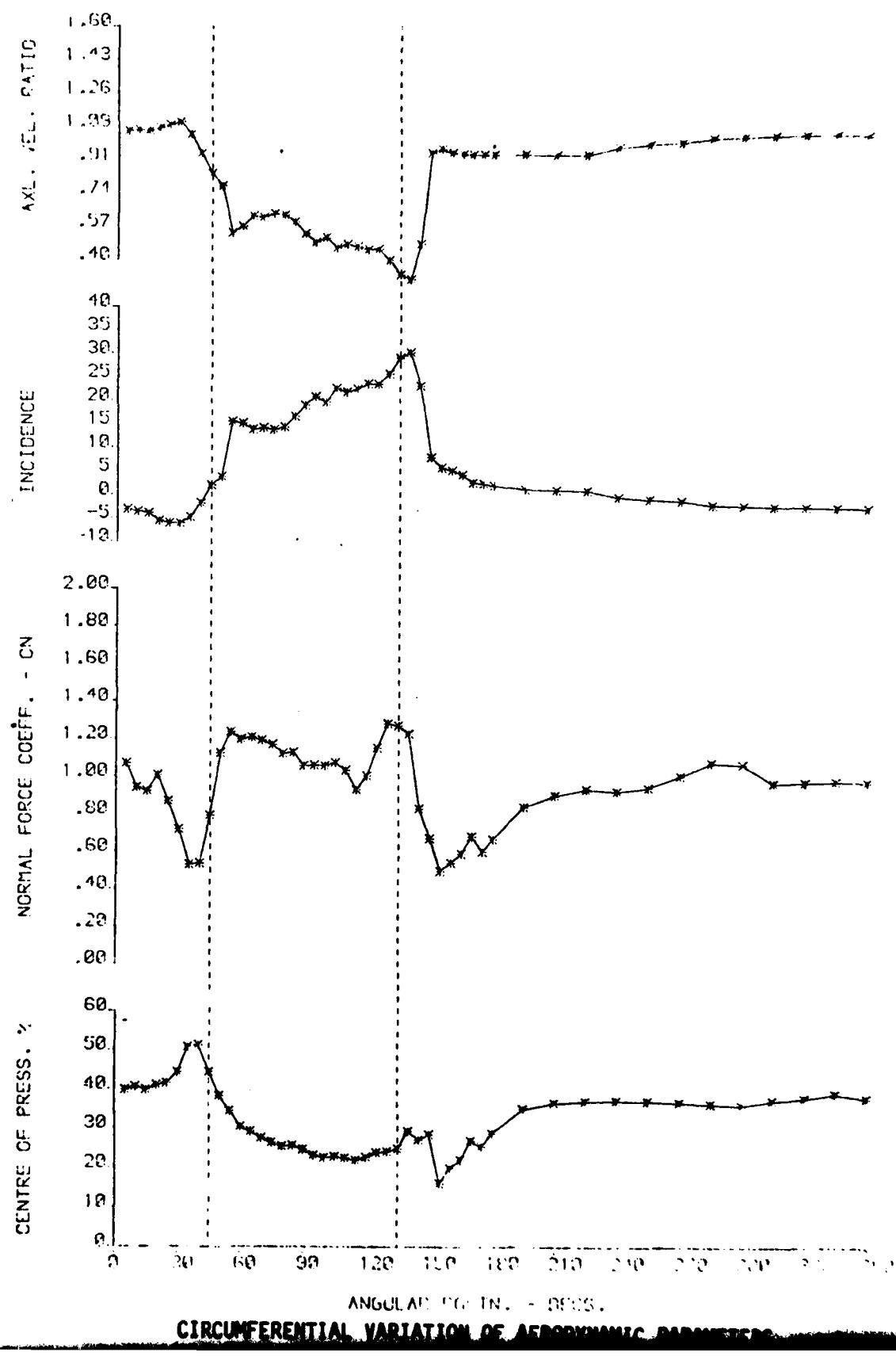


FIG. 16d

NORMAL FORCE VS. INCIDENCE -- TEST 6

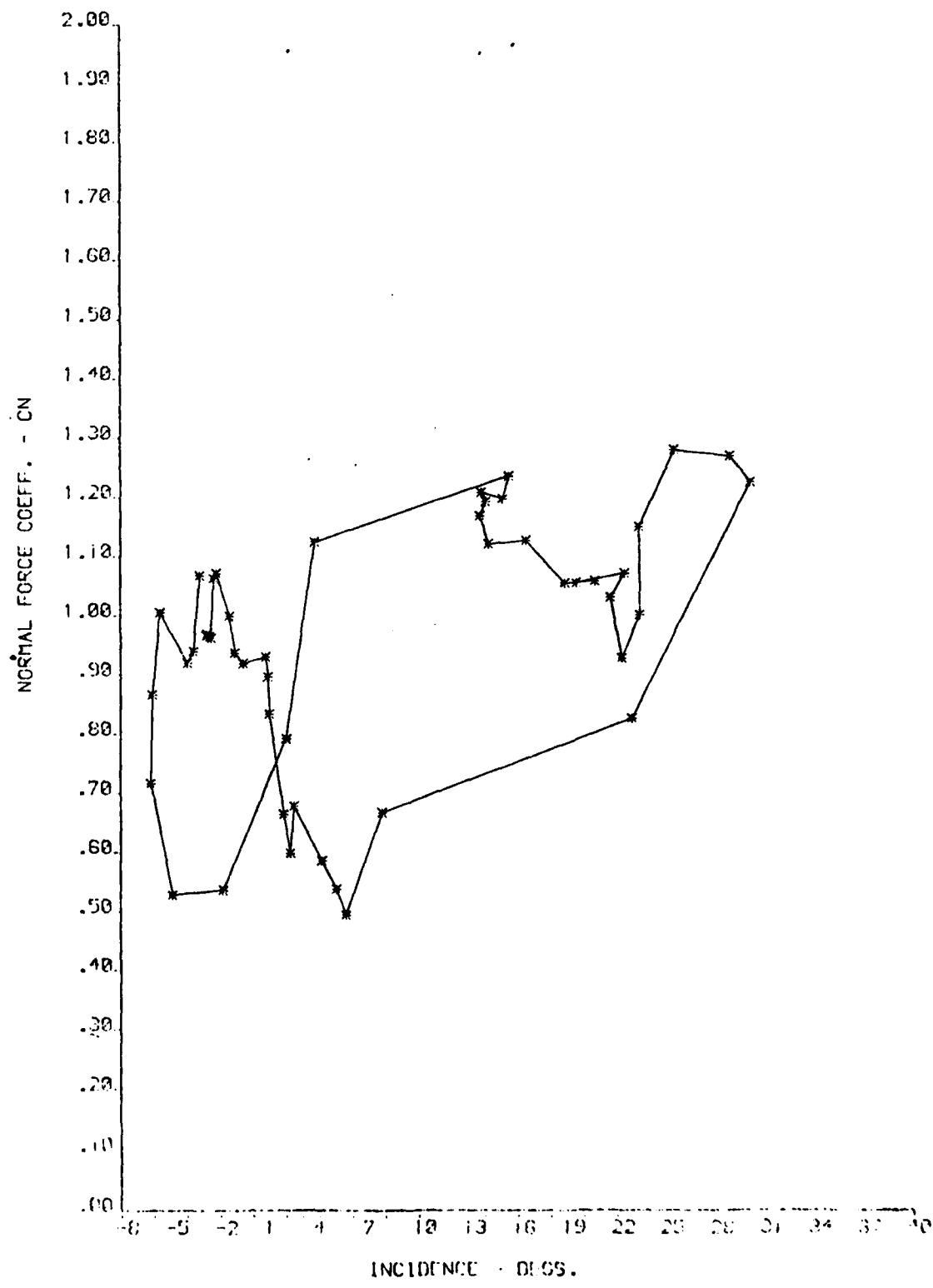
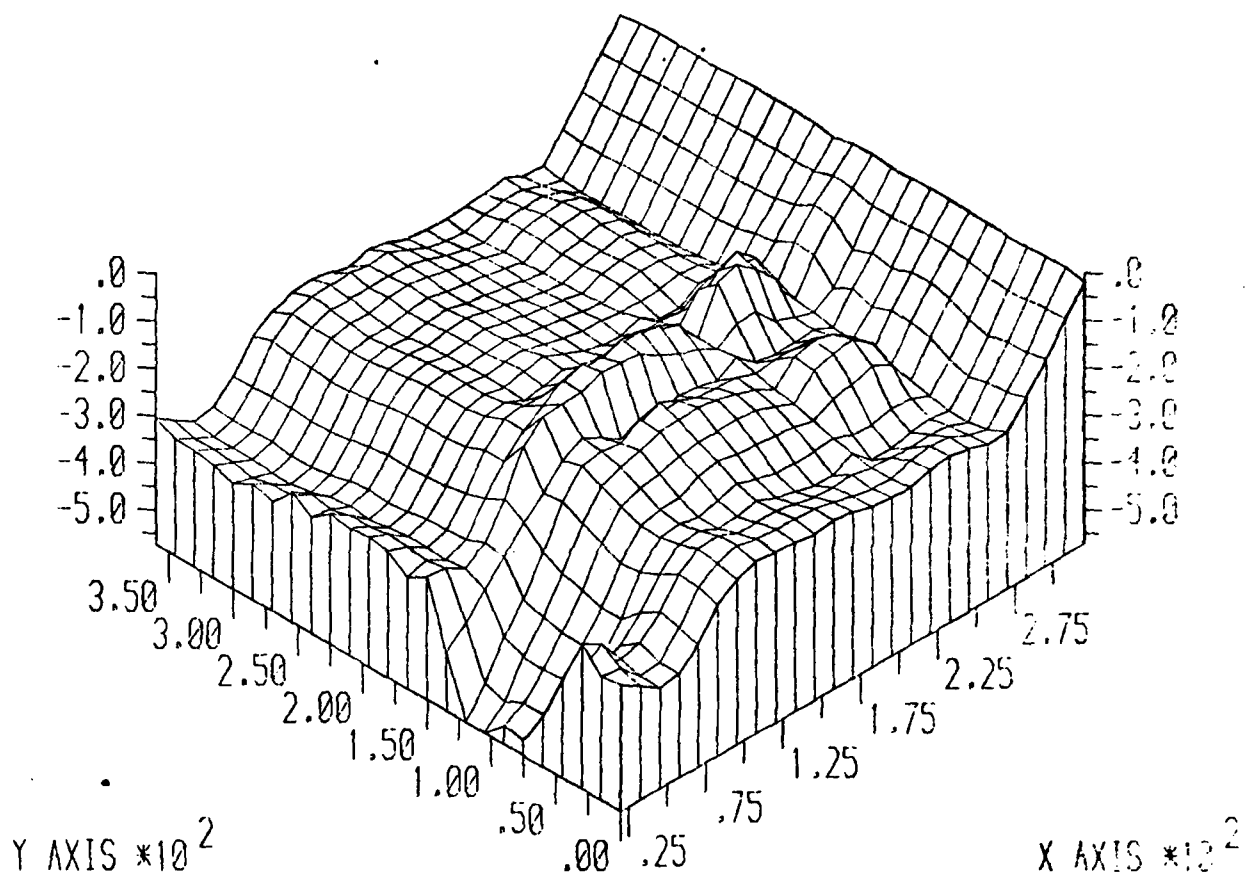


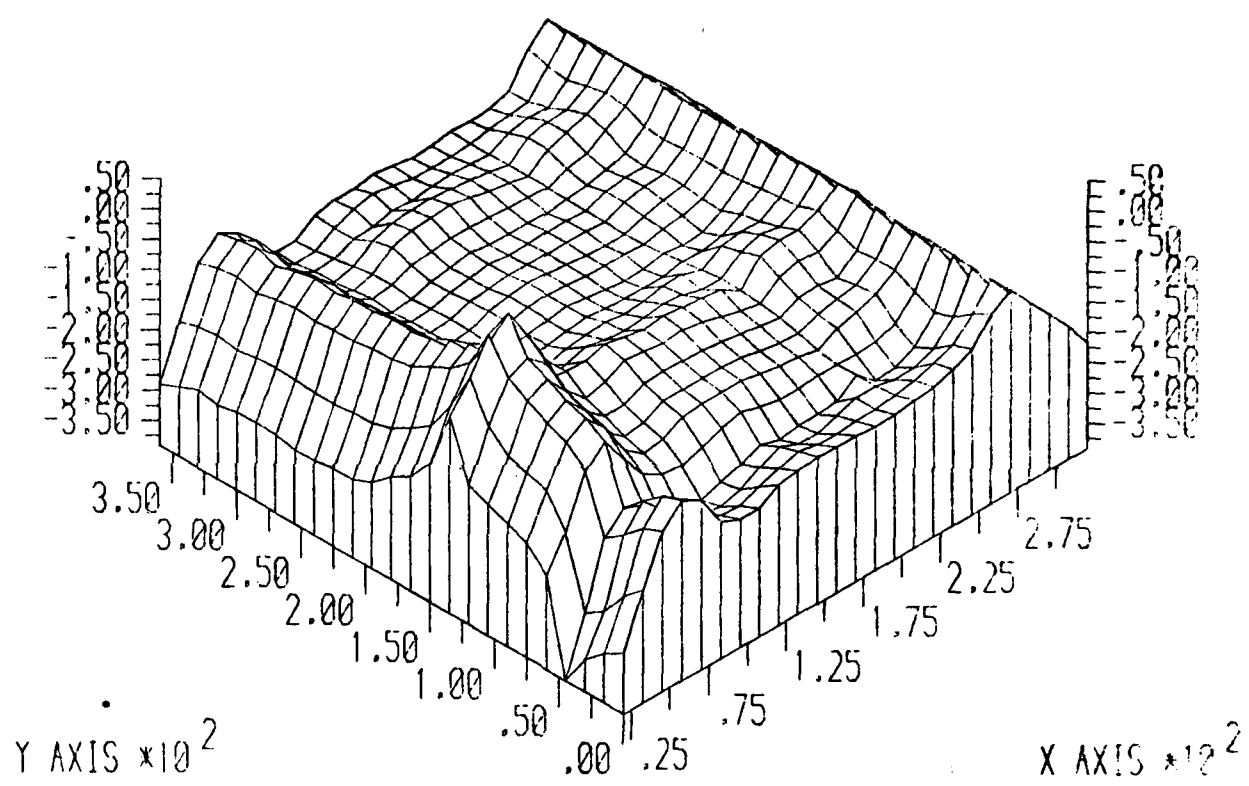
FIG. 17a



90° SQ. WAVE TEST @ 1250 RPM FLOW RATE NO-2

SUCTION SURFACE PRESSURE DISTRIBUTION

FIG. 17b

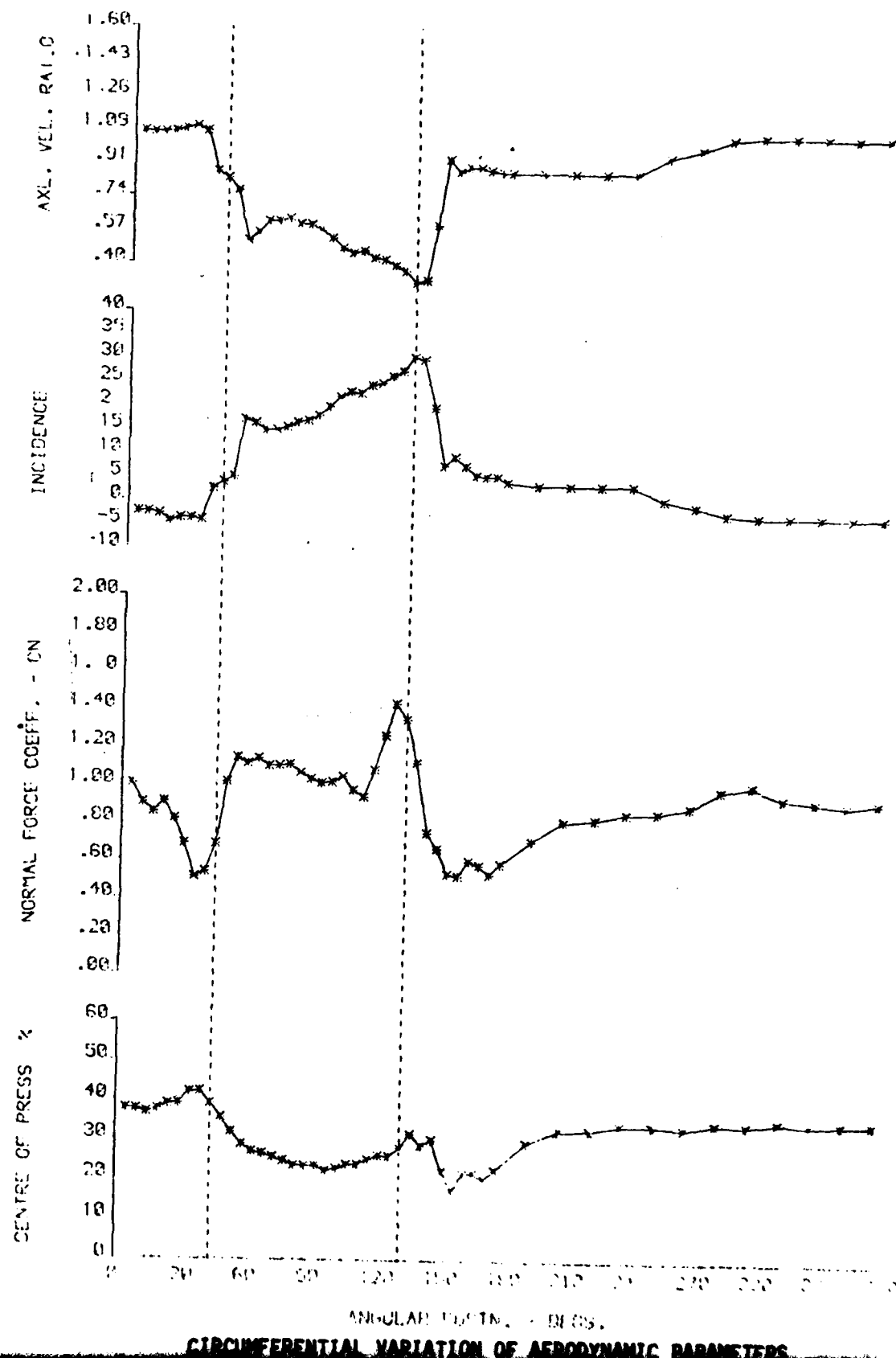


90° SQ.WAVE TEST @ 1250 RPM FLOW RATE NO=2

PRESSURE SURFACE PRESSURE DISTRIBUTION

FIG. 17c

PREDICTION OF AEROFOILS CLOSE TO SQUARE WAVE IN JEN TEST 7



CIRCUMFERENTIAL VARIATION OF AERODYNAMIC PARAMETERS

FIG. 17d

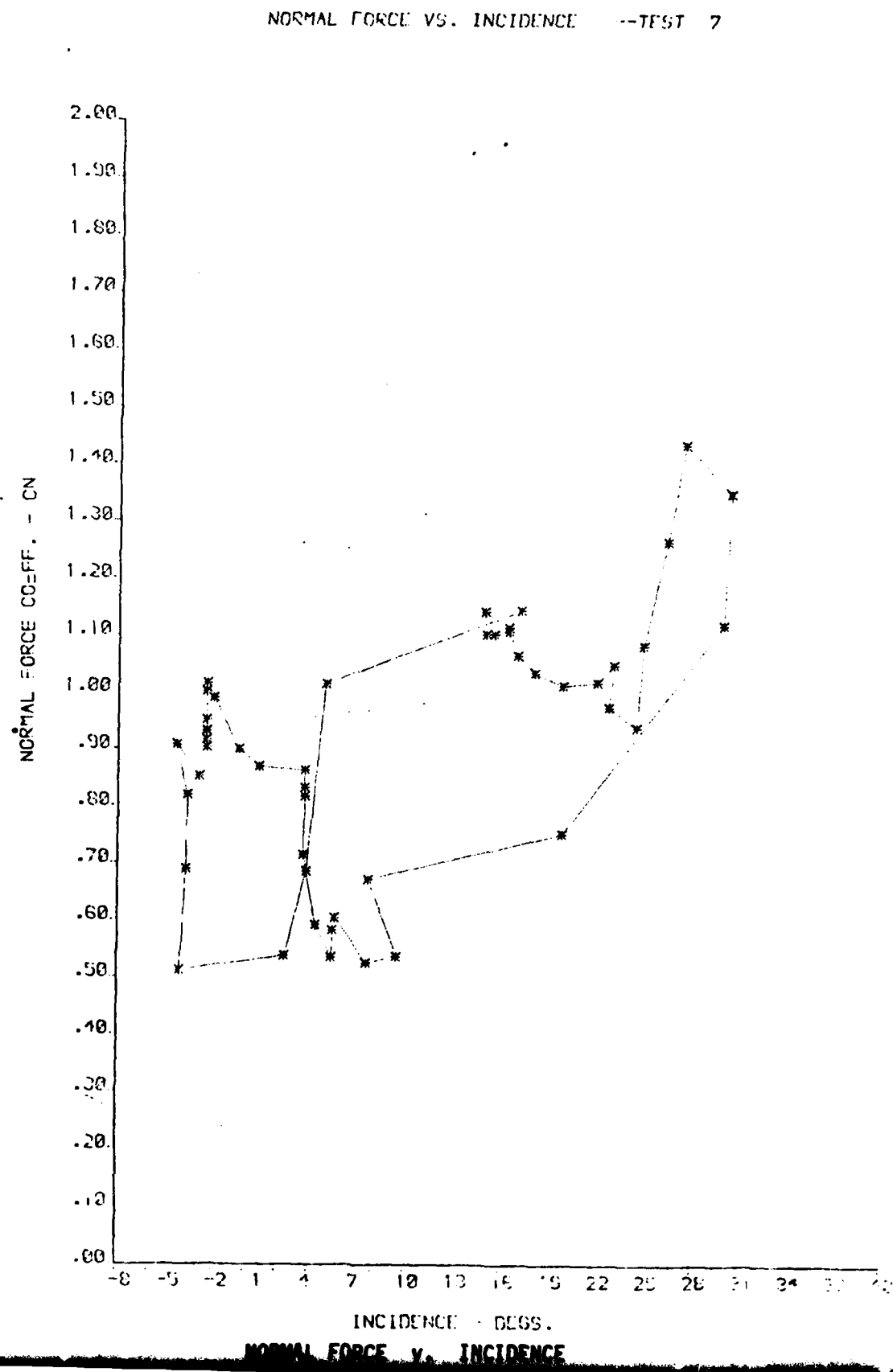
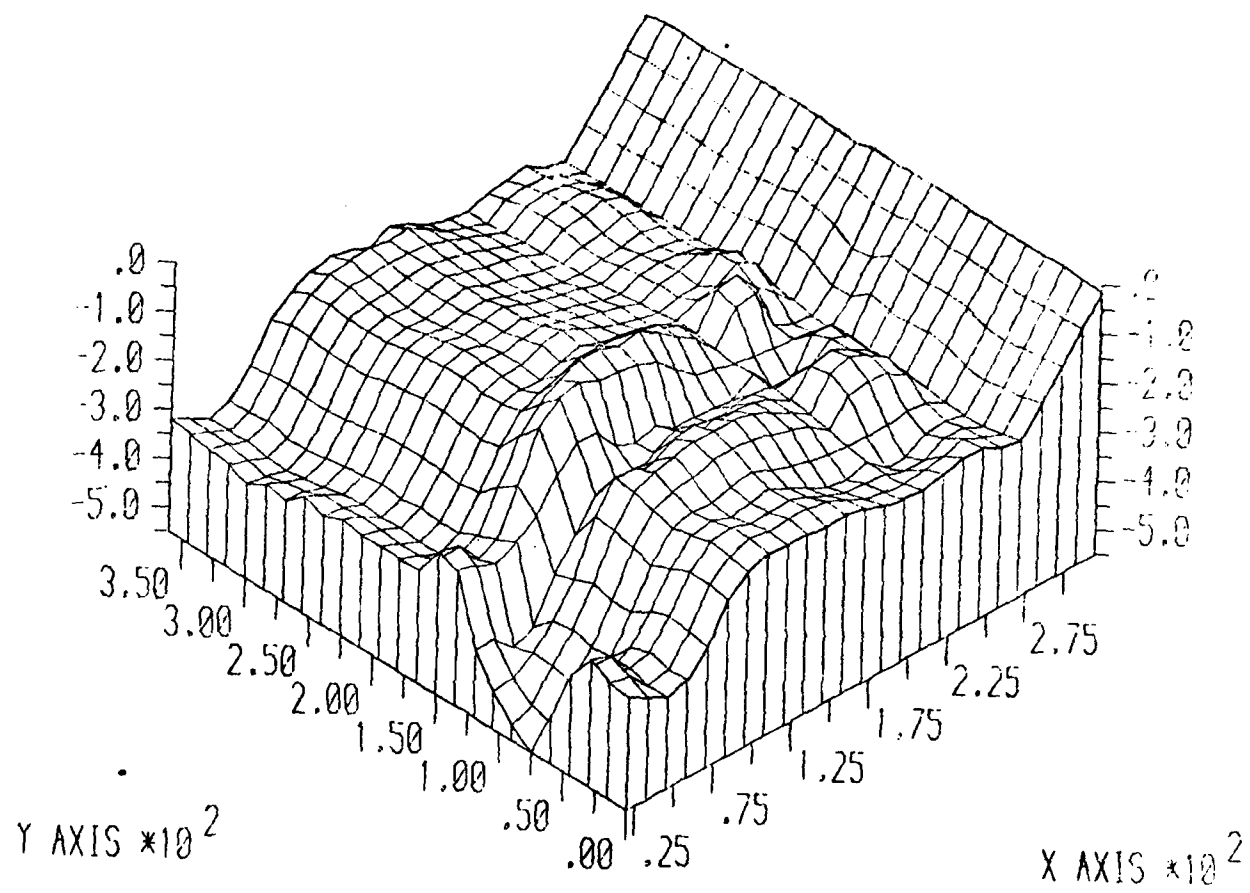


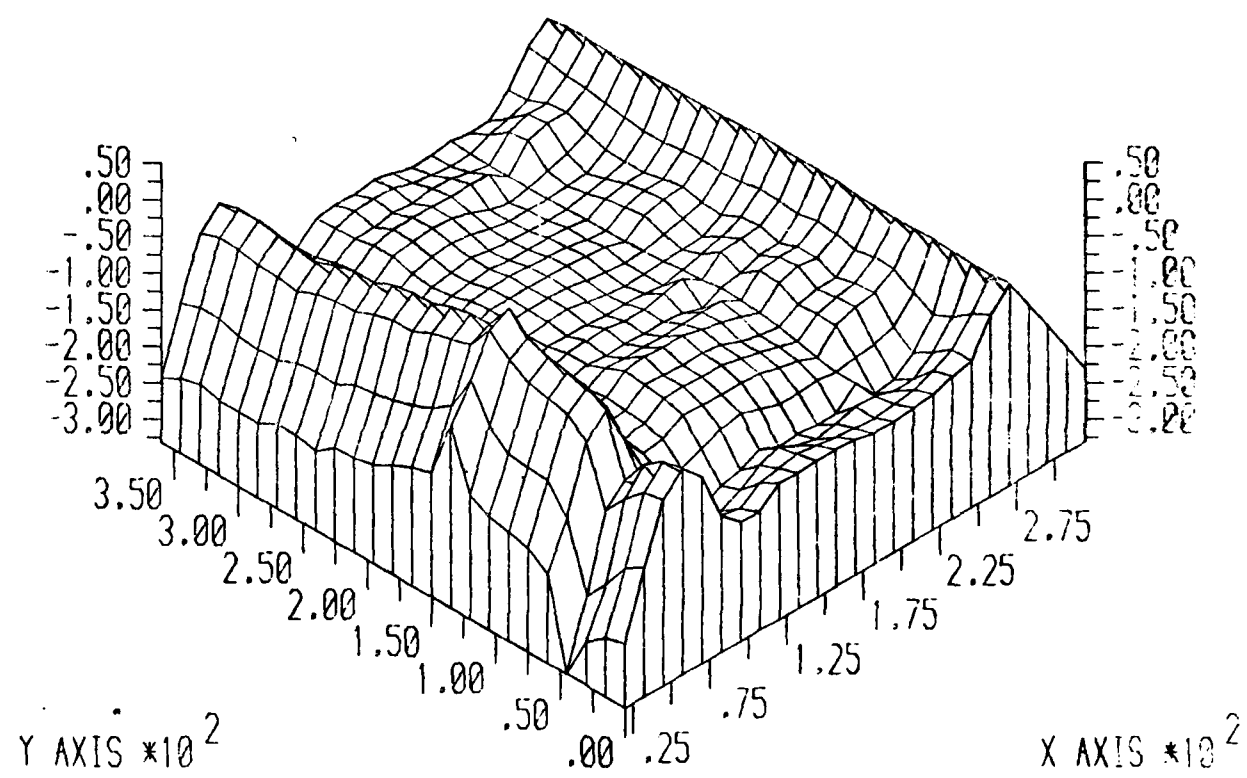
FIG. 18a



90° SQ. WAVE TEST @ 1250 RPM FLOW RATE NO=3

SURCTION SURFACE PRESSURE DISTRIBUTION

FIG. 18b



90° SQ. WAVE TEST @ 1250 RPM FLOW RATE NO=3

PRESSURE SURFACE PRESSURE DISTRIBUTION

FIG. 18c

ROTOR RESPONSE TO SQUARE WAVE SCREEN - TEST 8

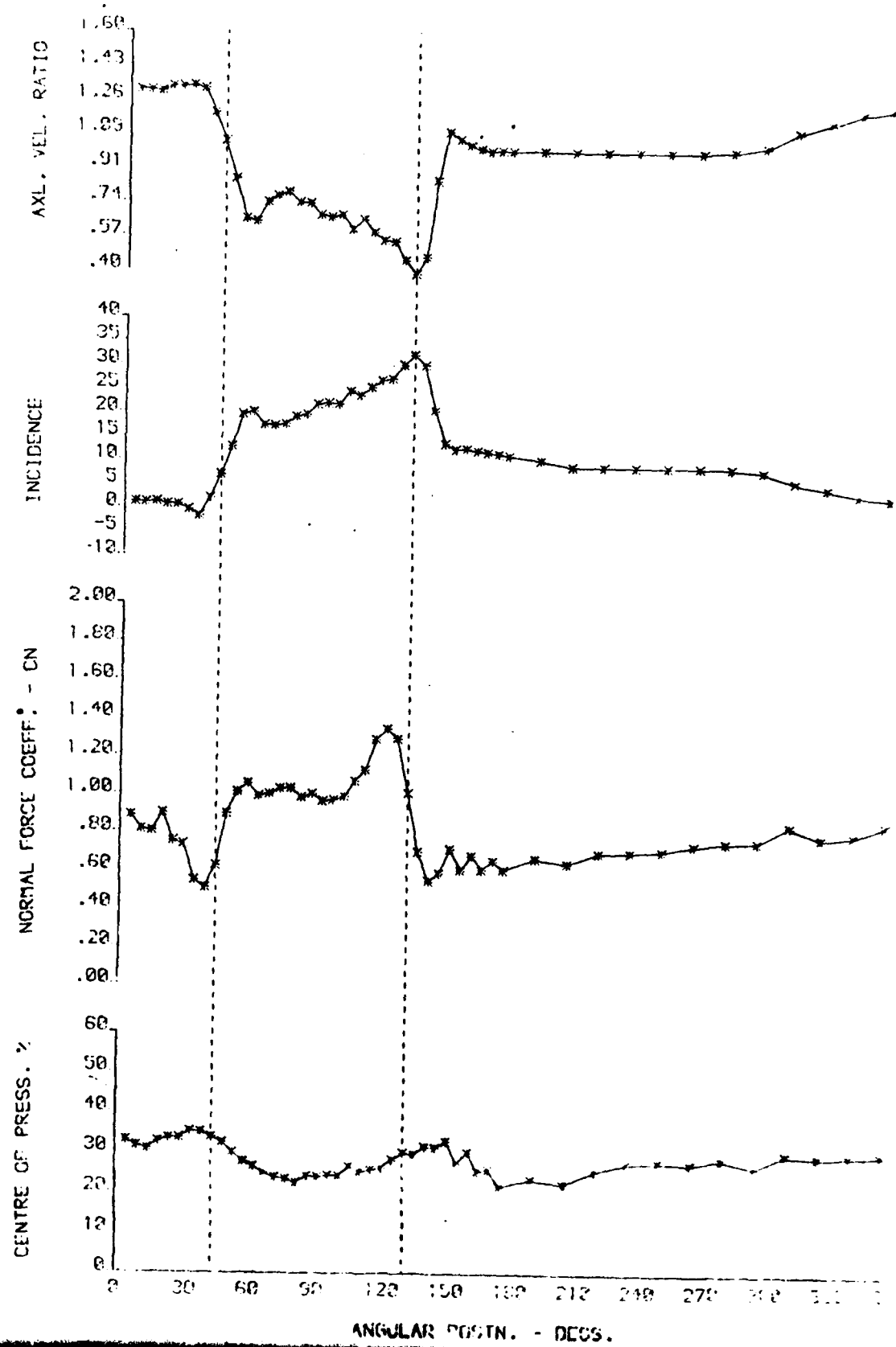
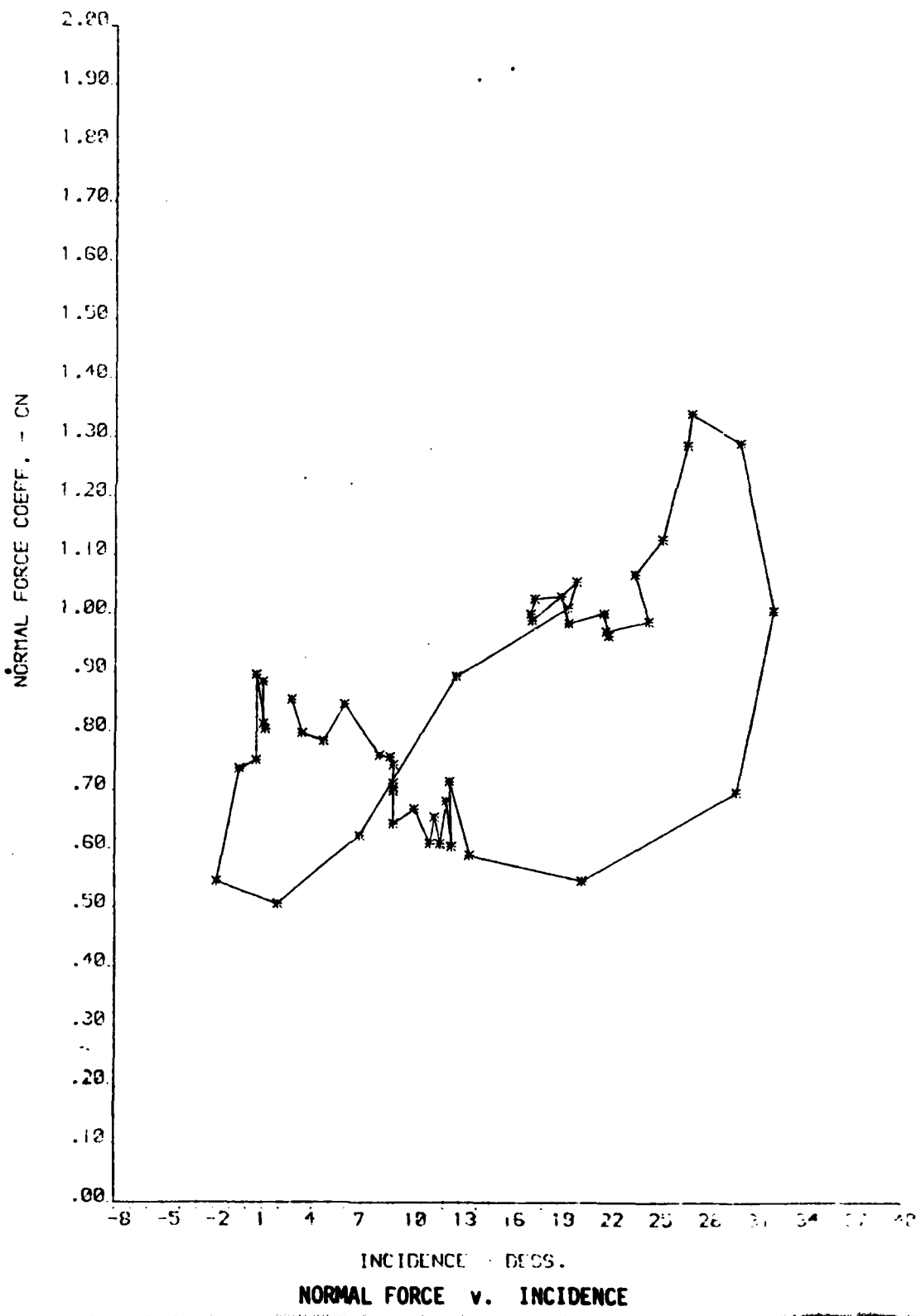


FIG. 18d

NORMAL FORCE VS. INCIDENCE -- TEST 8



AD-A102 330

CRANFIELD INST OF TECH (ENGLAND) SCHOOL OF MECHANICA--ETC F/6 13/7
UNSTEADY EFFECTS OF CIRCUMFERENTIAL PRESSURE DISTORTED INLET FL--ETC(U)
JUN 81 R E PEACOCK AFOSR-77-3305

UNCLASSIFIED

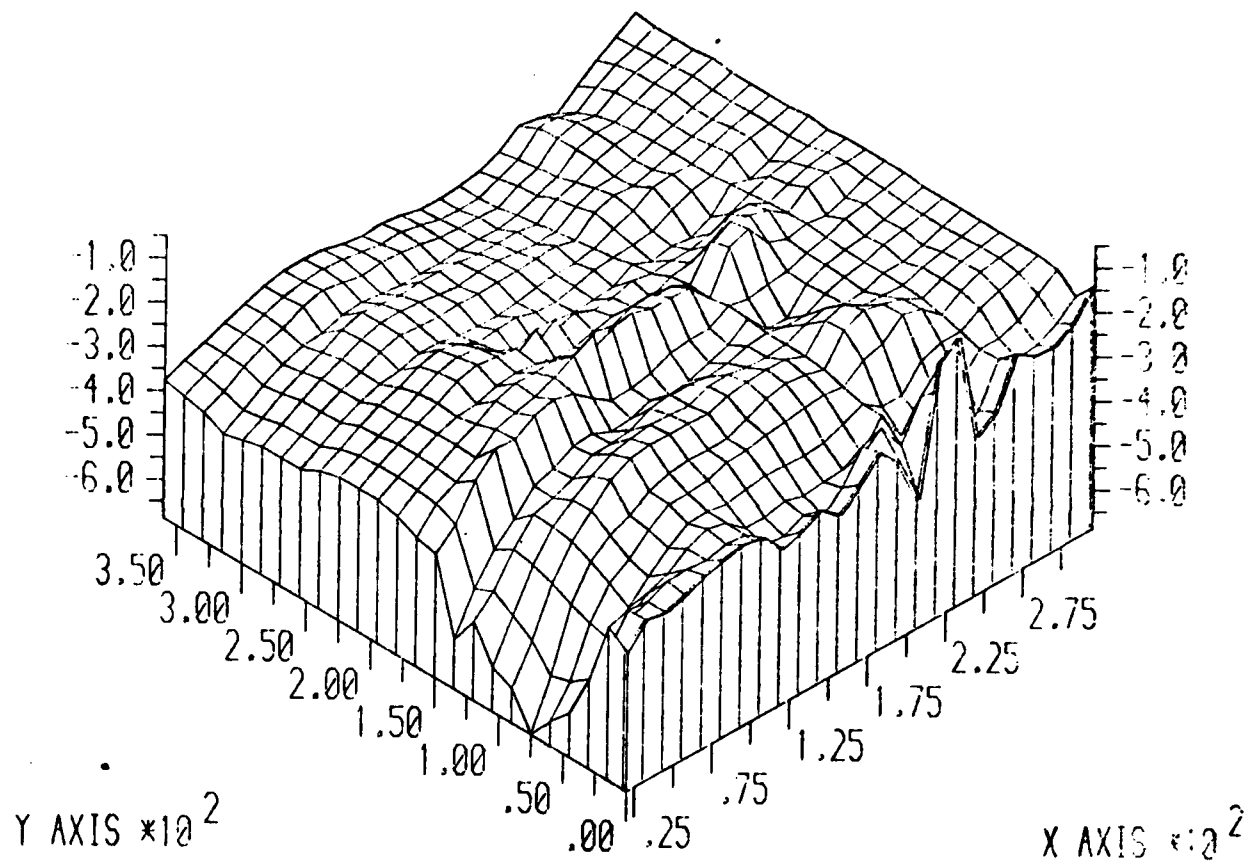
AFOSR-TR-81-0604

NL

2 of 2
AFOSR-77-3305

END
DATE
FILED
5-82
DTIC

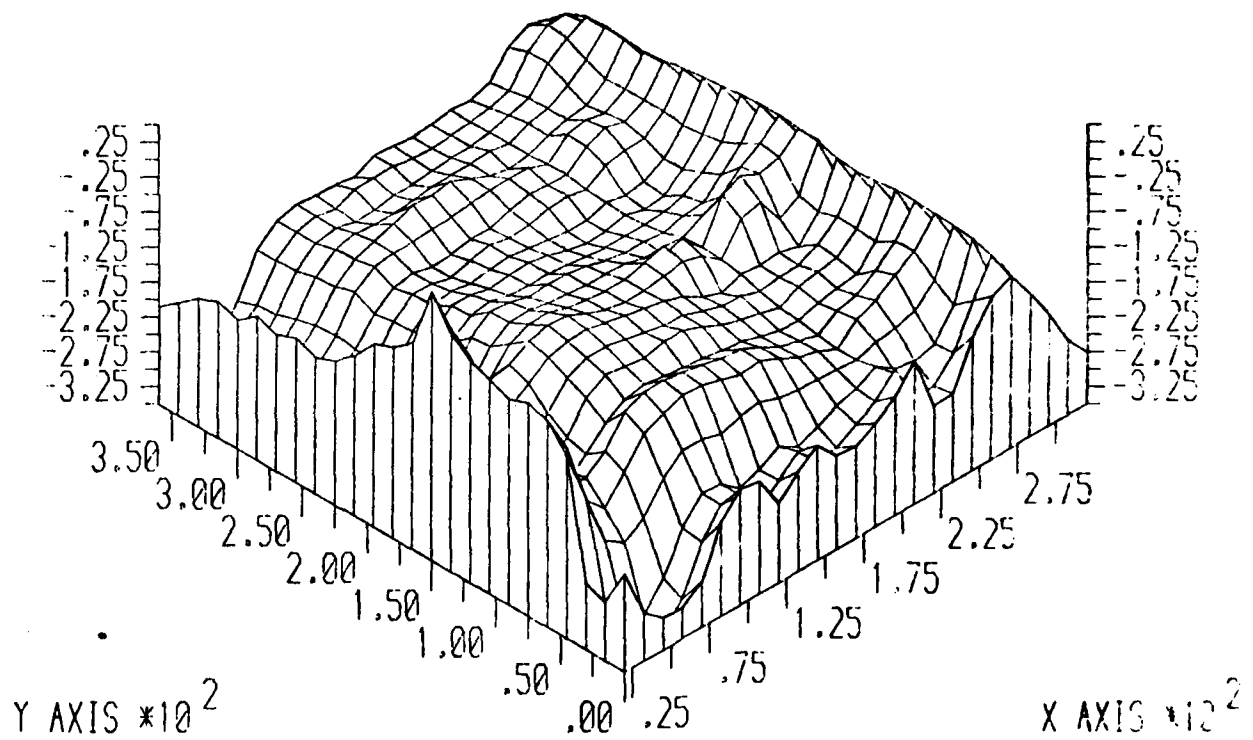
FIG. 19a



120' SQ. WAVE TEST 1000 RPM FLOW RATE NO-1

SUCTION SURFACE PRESSURE DISTRIBUTION

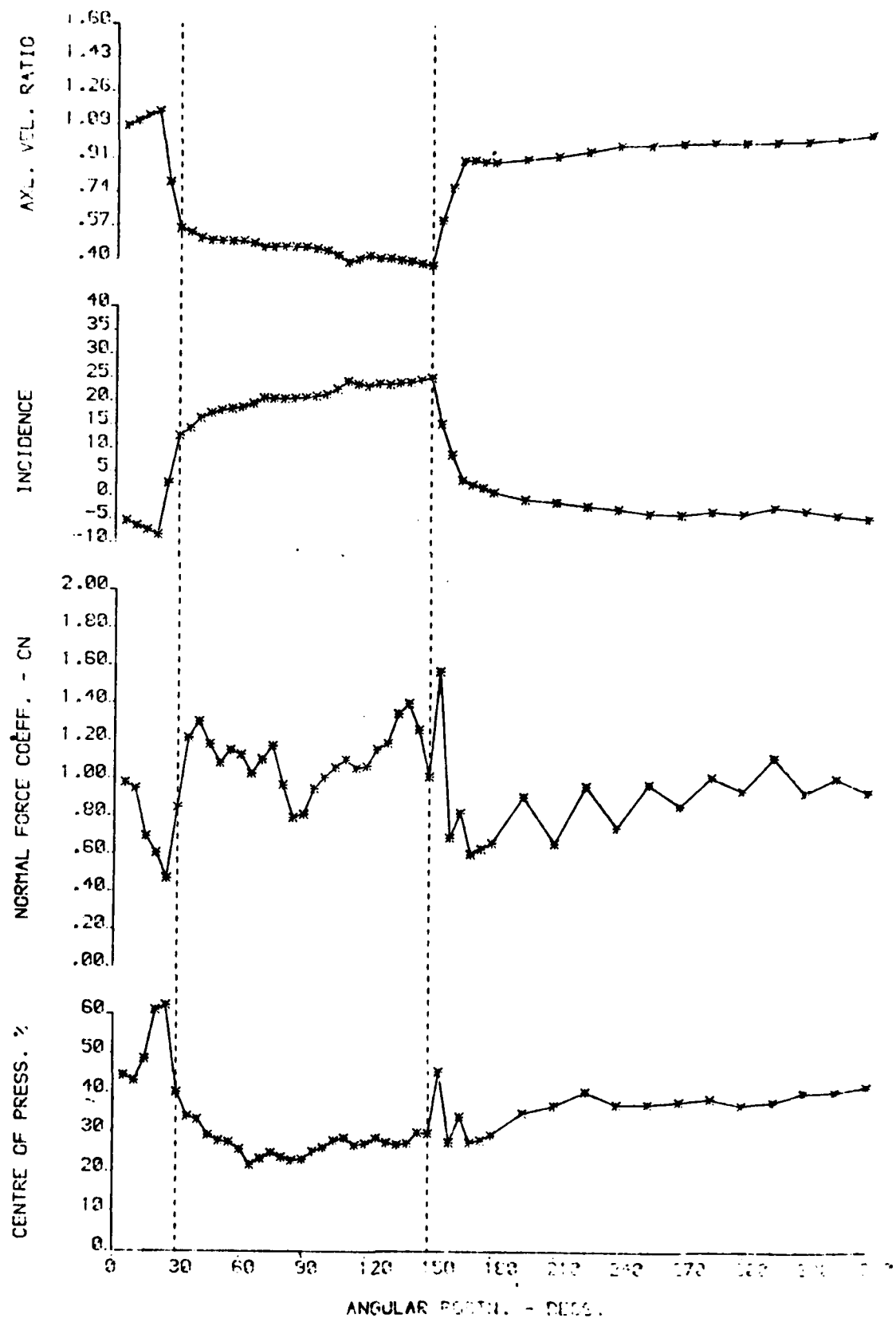
FIG. 19b



120° SQ. WAVE TEST 1000 RPM FLOW RATE NO: 1

PRESSURE SURFACE PRESSURE DISTRIBUTION

FIG. 19c
ROTOR RESPONSE TO SQUARE WAVE SCREEN -- TEST 1



NORMAL FORCE VS. INCIDENCE --TEST 1

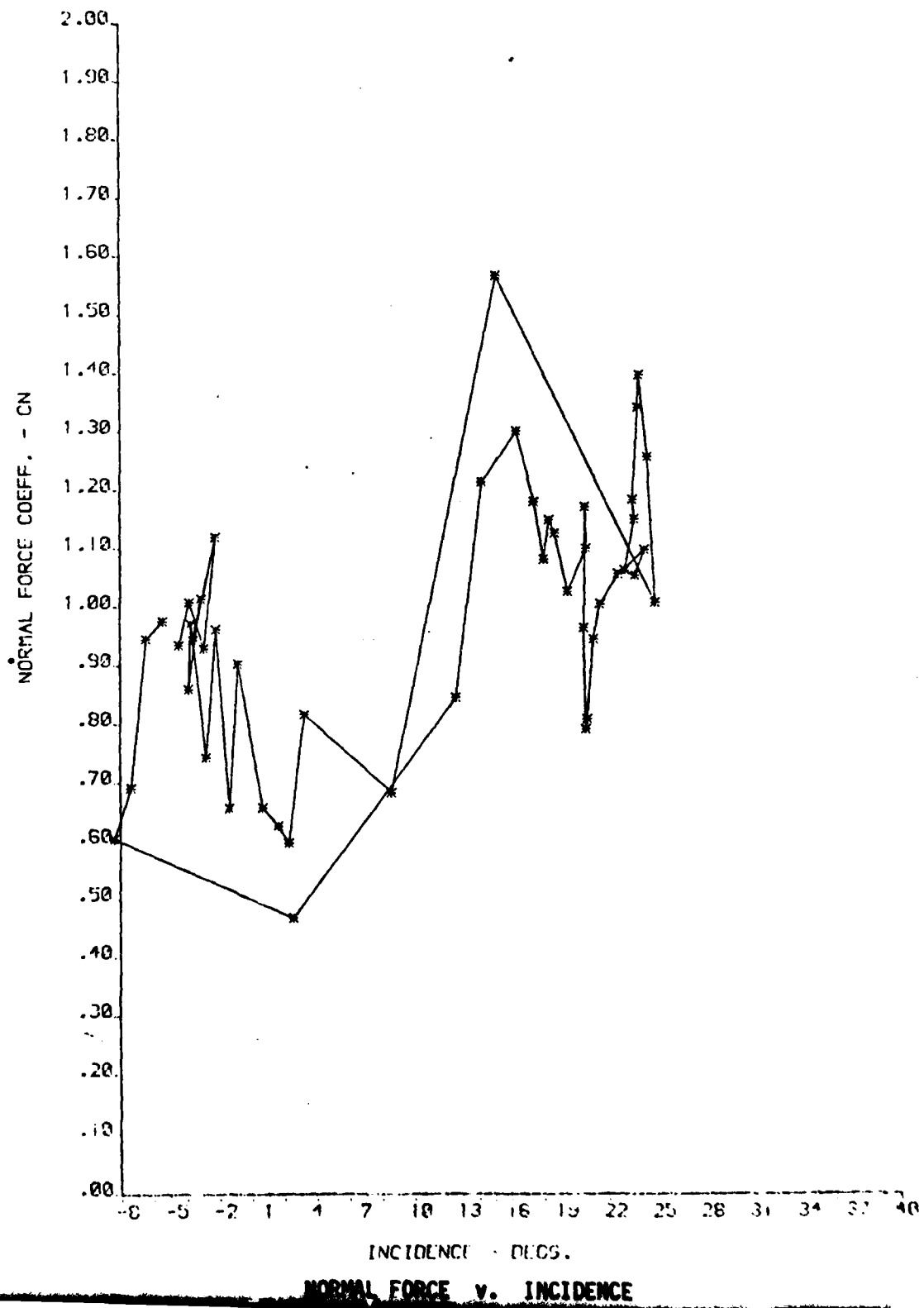
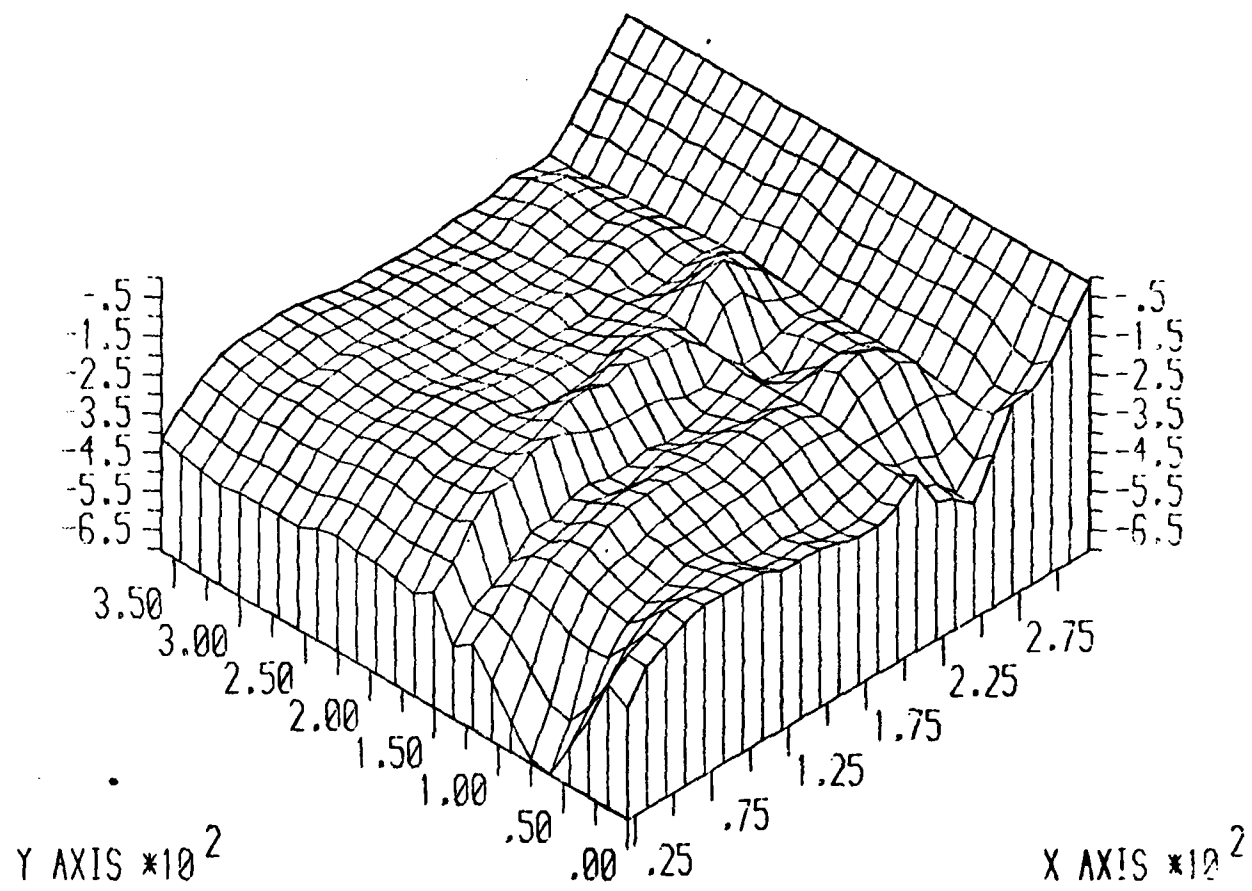


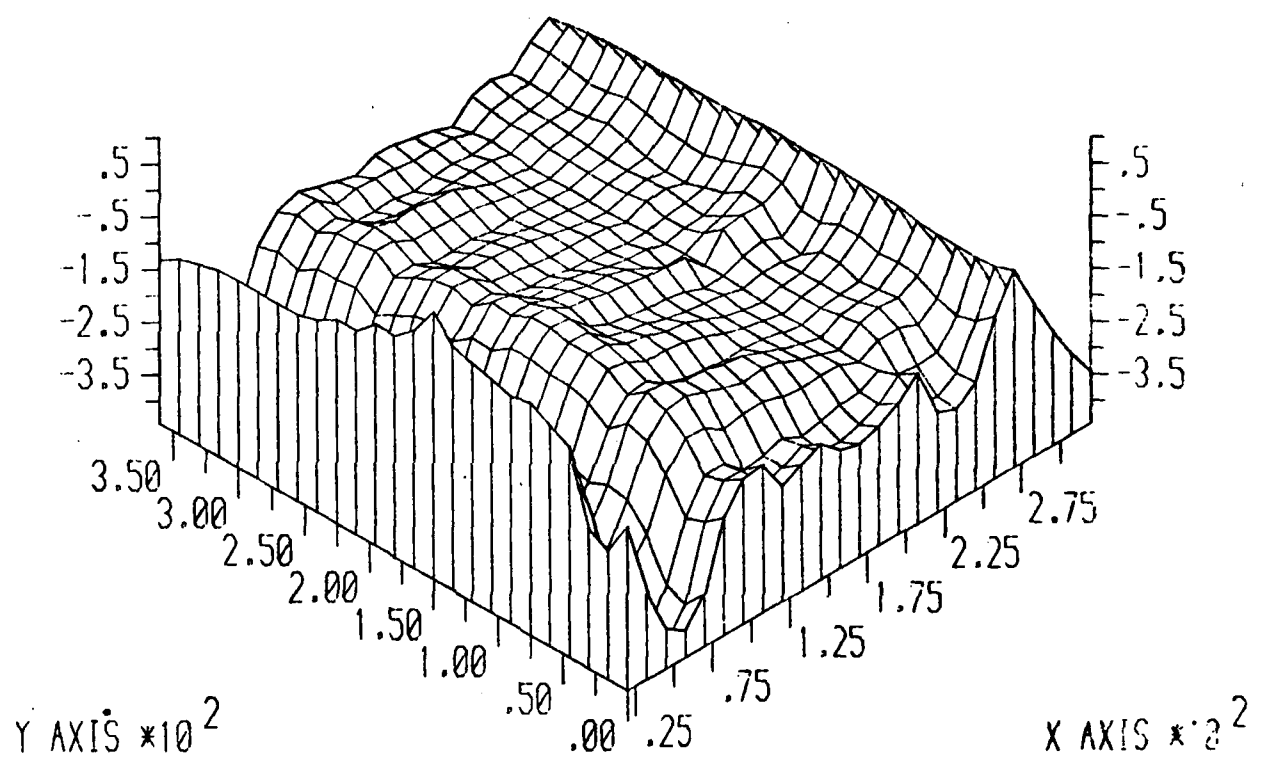
FIG. 20a



120° SQ. WAVE TEST @ 1000 RPM FLOW RATE NO=2

SUCTION SURFACE PRESSURE DISTRIBUTION

FIG. 20b



120° SQ. WAVE TEST @ 1000 RPM FLOW RATE NO=2
PRESSURE SURFACE PRESSURE DISTRIBUTION

FIG. 20c

ROTOR RESPONSE TO SQUARE WAVE SCREEN -- TEST 2

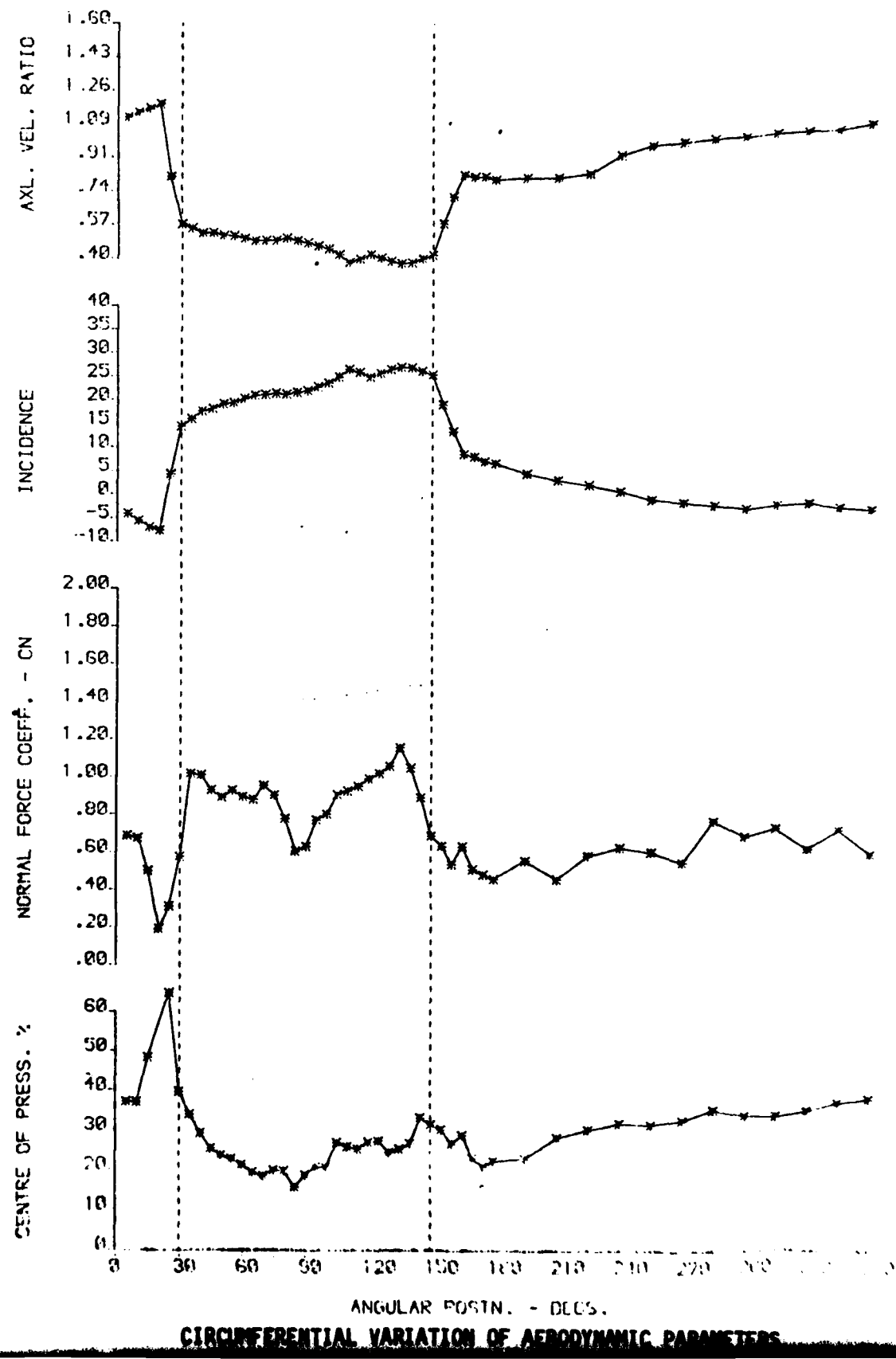


FIG. 20d

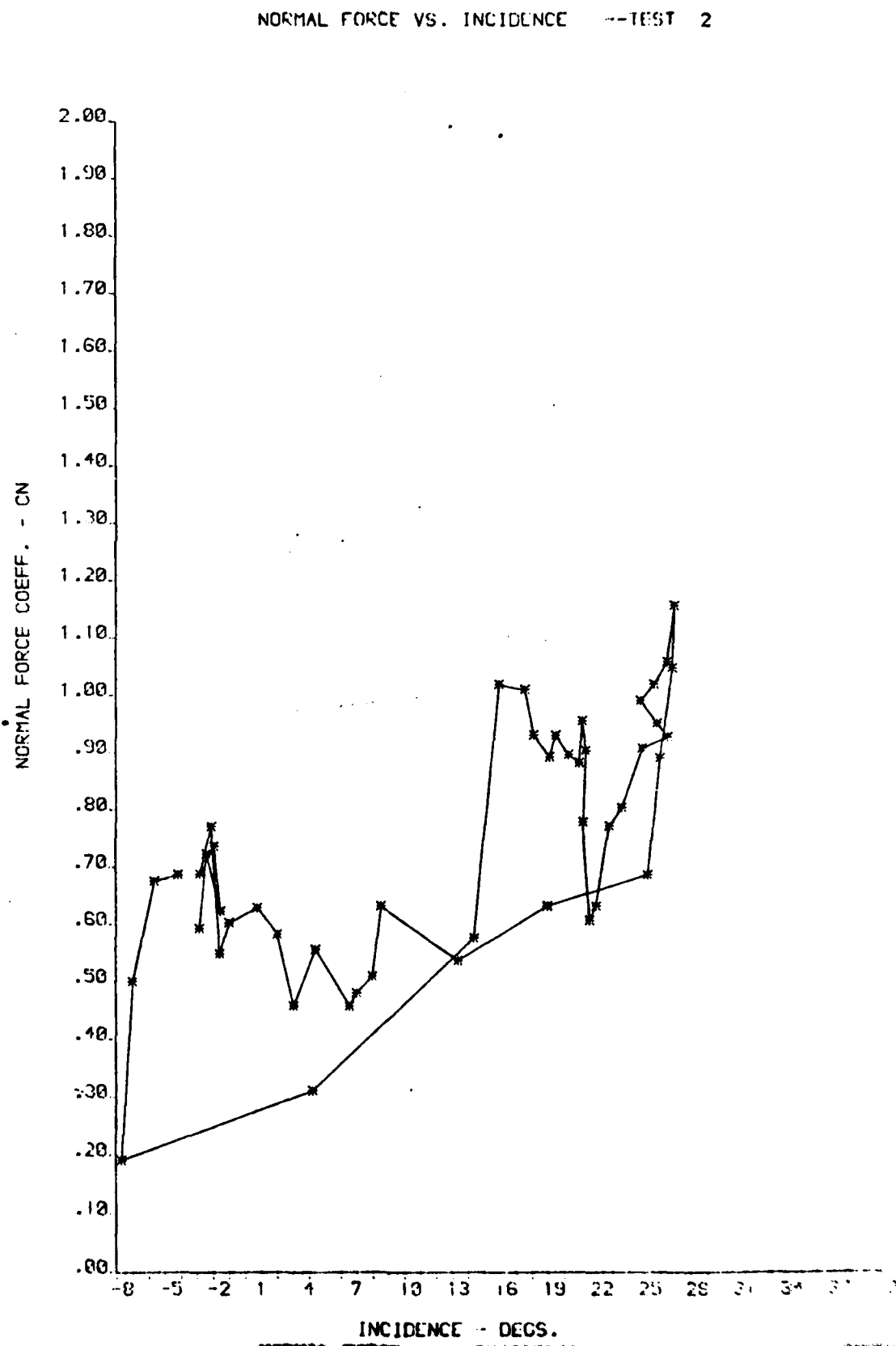
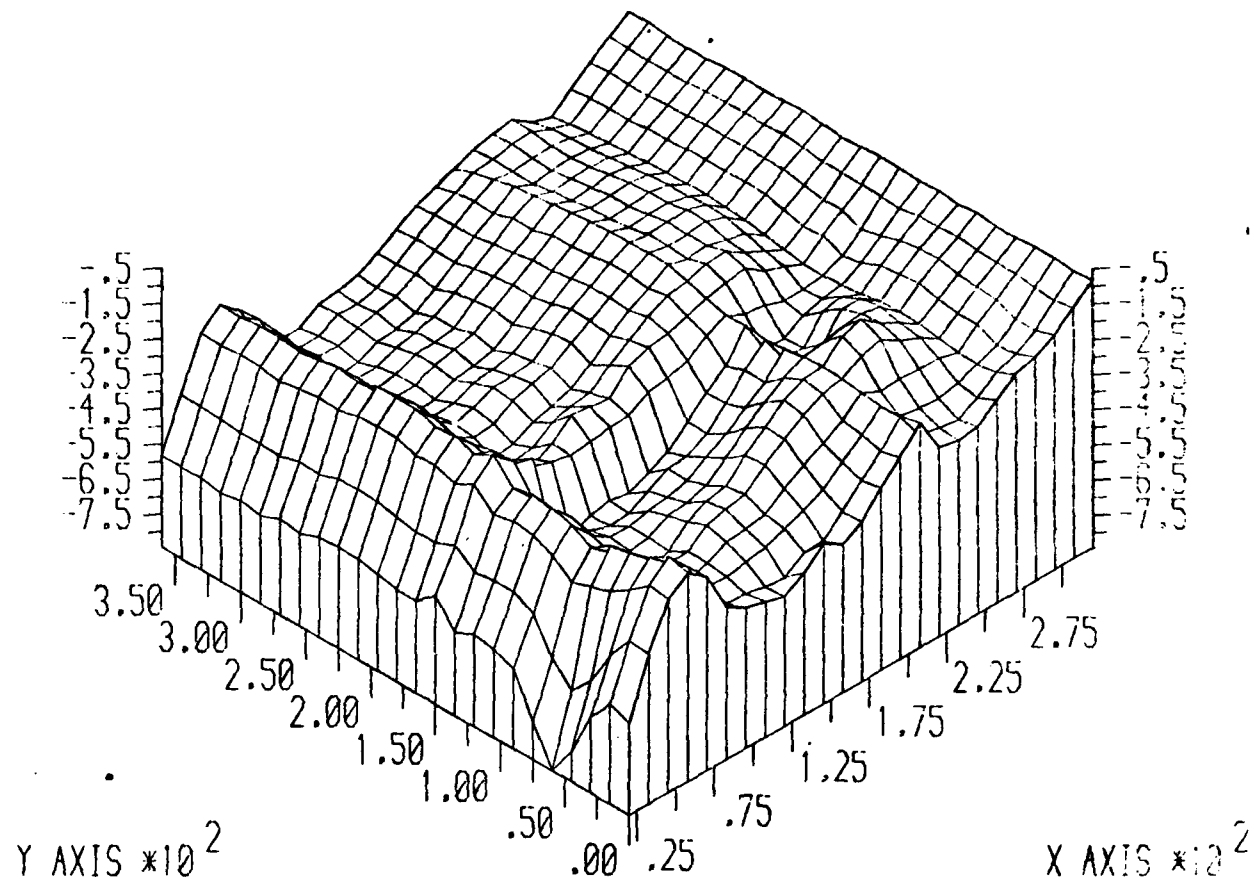


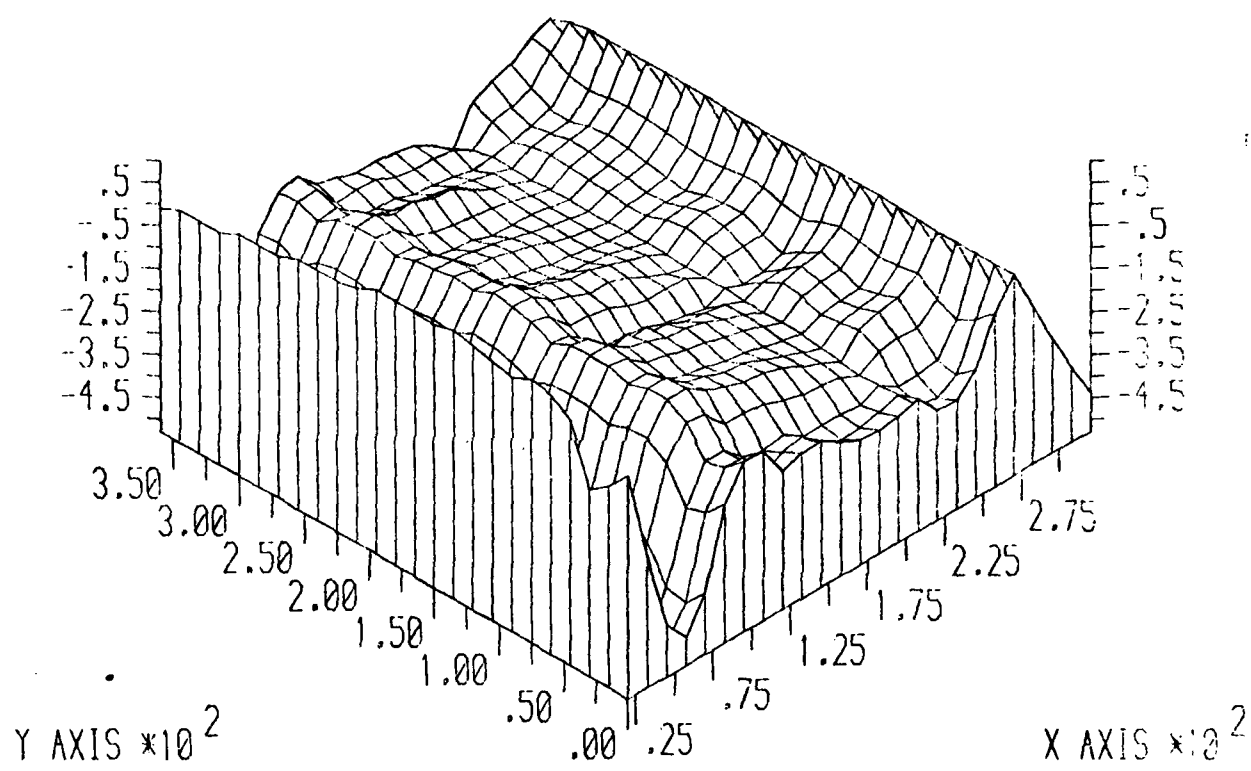
FIG. 21a



120° SQ. WAVE TEST @ 1000 RPM FLOW RATE NO-3

SUCTION SURFACE PRESSURE DISTRIBUTION

FIG 21b

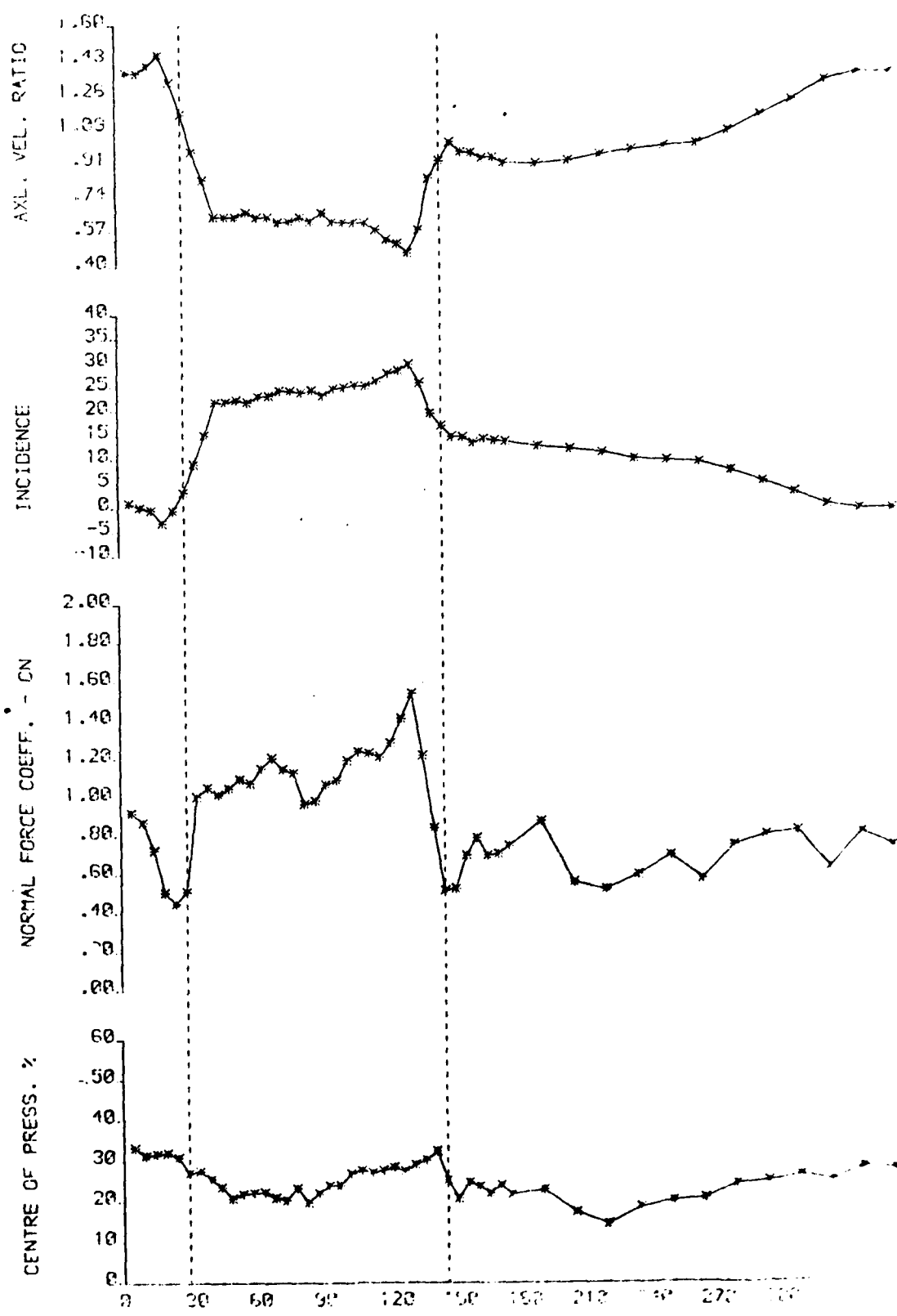


120° SQ. WAVE TEST @ 1000 RPM FLOW RATE NC=3

PRESSURE SURFACE PRESSURE DISTRIBUTION

FIG. 21c

PILLOW RESPONSE TO SQUARE WAVE SCREEN - TEST



NORMAL FORCE VS. INCIDENCE --TEST 3

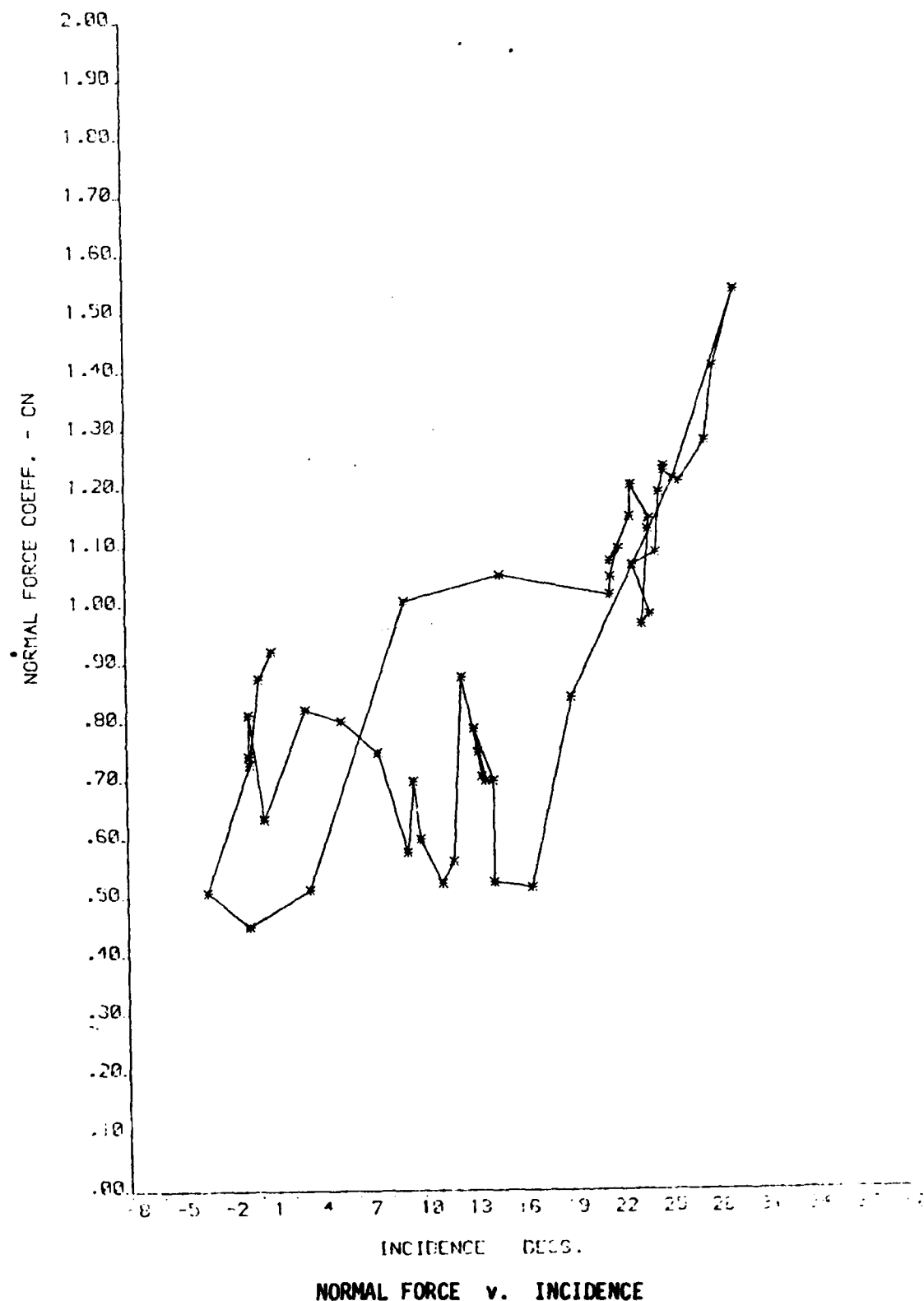
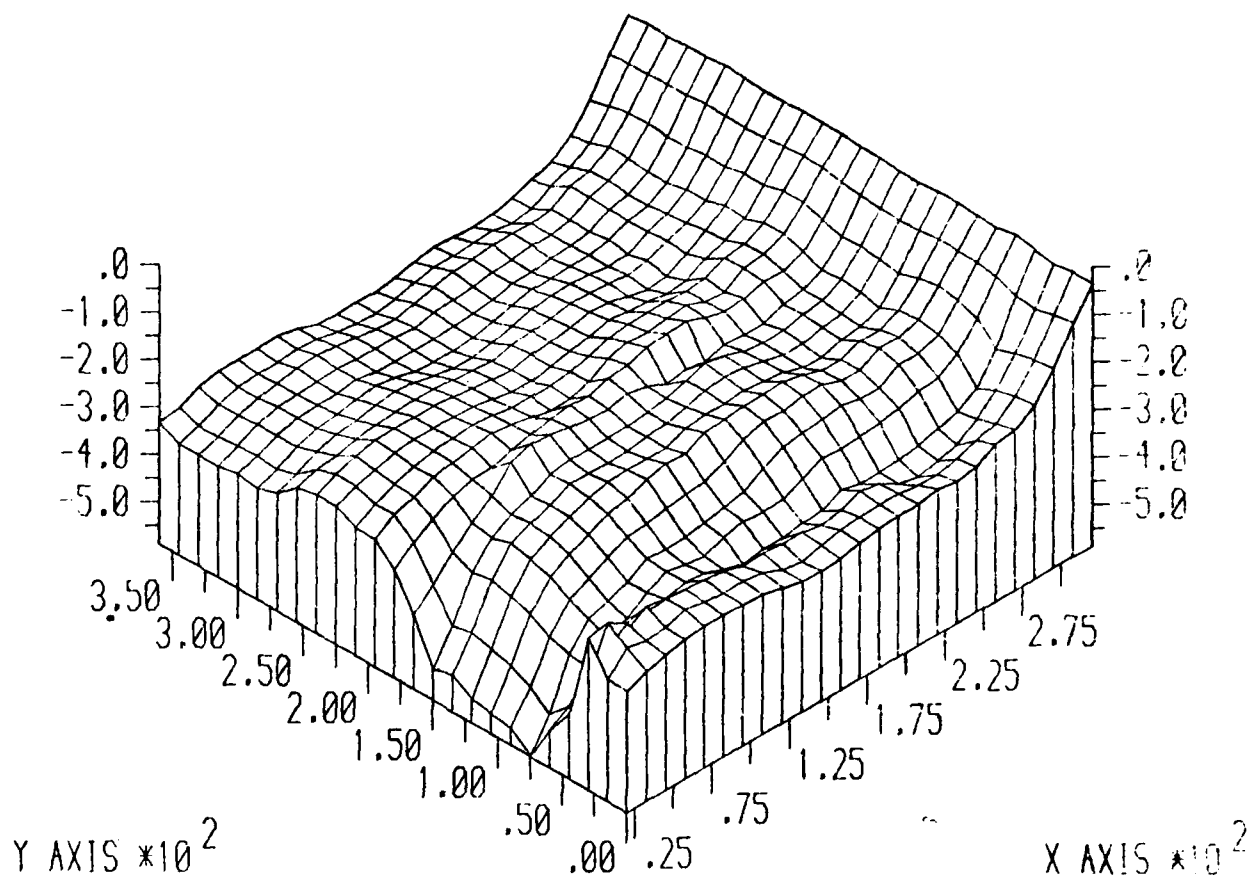
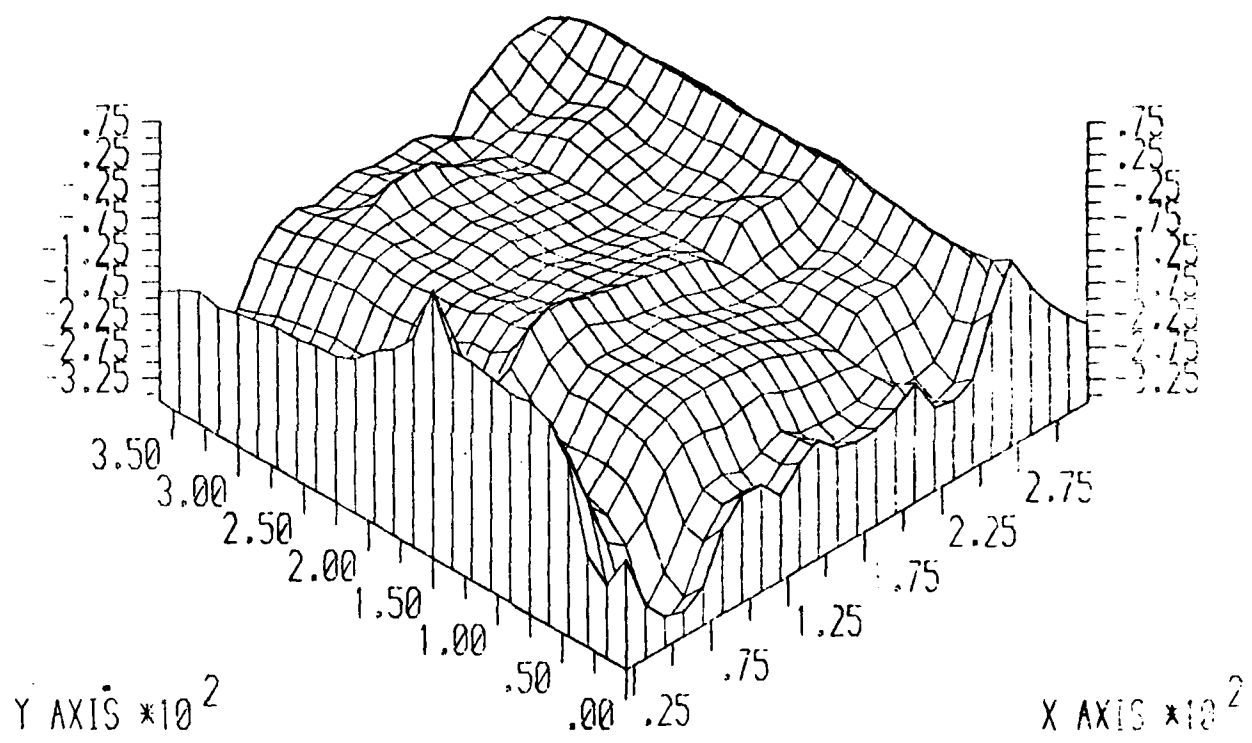


FIG. 22a



120° SQ.WAVE TEST @ 1250 RPM FLOW RATE NO=1
SUCTION SURFACE PRESSURE DISTRIBUTION

FIG. 22b



120° SQ.WAVE TEST @ 1250 RPM FLOW RATE NO=1

PRESSURE SURFACE PRESSURE DISTRIBUTION

FIG. 22c

PULSE RESPONSE TO SQUARE WAVE INPUT - TEST 1

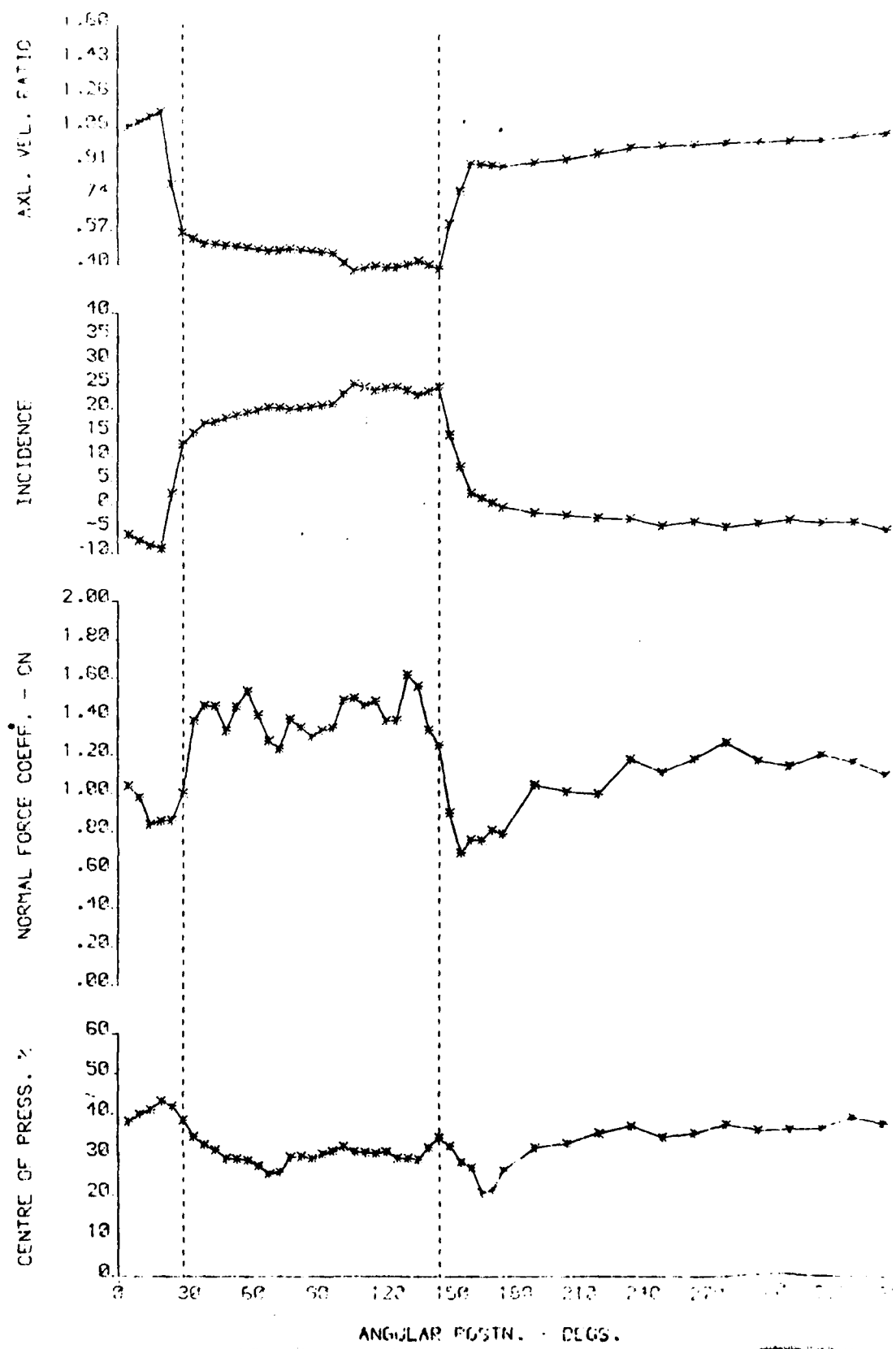


FIG. 22d

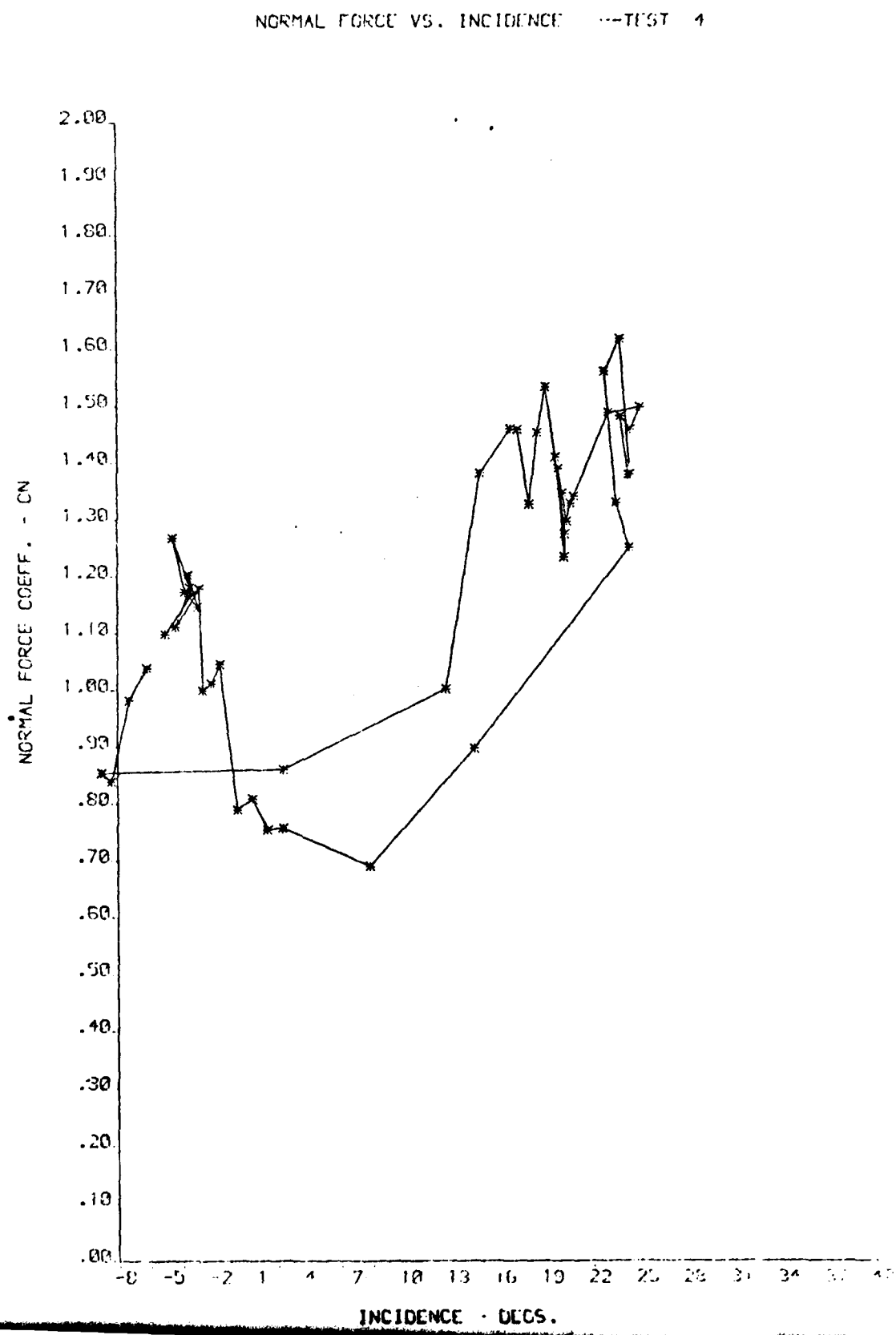
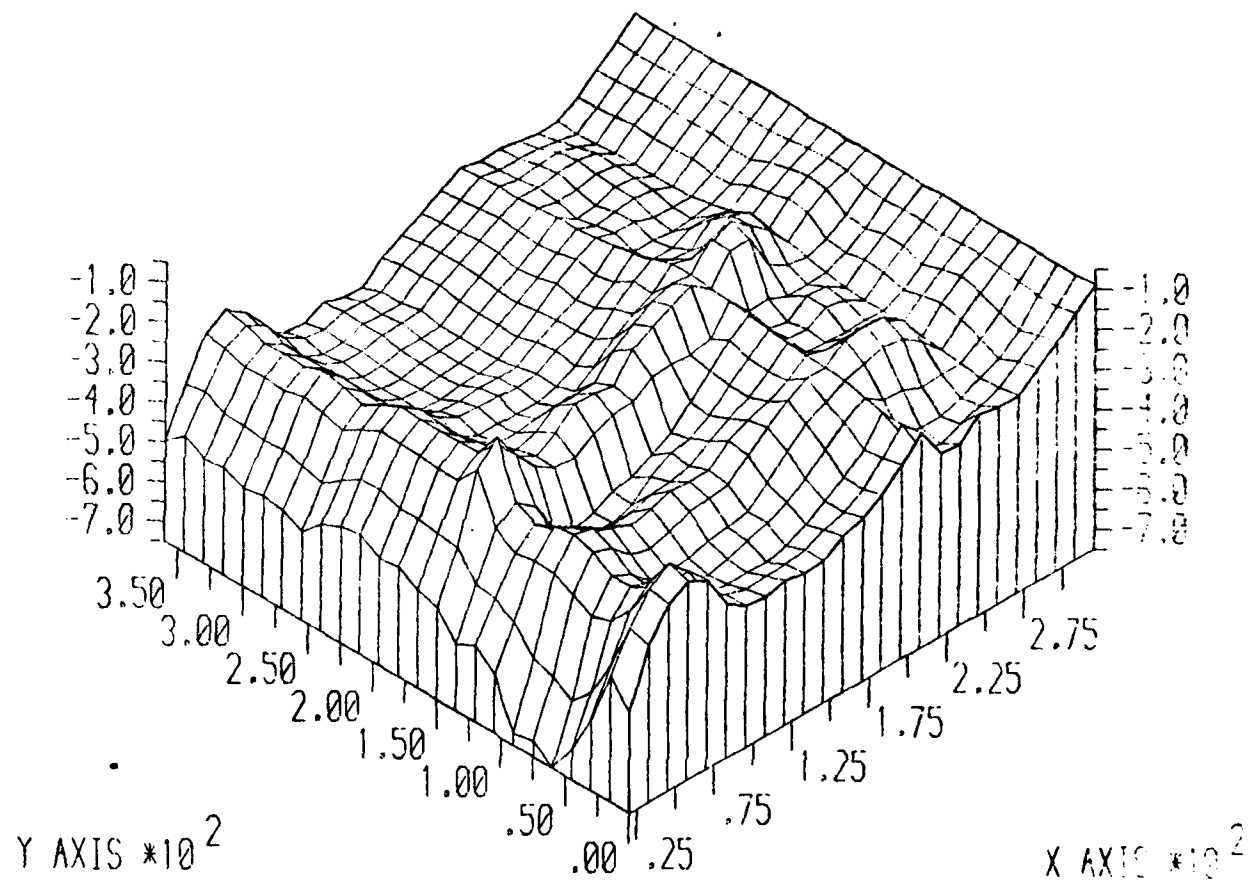


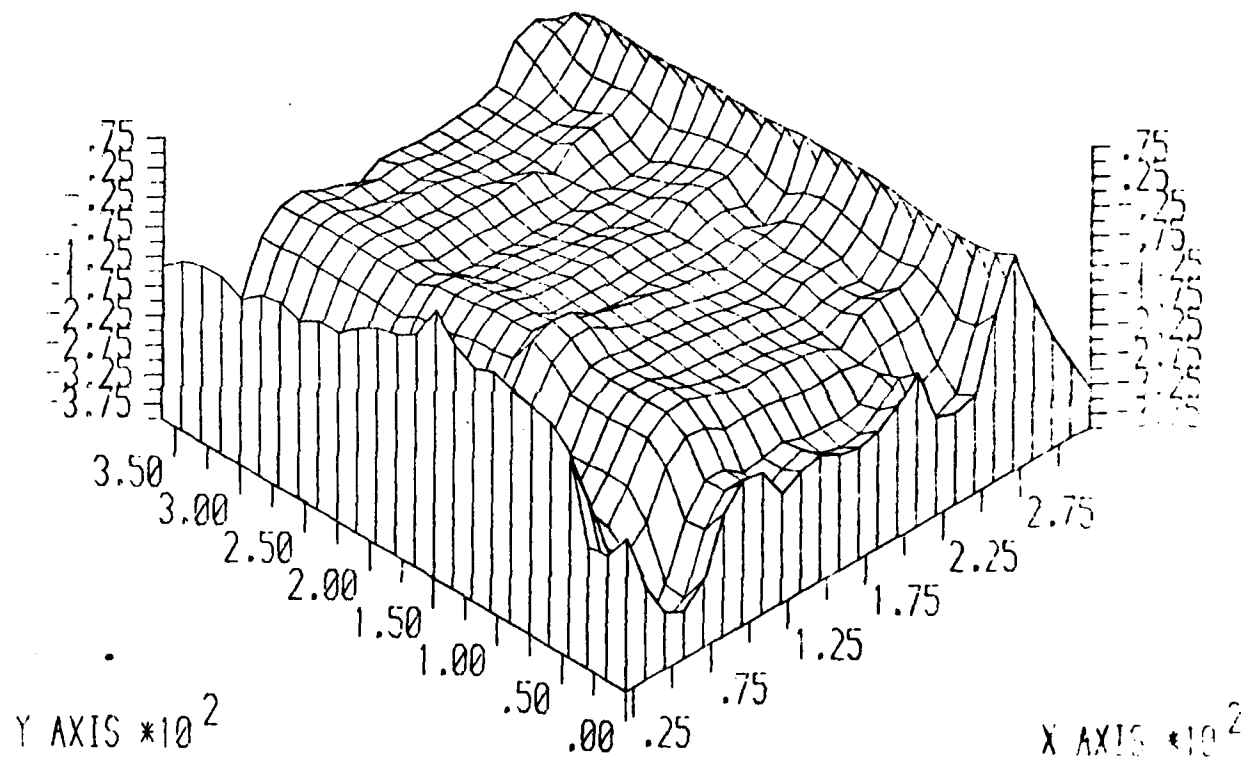
FIG. 23a



120° SO.WA /E TEST @1250 RPM FLOW RATE NO-2

SUCTION SURFACE PRESSURE DISTRIBUTION

FIG. 23b



120° SQ.WA VE TEST @1250 RPM FLOW RATE NO=2

PRESSURE SURFACE PRESSURE DISTRIBUTION

FIG. 23c

ROTOR RESPONSE TO SQUARE WAVE WIRELEN - TEST 5

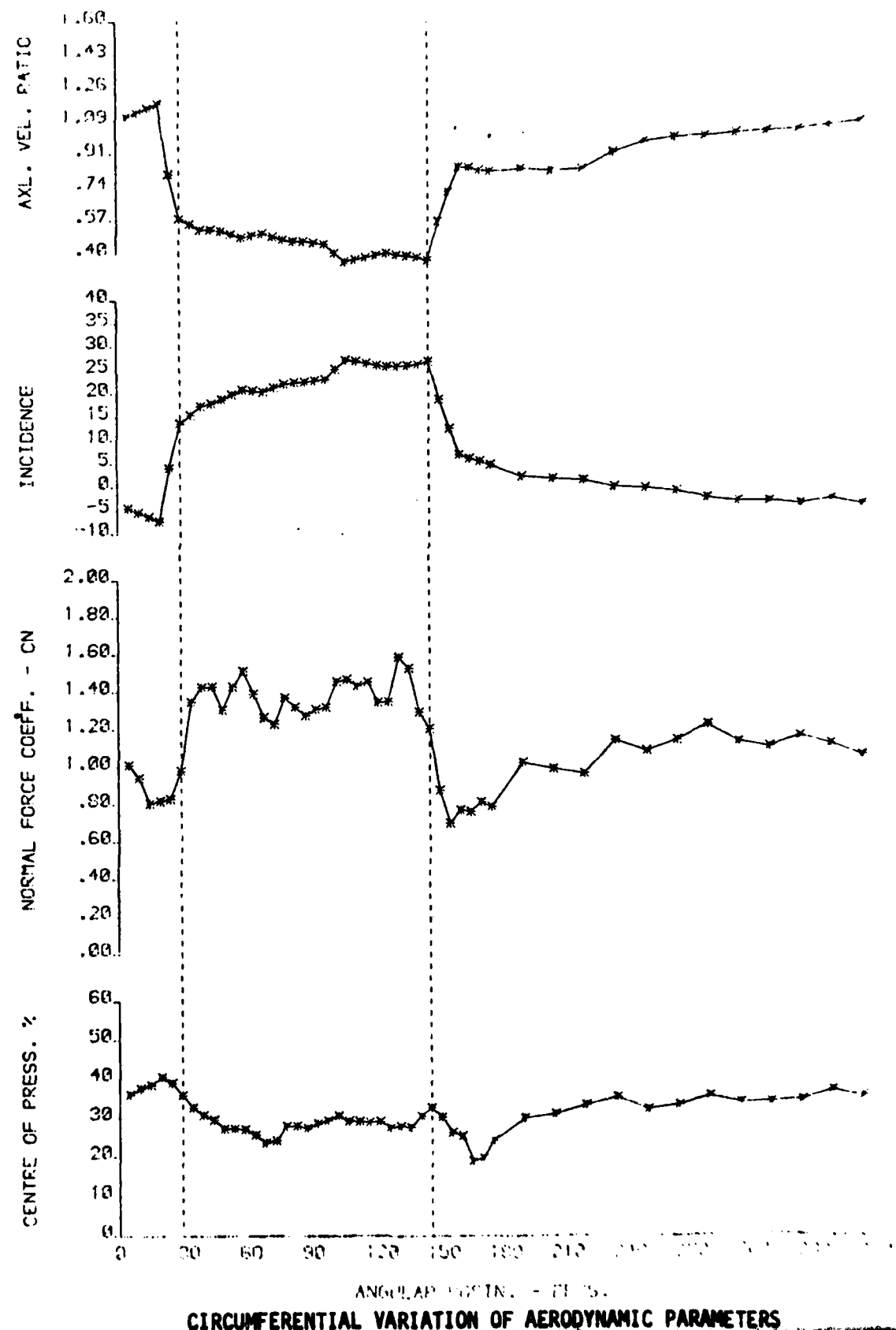


FIG. 23d

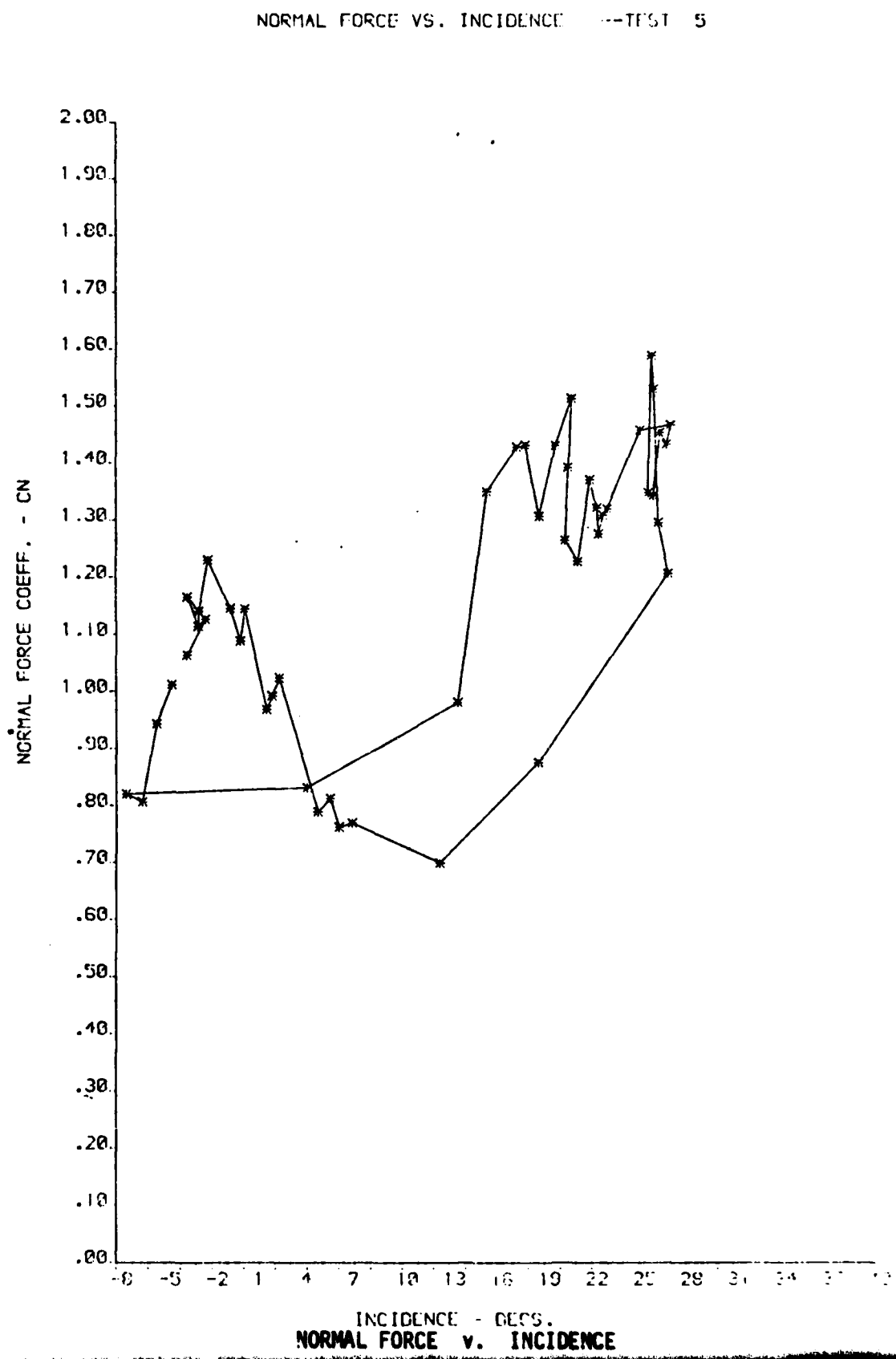
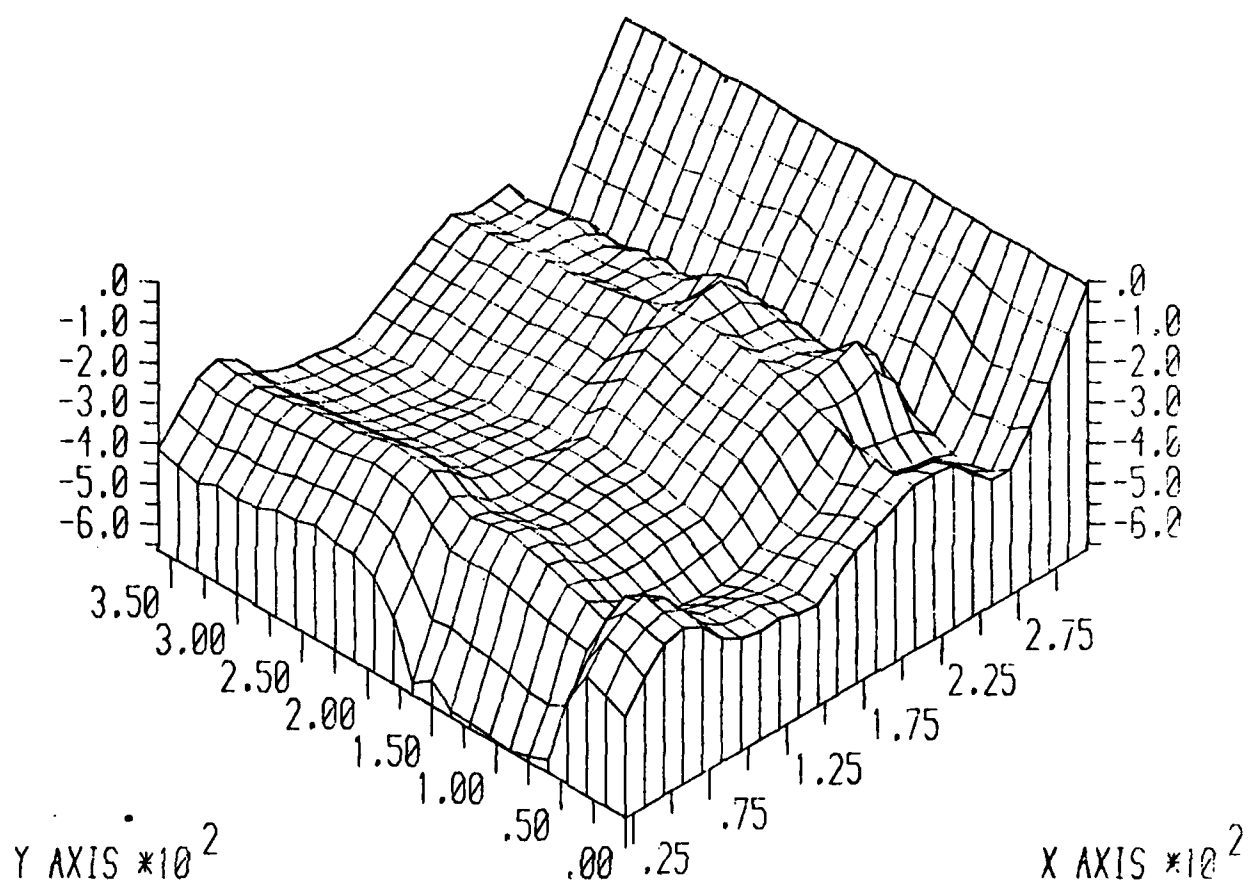


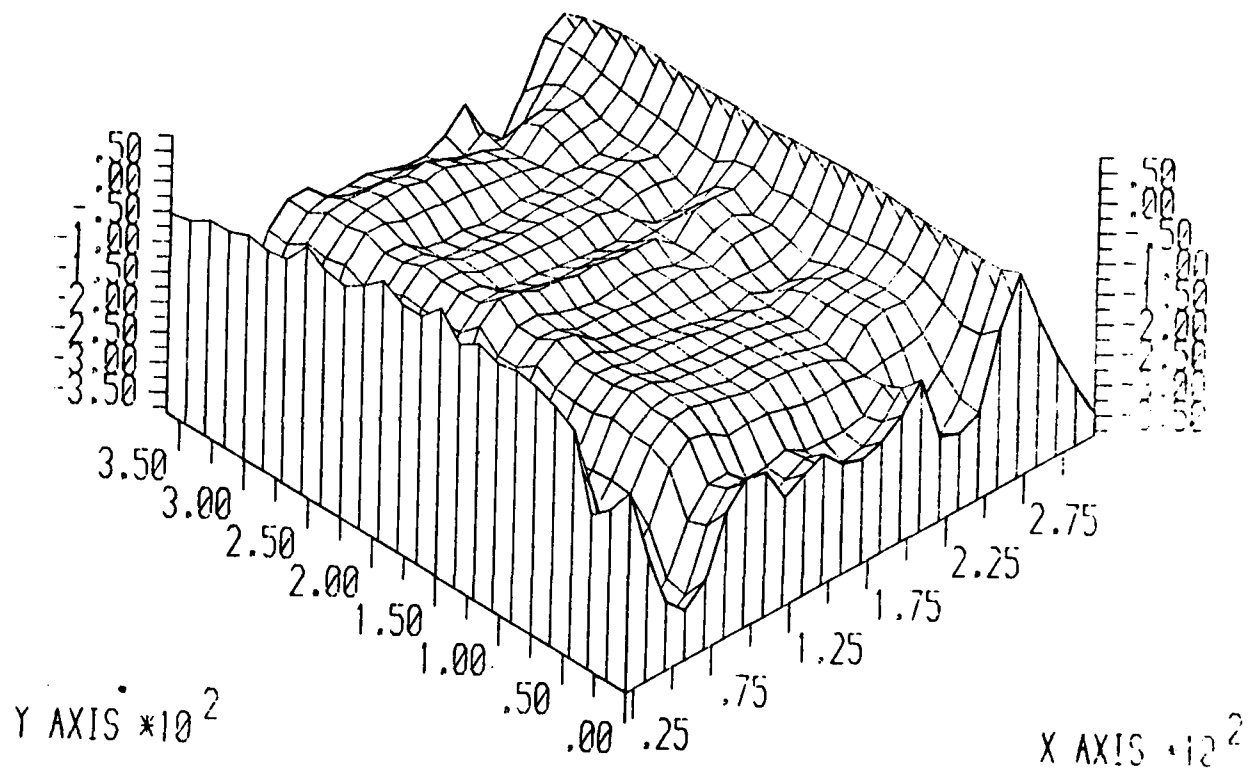
FIG. 24a



120° SQ.WAVE TEST @1250 RPM FLOW RATE NO=3

SUCTION SURFACE PRESSURE DISTRIBUTION

FIG. 24b



120° SQ. WAVE TEST @ 1250 RPM FLOW RATE NO-3

PRESSURE SURFACE PRESSURE DISTRIBUTION

FIG. 24c

ROTOR RESPONSE TO SQUARE WAVE SCREEN - TEST 6

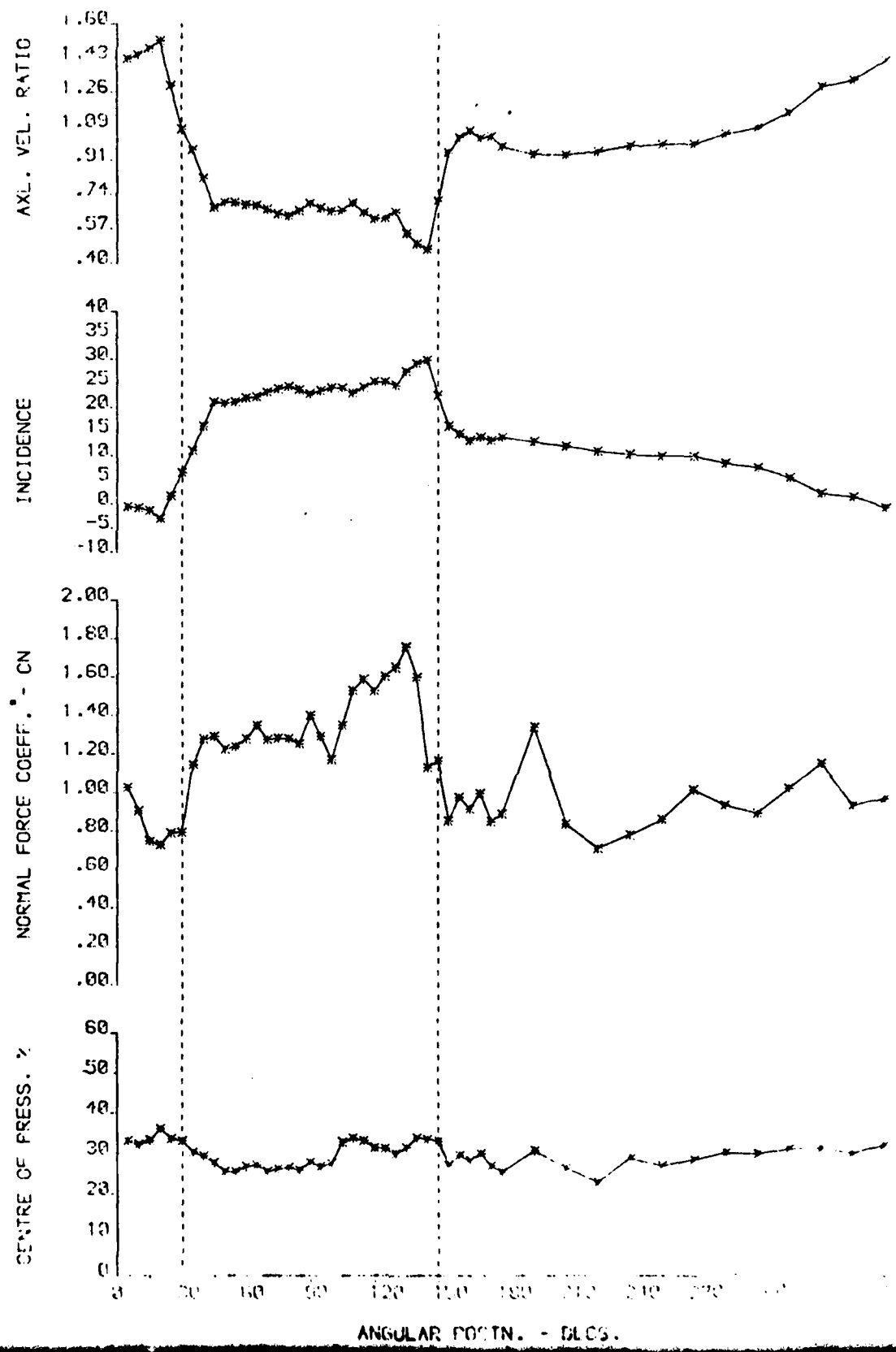


FIG. 24d

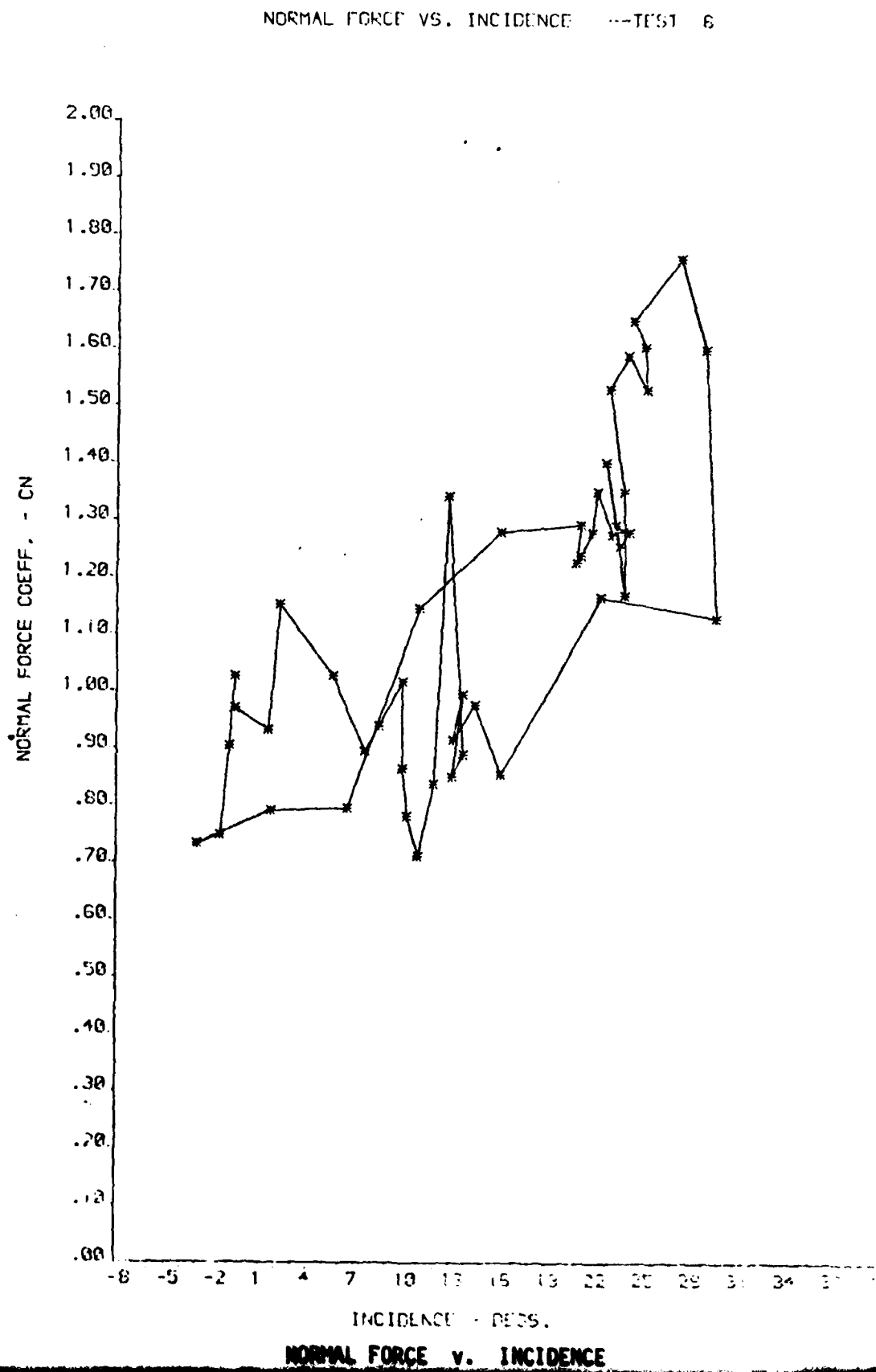
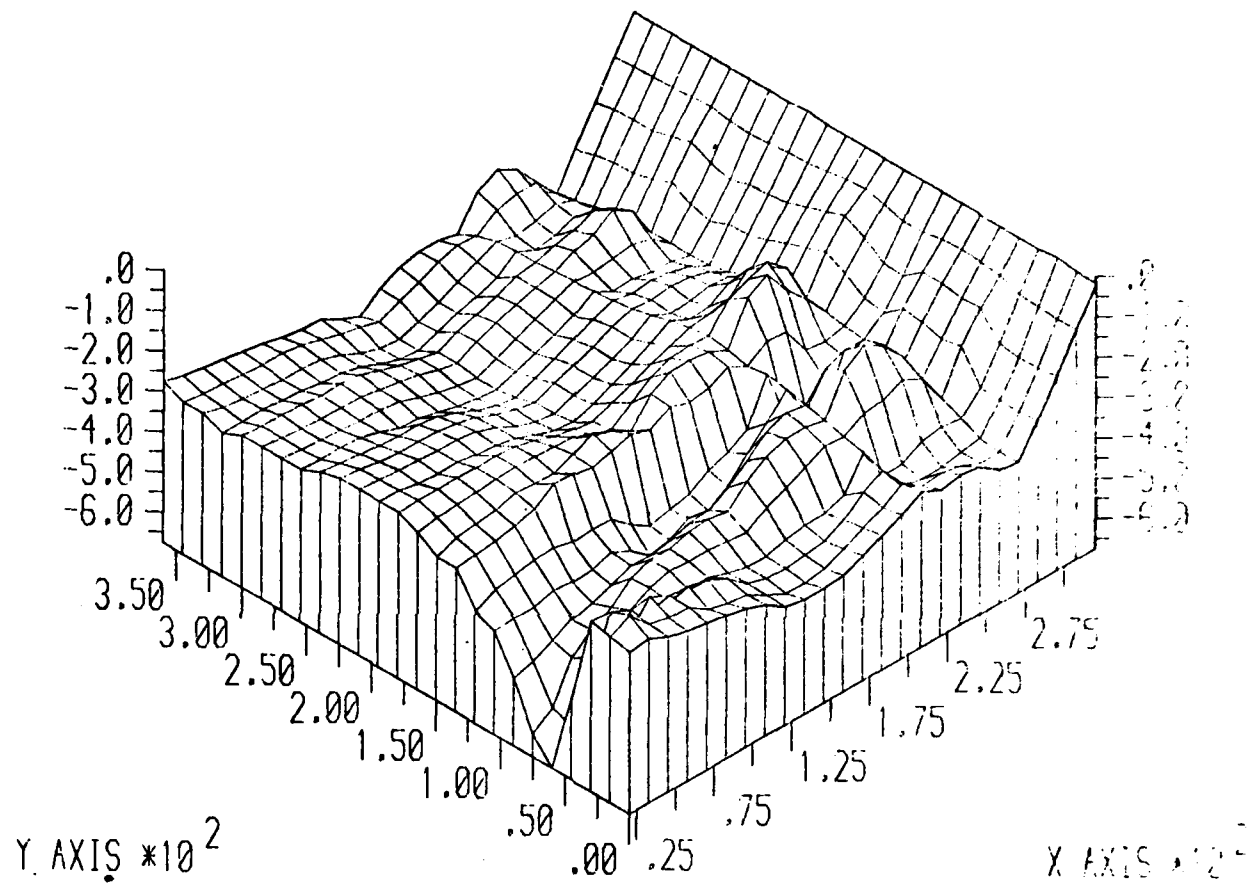


FIG. 25a



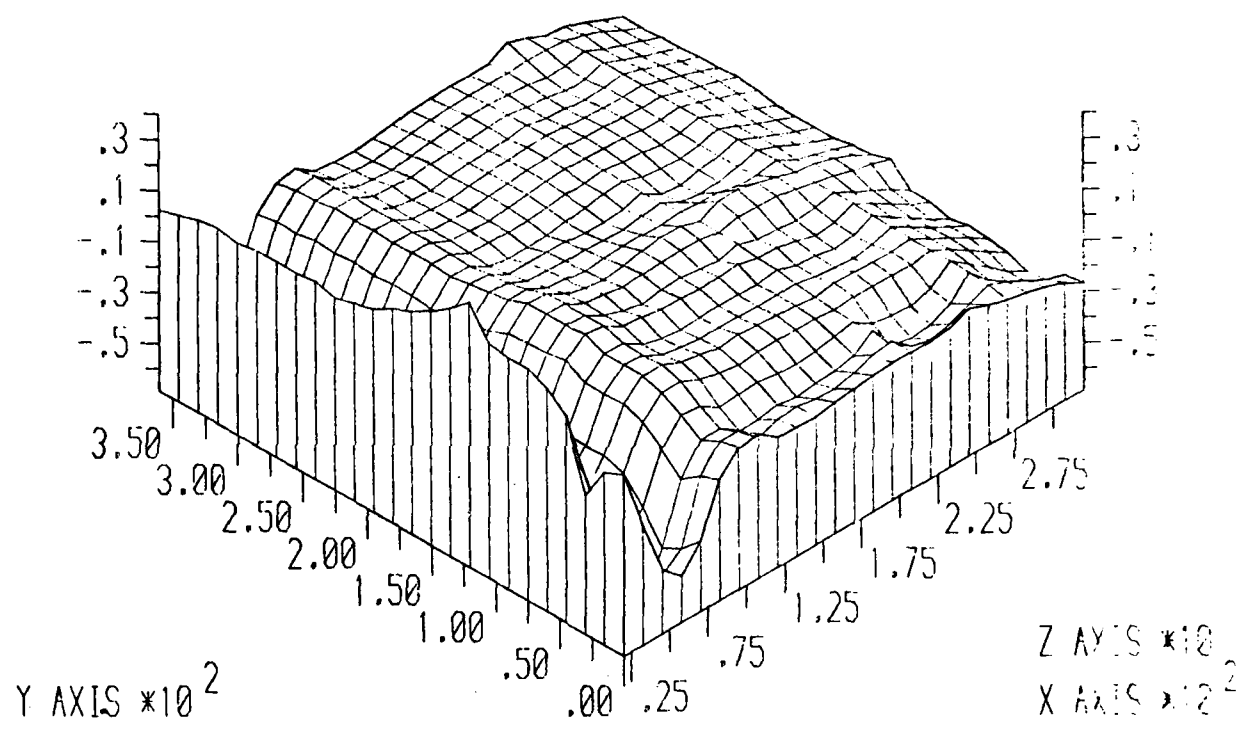
90° SQ. WAVE TEST @1000 RPM FLOW RATE NC=1

SUCTION SURFACE PRESSURE DISTRIBUTION

GDR7

11/08/80 20.54

FIG. 25b



90° SQ. WAVE TEST @1000 RPM FLOW RATE NC=1

PRESSURE SURFACE PRESSURE DISTRIBUTION

GDR7

11/08/80 20.57

FIG. 25c

ROTOR RESPONSE TO SQUARE WAVE SCREEN - TEST 1

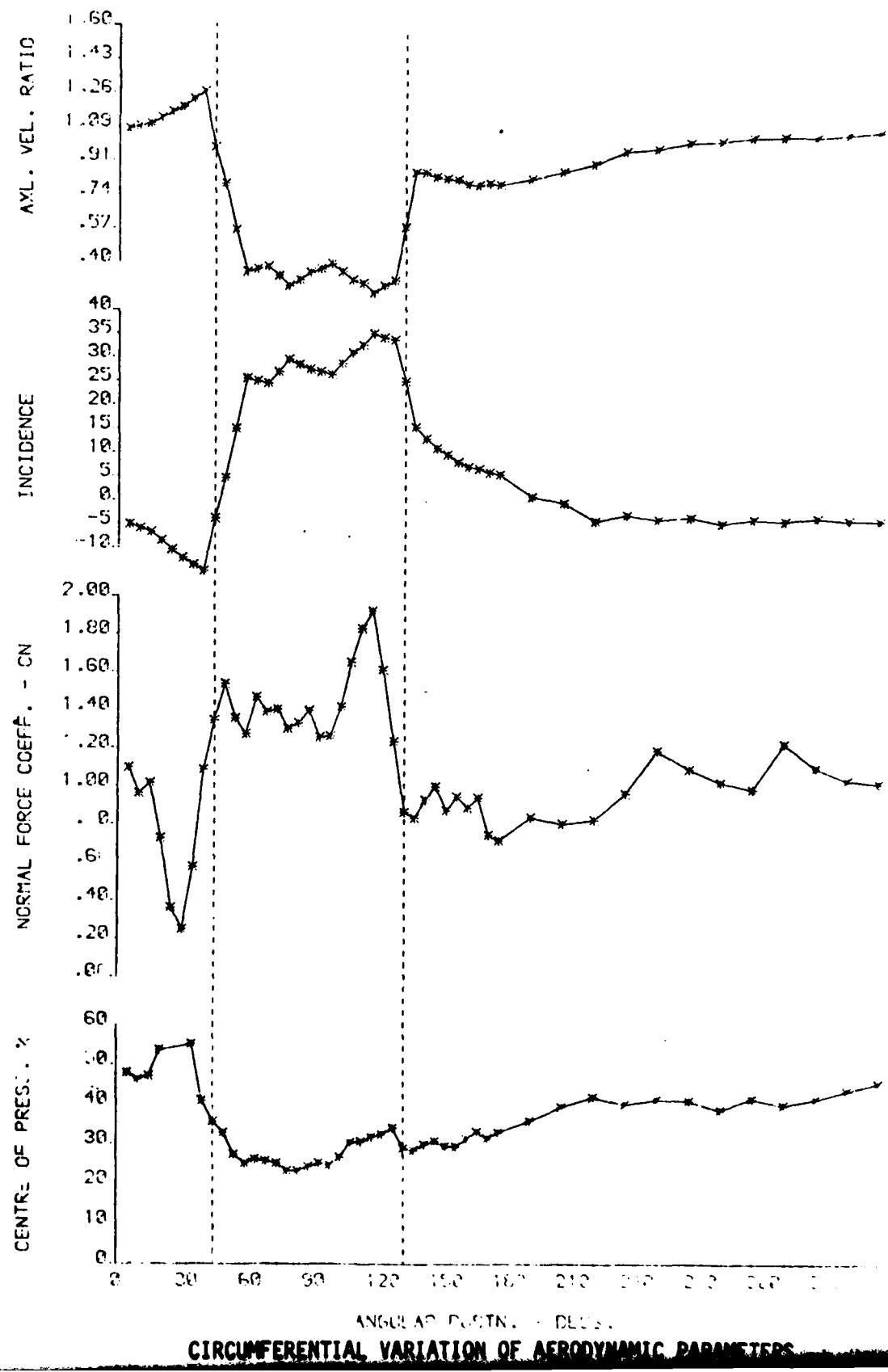


FIG. 25d

NORMAL FORCE VS. INCIDENCE --TEST 1

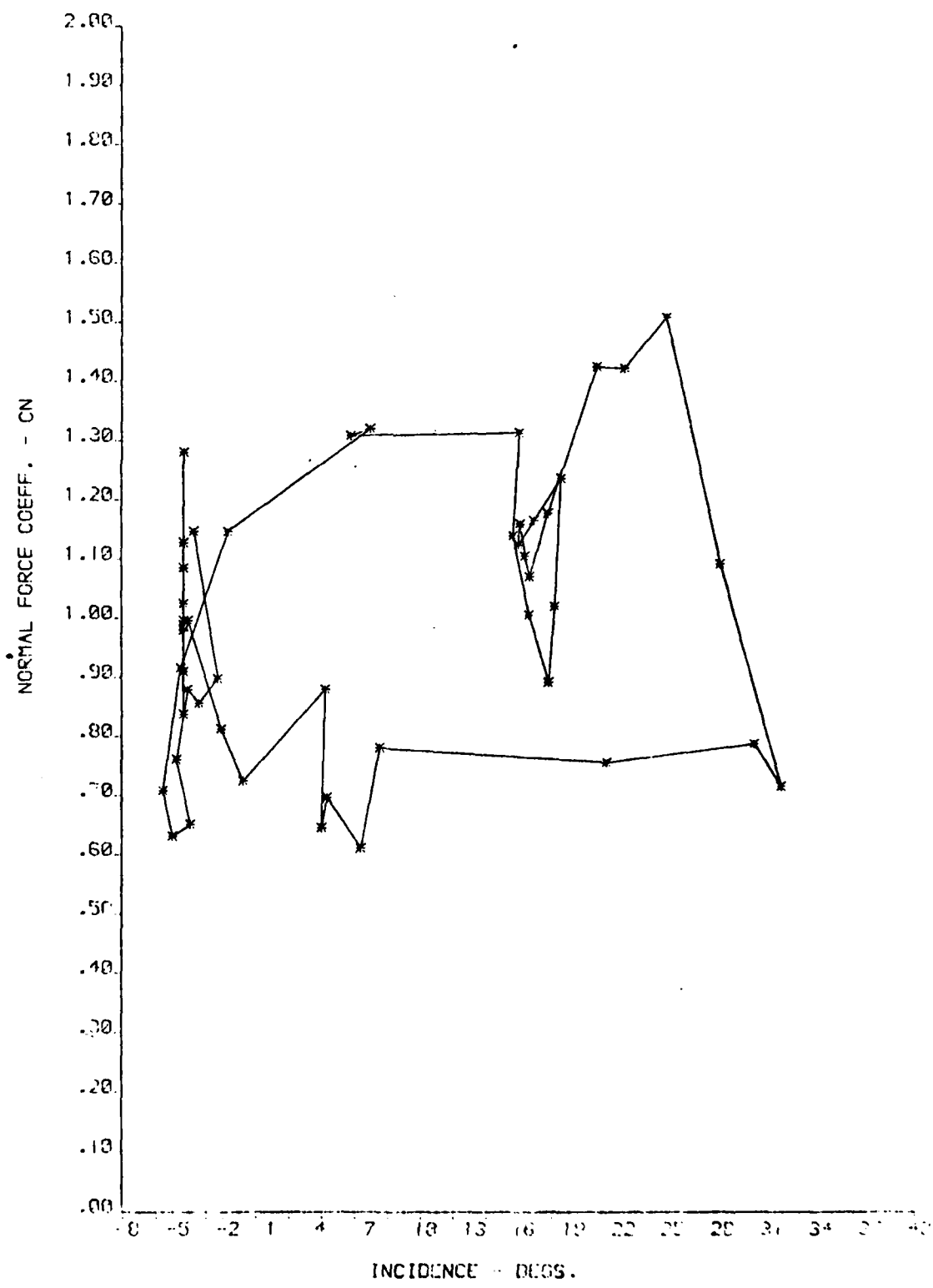
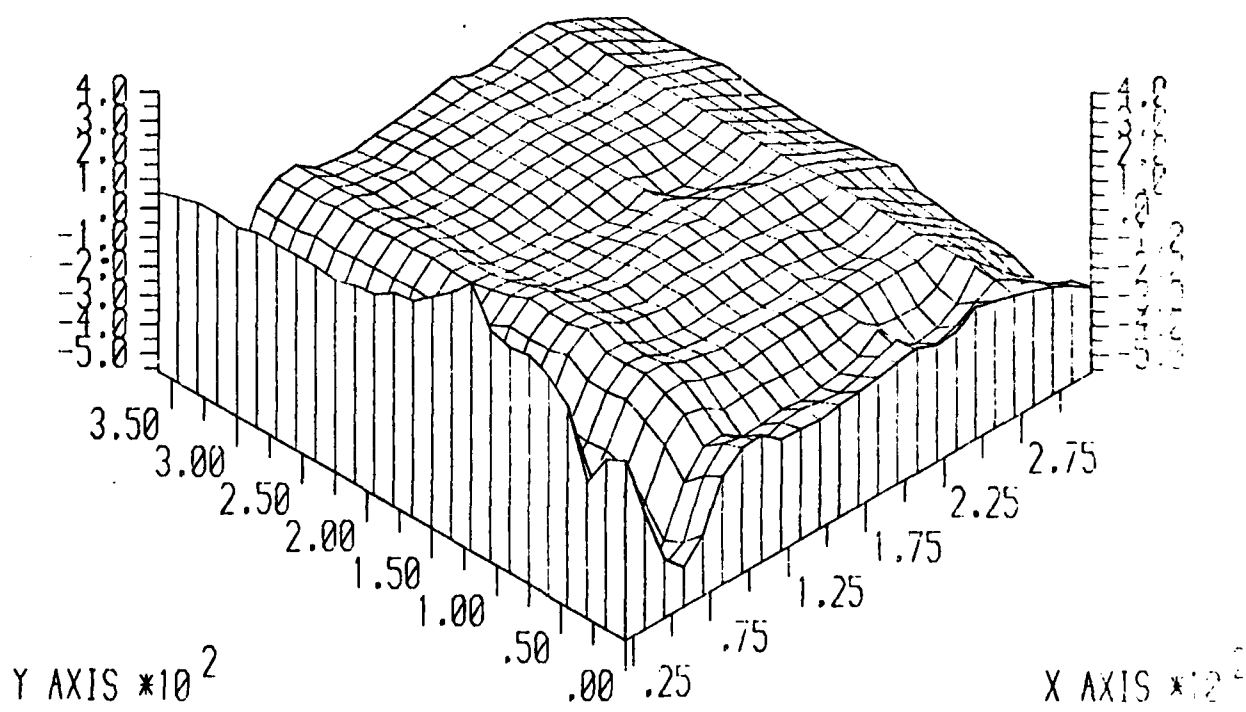


FIG. 26a



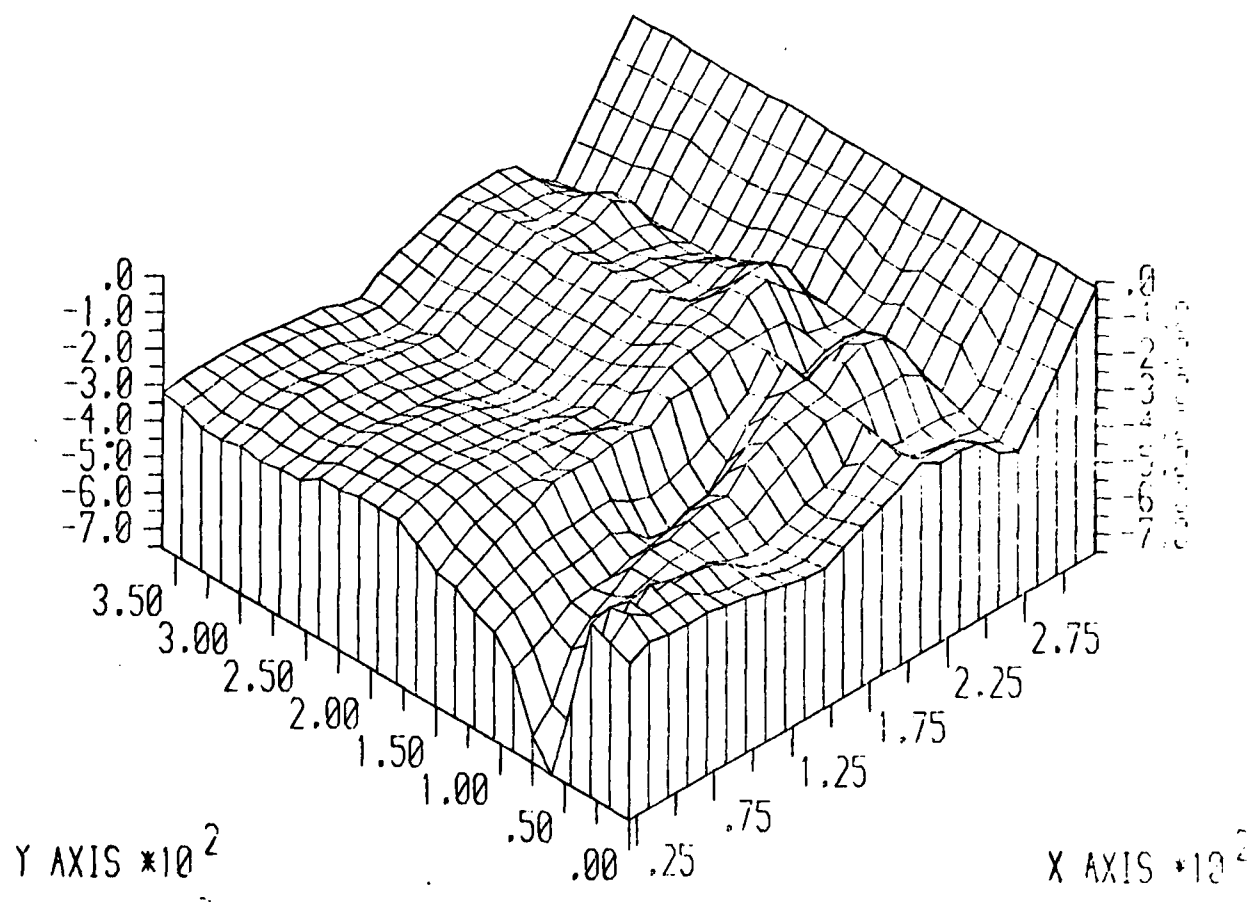
90° SQ.WAVE TEST @ 1000 RPM FLOW RATE NO: 2

SUCTION SURFACE PRESSURE DISTRIBUTION

GDR7

11/08/90 20.45

FIG. 26b



90° SQ. WAVE TEST @ 1000 RPM FLOW RATE NO-2

PRESSURE SURFACE PRESSURE DISTRIBUTION

GDR7

11/08/82 20.42

FIG. 26c

ROTOR RESPONSE TO SQUARE WAVE SCREEN - 1/10

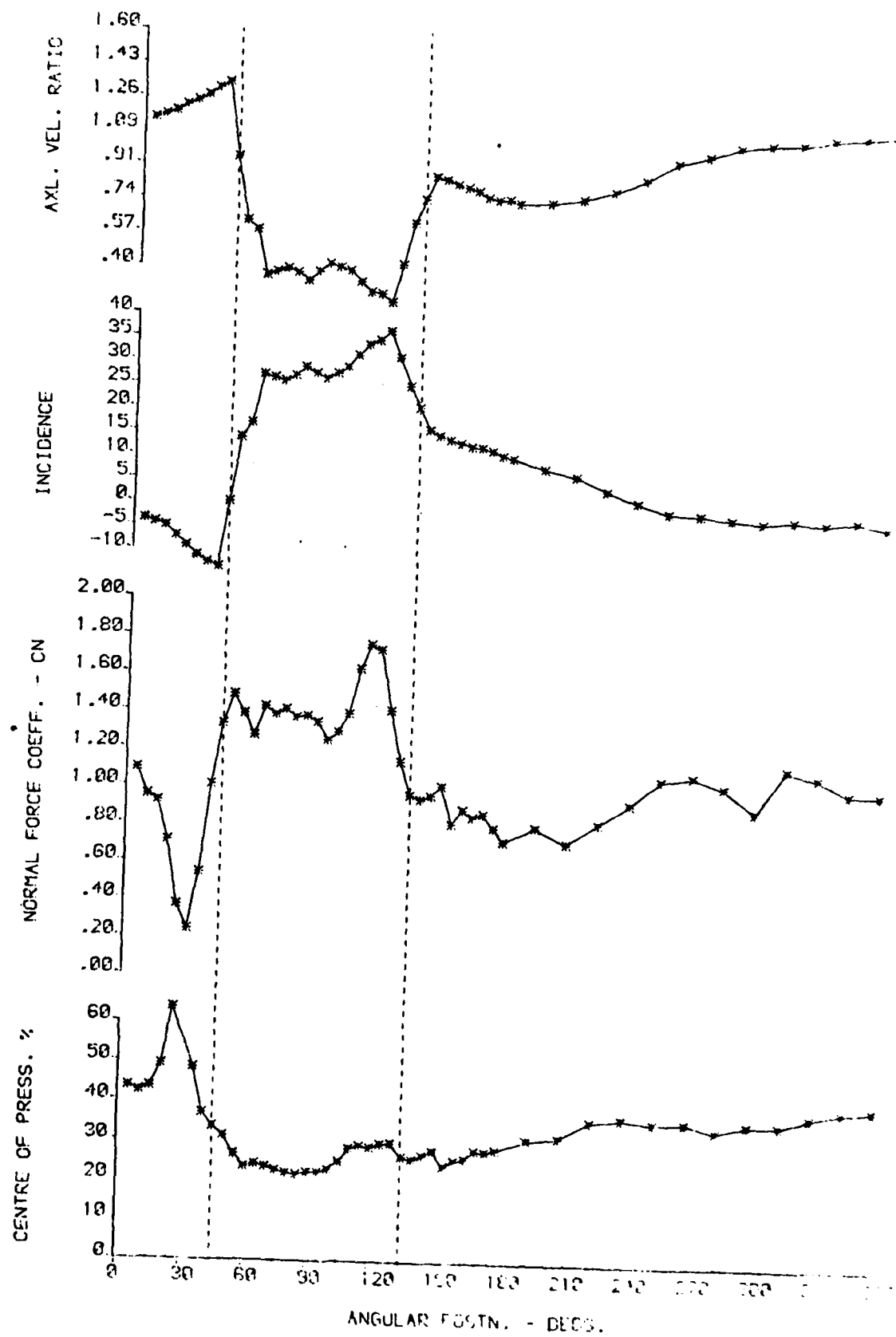


FIG. 26d

NORMAL FORCE VS. INCIDENCE --TEST 2

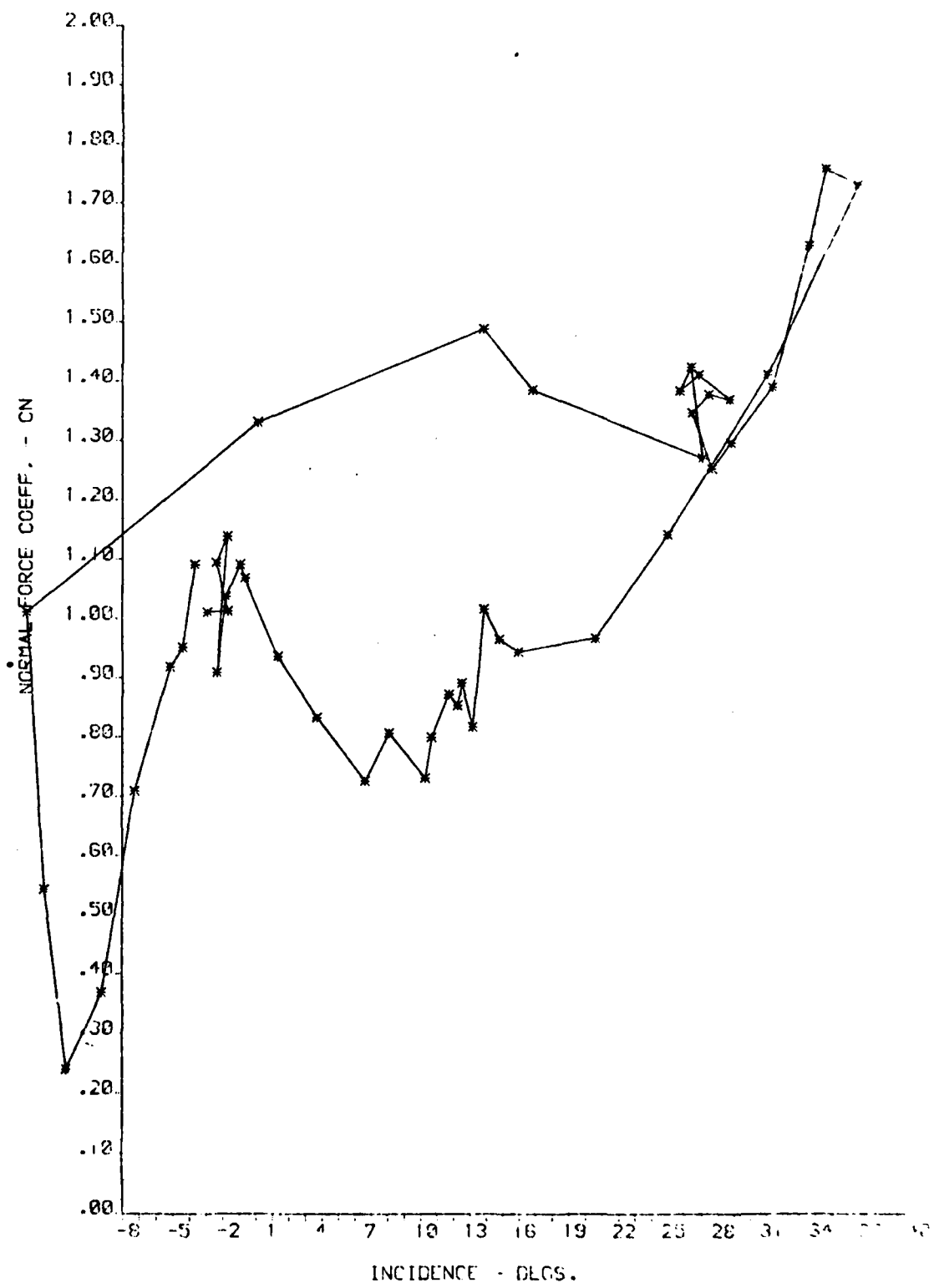
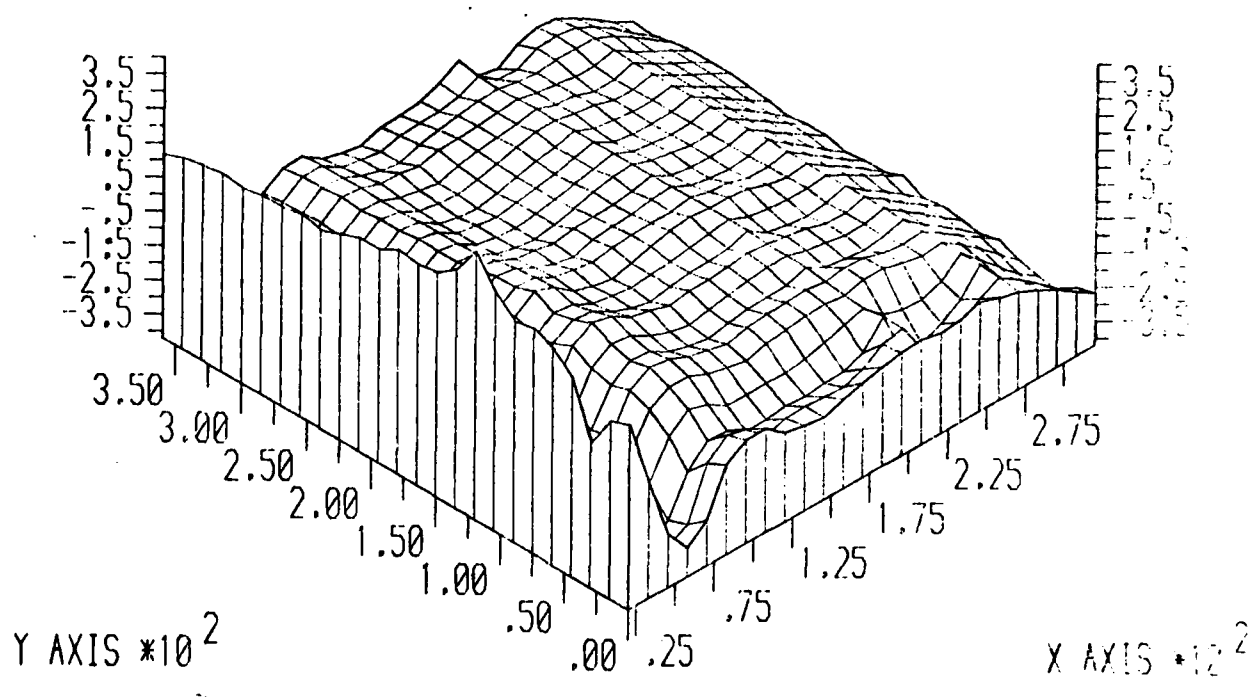


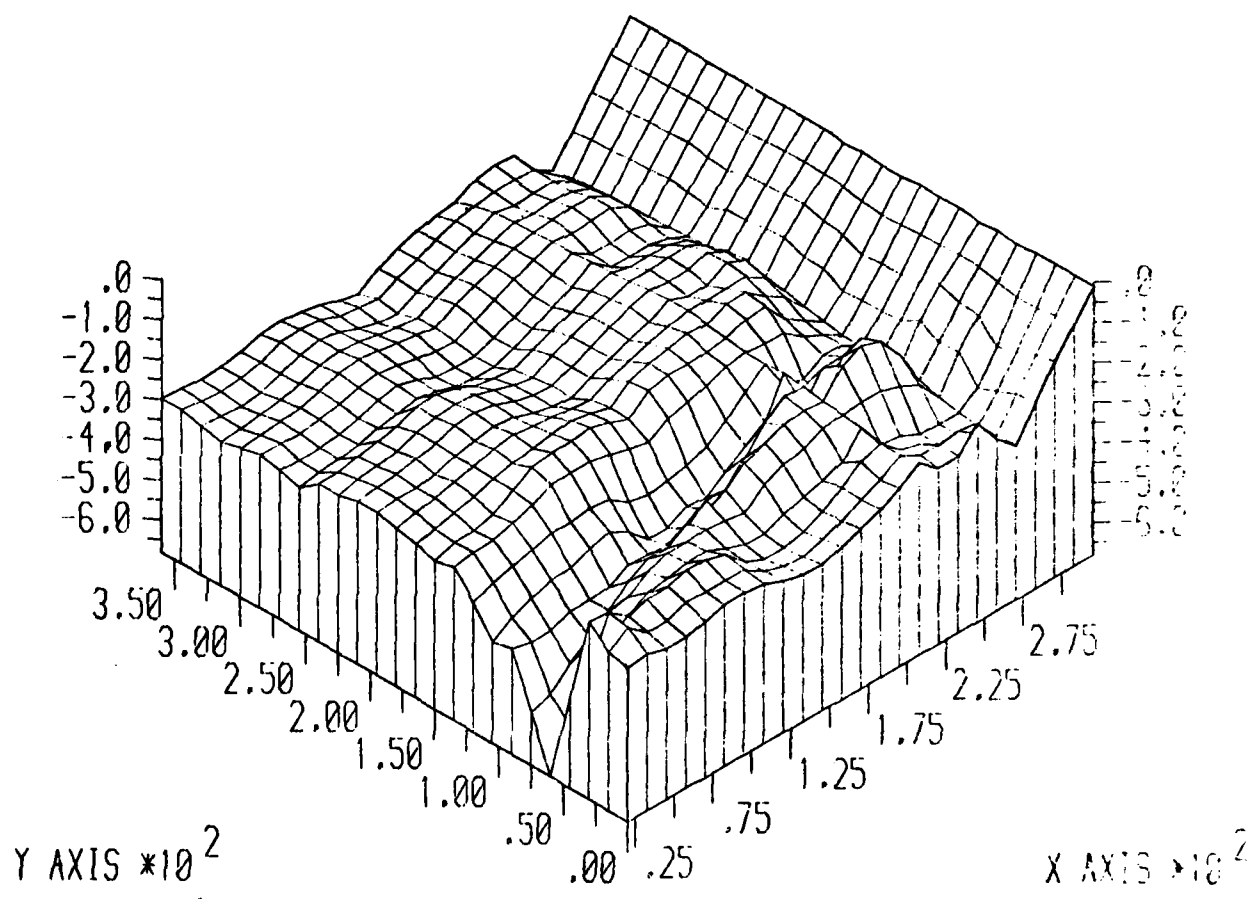
FIG. 27a



90° SQ.WAVE TEST @ 1000 RPM FLOW RATE NO. 3

SUCTION SURFACE PRESSURE DISTRIBUTION

FIG. 27b



90° SG. WAVE TEST @ 1000 RPM (FLOW RATE NO. 3)

PRESSURE SURFACE PRESSURE DISTRIBUTION

FIG. 27c
ROTOR RESPONSE TO SQUARE WAVE SCREEN - TEST 3

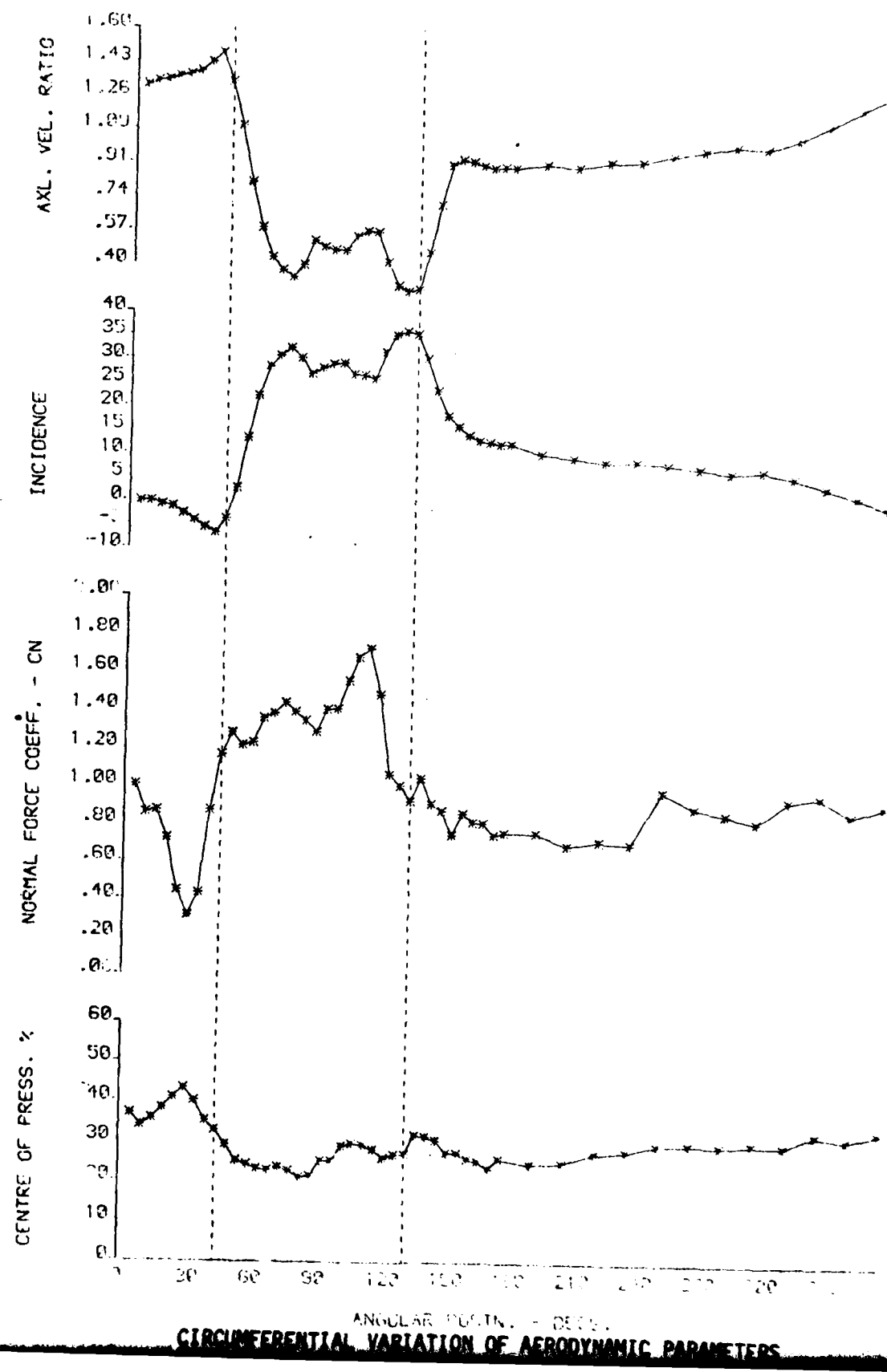


FIG. 27d

NORMAL FORCE VS. INCIDENCE --TEST 3

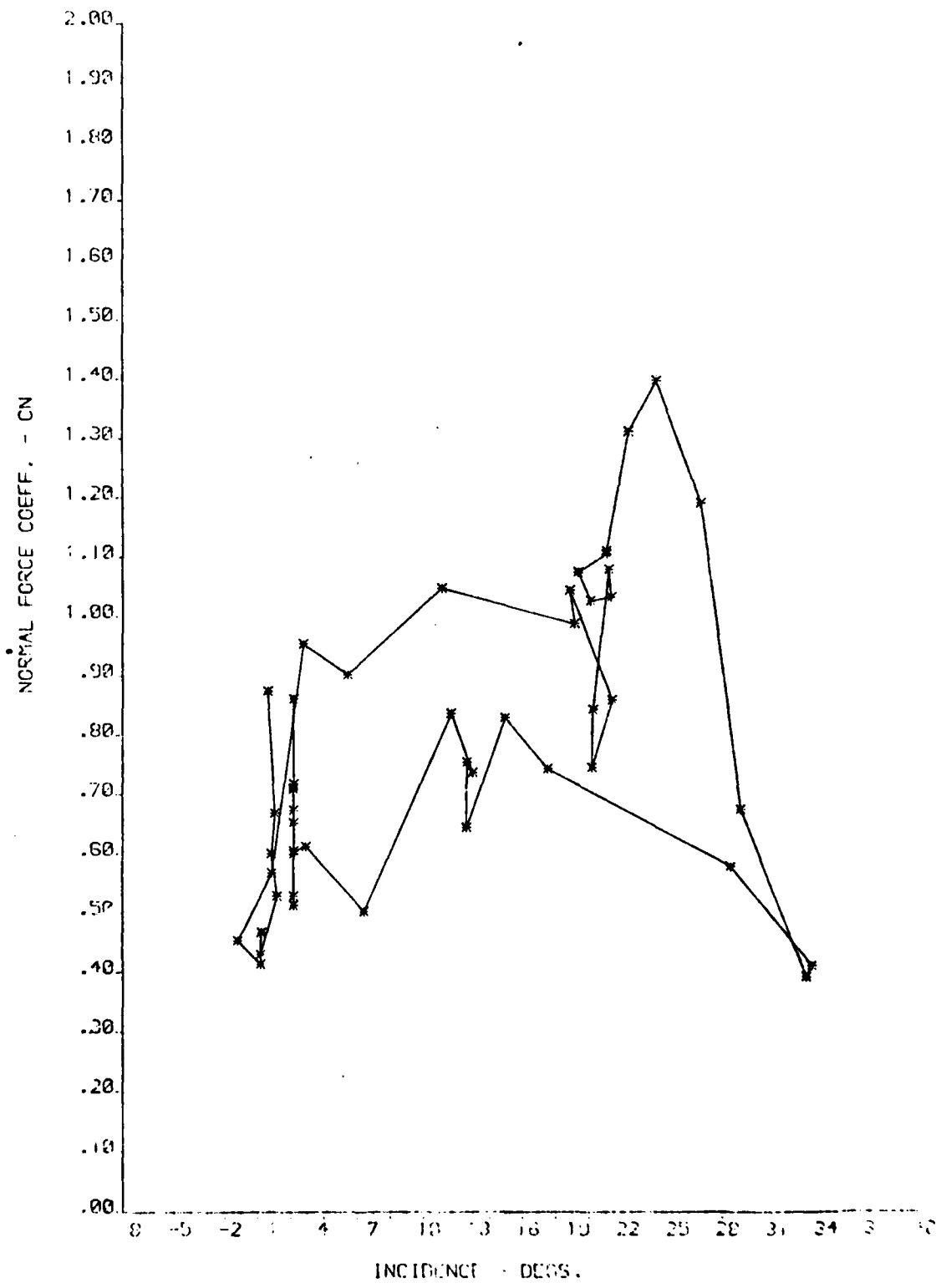
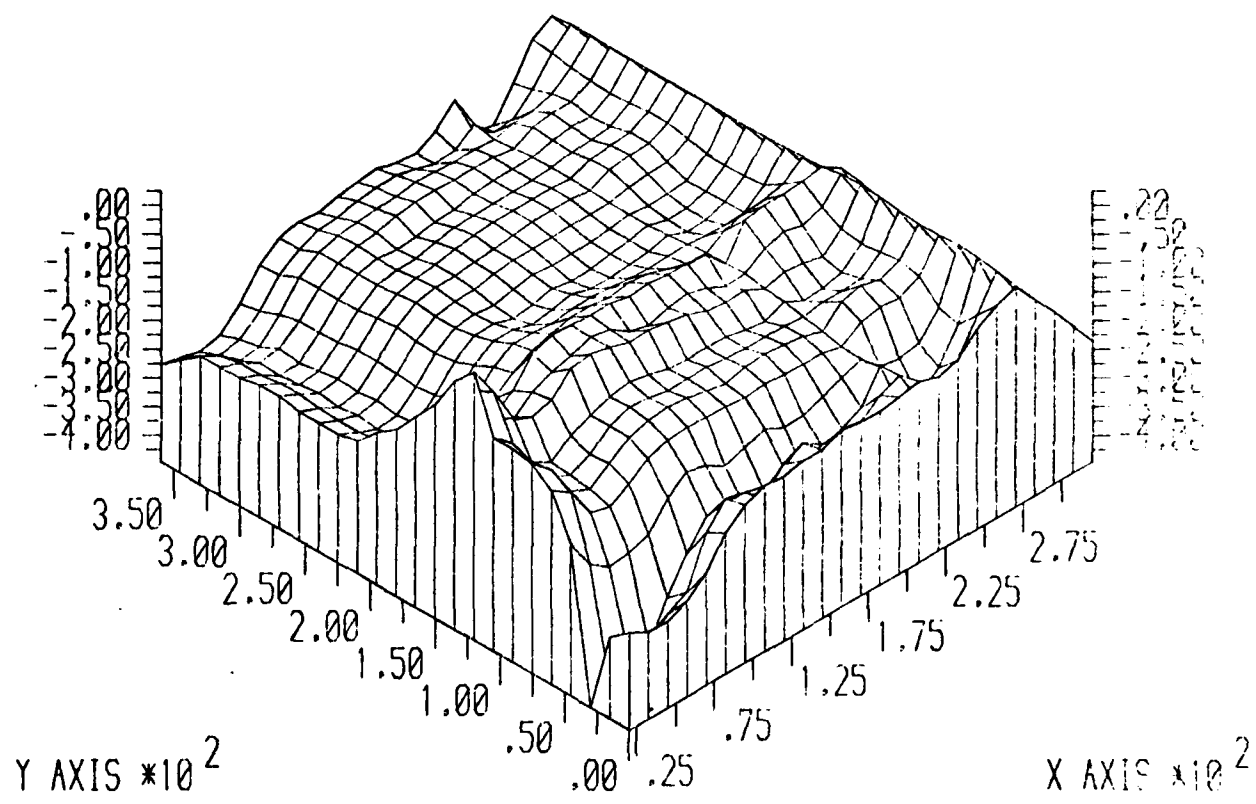


FIG. 28a



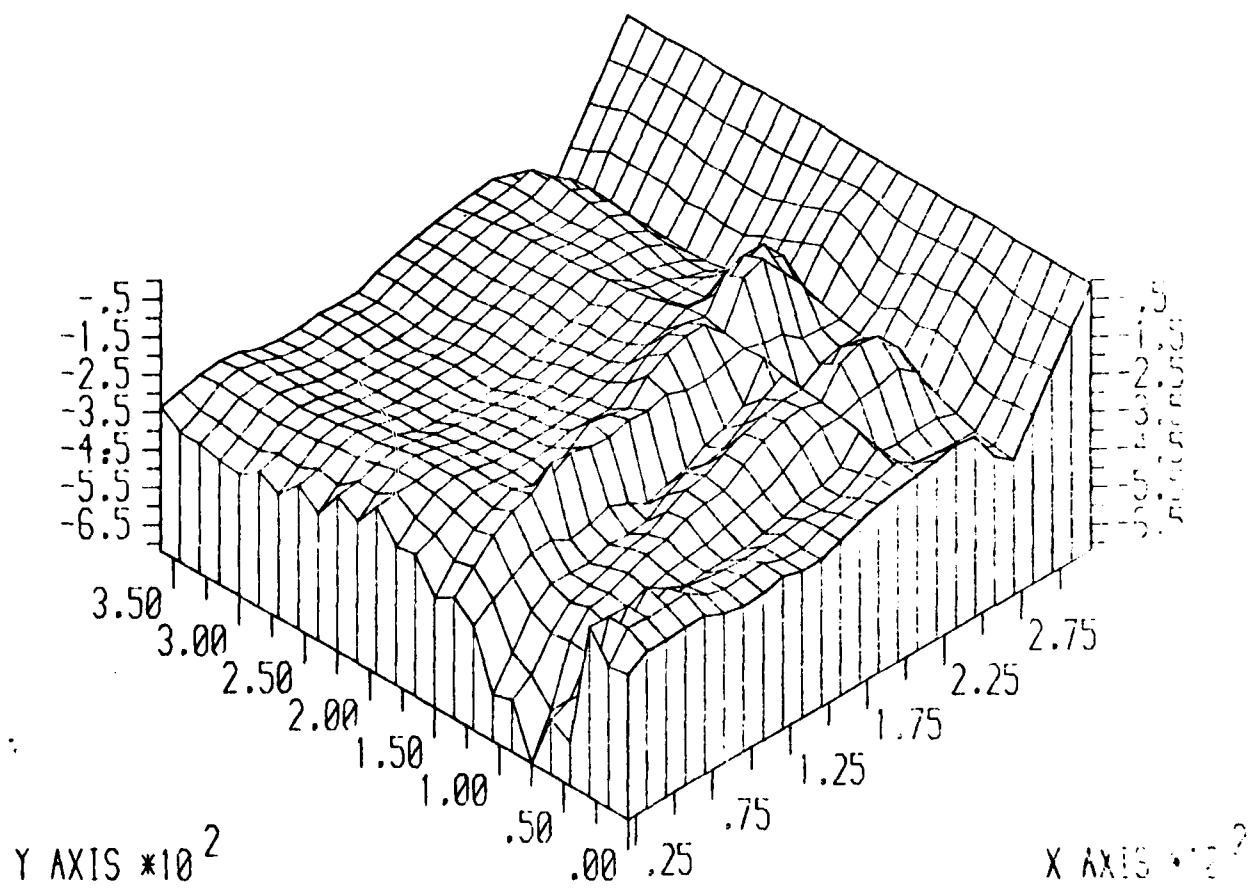
90° SQ. WAVE TEST @ 1250 RPM FLOW RATE NO=1

SUCTION SURFACE PRESSURE DISTRIBUTION

GDR7

22/08/80 17.26

FIG. 28b



90° SQ. WAVE TEST @ 1250 RPM FLOW RATE NG=1

PRESSURE SURFACE PRESSURE DISTRIBUTION

FIG. 28c

ROTOR RESPONSE TO SQUARE WAVE SCREEN -- TEST 6

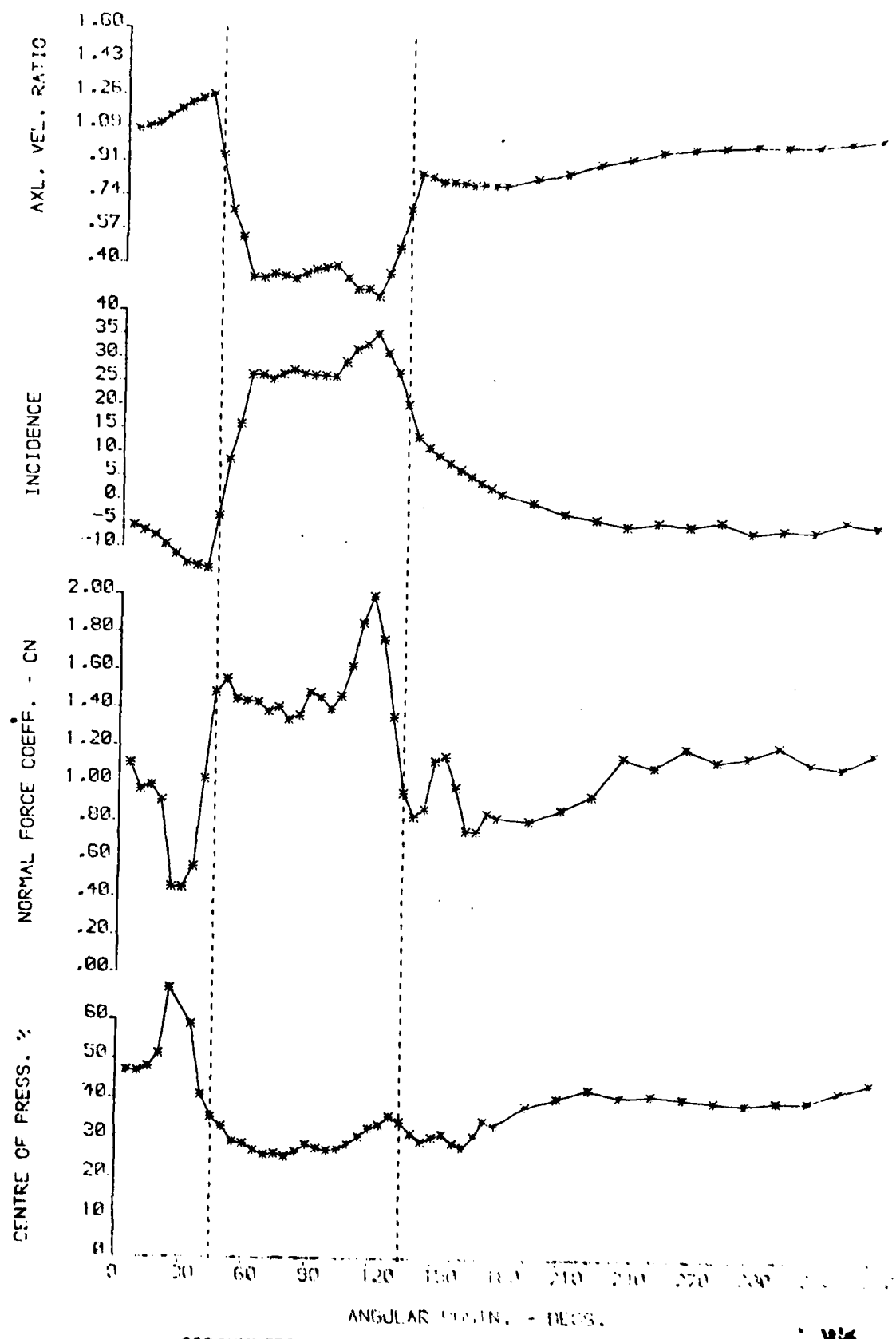


FIG. 28d

NORMAL FORCE VS. INCIDENCE --TEST 6

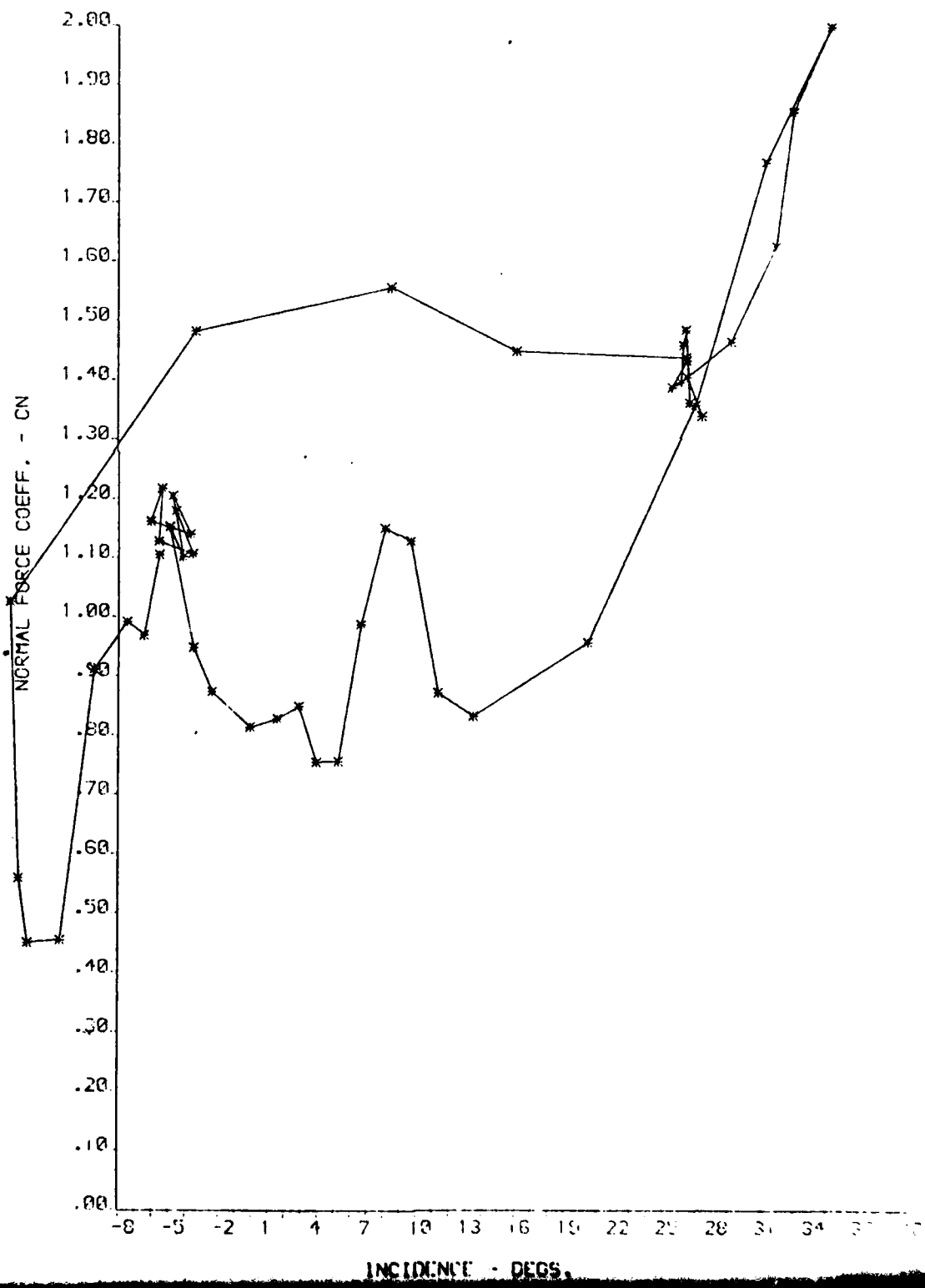
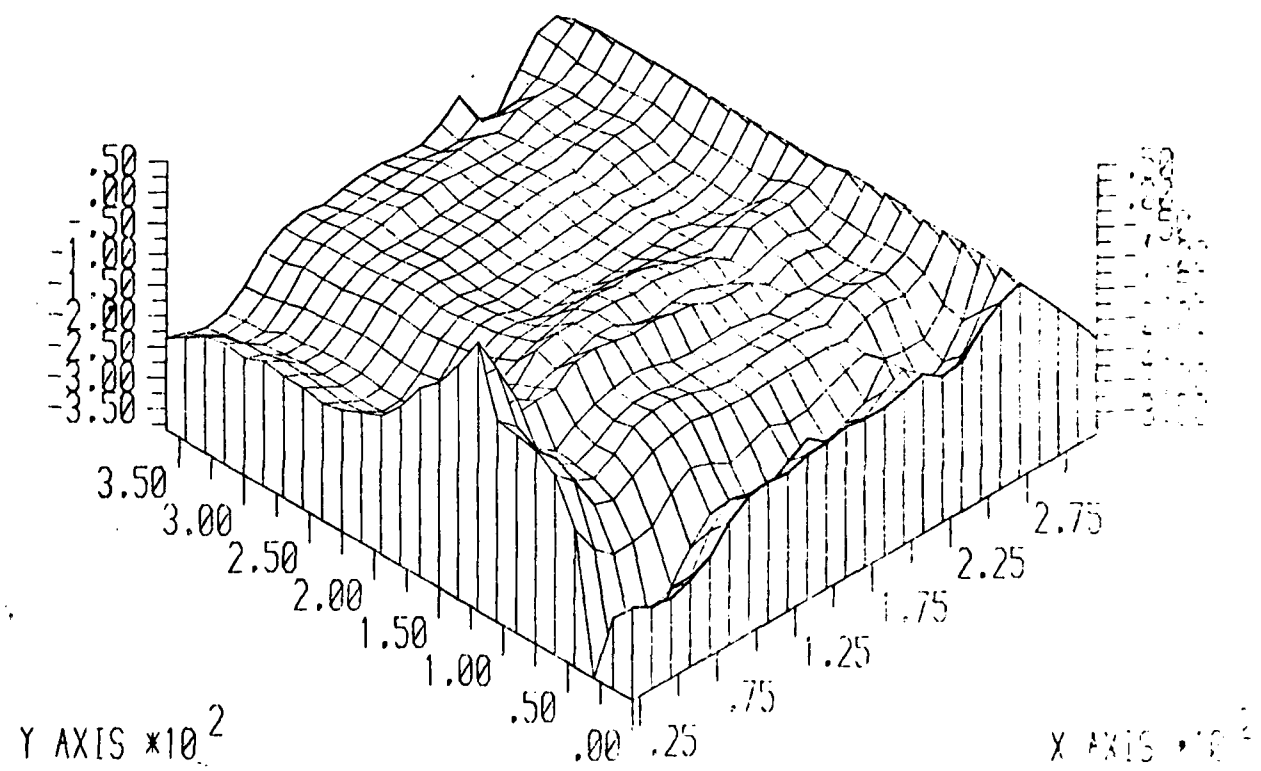


FIG. 29a



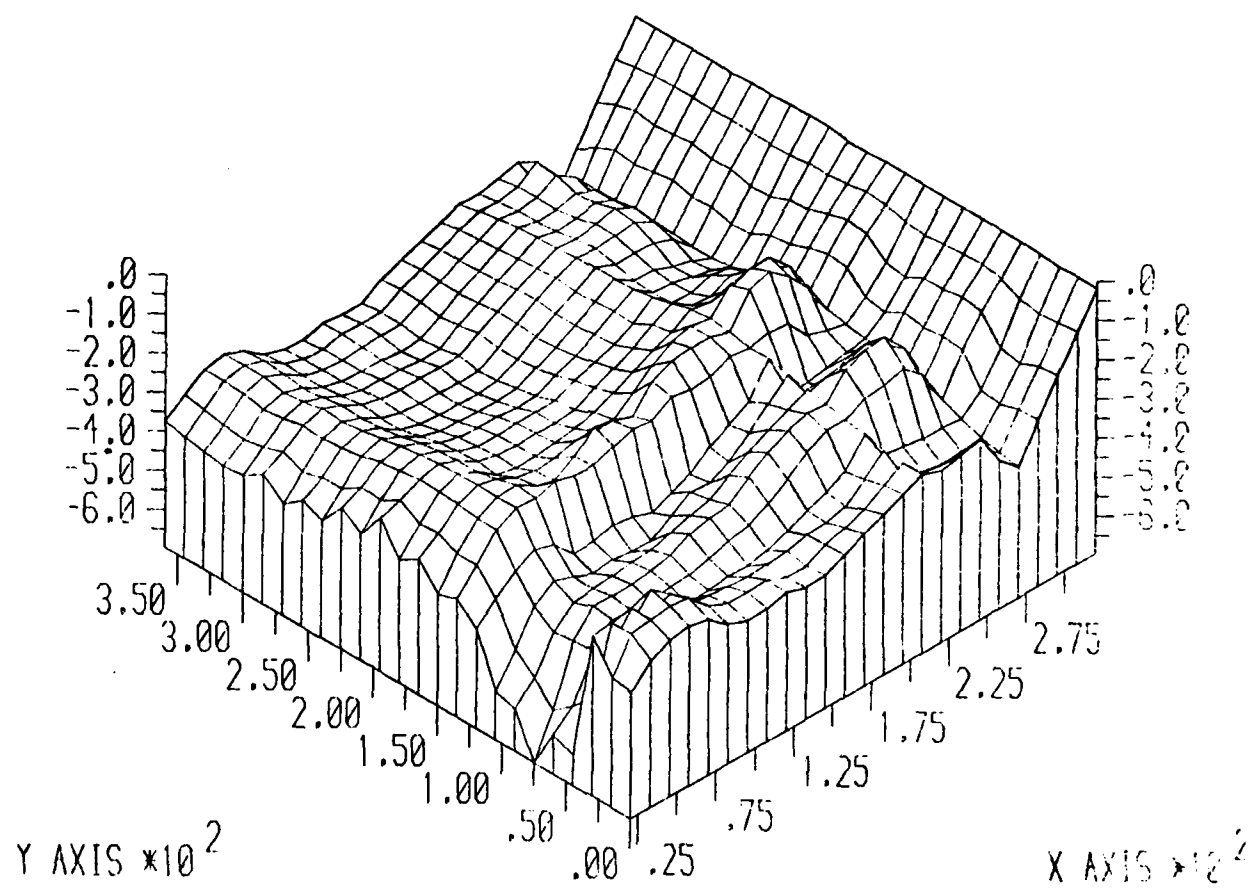
90° SQ.WAVE TEST @ 1250 RPM FLOW RATE NO. 1

SUCTION SURFACE PRESSURE DISTRIBUTION

GDR7

18/08/80 21.55

FIG. 29b



90° SQ.WAVE TEST @ 1250 RPM FLOW RATE NO:2

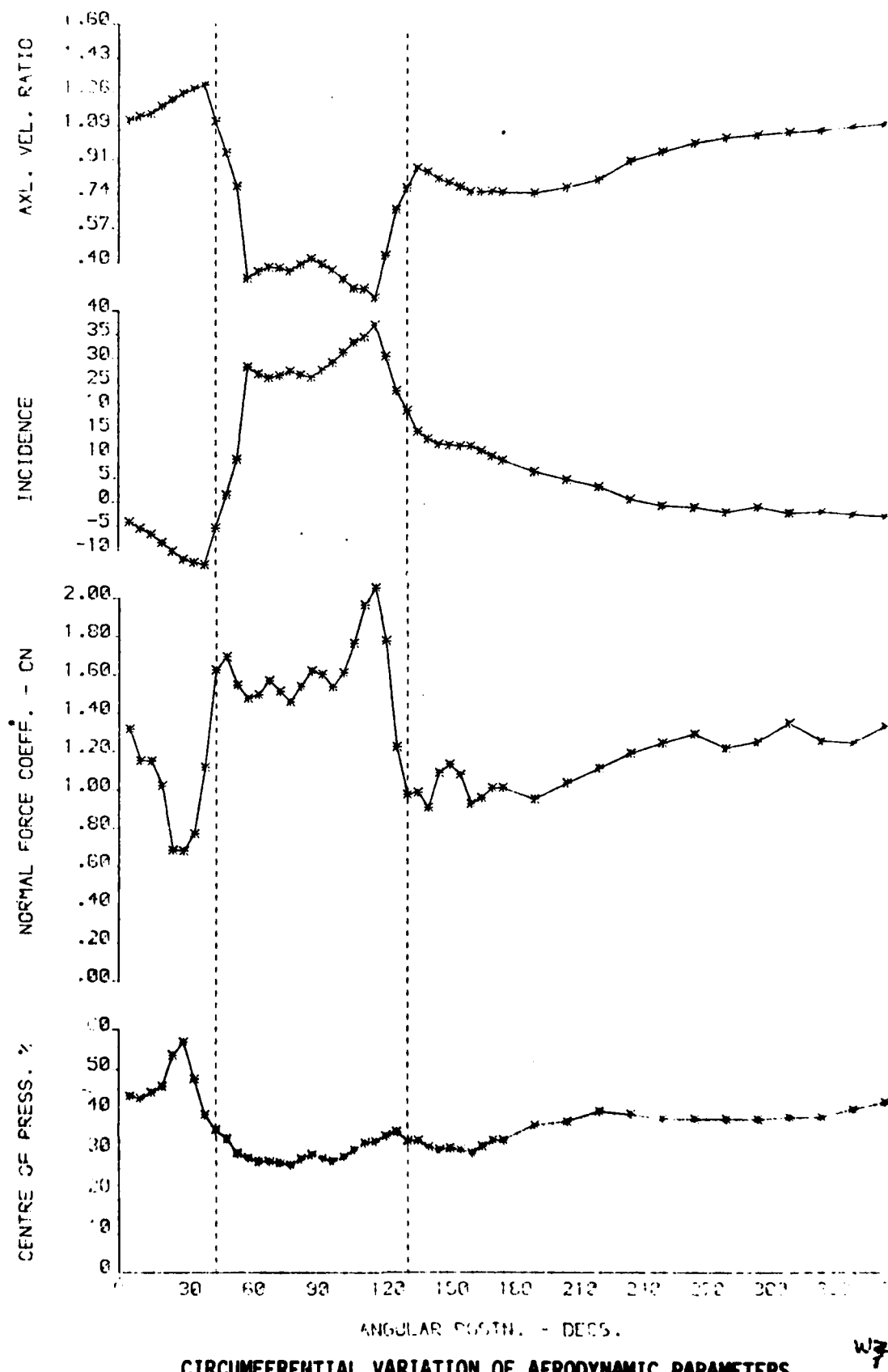
PRESSURE SURFACE PRESSURE DISTRIBUTION

GDR7

18/08/80 21.52

FIG. 29c

ROT. R. RESPONSE TO SQUARE WAVE SCREEN -- TEST 7



W7

FIG. 29d

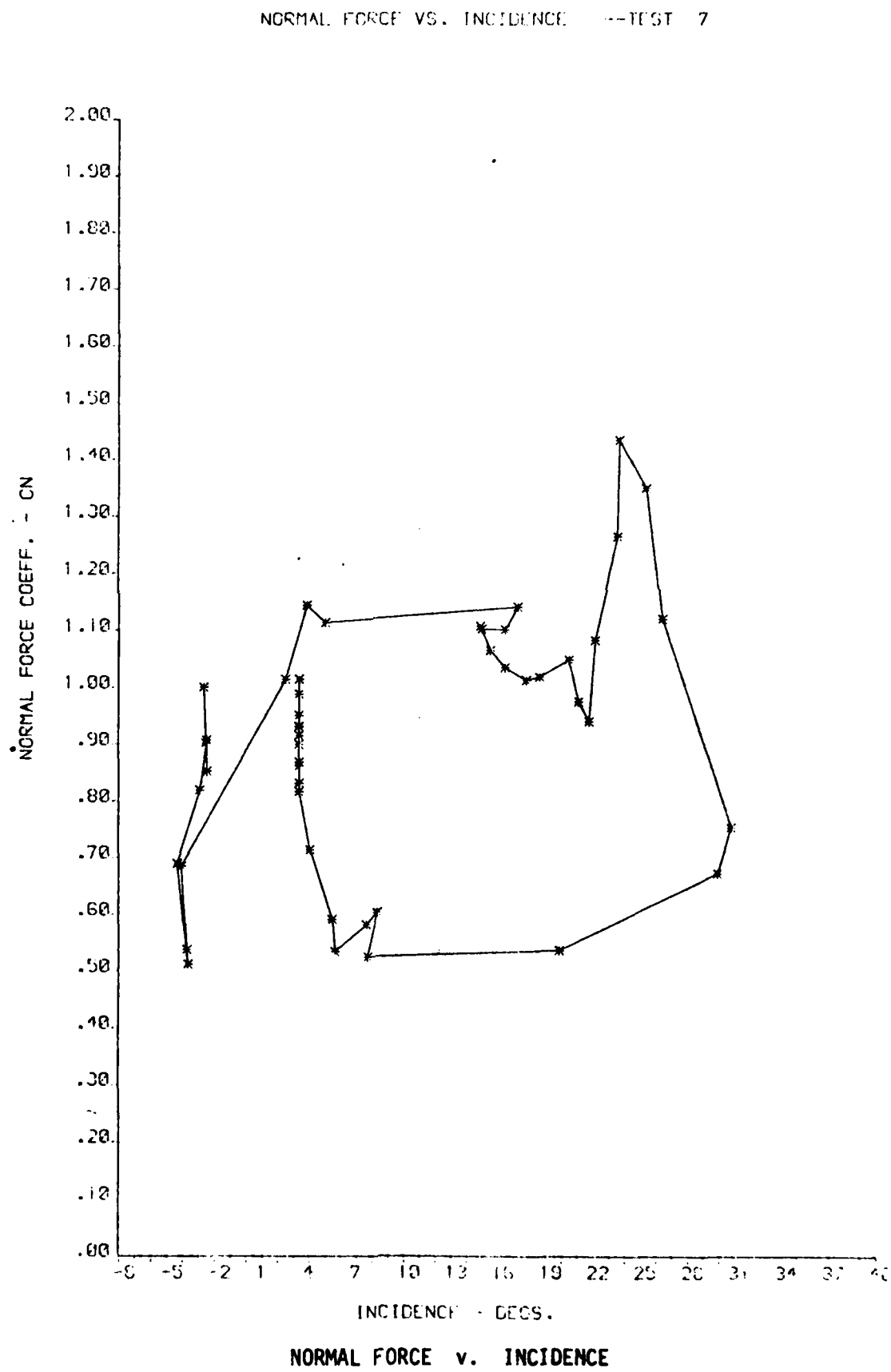
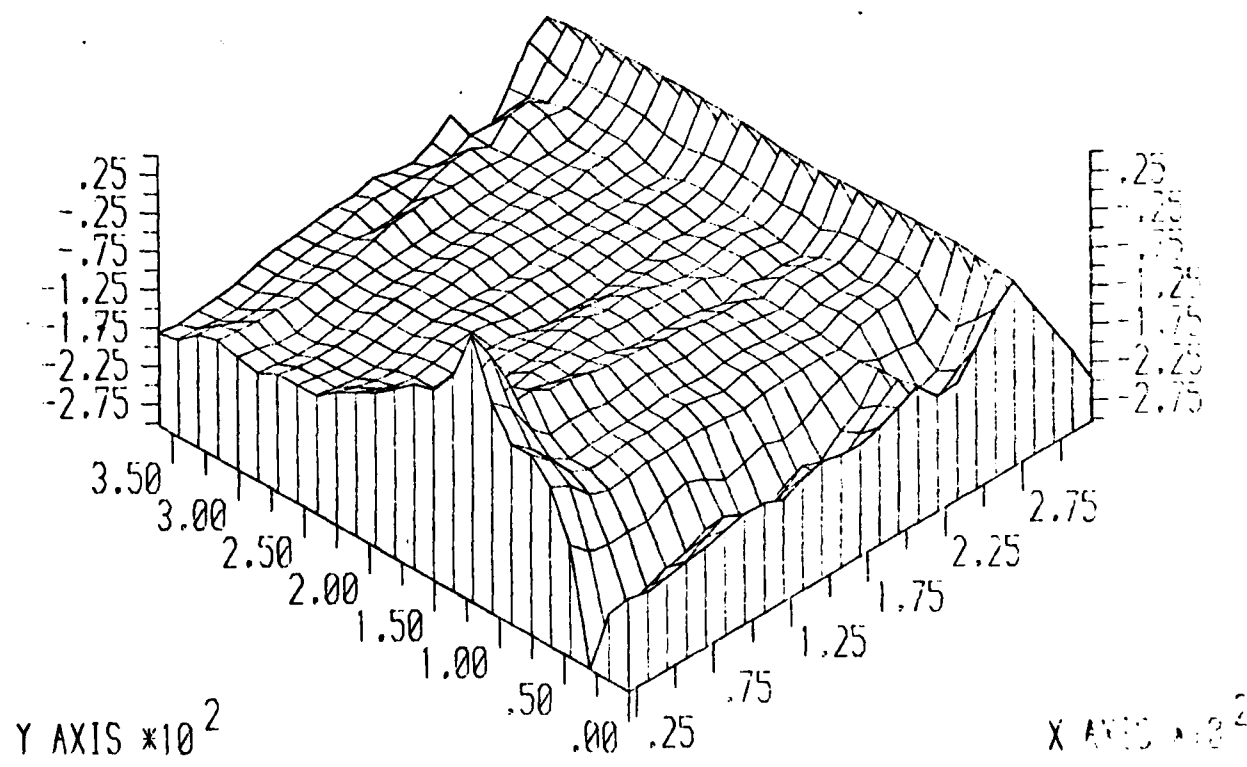


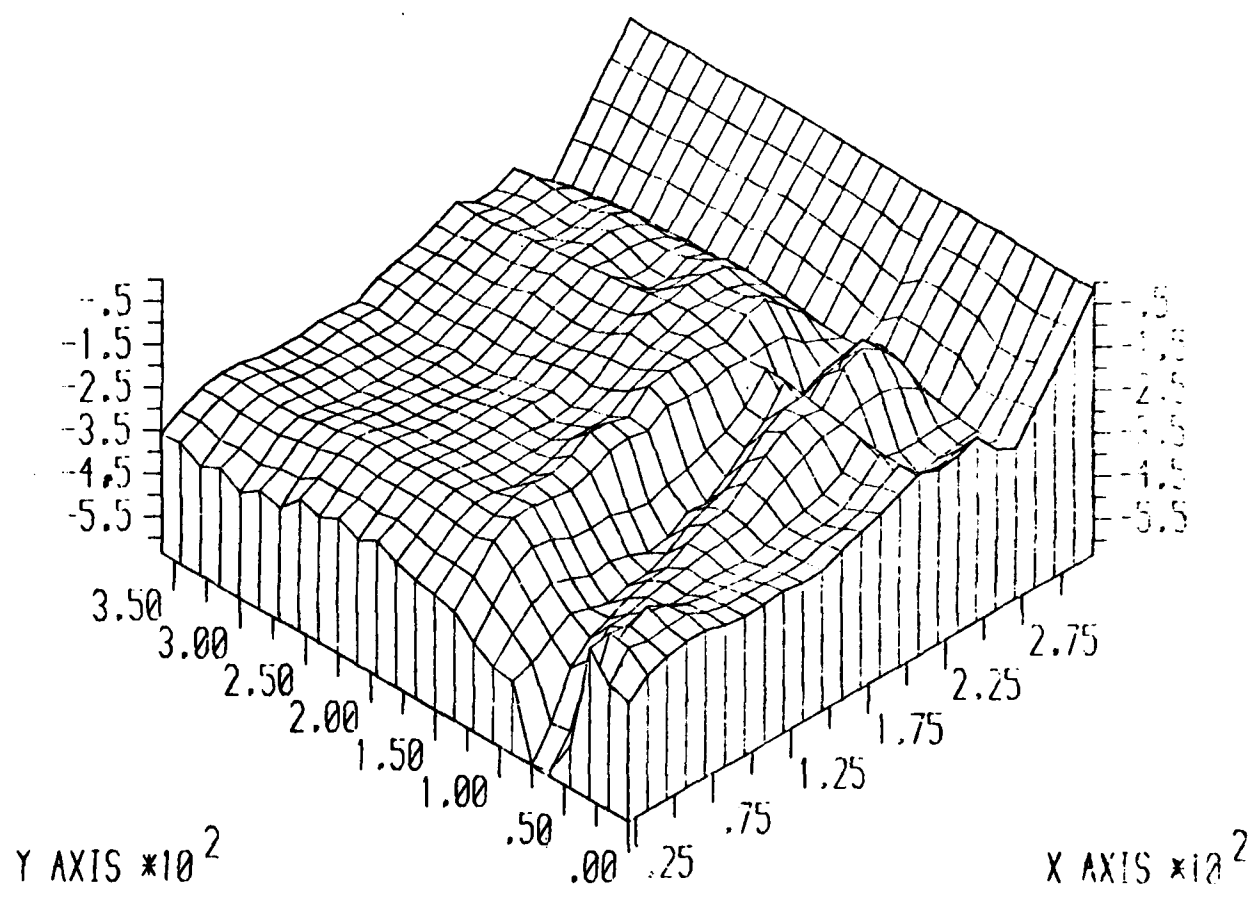
FIG. 30a



90° SG. WAVE TEST @ 1250 RPM FLOW RATE NO=3

SUCTION SURFACE PRESSURE DISTRIBUTION

FIG. 30b



90° SQ. WAVE TEST @ 1250 RPM FLOW RATE NO:3

PRESSURE SURFACE PRESSURE DISTRIBUTION

FIG. 30c

ROTOR RESPONSE TO SQUARE WAVE SCREEN -- TEST 8

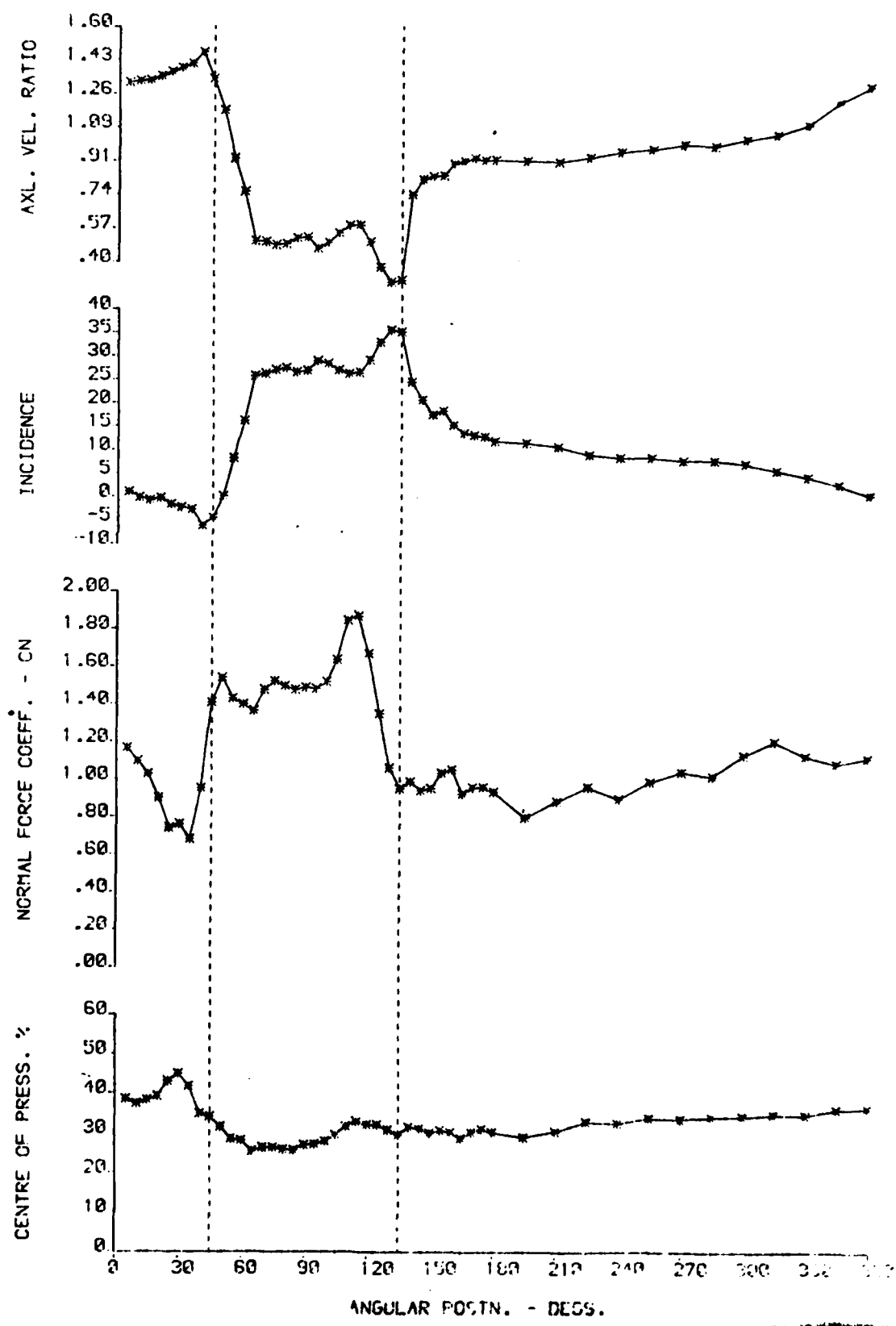
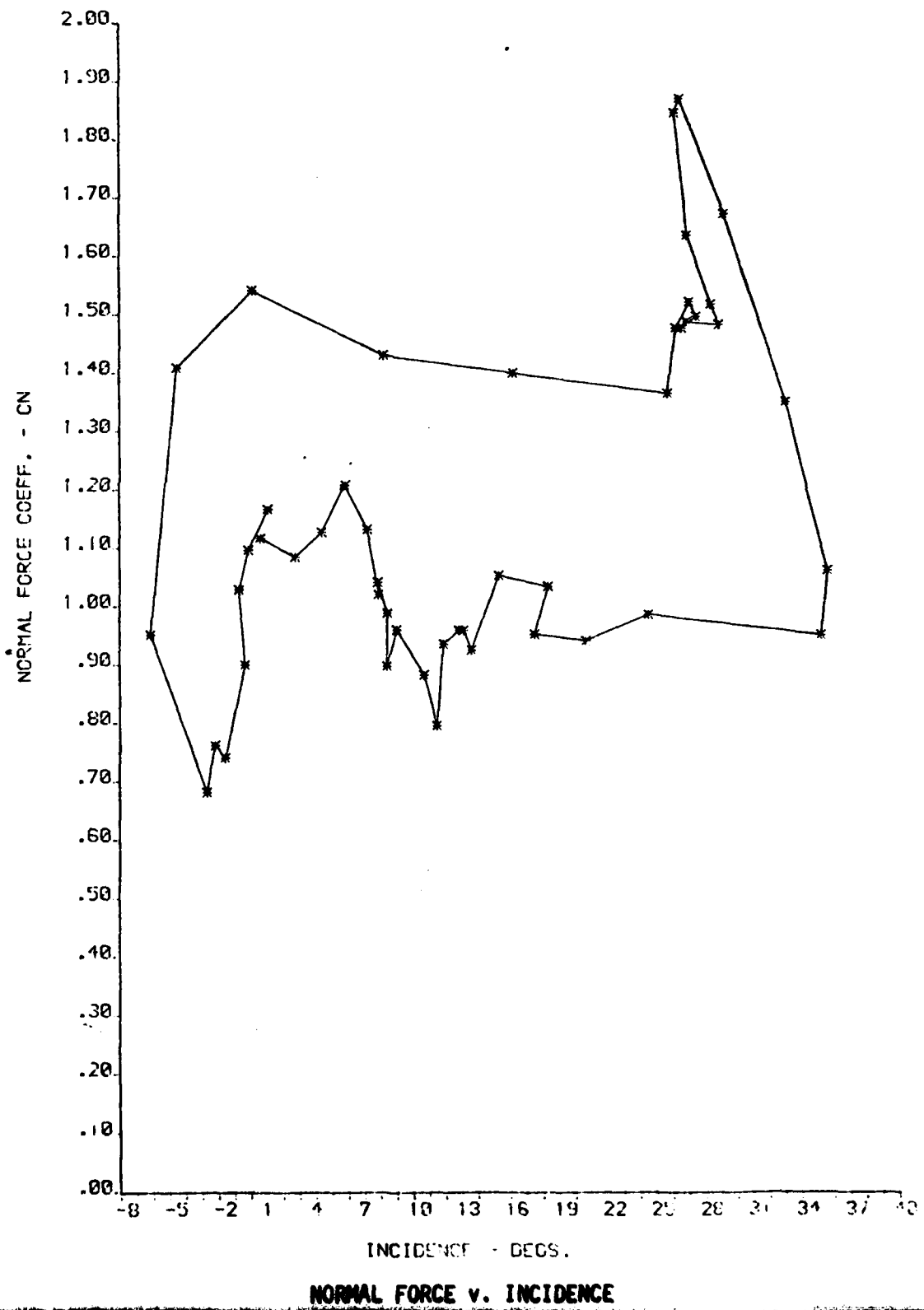


FIG. 30d

NORMAL FORCE VS. INCIDENCE --TEST 8



REPORT DOCUMENTATION PAGE		READ INSTRUCTIONS BEFORE COMPLETING FORM
1. Report Number AFOSR-TR- 81-0604	2. Govt Accession No.	3. Recipient's Catalog Number
4. Title (and Subtitle) UNSTEADY EFFECTS OF CIRCUMFERENTIAL PRESSURE DISTORTED INLET FLOWS IN COMPRESS- ORS.	5. Type of Report & Period Covered FINAL 1977-1981	
7. Author(s) R. E. PEACOCK	6. Performing Org. Report Number AFOSR-77-3305	
9. Performing Organization Name and Address CRANFIELD INSTITUTE OF TECHNOLOGY CRANFIELD BEDFORD GREAT BRITAIN	10. Program Element, Project, Task Area & Work Unit Numbers <i>61102F 2307/A4</i>	
11. Controlling Office Name and Address AFOSR BOLLING AFB DC 20332	12. Report Date JUNE 1981	
14. Monitoring Agency Name and Address EUROPEAN OFFICE OF AEROSPACE RESEARCH AND DEVELOPMENT LONDON GREAT BRITAIN	13. Number of Pages <i>146</i>	
16. & 17. Distribution Statement Approved for public release; distribution unlimited.	15. UNCLASSIFIED	
18. Supplementary Notes		
19. Key Words TURBOMACHINERY, COMPRESSORS, UNSTEADY AERODYNAMICS INLET MALDISTRIBUTION EFFECTS.		
20. Abstract A STUDY WAS COMPLETED OF UNSTEADY FLOW EFFECTS UPON COMPRESSOR ROTORS. ON-ROTOR INSTRUMENTATION WAS USED IN CONJUNCTION WITH A CUSTOM-DESIGNED PERIPHERAL DATALOGGER TO ESTABLISH THE UNSTEADY AERODYNAMIC RESPONSE BOTH TO A SERIES OF UPSTREAM SCREEN GENERATED DISTORTIONS AND TO ROTATING STALL, WITH AND WITHOUT SCREENS		